‘1-, 2- and 3-Dimensional Phenylene-based Materials for Optoelectronic Applications’

Dissertation zur Erlangung des Grades

„Doktor der Naturwissenschaften“

am Fachbereich

Chemie, Pharmazie und Geowissenschaften

der Johannes Gutenberg-Universität Mainz

Vorgelegt von

Luke D. Oldridge

Geb. in Dunedin, New Zealand

Mainz 2005

1 Introduction

1.1 General introduction

There has been no technology that has affected every area of our society as much as synthetic polymers. The development and production of plastics has had an impact on every aspect of our lives; it is used to package the food we buy, as housing for our appliances and as a superior material for countless applications.

Plastics are synthesised, and so the properties of the end product can be designed to correspond to the desired properties by manipulation of the molecular structure. Due to recent advances in synthesis, commercial plastics can nowadays be fine-tuned for most desired properties, simply by alteration of their chemical structure. The characteristics of plastics that make them such a versatile material include chemical resistance, low heat and electrical conductance, high strength to weight ratio, and easy processability. This makes synthetic polymers useful for a range of functions from storing nitric acid, as insulation for electricity cables, and as the frame structure on space stations.

The plastic era began in 1862, when Alexander Parkes revealed a cellulose derivative that could be moulded at elevated temperatures but kept its shape when cooled. The first thermoplastic, a substance molded under heat and pressure into a shape that is retained after the heat and pressure is removed, was discovered in 1866 as an alternative for ivory for use in billiard balls. Celluloid, made from cellulose nitrate and camphor, became a widely used material, however as more advanced plastics were discovered its usefulness declined. The next important innovation came in 1907 when Leo Baekeland developed Bakelite, the first thermoset plastic (materials that once hardened in a mould, cannot be burnt, melted, or redissolved). Many plastics have been developed since; cellophane in 1913 as a flexible wrap, nylon and polyvinyl chloride (PVC) in the 1920's, polyethylene in 1933, and Teflon as a non-stick surface in 1938. Plastics have had an influence in many industries, from revolutionising the music industry in 1948 with the development of the long-playing record (LP), to changing the way clothes are worn with the introduction of spandex

(Lycra) in 1959 by DuPont, a stretchable material to replace rubber in swim wear, girdles and gym clothing.

In the field of electronics and optics, plastics originally fulfilled only the requirements of packaging and insulating. However, this changed in 1977 with the serendipitous discovery of electrically conducting organic polymers based on polyacetylene.[1,2] Heeger, MacDiarmid and Shirakawa discovered that when a film of polyacetylene was doped with a halogen, the conductivity of the films increased dramatically, by up to 7 orders of magnitude. Inorganic semiconductors had already had an enormous impact on the development of many technologies, and the promise to combine the well-known properties of organic polymers with the properties of inorganic semiconductors and metals generated interest in both academia and industry. Thus, a new field of research with potential to revolutionize the electronic industry as a whole was born, namely, conducting polymers.

1.2 Conjugated Polymers

The structure of the first reported conjugated polymer, polyacetylene, is shown in Figure 1.1. The alternating double and single bonds in the structure enable complete delocalisation of pi-electrons along the polymer chain. Upon doping, i.e. on partial oxidation or reduction, charge carriers are created which are mobile not only along the polymer chains but also between successive chains. This conjugation is also responsible for the strong absorption of radiation in the UV/visible range.

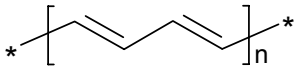

Figure 1.1. Structure of polyacetylene.

While polyacetylene was the first conducting polymer, it was not useful as a material for industrial applications due to its instability in air and the difficulties associated with processing the insoluble material. Fortunately, the field of conjugated polymers was not restricted to polyacetylene, and research into more stable polymers

commenced with investigations into aromatic polymers. Some examples of aromatic conjugated polymers are shown in Figure 1.2. These conducting polymers differ from polyacetylene for three fundamental reasons: they have non-degenerate ground states due to the energy difference between the two mesomeric forms, quinoid and aromatic; higher stability; and structural versatility that stems from the ability to control the monomer structure, which can lead to a range of electronic properties.[3]

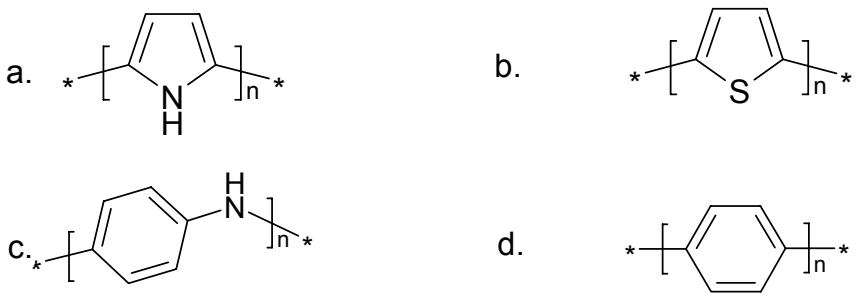

Figure 1.2. Structure of several aromatic conjugated polymers: a. poly(pyrrole); b. poly(thiophene); c. poly(aniline); d. poly(phenylene).

Early investigations into conjugated polymers followed the development of electropolymerisation techniques in the 1980s. This was as a consequence of the report in 1979 of the oxidative electropolymerisation of pyrrole to yield highly conducting films of poly(pyrrole), Figure 1.2a.[4-6] This electropolymerisation technique was promptly applied to other aromatic compounds to give conducting polymers such as poly(thiophene) (Figure 1.2b.),[5] poly(aniline) (Figure 1.2c.),[7,8] and poly(phenylene) (Figure 1.2d.).[9,10]

An advantage of this electropolymerisation to obtain conducting polymers is that insoluble thin films are prepared in one step. However the motivation to use conjugated polymers is that they could combine the electronic properties of metals and inorganic semiconductors with the processability and mechanical properties of synthetic polymers. Electropolymerisation has a slight disadvantage in that the regioregularity of the units in the polymer chain cannot be guaranteed.[3] This results in polymers with reduced performance as the effective conjugation length, *i.e.* the oligomeric length at which saturation of molecular properties occurs, is reduced due to coupling defects.

The chemical synthesis of conjugated polymers allows for the easy substitution of the monomer units and for a higher regioselectivity during the polymerisation reaction. As a result, the field of conjugated polymers has advanced significantly in the past two decades with extensive studies into a multitude of new, readily processable conducting materials.

1.2.1 Phenylene as the backbone-Poly(para-phenylene) derivatives

Initial attempts to make poly(aniline) and poly(acetylene) processable concentrated on introducing substituents onto the monomer units.[11,12] However, this induced a twisting of the polymer backbone due to unfavourable steric interactions, which yielded processable but poorly conjugated polymers with reduced conducting properties. The first processable and conducting polymers were based on poly(3-alkylthiophene), Figure 1.3.[13-15]

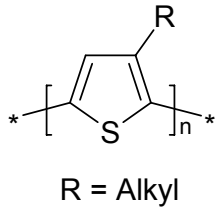

Figure 1.3. Structure of Poly(3-alkylthiophene).

The polymerisation of thiophenes yielded the first soluble conducting polymers, which was rapidly followed by reports of many processable conducting polymers. One such conjugated system that has been studied extensively in recent years is poly(*para*-phenylene) (PPP), the structure of which is shown in Figure 1.4.

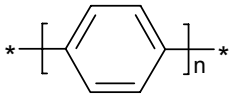

Figure 1.4. Poly(para-phenylene).

The unsubstituted phenylene polymer is insoluble and hence not processable. Thin films of this material were first made by a precursor method. The radical

polymerisation of a diacetate precursor yields a soluble polymer, which can be thermally converted to PPP.[16] The synthetic route is shown in Scheme 1.1. This method towards PPP synthesis gives approximately 15 % 1,2-linkages.[16]

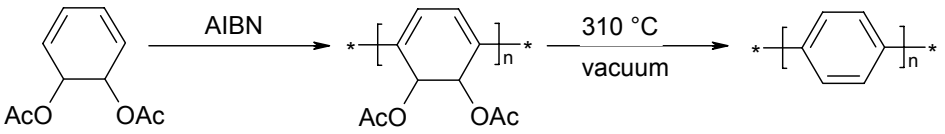

Scheme 1.1. Precursor route to PPP.

While the use of precursor methods to overcome the insolubility of PPP is effective, soluble analogues of PPP are necessary in order to obtain fully processable conjugated materials. This processability is important for certain applications, for example when the substrate or other component of a device cannot be heated to 310 °C. The early soluble PPP's were based on poly(2,5-dialkyl phenylenes).[17,18] The first reports of substituted PPP's were unsatisfactory in that the molecular weights of the materials were too low.[18] These low molecular weight oligomers were synthesised by the nickel (0) mediated Yamamoto-type polymerisation of 1,4-dibromo benzene derivatives, to give a material with a degree of polymerisation of approximately 13.[18] Oligomers of this length are of the same order as the mean conjugation length of PPP's. PPP's of significantly higher molecular weight were synthesised by the palladium catalysed Suzuki polymerisation of a 4-bromo-2,5-dialkylbenzeneboronic acid.[17,18] The synthetic route to high molecular weight soluble PPP's is shown in Scheme 1.2.

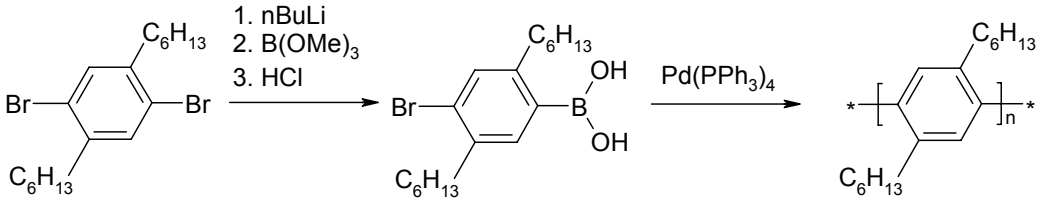

Scheme 1.2. Suzuki polymerisation for PPP synthesis.

The length of the alkyl chains has an effect on the physical properties of the polymer, with solubility increasing with increasing chain length. However, the steric interactions between the alkyl chains on adjacent benzene rings in the polymer chain

cause a substantial twist of the phenylene rings out of the plane. This leads to less effective conjugation along the chain, and is usually accompanied by a reduction in the fluorescence quantum yield. One method to eliminate the twist in the polymer is to lock in the planarisation by introducing methylene bridges to form a ladder PPP (LPPP).[19,20] A Suzuki polymerisation of an aryl ketone, followed by a polymer analogous reduction and subsequent Friedel-Crafts ring closure yields a planar ladder polymer.[19,20] A general reaction sequence is shown in Scheme 1.3.

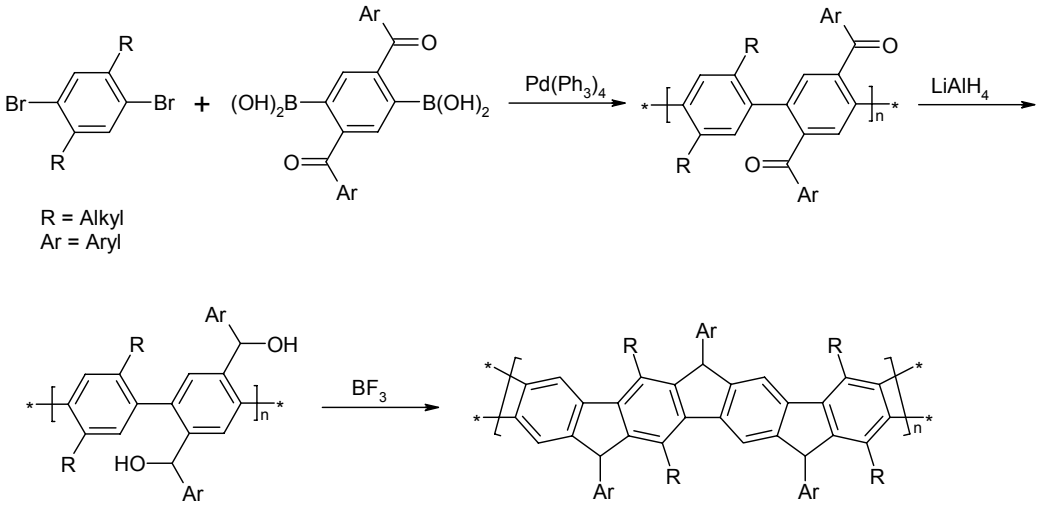

Scheme 1.3. Route to ladder-PPP.

The ladder formation occurs with a high level of regularity, and no evidence of defects such as cross-linking or incomplete ring closure can be detected.[19,20] The thermal stability and degree of rigidity is higher for these ladder-type polymers than the one-dimensional analogues.[19-21] A number of synthetic strategies to prepare LPPP's exist, and a range of polymers have been reported.[22] The fluorescence spectra of these materials in the solid state show a broad emission between 650 nm and 450 nm, compared to a narrow emission at 450 nm in solution. This is attributed to the formation of excimers in the solid state due to the π–π stacking between the planar conjugated polymer chains. This bathochromic shift of the emission in the solid state renders the LPPP inadequate for a number of applications. With the aim to obtain a material with properties intermediate to PPP and LPPP, a number of polymers, which consist of structures intermediate between LPPP and PPP, have been reported. Two of these intermediate step ladder polymers are shown in Figure 1.5.

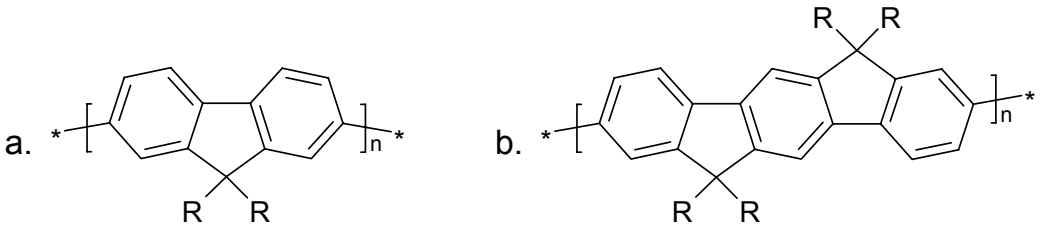

Figure 1.5. Examples of step ladder polymers. a. Poly(dialkylfluorene) b. Poly(tetraalkylindenofluorene).

The first attempts to synthesise soluble poly(fluorenes) with the attachment of solubilising alkyl substituents at the 9-position were reported in 1989.[23] The oxidative polymerisation using $FeCl_3$ yielded low molecular weight materials and the coupling was not regioselective either.[23] However, the use of metal catalysed aryl-aryl cross coupling reactions allowed the synthesis of higher molecular weight polymers, which are structurally well defined. In addition to the Suzuki polymerisation mentioned above, the Yamamoto nickel(0) catalysed cross coupling of dihaloaryl monomers, and the palladium catalysed Stille-coupling of distannyl- and dihaloaryl monomers, have been successfully applied to the synthesis of conjugated polymers. [24-26] Pei and Yang, at Uniax, reported the first transition metal catalysed polymerisation of a fluorene derivative in 1996.[27] Since then, due to the optical and electronic properties of the various poly(fluorenes), *ie.* emission in the blue region of the spectrum and a small Stokes shift, there has been considerable interest in the development of this class of materials, both in academia and industry.[28-30]

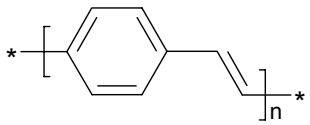

Figure 1.6. Structure of Poly(phenylene vinylene).

The discovery of conducting polymers led to a large amount of work being undertaken to investigate the electrical properties of these materials. Most of the work prior to 1990 was concerned with studies on the conductivity of these materials, however the work of Friend and Holmes *et al.* showed that poly(phenylene vinylene) (PPV) could generate light with the application of an electrical field, Figure 1.6.[31] This discovery initiated a new field of research, which incorporates both chemists and

physicists, in an effort to develop polymeric optoelectronic technologies and materials for commercial applications.

1.3 Organic Light Emitting Diodes

1.3.1 Introduction

Photoluminescence (PL) is the emission of light from a material, as a consequence of the optical absorption and subsequent radiative decay of an excited state. In contrast, electroluminescence (EL) is the non-thermal generation of light due to the application of an electric field to a substrate. The two processes differ in the way in which the excited state of the emitting material is formed. In PL, absorption of a photon excites an electron from the highest occupied molecular orbital (HOMO) to the lowest unoccupied molecular orbital (LUMO). Following this electronic transition, the excited state can relax back to the ground state by radiative decay, with the excess energy lost as a photon of light. In EL, the excited state is formed by the injection of an electron into the LUMO and hole to the HOMO, as a result of the applied electric field. The addition of a positively charged hole is in reality the removal of a negatively charged electron, but it is simpler to discuss in terms of hole addition. If this excited state is a singlet, it is identical to the one formed by absorption of a photon, and so can also relax to the ground state by radiative decay. The two processes are illustrated in Figure 1.7.

EL was first observed from an inorganic material, a dispersion of ZnS phosphor powder in an isolator between two electrodes. The first commercially available light emitting diodes (LED's) were introduced in the 1960's by General Electric, and were based on the inorganic semiconductor GaAsP.[32] The first LED's emitted red light, as determined by the band gap of the semiconducting material. Orange, yellow and green LED's followed with the development of new inorganic semiconductors, generally from elements from groups III and IV of the periodic table such as GaAs, InGaP and GaAsInP.[33] Larger band gap materials, and so LED's of shorter wavelength, were difficult to obtain. However blue LED's based on SiC, ZnSe or GaN were developed, but demonstrated lower device efficiencies and performance.[33]

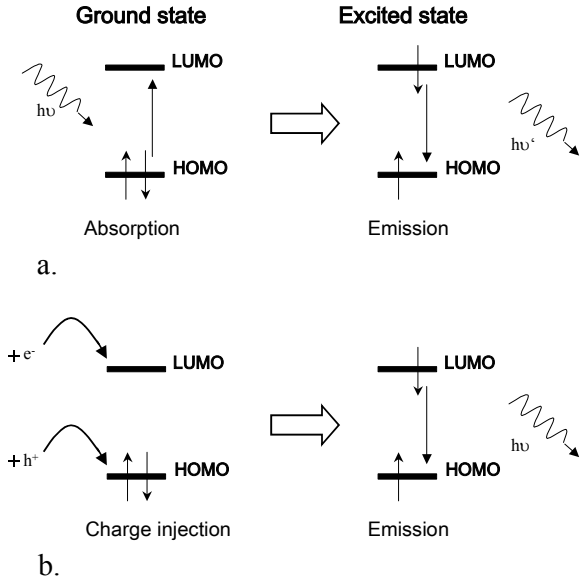

Figure 1.7. a. PL. Absorption of a photon results in an electron being excited to the LUMO of the material. The excited state radiatively decays with the emission of a photon. b. EL. The injection of an electron to the LUMO and a hole to the HOMO results in an excited state. The excited state radiatively decays with the emission of a photon.

LED research focused on both the production of new materials and the development of device technologies; research previously undertaken in the silicon industry. In contrast to the silicon industry however, the materials used in LED's are comparatively complex and difficult to produce, and so the development of LED technologies is behind those developed for the silicon industry.[33] Therefore there still remain concerns regarding cost, size of crystal growth, defect densities and the volumes of the devices produced.[33]

One potential solution for the issues associated with inorganic LED's is to use organic materials as the active component, as problems such as cost and size of the emitting area are easily resolved for theses types of materials. EL was first observed from anthracene in the 1960's, however driving voltages in the order of 100 V were required.[34,35] While the device performance of anthracene was significantly lower than for inorganic LED's, this was proof that EL was not confined to inorganic materials. The device efficiencies, brightness, lifetime and operating voltages of

organic LED's (OLED's) were not competitive compared to those containing inorganic materials until 1987, when organic fluorescent dyes were incorporated into working devices.[36-39] This revived the interest in OLED's for commercial use.

In the fabrication of LED's with organic dyes or inorganic substrates as the active material, thin films of the emitting layer are required. This is achieved by sublimation or vapour deposition, both methods which are expensive and not suited to the production of large-scale devices. Polymers are readily deposited as thin films over large areas from solution, using techniques such as spin coating or a doctor blade. This processability, as previously mentioned for conjugated polymers, makes EL from polymeric materials attractive for commercial applications.

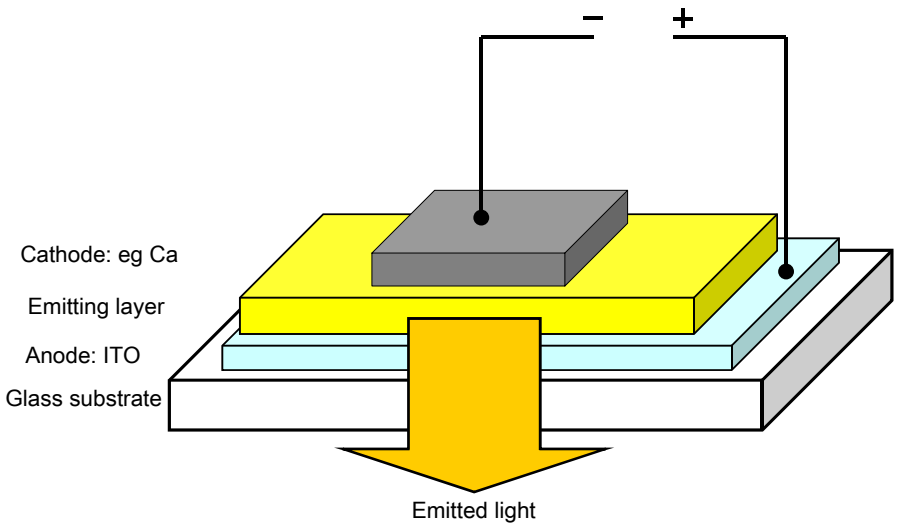

Figure 1.8. Schematic diagram of single-layer OLED. An applied voltage to the cathode and anode results in the emission of light.

The first polymer based OLED's were reported by Holmes and Friend *et al.* in 1990, using PPV as the active material[31]. By depositing a precursor polymer by spin coating, then thermally converting the film to PPV, robust and uniform films of approximately 100 nm can be produced. If the films are deposited on a conducting transparent substrate, such as indium tin oxide (ITO) coated glass (anode), and a low

work function electropositive metal, such as Ca or Mg, is deposited on top, as cathode, an OLED is produced. A schematic diagram of a polymer OLED is shown in Figure 1.8.

When an external voltage above a specific threshold value that is dependant on the material, is applied at the electrodes, charge carriers are injected into the emitting layer. Holes are injected at the anode and electrons at the cathode, and in the presence of an electric field, $> 10^5$ Vcm^{-1}, the charge carriers move through the active layer, and non-radiatively decay at the opposite electrode.[40] Some charge carriers combine to form a hole and electron pair, or exciton, which can be triplet or singlet excited states. The singlet excited state can radiatively relax with the emission of a photon, to give EL.

A number of parameters are used to assess the performance of an OLED. The most common measures of OLED performance are:

- *Internal efficiency* The most common measure of quantum efficiency is internal efficiency, the ratio of the number of photons emitted per electron injected. This figure cannot be measured directly.
- *External efficiency* Not all of the light generated reaches the viewer and so the external efficiency is a factor of $2n^2$ lower than the internal efficiency, where n is the refractive index of the polymer. Typical values for the external quantum efficiency range between 0.1-5 %.[41]

$$\eta_{int} = 2n^2 \eta_{ext}$$

- *Power efficiency* The ratio of output light power to the input electric power, power efficiency, cdA^{-1}, can be calculated by multiplying the external efficiency by the ratio of the mean photon energy (E_p) and the drive voltage (U). High power efficiency is required for long device lifetimes.

$$\eta_{pow} = E_p U^{-1} \eta_{ext}$$

- *Luminous efficiency* The luminous efficiency, measured in lumens per watt (lmW^{-1}) takes into account that the human eye is more sensitive to certain colours. The luminous efficiency is determined by multiplying the power efficiency by the luminous efficacy (S), as defined by the Commission de L'Eclairage (CIE).[42]

$$\eta_{lum} = \eta_{pow} S$$

- *Luminance* The brightness of a device, in cdm^{-2}, is also used to estimate the efficiencies of devices. The Luminance is sometimes reported as a function of current density. An average laptop display has a luminance in the order of 100 cdm^{-2}.[33,40]

1.3.2 Multilayer OLED's

Most conjugated polymers are intrinsic p-type conductors, *ie* positively charged holes have a higher charge carrier mobility through the material compared to electrons.[33] As a consequence, excitons tend to be formed close to the cathode-polymer interface, which affects the lifetimes and efficiencies of the devices. To overcome this problem either an emissive material with a balanced charge injection and mobility must be used, or the device construction must be such that the recombination zone is shifted more to the centre of the emitting layer. One technique to shift the position of the recombination zone is to use multilayer devices.

An early attempt to balance the charge injection involved the incorporation of a cyano-substituted polymer (CN-PPV) with a high electron affinity.[43] The soluble polymer was synthesised by a Knoevenagel condensation, as shown in Equation 1.

Equation 1. Knoevenagel condensation polymerisation of cyano-substituted PPV (CN-PPV).

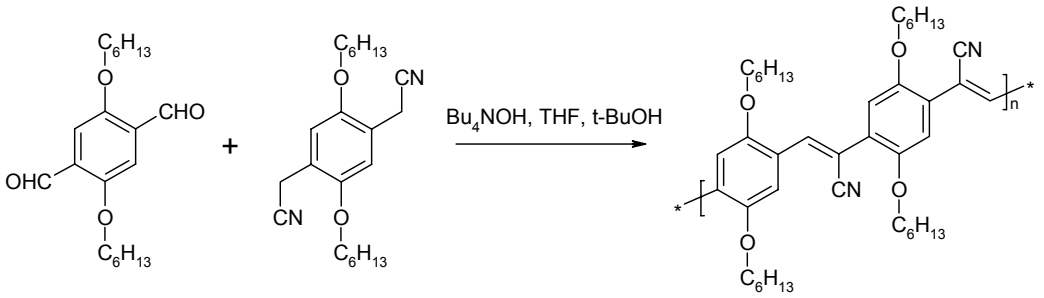

An OLED was produced with CN-PPV as the emissive layer, and red emission with a 0.2 % η_{int} was observed.[43] The η_{int} was not affected by exchanging the cathode from calcium to aluminium, suggesting that the electron injection is improved by the introduction of cyano groups, and that other processes at the anode now determine the device efficiency.[43]

The authors incorporated the CN-PPV with PPV into a two-layer device, in order to balance the charge injection. By first depositing a thin film of insoluble PPV via the precursor route as a hole transporting layer, then spin coating the CN-PPV, an OLED with an η_{int} of 4 % was produced.[43] While larger driving voltages were needed for the thick two layer device compared to the single layer device, the required field (drive voltage/film thickness) was reduced, indicating a significant improvement in charge injection.[43]

The emission from the two-layer device was found to only occur from the lower band gap, cyano substituted PPV. In order to understand the emission and efficiency of the two-layer OLED, the schematic energy level diagram must be considered, Figure 1.9. The authors found that the levels of the HOMO, or ionisation potential (IP), and the LUMO, or electron affinity (EA), of CN-PPV were 0.6 and 0.9 eV lower respectively than for PPV.[43] These present a significant barrier at the polymer heterojunction for both holes and electrons, which leads to charge confinement. Excitons are produced when either a hole or an electron tunnel through the barrier.[43] When the exciton is formed in the CN-PPV layer, it can radiatively decay to emit light and when the exciton is formed in the PPV layer, it diffuses into the lower energy CN-PPV layer where it emits. Therefore, the exciton generation must occur close to

the polymer interface, so that the emission is from the polymer with the lowest energy gap.[43]

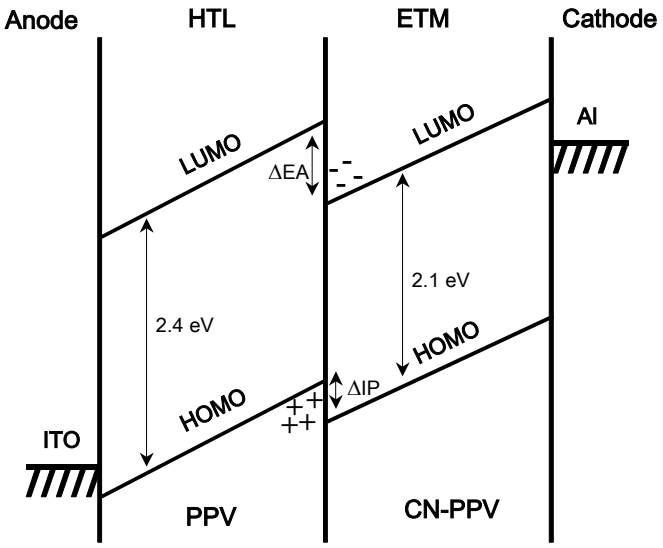

Figure 1.9. Schematic energy level diagram for a two-layer OLED. The relative energy levels of the HOMO and LUMO of the hole transporting layer (HTL) and the electron transporting material (ETM) and the Fermi levels of the electrodes are shown. The difference in electron affinity (EA) and ionisation potential (IP) between the HTL and the ETM is shown.

1.3.3 Electron transporting materials

A balanced injection of both types of charge carriers, holes and electrons, is required to produce an EL device with high quantum efficiency. Most conjugated polymers are intrinsic p-type conductors, *ie* hole conductors, and there are relatively few examples in the literature on n-type conjugated polymers.[33,44,45]

For a material to be successful as an electron transporting material (ETM), a number of properties are required: (i) reversible reduction; (ii) EA and IP values that match the p-type material and electrodes to minimize the energy barriers for charge injection; (iii) high electron mobility; (iv) high glass transition temperature and thermal stability; (v) processability; (vi) amorphous morphology.[45] Among these properties, a high electron mobility is the most challenging to obtain. Typically, the hole mobility is found to be higher than the electron mobility.[45] Electron transport,

which can be regarded as a one-electron reduction of a neutral moiety and the oxidation of its anion, requires the formation of stable anions, and the presence of impurities such as molecular oxygen can lead to trapping of the electron.[45] High electron mobilities have been reported for some single organic crystals, suggesting that there is no inherent limitation to achieve high mobility in organic n-type materials, however, the challenge is to achieve air-stable electron transport with high mobilities under ambient conditions.[45]

Most ETM's are electron deficient heteroaromatics. Quinoline and quinoline-based polymers are two of the more widely studied ETM's in OLED's.[45,46] Many other classes of compounds have also been looked into as potential ETM'S. These include metal chelates[38], various nitrogen containing heteroaromatics[47-52], and perfluorinated aromatics[53,54].

The most extensively investigated class of ETM's to date is the oxadiazole containing materials. The success of 2-(4-biphenyl)-5-(4-*tert*-butylphenyl)-1,3,4-oxadiazole (PBD), Figure 1.10, in organic EL devices in 1988 ensured a continued use of these types of materials in OLED's as ETM's.[36-39,55-58] The incorporation of PBD with a triphenylamine derivative as an emissive material in a bilayer OLED resulted in an increase in the quantum efficiency by four orders of magnitude.[37,39,45]

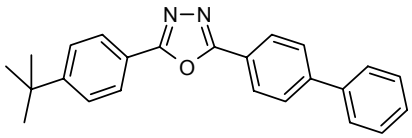

Figure 1.10. Structure of PBD.

Oxadiazoles are electron deficient, meaning they have poor hole acceptor capabilities. PBD is often used as ETM's because of its availability in high purity (purified by sublimation) and it can be blended with EL polymers.[40] Blending of two materials can lead to phase separation and crystallisation however, and more complex device architectures must sometimes be used, *eg.* solid dispersion of PBD in an insulating polymer such as poly(methyl methacrylate) (PMMA).[59] While higher drive voltages are required for OLED's containing an ETM layer of a PBD-PMMA blend,

the η_{ext} for a device with and without the ETM layer are 1.1% and 0.07% respectively.[59]

Oxadiazoles have also been used as components of n-type polymers, where they are expected to have higher glass transition temperatures and are less susceptible to crystallisation under device operation when compared to the oligomeric oxadiazole containing compounds.[45] The processability of an oxadiazole polymer by spin coating was an additional benefit of polymeric oxadiazole. However, the solubility of most of the phenyloxadiazole copolymers initially reported was low.[60] The introduction of solubilising alkoxy chains on the benzene units gave a soluble material, which gave an increase in the η_{ext} of a bilayer PPV OLED by a factor of 25.[61]

The oxadiazole moiety has also been introduced into polymers as pendant sidechains. In comparison with the unsubstituted analogue, upon oxadiazole substitution in PPV, a 56 fold increase in η_{ext} was observed.[62] Oxadiazole functionality has also been incorporated into polyfluorene to improve charge injection and transport and one such synthesis is depicted in Scheme 1.4. The monomer was copolymerised in a Suzuki polymerisation to give the copolymer illustrated in Scheme 1.4.[63] The polymer was incorporated into an OLED which yielded an η_{ext} of 0.52%, which is better than the unsubstituted poly(fluorene) with an η_{ext} of 0.2%.[63,64]

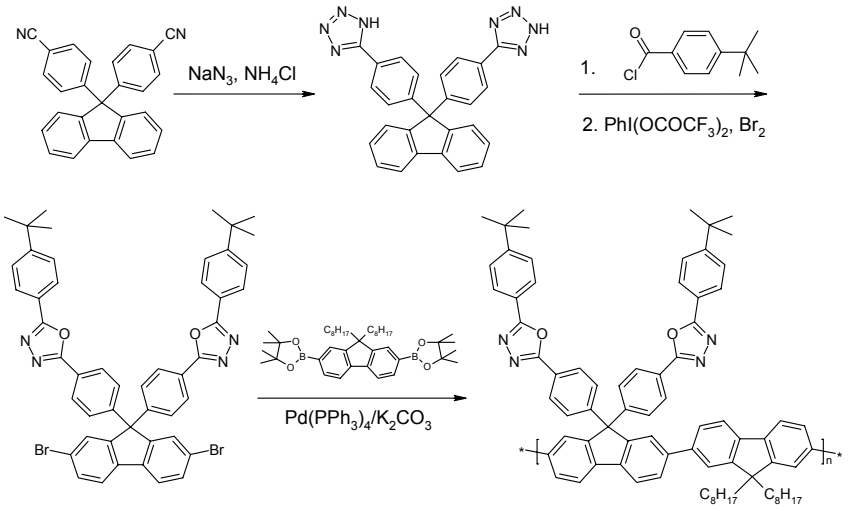

Scheme 1.4. Synthetic route to oxadiazole substituted poly(fluorene).

The fluorenone moiety has been described as an undesirable defect in polyfluorenes, and will be discussed later in terms of the long wavelength emission in blue emitting OLED's.[30,65] A keto functionality is electron withdrawing and the fact that the electrons are trapped at this moiety in device operation suggests that polymers based on this may be useful ETM's.

Fluorenone containing poly(fluorenes) have been synthesised in the past for use in OLED's[66,67] In these cases, the fluorenone unit was incorporated as a statistical co-monomer with dialkylfluorene in a Yamamoto or Suzuki polymerisation. The solubility of the resulting polymers was related to the amount of fluorenone present, with ratios above 1:1 yielding materials that are insoluble in most organic solvents.[67] Devices constructed from these copolymers showed a green EL, with a maximum at 550 nm.[66] The long wavelength emission was dominant when the amount of fluorenone unit was as low as 1%, suggesting efficient exciton energy transfer to the moiety in addition to charge trapping.[66] The η_{ext} of the devices prepared were as high as 0.19% with brightness of 3340 cdm^{-2}, compared with 0.07% and 280 cdm^{-2} for the poly(fluorene) without fluorenone.[66]

Poly(fluorenone) is an insoluble material, however it has been incorporated as the active layer in an OLED.[68,69] In order to overcome the insolubility of the material the authors deposited a processable precursor poly(fluorene ketal), which was deprotected to the ketone by treatment with dichloroacetic acid, Scheme 1.5.[68,69] Cyclic voltammetry measurements showed the polymer to have a LUMO at –3.3 eV.[68] This value is comparable to the work function of a magnesium electrode, -3.7 eV,

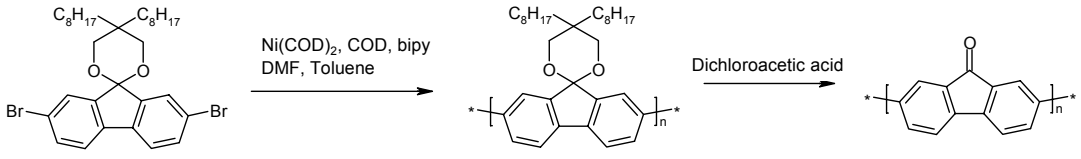

Scheme 1.5. Synthetic route to poly(fluorenone) via precursor.

A cathode was applied to the film of deprotected poly(fluorenone) on an ITO covered substrate, and EL with a maximum of 580 nm was observed.[69] η_{ext} values were not reported. While the emission from the poly(fluorenone) was not blue, the low lying LUMO of the material prevents impurities such as oxygen from capturing electrons.[69] Hence, this trap-free material can be used as an ETM in an OLED.

1.3.4 Blue emission from OLED's

The fabrication of LED's that emit light in the blue part of the visible spectrum is generally difficult and expensive. For blue emission from the active luminescent material, a HOMO-LUMO energy gap of 2.7-3.0 eV is required.[33] Due to this high energy gap, the lifetime and colour stability of blue emitting OLED's are the least resolved for commercial applications, and research into novel materials for this application is ongoing.

Unsubstituted PPP was incorporated into a one layer OLED in 1992.[70,71] Similar to the first PPV OLED's, the PPP active layer had to be deposited as a soluble precursor that was thermally treated to give the active material. The first simple one layer device, ITO/PPP/Al, had an emission maximum of 459 nm and an η_{ext} of 0.05%.[70,71]

The research efforts to produce soluble PPP derivatives have been discussed in Section 1.2.1. The fabrication of OLED's from soluble active materials is obviously preferable for commercial applications, as the treatment of a device to 310 °C in a high vacuum is costly and difficult for large-scale manufacturing. While PPP and its derivatives have high thermal and oxidative stability, single layer OLED's of these materials exhibit comparably low EL efficiencies.[33] Not surprisingly, much more efficient devices have been constructed using a multi-layer configuration.[72]

The substituents on a PPP backbone can cause significant twisting between the adjacent benzene rings, and although this leads to a hypsochromic shift, it is accompanied by a reduction of the fluorescence quantum yield.[33] This twisting can be removed by planarising the polymeric backbone, to give LPPP's.[19,20] OLED's based

on these materials initially give blue EL, however as operating times increase a yellow emission band becomes prominent, attributed to aggregate formation.[73] This emission could be suppressed by incorporating oligo-phenylene spacers between ladder segments, introducing substituents at the bridge head position or diluting the LPPP in a PVK matrix.[74,75]

With a structure intermediate to LPPP and PPP, the so-called stepladder polymers based on monomers of fluorene have become widely used in OLED fabrication. The high solution and solid state fluorescence quantum yields and thermal and chemical stability of these polymers, as well as the ease of substitution at the 9-position, make these materials promising candidates for blue emitting OLED's.[76-80] OLED's fabricated with poly(9,9-dialkylfluorenes) have been reported with high η_{lum}, up to 20 lmW^{-1}, with a turn-on voltage of 2 volts.[81] Poly(fluorenes) have also been utilized as the blue emitting material in multi-colour devices, where red, green and blue EL can be observed by varying the strength or polarity of the electric field.[82-84]

The EL of poly(fluorenes) is close to the violet part of the spectrum, and not a 'true' blue. In order to tune the emission of the polymers to a colour the human eye is more sensitized towards, Müllen *et al.* synthesized the next higher analogue to poly(fluorene), poly(indenofluorene).[85] Like fluorene, indenofluorene can be easily polymerized using various metal mediated reaction types, such as Suzuki or Yamamoto, and can be functionalised with various groups at the 6 and 12 position. The Yamamoto polymerization of indenofluorene is illustrated in Equation 2.

Equation 2. Yamamoto polymerisation of 2,8-dibromo-6,6,12,12-tetraalkylindenofluorene.

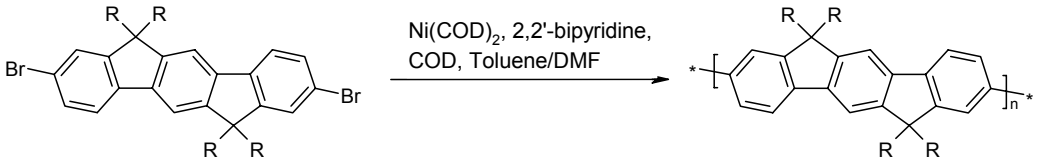

R = alkyl

As expected, the emission of poly(indenofluorene) at 432 nm is between that of poly(fluorene), 415 nm, and LPPP, 470 nm.[85] OLED's fabricated from tetraoctyl substituted and tetraethylhexyl poly(indenofluorene) were constructed.[86] The EL

spectrum of the octyl substituted polymer shows a broad peak, with a maximum at 567 nm, to give a green/yellow emission. The device had a η_{lum} of 0.16 lmW^{-1} and showed a stable luminance, with a predicted half-life of 5000 hours.[86] In contrast, the ethylhexyl substituted device produced an EL spectrum with a maximum at 429 nm, to give blue emission. This luminance rapidly decayed, with a half life of 0.8 hours, and an increase in the required driving voltages. This was accompanied by a bathochromic shift of the EL spectrum.[86] The authors propose that the long wavelength emission is attributed to the formation of aggregates, and while the linear octyl chains form said aggregates during the device fabrication that are stable, the branched ethylhexyl substituted polymers undergo a reordering under the electric field.[86] However, as the absorption spectra for the polymers is the same for solution and solid state, it is more likely excimer formation rather than an aggregate of ground state species.

Tapping-mode atomic force microscopy of the polymers shows that while the octyl substituted polymers show fibrillar morphology, a result of a long range regular packing between the π systems, the ethylhexyl substituted polymers shows no such fibrillar morphology.[86] This suggests that the bulky chains prevent a close stacking of the π systems, and so no long range ordering exist. As it is not possible to study the polymer films in the OLED's with this method without affecting the nature of the morphology, it is not known whether there is a change in morphology of the ethylhexyl substituted polymer films under device operating conditions.[86]

In order to produce stable blue emission, substituents with greater bulk were attached to indenofluorene. The synthesis of poly(tetraarylindenofluorene) is shown in Scheme 1.6.[87] As aryl substituents cannot be attached directly to indenofluorene, as is the case for alkyl chains, an alternate route is used. The indenofluorene moiety has to be formed by a ring closure reaction, a BF_3 mediated Friedel-Crafts ring closure, after the addition of the aryl groups.

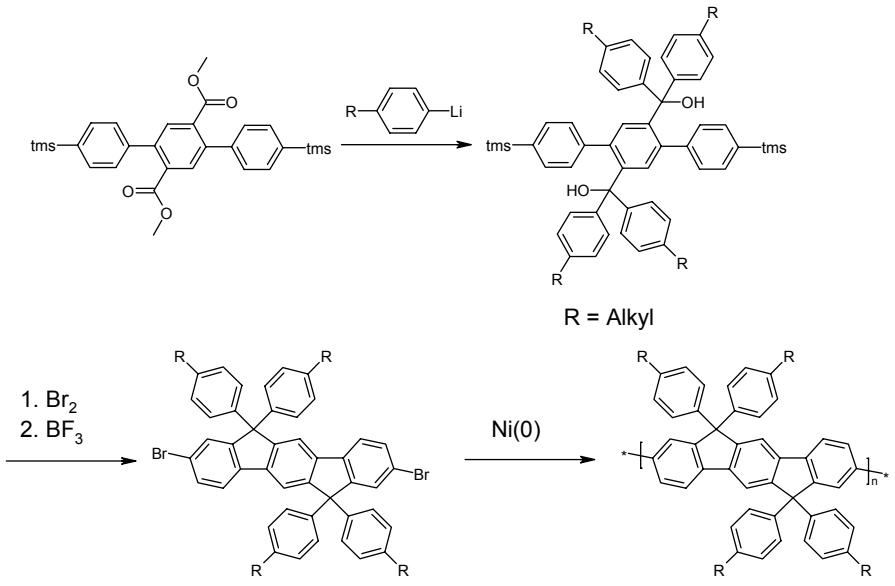

Scheme 1.6. Synthesis of poly(tetraarylindenofluorene).

OLED's fabricated from this material showed a blue emission with a maximum at 434 nm, which was stable under the testing conditions, *i.e.* argon atmosphere and low driving voltages.[87] While a long wavelength tail between 500 nm and 650 nm was observed in the EL spectrum, this became prominent only when the device was placed under increasing stress.[87]

Further analogues of indenofluorene have since been synthesized. The ladder-type pentaphenylene, Figure 1.11, has a narrow PL emission band with a maximum at 445 nm.[88] The polymer was incorporated into a single layer OLED, with an EL emission maximum at 445 nm, a luminance of over 200 cdm^{-2}, and no long wavelength emission with device operation under glove box conditions.[88]

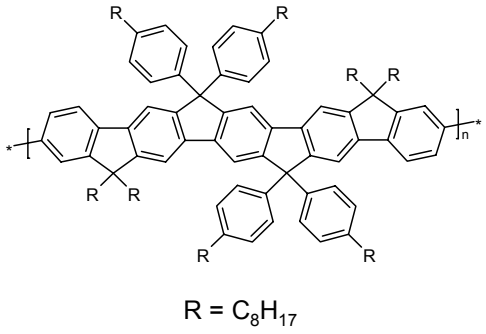

Figure 1.11. Structure of poly(pentaphenylene).

While the lifetimes and stability of blue emitting OLED's has been increasing steadily, it is important to understand the nature of the long wavelength emission in devices. With respect to poly(indenofluorenes), the authors attributed the unwanted emission as arising from aggregate, or excimer formation.[86] This hypothesis is supported by the fact that by introducing bulky substituents such as branched chains or dendritic systems, the long wavelength emission is suppressed.[76,86,87,89-91] However there is further experimental evidence that does not seem to support this explanation, and a significant amount of work has been undertaken to understand the processes involved with the emission.

1.3.5 Long wavelength emission: excimers or defects?

Early research into blue emitting OLED's determined that the production of pure blue light was hampered by a longer wavelength emission, and that the low energy tail or band in the EL spectrum affected the colour purity of the devices. This was first described as aggregate or excimer formation.[76,86,87,89-91]

Excimer formation is the interaction between an excited chromophore and an unexcited neighbour, which gives a more delocalised, lower energy excited state complex.[76] Poly(fluorenes), which can be described as rigid rods, are known to form nematic phases, and so can be pre-organised into the structural arrangement necessary for the π-π interaction of an excimer.[76,92]

Several results imply excimer formation as the lead source of long wavelength emission. As described for two poly(indenofluorene) derivatives previously, the transition from bulky ethylhexyl chains to linear octyl chains severely alters the solid state PL and EL measured.[86] Further indication of the effects of steric bulk is evident in examples when aryl substituents are pendant on a poly(indenofluorene) or large polyphenylene dendron side chains are attached to poly(fluorene).[87,89] In these instances, the long wavelength emission in EL and solid state PL is suppressed. Other approaches include the addition of bulky end groups, co-polymerisation, and blending.[93-95] There is little argument that the separation of the polymer chains reduces the prevalence of long wavelength emission.

A chromophore in an excited state can relax to the ground state through many different processes, including intermolecular and intramolecular interactions. However while in an excited state, the system can undergo both physical, *i.e.* reorientation or aggregation, and chemical, *i.e.* dissociation or oxidation, changes.[76] In terms of OLED's, the possibility of oxidation as a process to form low energy chromophores is apparent, as the lifetimes of devices are significantly improved when run under vacuum or glove box conditions.

Bliznyuk *et al.* studied the degradation mechanisms of OLED's utilizing spectroscopic techniques, chemical and structural analysis.[76] Using FTIR, they probed films of poly(dihexylfluorene) as pristine samples, as samples photodegraded in air and under a nitrogen atmosphere, and as a electrically degraded sample in a device.[76] The sample photodegraded under nitrogen and the fresh polymer film did not show the appearance of a vibrational band in the region of a carbonyl stretch, whereas the sample photodegraded under air showed such a band. While the spectra obtained from the electrically degraded devices are complicated by additional oscillations due to interference of the IR beam reflections from the interfaces of the device, the authors state that no carbonyl stretch is observed.[76] The presence of oxygen is also tested for by X-ray photoelectron spectroscopy, and is found in significant quantities only in the sample photodegraded in air, and close (< 1 nm) to the ITO anode in the electrically degraded sample. The authors proposed that there are two different mechanisms in operation; a photo oxidation process to form fluorenone centres (Figure 1.12), and a physical degradation to form excimers.[76]

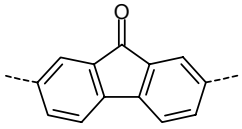

Figure 1.12. Structure of fluorenone.

The opposing opinion to the excimer formation hypothesis is that it is the formation of defect sites, namely oxidation to form fluorenone in the poly(fluorene) case, that is responsible for the long wavelength emission observed in OLED's. These

keto sites can be regarded as guest emitters, which efficiently trap singlet electrons created on the conjugated backbone.[65] There are two possible pathways to the generation of the ketone moiety. If the alkylation of fluorene does proceed to completion, the monoalkyl fluorene can be oxidised during the polymerisation reaction.[30,65] The proposed mechanism is shown in Scheme 1.7. The authors postulate that the reactive Ni(0) species used in the polymerisation of fluorene reduce the monoalkyl fluorene to a fluorenyl anion, with the formation of hydrogen. These anions can form hydroperoxide when exposed to oxygen, which can undergo a rearrangement to yield the fluorenone moiety.[30,65] This susceptibility to oxidation of the monoalkylated fluorene is clear when the solid state PL spectrum of poly(monoalkylfluorene) and poly(dialkylfluorene) is compared. The dialkylated films show no longwavelength emission, whereas the monoalkylated polymer shows significant low energy emission in the solid state.[65] A rigorous purification of the fluorene monomers to ensure that there is no monoalkylated fluorene results in pure blue EL, with a reduced long wavelength component.[96]

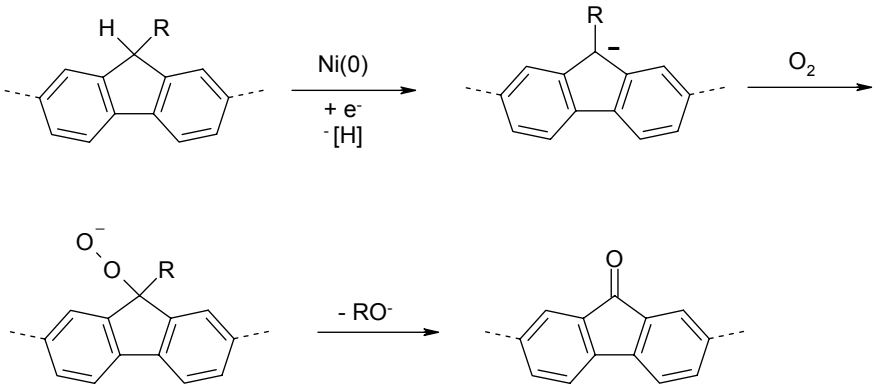

Scheme 1.7. Proposed scheme for generation of fluorenone during fluorene polymerisation.

In addition to the formation of keto defect sites during the synthesis of the polymer, these defects can be formed as a result of photo or electro oxidation.[30,65] The solid state PL spectra of a poly(dialkylfluorene) under UV illumination and the EL spectra of the same material run under ambient conditions show a clear increase in the relative amount of long wavelength emission with respect to time.[30,65] The FTIR spectra of the film under UV irradiation show an increase of the carbonyl stretching

band at 1721 cm^{-1} with respect to time.[30,65] The authors attributed this to the formation of emissive keto defect sites upon photo- and electrodegradation.[30,65]

The evidence for the presence of fluorenone defects in the main poly(fluorene) chain is clear. However, this does not exclude the formation of excimers as the source of the low energy emission. It has been postulated that the presence of fluorenone moieties in the polymer chain, with its planar structure, low steric hindrance and its tendency to induce interchain dipole-dipole interactions due the polar nature of the carbonyl, results in an increase in excimer formation.[67]

Evidence for the formation of excimers and keto defects has been introduced in the preceding paragraphs, but the low energy radiative pathway has not been established. Studies on the PL decay dynamics of fluorenone-fluorene oligomers and polymers can provide valuable information on the nature of the emitting chromophores.[66] A single exponential PL decay suggests the presence of a single emitting chromophore, whereas multiexponential decays would suggest complex kinetics of monomeric and excimer species.[66] The dilute solution time resolved PL shows that the blue emission at 416 nm has a single exponential decay with short lifetimes, less than 400 ps. The green emission at 525 nm for all copolymers had a longer lifetime of 5 ns, and follows a single exponential decay kinetics.[66] The long lifetimes observed for the green emission band are similar to those previously reported for fluorenone.[97] The decay kinetics for the thin film emission are similar to those from solution, with the green emission fitting a single exponential, which would not be expected for excimer emission in thin films.[66] This single exponential PL decay of the long wavelength band, as well as the observed similarity in delayed PL kinetics for the range of fluorenone-fluorene copolymers, suggests that the green emission originates from an on-chain monomeric fluorenone defect rather than from the formation of excimers of fluorenone or fluorene.[66]

The observed solvatochromism of the low energy band in poly(monoalkylfluorene) is further evidence for the assignment of this band to fluorenone defect sites.[30] Poly(monoalkylfluorene) was used as a poly(fluorene) example with increased defect concentration. As the polarity of the solvent increases, the low energy emission band decreases.[30] With increasing polarity the solvent

molecules are more closely bound to the permanent dipole moment of the fluorenone in its excited state. This favours non-radiative decay pathways through solvent quenching.[30] This effect is not concentration dependent, further evidence against excimer formation as the origin of the green emission.[30]

The experimental evidence tends to suggest that the fluorenone guest emitters in the poly(fluorene) trap singlet excitons from the polymer backbone by a dipole-dipole induced direct energy transfer of the Förster-type or an excitation energy migration assisted Förster-type transfer process.[30] This trapping process is the dominant pathway for excited state relaxation in the solid state.[30] The strong influence of the intermolecular interactions, such as the addition of sterically bulky substituents on the polymer chain, on the strength of the green emission was attributed to the interference to the formation of aggregates or excimers. However, if the migration of the excitons is viewed as an inter- and intrachain process, then the rate of migration to low energy traps is lower for polymer chains which have less intermolecular interactions, *i.e.* further apart. When the polymer chains are well packed, the excitons can migrate to the low energy fluorenone defect trapping sites easily. However, as the packing of the chains is impeded with the substitution of bulky groups, the rate of interchain migration is lower, and smaller ratios of excitons are trapped at the defect sites.

In addition to the rate of interchain migration, the chemical route to the fluorene monomer with bulky substituents is different compared to the routine literature route to poly(dialkylfluorenes). As the synthesis does not require the direct substitution on the fluorene moiety, rather the fluorene unit is formed by a Friedel-Crafts ring closure reaction, *c.f.* Scheme 1.6, it is less likely to form the mono-substituted monomers. Hence, this approach minimizes the amount of monosubstitution at the 9-position of the fluorene, which in turn generate keto defect sites either during synthesis or device operation. Furthermore, arylene-type substituents are more stable to photo-and electrooxidative degradation, and so produce OLED's with higher colour stability.[30]

While there is evidence for both excimer formation and defect emission as the origin of the long wavelength emission in poly(fluorenes), the hypothesis of defect formation can explain all the experimental evidence to date. Strategies to reduce

either the formation or the influence of keto defects are essential in order to fabricate blue emitting OLED's with long lifetimes and high stability.

1.4 Oligomers-linear conjugated segments

Whereas polymers are made of a large number of units linked in a repetitive fashion, oligomers contain only a few of these units, *ie* a lower homologue. It is not constructive to assign a particular molecular weight as the borderline between polymer and oligomer, but a feature of oligomers is that increasing the size affects the materials physical properties, until a convergence limit is reached.[98] When the increasing number of units no longer affects the physical properties, the material may no longer be regarded as an oligomer. A systematic study of physical properties with oligomer size helps to establish structure-property relationships of a polymer. The relationships for monodisperse materials can be extrapolated to give predictions for the properties of the analogous, defect free, polymeric compound.

An oligomer does not necessarily have to be utilised only as a polymer model, but can constitute an active material. Oligomers of thiophene, such as α-sexithiophene, Figure 1.13, have been used as the active component in molecular electronic and optical devices since 1989.[99-103] Sexithiophene was incorporated as the active material in an organic field effect transistor (OFET), with the resulting charge carrier mobilities and transistor characteristics found to be superior to those of the analogous poly(thiophene) transistor.

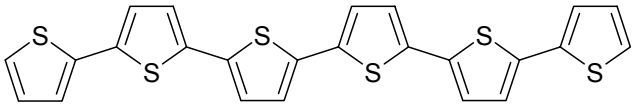

Figure 1.13. Structure of α-sexithiophene.

There has been much research into oligomers and oligomer synthesis in general, and into oligomers of conjugated materials in particular, for their use as the active compounds for optoelectronic applications.[98,104,105] A comprehensive review of the research regarding conjugated oligomers can be found in the literature, and is outside the scope of this thesis.[98,104,105]

The first synthesis of defined oligomers of fluorene was achieved using a random synthesis in 1998.[106] By introducing a monofunctional fluorene into the reaction mixture at the onset of the polymerisation, the formation of oligomers and low molecular weight polymers was observed by GPC analysis.[106] The differing molecular weight oligomers were separated from the polymer fraction, and each other, using HPLC. This afforded oligomers from n = 3 to n = 10 to be separated and characterised fully.[106] FD-MS showed that the fluorene end-capping unit is present at each end of the oligomers, which is important when considering the effect of the end-group on the properties of the oligomers.[106]

The purification of a crude reaction mixture to obtain discrete fluorene oligomers by HPLC requires a large amount of effort. A step-by-step approach was utilised in 2000 to prepare well-defined monodisperse oligofluorenes.[107] The step-by-step synthesis of the fluorene dimer, trimer and tetramer is shown in Scheme 1.8.

The odd number oligomer, *eg* n = 3, was synthesised by the Suzuki cross-coupling reaction of 2,7-dibromo-9,9-dihexylfluorene with 2-boronic ester-9,9-dihexylfluorene.[107] The fluorene dimer was synthesised by the nickel (0) catalysed homocoupling of 2-bromo-9,9-dihexylfluorene.[107] The subsequent bromination with alumina supported copper (II) bromide, and Suzuki cross-coupling reaction with 2-boronic ester-9,9-dihexylfluorene afforded the tetramer.[107] Higher analogues were not synthesised.

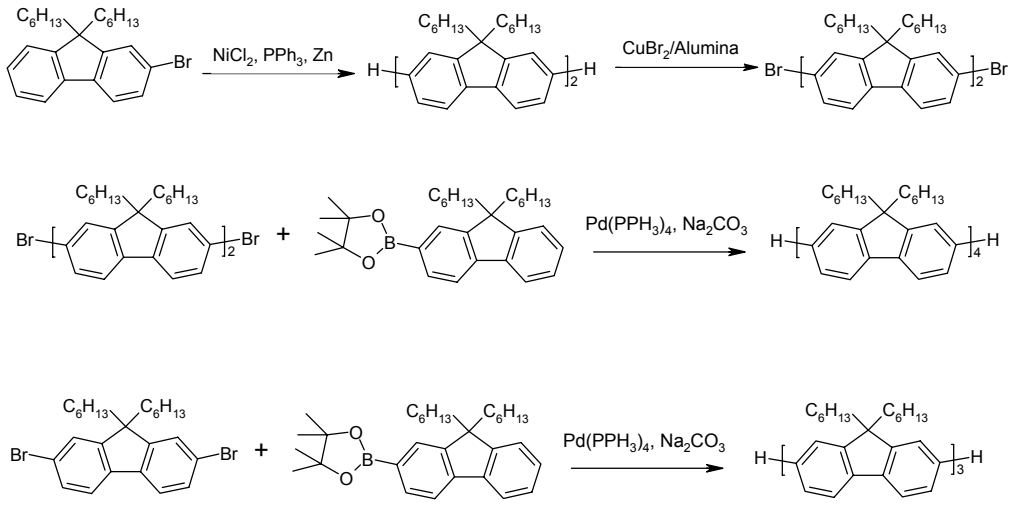

Scheme 1.8. Step-by-step synthesis of fluorene dimer, trimer and tetramer.

While it is certainly easier to synthesise longer oligomers via the random approach, the amount of material that can be obtained is limited by the quantity of crude polymerisation product that can be purified by HPLC. Conversely, while large quantities of low oligomer size can easily be synthesised utilising the step-by-step approach, for the fluorene case the higher oligomers get progressively more synthetically challenging.

1.5 Columnar bypass-sidestepping the defects

1.5.1 Introduction to hexa-peri-hexabenzocoronene (HBC)

The charge carrier mobility of a semiconducting material is an important factor governing its performance in electronic and optoelectronic devices. In organic semiconductors this mobility is strongly dependent on the morphology of the material, and as such can be improved by introducing long-range supramolecular order in the solid state.[33,40,108] In the case of conjugated polymers, the rigid-rod chains with solubilising alkyl substituents form lamella-type face-to-face alignment of the π-systems.[33,40] The charge carrier mobility is sensitive to a reduction in the long-range order of the polymer chains.[33,40] The degree of polydispersity of a polymeric semiconductor, as well as structural defects in the chain influence the formation of

perfect order between the chains.[33,40] These factors are intrinsically difficult to address in the construction of polymer devices. Alternate organic semiconductor materials that are monodisperse and possess the ability to form structures with long-range order are attractive as the active component in organic devices, as they can be produced defect-free.

Polycylic aromatic hydrocarbons (PAH's) are a stable class of disc-type organic molecules that include pyrene and coronene. The two-dimensional π-system of PAH's can be substituted with alkyl groups to form the combination of rigid core with soft shell, similar to conjugated polymers.[108] Under certain conditions this can result in PAH's that melt into discotic columnar mesophases, which possess long-range order through the π-systems of the discs. These discotic columns have been previously shown to possess a high charge carrier mobility.[109] These disc-type molecules with long-range ordering are attractive for use as the active component in OFET and photovoltaic (PV) devices as they can be produced defect-free and processed from the melt due to their lower viscosity, which can also result in a certain degree of self-healing of the columns in the devices.[108] The modification of the size and substitution pattern of PAH's can lead to materials with different electronic properties and phase behaviour. As a result, there has been much research into the synthesis and characterisation of PAH based materials.[108,110,111]

One class of PAH's are the hexa-peri-hexabenzocoronene (HBC) derivatives, shown in Equation 1.3. Unsubstituted HBC has hexagonal symmetry, and as it is a homologue of benzene, is sometimes referred to as super-benzene.[110] HBC was first prepared in 1958 by Halleux and co-workers by the oxidative intramolecular cyclodehydrogenation of hexaphenylbenzene (HPB) using aluminium (III) chloride in the melt, as shown in Equation 1.3. This cyclisation was achieved at room temperature in 1995 with the addition of copper (II) salts to an inert solvent under Lewis acid conditions.[112] This yielded the fully aromatised target HBC in quantitative yields, however for alkyl substituted HPB's the alkyl groups could undergo migration or cleavage when aluminium (III) chloride was used as the Lewis acid.[112] When iron (III) chloride, a weaker acid, was used the degree of unwanted side reactions was

reduced.[113] Iron (III) chloride could also act as the oxidant, which meant that the copper salts were no longer needed.[113]

Equation 1.3. Oxidative intramolecular cyclodehydrogenation of HPB to yield HBC.

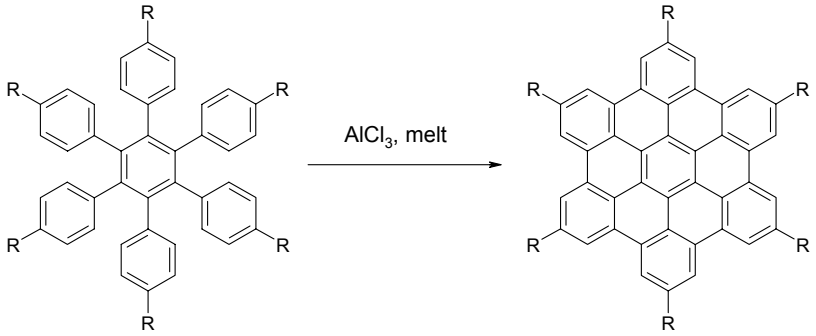

The phase behaviour of HBC's depends strongly on the nature of the substituents.[108,111,114] When HBC is hexa-substituted with long n-alkyl chains the molecules self-assemble to form columnar aggregates, and above a critical temperature form a discotic liquid-crystalline phase.[115] In this phase, the alkyl chains are molten and the central cores stack to form graphite wires. The π-stacking between the HBC discs allows for high charge transport due to the overlap of the π-orbtals and the extended π-system.[116]

There are two methods to prepare the precursor HPB molecules; the cyclotrimerisation of tolanes or the Diels-Alder cycloaddition of a tolane with a tetraphenylene substituted cyclopentadienone.[108] The two methods are presented in Scheme 1.9. The use of transition metal catalysed cyclotrimerisations yields HPB molecules with hexafold symmetry. A more versatile synthesis is available in the Diels-Alder cycloaddition, as the substituents on the tolane and cyclopentadienone can be selected to result in a range of HPB's.[108] This allows for the synthesis of a variety of HBC molecules with differing substitution patterns, as required for the properties of the end product.

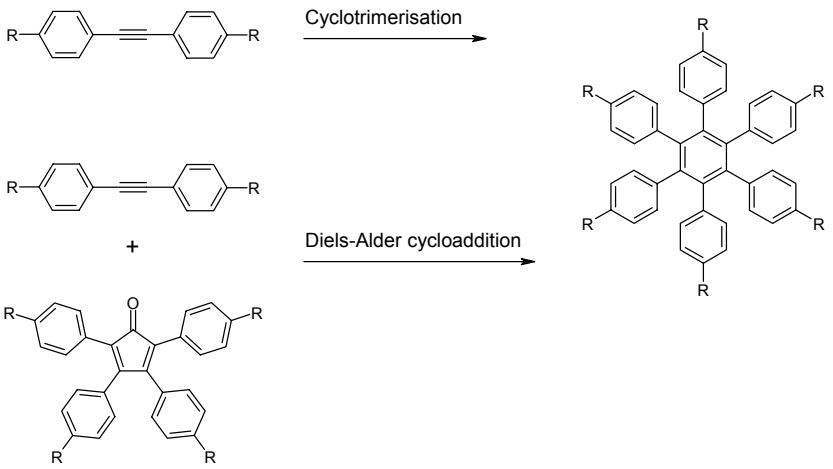

Scheme 1.9. Synthetic route to HPB via cyclotrimerisation or Diels-Alder cycloaddition.

There are a considerable number of potential substituents and substitution patterns possible for HBC, to yield materials that may have a wide range of electronic properties and phase behaviours. A number of reviews are available, which illustrate the scope of HBC research.[108,111,114]

HBC based materials have been used in a variety of organic devices. One of the most important applications of HBC's is as the active material in organic field effect transistors (OFET's).[117-119] A transistor is a three-terminal semiconductor device that provides current amplification. A field-effect transistor has gate, source, and drain electrodes and is a voltage controlled device, *ie* the amount of current flowing between the source and drain at a given potential depends on the gate voltage.[120] The transistor became the building block for all modern electronics and the foundation for microchip and computer technology. The mobility of charge in OFET's however, is the characteristic of organic semiconductors that limits their widespread use.[121-123] In order to compete with amorphous silicon based FET's, OFET's should have a field effect mobility in the range of 1 $cm^2V^{-1}s^{-1}$.[121] At present only pentacene based OFET's have a majority carrier mobility comparable with amorphous silicon.[121]

1.5.2 Discotic materials in OFET's-scope of HBC

In the preparation of an OFET the edge-on morphology, as opposed to face-on or homeotropic alignment, of the HBC active material is important. However, the

flow of charge is one-dimensional between the electrodes, and so the edge-on columnar structures must be orientated to span the gap between the source and drain electrodes if a device is to display a high charge carrier mobility.[108] Also, the film must be domain free as local defects at grain boundaries can trap charge carriers and decrease the performance of a device.[119] To obtain these orientated columnar films, more sophisticated preparation techniques are required.

One method to align the discotic HBC between the electrodes is to introduce an alignment layer under the semiconducting material.[117] An OFET was prepared by van de Craats *et al*. with a friction orientated poly(tetrafluoroethylene) (PTFE) alignment layer deposited on the insulator layer.[117] HBC substituted with a branched alkyl chain was deposited on this alignment layer by casting from solution with slow solvent evaporation, to form aligned columnar films.[117] The devices obtained from this method showed on/off ratios of 10^4, and OFET charge carrier mobilities of up to 1.0-0.5 x 10^{-3} cm^2 $V^{-1}s^{-1}$.[117] To compare, an OFET prepared by spin-coating onto the substrate, to give unaligned HBC films, was prepared. This had mobilities of 1.0 x 10^{-5} cm^2 $V^{-1}s^{-1}$, two orders of magnitude less than for the aligned films.[117] The OFET mobilities measured are two orders of magnitude less than the intrinsic values obtained using pulse-radiolysis time-resolved microwave conductivity.[116] This could be due to poor contact between the electrodes and the semiconducting material in the device, or due to intramolecular packing defects that act as barriers to charge carrier movement along the column.[119]

The introduction of an alignment layer is essential for the deposition of HBC films with long-range order in a desired orientation. Directional alignment of columnar structures can be achieved on untreated glass by solution processing using the technique of zone-casting.[118] A solution of HBC is deposited from a stationary slit-like nozzle onto a moving substrate, where both the nozzle and substrate are thermally controlled.[118] The temperature and concentration gradient order the columnar structures parallel to the direction of substrate movement, with the rates of substrate motion and solution deposition optimised for stationary film forming conditions.[118] Atomic Force Microscopy (AFM) studies demonstrated the long range order and alignment of the prepared films.[118]

OFET's were prepared using the zone-casting technique to deposit aligned HBC (n-$C_{12}H_{25}$ substituted) semiconductor layers in devices with a top-contact configuration.[119] A transistor field effect mobility of 1 x 10^{-2} cm^2 $V^{-1}s^{-1}$ was obtained for device operation parallel to columnar alignment, with on/off ratios of 10^4.[119] This represents an increase of an order of magnitude for the carrier mobilities in OFET's obtained from zone-casting compared to those prepared with a PTFE alignment layer.[117,119] This increase in mobility is attributed to the increased columnar order and orientation of the HBC columnar films prepared from zone-casting compared to those prepared with an alignment layer.[119] The high field effect mobilities of OFET's prepared by the zone-casting of HBC molecules demonstrates the potential of this combination of technique and material for future commercial use in plastic electronics.

1.6 General motivation

There is considerable potential for the field of plastic electronics, from OLED's to OFET's to PV devices. While some crucial areas have been extensively worked on, there are still questions to be answered regarding such things as stable blue OLED's, improved OFET performance and increased efficiencies in organic PV devices.

1.6.1 Dendronised polymers

The dendronisation of poly(fluorenes) with shape persistent oligo-phenylenes has been shown to improve the colour stability of OLED's fabricated with the dendronised material. [89,124] The effect of the dendronisation, in terms of the reduction in the long wavelength emission, can be viewed as a decrease in exciton migration to defect sites in the polymer, due to an increased separation of the poly(fluorene) chains.[124,125] In terms of a solution to the problem of defect emission, the shielding of the conjugated polymer by a dendritic shell appears to be a viable solution.[124,125]

Although these initial results have been encouraging, there is still room for improvement and development. An improved synthetic route to dendronised poly(fluorenes) is one objective, particularly for the preparation of a series of dendronised polymers with diverse functionalities on the periphery. The inclusion of functionalities to improve the charge injection and charge transport characteristics of poly(fluorene), in addition to the suppressed aggregation, is likewise attractive.

The previously reported syntheses of dendronised poly(fluorene) have their advantages and disadvantages, depending on the synthetic approach.[89] The synthesis of the dendronised macromonomer via the divergent route, *ie* the dendrons formed from the monomer core, yields a material containing benzylic linkages. However, in terms of long term material stability, such linkages are undesirable since they are susceptible to oxidation. The macromonomer without the benzylic linkage was synthesized by the convergent route. This means the dendron must be synthesised and attached to the monomer unit, which is unattractive for the synthesis of a series of different compounds.

Not only does dendronisation suppress aggregation, it also allows for the attachment of additional functional groups to the polymer chain in high concentrations. As the generation of the dendrons increases, the number of functionalities attached to each monomer unit also grows. This may dramatically influence the properties of the final polymer, for as the concentration of functional moieties increases, they may begin to dominate the properties of the bulk material.

A new and improved synthetic route to dendronised poly(fluorenes) is proposed. The method involves the divergent synthesis of a fluorene macromonomer. This allows for the synthesis of an intermediate that can be easily transformed into a series of novel macromonomers, while improving the properties of the previously reported generic first generation dendronised poly(fluorene). The incorporation of moieties previously shown to improve charge injection and charge transport, onto the periphery of the dendronised monomers is presented.[126] As the functional groups are attached at the periphery of the dendron units, they are included at a higher concentration per repeat unit than previously reported. It is anticipated that this increase in the amount of moiety will result in an increase in the desired charge injection and transport properties of the polymer.

In addition to functional groups with charge injection and transport properties, further generations of dendrimer can be attached to the fluorene unit. This is achieved in an analogous fashion to the synthesis of higher generation dendrimers previously prepared in the group.[127,128] In addition to the synthetic novelty, the deprotection and further coupling reaction to obtain a second generation fluorene monomer has two goals. The second generation dendronised poly(fluorene) is expected to be even more efficiently shielded, and so the polymer chain should be held at greater distances apart. This should decrease the interaction between the polymer chains, resulting in less long wavelength emission. Secondly, the attachment of a higher generation dendron can sometimes be expected to increase the solubility of a polymer, which is desirable. The steric effects of the bulky second generation dendron on the polymerisation reaction can also be investigated.

The polymerisation of these new macromonomers by common methods such as Yamamoto polycondensation is reported, and the characteristics of the novel polymers are presented. Any material that shows promise as the active component in an OLED will be incorporated into a device, and the performance determined. Of interest will be the turn on voltage and colour stability of the device.

As mentioned in Section 1, the emission maxima of poly(fluorene) materials are generally considered to be too hypsochromically shifted compared to what is perceived to be a true blue emission. The previous approach to produce a material that emits at a longer wavelength was to increase the length of the repeat unit of the polymer, *ie* to prepare poly(indenofluorene).[85] To date the largest group pendent to the indenofluorene backbone is an aryl group, which resulted in an increased colour stability.[87] While the performance of the tetraaryl substituted polymer was improved compared to the tetraalkyl case, there is a need to investigate whether the dendronisation approach can further enhance the performance of poly(indenofluorene) based OLED's.

The synthetic route to dendronised poly(indenofluorene) is presented. The synthesis of this novel polymer is achieved utilising a variation of the synthetic route to produce dendronised poly(fluorene). The differences in the properties of the polymer with respect to the first generation dendronised poly(fluorene) will be discussed.

Poly(p-phenylene ethynylene) (PPE), consisting of alternating benzene rings and triple bonds, is a rigid linear polymer. PPE's exhibit higher quantum efficiencies compared to PPV's due to the decreased potential of non-radiative decay pathways.[129,130] The solution PL maximum of PPE with alkoxy sidechains is about 475 nm, depending on the alkyl group, whereas in the solid state, the PL spectra are broader and bathochromically shifted with a maximum at 530 nm.[129,130] A PPE with Fréchet dendrons was prepared previously.[131] The dendrons suppressed aggregation, and a narrow blue emission was observed.[131] The incorporation of shape persistent oligo-phenylene dendrons should be more efficient for the suppression of aggregates, to yield a material suitable for use in an OLED.

The synthesis of a PPE with oligo-phenylene dendrons is presented. Similar to the other synthetic routes, this synthesis uses the Diels-Alder cycloaddition to form the oligo-phenylene dendrons. The polymerisation reaction, and the resulting dendronised polymer, will be discussed in light of recent reports on a similar derivative of PPE.[132]

1.6.2 Electron transporting materials

The incorporation of electron transporting moieties onto the poly(fluorene) skeleton is a potential method of improving the device performance of OLED's. While investigating potential synthetic pathways to attach oxadiazole to poly(fluorene), Jen *et al.* published their results from a fluorene copolymer.[63] The Suzuki polymerisation yielded a material with a molecular weight of 1.3 x 10^3 $gmol^{-1}$, possibly due to poor solubility of the oxadiazole sidechain.[63]

The synthesis of a processable oxadiazole containing poly(fluorenes) is an important goal towards more efficient blue OLED's. Two synthetic approaches to obtain fluorene monomers with oxadiazoles in the side chain are proposed. The novel synthesis of an oxadiazole-substituted dibromofluorene is presented. Using a preformed oxadiazole building block, the same bisoxadiazole substituted fluorene monomer first reported by Jen *et al.* is synthesised.[63] The two-step synthetic approach is advantageous in that it uses common starting materials.

The other approach is a variation of the previously reported route by Jen *et al.*, where a monomer with the longer decyl solubilising group is synthesised. It is envisioned that the long alkyl chain will impart greater solubility on the oxadiazole fluorene monomer. The polymerisation of this monomer using Yamamoto conditions is presented. The synthesis of the homopolymer is hoped to extend the positive effect of oxadiazole moiety on the EQE of poly(fluorene) based OLED's, due to the increased concentration of the oxadiazole moiety.

The use of poly(fluorenone) as an electron transporting material in OLED`s is largely limited by the lack of availability of a solution processable form of the

material.[68,69] The planar nature of fluorenone, and the fact that the normal substitution position for fluorene molecules is blocked, has until now made poly(fluorenone) an insoluble material. A soluble poly(fluorenone), which can be easily processed, is attractive as a potential ETM. In the previous section it was demonstrated how shape persistent oligo-phenylene dendrimers inhibit the aggregation behaviour of poly(fluorene) based materials. Thus, a dendronised fluorenone polymer is expected to be soluble and processable.

The novel synthesis of the first soluble poly(fluorenone) is presented. The synthetic route includes the functionalisation of the 4 position of a fluorenone monomer with an oligo-phenylene dendrimer. The Yamamoto polycondensation of the fluorenone monomer to obtain a soluble polymer is described, and the properties of the material discussed.

1.6.3 Indenofluorene based materials

Oligomers of conjugated materials have been used as the active material in plastic electronic devices, such as thiophene oligomers in OFET's.[99-103] Monodisperse oligomers can possess high quality device characteristics as a result of the ability of the identical molecules to pack efficiently. This efficient packing leads to intermolecular coupling of π-electrons on neighbouring molecules, which allows for the facile charge mobility.[117] As straight moieties like indenofluorene should inherently pack better than bent moieties like fluorene, the synthesis of indenofluorene oligomers may yield novel, useful conjugated materials. These materials could be utilised as the active material in OFET's, OLED's or organic solar cells.

Whereas fluorene oligomers are easily synthesised, due to the commercial availability of a mono-functionalised fluorene, the synthesis of an indenofluorene oligomer is not trivial. [107] No commercial source or literature reference of mono-functionalised indenofluorene is available. The key challenge with any synthetic approach is the hetero-functionalisation of an indenofluorene moiety. For the purpose of indenofluorene oligomers synthesis, this could either involve a mono-bromination

reaction or a reaction of just one halide of a dibromo indenofluorene. The alternate method is to synthesise the indenofluorene moiety in such a way that a mono-functionalised product is obtained. These various approaches will be presented and discussed.

The role of excimer and ketone formation in the colour instability of poly(fluorene) based OLED's was discussed in depth in Section 1. In order to eliminate the unwanted long wavelength emission from blue emitting poly(fluorene), the limitation of ketone formation and the ability for the polymers to π-stack has been shown to be beneficial.[76,86-89,91] While the radiative pathway for the long wavelength emission in poly(fluorene) is established, this does not necessarily mean that the same pathways are responsible for the long wavelength emission in other blue emitting conjugated materials. OLED's with poly(tetraalkyl-indenofluorene) as the active material also show long wavelength emission on device operation, however this was improved by the substitution of aryl groups for the alkyl sidechains.[87] This again raises the question however, as to what role the aryl groups play in reducing the low energy emission.

The aryl groups are significantly more bulky than the alkyl groups and so would prevent stacking, but this could reduce the excimer formation or decrease the rate of exciton migration to low energy defect sites. Aryl groups are less susceptible to oxidation when compared to alkyl groups, and so less likely to form defect ketone sites. Also, the synthetic route to the aryl substituted monomers is such that it is not possible to form a monosubstituted bridge head, which is known to be more prone to oxidation.[65,96] While the structures of fluorene and indenofluorene are similar; the radiative pathway for the long wavelength emission may not be the same. Therefore it is important to investigate the potential mechanisms for the appearance of the long wavelength emissions. The understanding of the processes that result in unwanted emission in an OLED is important for all active polymer materials if this emission is to be reduced or removed. While the pathways for this emission in poly(fluorene) based OLED's have been extensively discussed in the literature, there is little discussion regarding this problem with respect to poly(indenofluorene). [30,65,76]

One method to elucidate the nature of the long wavelength emission is through extensive spectroscopic analysis of the material. To facilitate these experiments it is important to have a model of the suspected defect structure, in order to compare it with the experimental results from the device operation. The synthesis and analysis of a potential defect structure in poly(indenofluorene) based OLED's will be presented.

1.6.4 Columnar bypass material

It is very difficult, if not impossible, to fabricate films completely absent of defects, even in organic crystals, due to entropy considerations.[119] High-resolution transmission electron microscopy images of zone-cast films of HBC show intramolecular defects.[119] Although these defects are infrequent and distributed throughout the film, they could represent a significant barrier to charge transport over the long distances between the electrodes.[119] While the contacts between the source and drain electrodes and the semiconductor are a significant barrier to efficient charge carrier mobility, the inherent defects found in the columnar structure represent a limitation to device performance based on discotic materials.

The charge carrier mobility in discotic HBC is confined along a single column, not between the columns. If a pathway existed where the charge could hop from one column to another when confronted with a defect site, the charges could by-pass any defect sites and continue to the drain electrode.

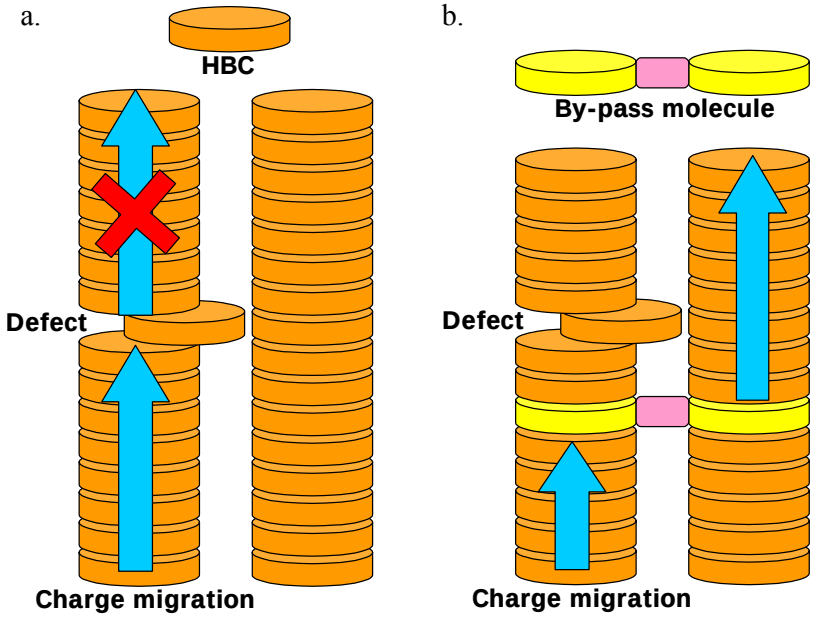

Figure 1.14. Graphical representation of by-pass mechanism for charge carriers in HBC columns. a. Column without by-pass molecule, charge migration stopped. b. Column with by-pass molecule, charge migration continues to the drain electrode.

For a molecule to work in a by-pass mechanism the anchoring ends must correctly fit into the HBC column and the linker must be conjugated to allow for the charge to flow to the neighbouring column. To this end, a pair of HBC molecules linked with an indenofluorene spacer was envisioned to act successfully as a by-pass molecule. The synthesis and characterisation of a by-pass molecule will be described, and attempts to incorporate the material in a blend of HBC molecules will be discussed.

1.7 References

(1) Chiang, C. K.; Fincher, C. R.; Park, Y. W.; Heeger, A. J.; Shirakawa, H.; Louis, E. J.; Gau, S. C.; Macdiarmid, A. G. *Physical Review Letters* **1977**, *39*, 1098-1101.

(2) Shirakawa, H.; Louis, E. J.; Macdiarmid, A. G.; Chiang, C. K.; Heeger, A. J. *Journal Of The Chemical Society-Chemical Communications* **1977**, 578-580.

(3) Roncali, J. *Chemical Reviews* **1992**, *92*, 711-738.

(4) Diaz, A. F.; Kanazawa, K. K.; Gardini, G. P. *Journal Of The Chemical Society-Chemical Communications* **1979**, 635-636.

(5) Tourillon, G.; Garnier, F. *Journal Of Electroanalytical Chemistry* **1982**, *135*, 173-178.

(6) Kanazawa, K. K.; Diaz, A. F.; Geiss, R. H.; Gill, W. D.; Kwak, J. F.; Logan, J. A.; Rabolt, J. F.; Street, G. B. *Journal Of The Chemical Society-Chemical Communications* **1979**, 854-855.

(7) Diaz, A. F.; Logan, J. A. *Journal Of Electroanalytical Chemistry* **1980**, *111*, 111-114.

(8) Huang, W. S.; Humphrey, B. D.; Macdiarmid, A. G. *Journal Of The Chemical Society-Faraday Transactions I* **1986**, *82*, 2385-2400.

(9) Schiavon, G.; Zotti, G.; Bontempelli, G. *Journal Of Electroanalytical Chemistry* **1985**, *186*, 191-199.

(10) Raultberthelot, J.; Simonet, J. *Journal Of Electroanalytical Chemistry* **1985**, *182*, 187-192.

(11) Leclerc, M.; Guay, J.; Dao, L. H. *Macromolecules* **1989**, *22*, 649-653.

(12) Leclerc, M.; Prudhomme, R. E. *Macromolecules* **1987**, *20*, 2153-2159.

(13) Sato, M.; Tanaka, S.; Kaeriyama, K. *Journal Of The Chemical Society-Chemical Communications* **1986**, 873-874.

(14) Hotta, S.; Rughooputh, D. D. V.; Heeger, A. J.; Wudl, F. *Macromolecules* **1987**, *20*, 212-215.

(15) Roncali, J.; Garreau, R.; Yassar, A.; Marque, P.; Garnier, F.; Lemaire, M. *Journal Of Physical Chemistry* **1987**, *91*, 6706-6714.

(16) Ballard, D. G. H.; Courtis, A.; Shirley, I. M.; Taylor, S. C. *Journal Of The Chemical Society-Chemical Communications* **1983**, 954-955.

(17) Rehahn, M.; Schluter, A. D.; Wegner, G. *Makromolekulare Chemie-Macromolecular Chemistry And Physics* **1990**, *191*, 1991-2003.

(18) Rehahn, M.; Schluter, A. D.; Wegner, G.; Feast, W. J. *Polymer* **1989**, *30*, 1054-1059.

(19) Scherf, U.; Mullen, K. *Macromolecules* **1992**, *25*, 3546-3548.

(20) Scherf, U.; Mullen, K. *Makromolekulare Chemie-Rapid Communications* **1991**, *12*, 489-497.

(21) Mullen, K. *Pure And Applied Chemistry* **1993**, *65*, 89-96.

(22) Scherf, U. *Journal Of Materials Chemistry* **1999**, *9*, 1853-1864.

(23) Fukuda, M.; Sawada, K.; Yoshino, K. *Journal Of Polymer Science Part A-Polymer Chemistry* **1993**, *31*, 2465-2471.

(24) Miyaura, N.; Yanagi, T.; Suzuki, A. *Synthetic Communications* **1981**, *11*, 513-519.

(25) Yamamoto, T.; Morita, A.; Miyazaki, Y.; Maruyama, T.; Wakayama, H.; Zhou, Z.; Nakamura, Y.; Kanbara, T.; Sasaki, S.; Kubota, K. *Macromolecules* **1992**, *25*, 1214-1223.

(26) Stille, J. K. *Angewandte Chemie-International Edition In English* **1986**, *25*, 508-523.

(27) Pei, Q. B.; Yang, Y. *Journal Of The American Chemical Society* **1996**, *118*, 7416-7417.

(28) Bernius, M. T.; Inbasekaran, M.; O'Brien, J.; Wu, W. S. *Advanced Materials* **2000**, *12*, 1737-1750.

(29) Leclerc, M. *Journal Of Polymer Science Part A-Polymer Chemistry* **2001**, *39*, 2867-2873.

(30) Scherf, U.; List, E. J. W. *Advanced Materials* **2002**, *14*, 477-487.

(31) Burroughes, J. H.; Bradley, D. D. C.; Brown, A. R.; Marks, R. N.; Mackay, K.; Friend, R. H.; Burns, P. L.; Holmes, A. B. *Nature* **1990**, *347*, 539-541.

(32) Holonyak, N.; Bevacqua, S. F. *Applied Physics Letters* **1962**, *1*, 82-83.

(33) Mitschke, U.; Bauerle, P. *Journal Of Materials Chemistry* **2000**, *10*, 1471-1507.

(34) Helfrich, W.; Schneide.W *Physical Review Letters* **1965**, *14*, 229-&.

(35) Pope, M.; Magnante, P.; Kallmann, H. P. *Journal Of Chemical Physics* **1963**, *38*, 2042-&.

(36) Adachi, C.; Tokito, S.; Tsutsui, T.; Saito, S. *Japanese Journal Of Applied Physics Part 2-Letters* **1988**, *27*, L713-L715.

(37) Adachi, C.; Tokito, S.; Tsutsui, T.; Saito, S. *Japanese Journal Of Applied Physics Part 2-Letters* **1988**, *27*, L269-L271.

(38) Tang, C. W.; Vanslyke, S. A. *Applied Physics Letters* **1987**, *51*, 913-915.

(39) Adachi, C.; Tsutsui, T.; Saito, S. *Applied Physics Letters* **1989**, *55*, 1489-1491.

(40) Kraft, A.; Grimsdale, A. C.; Holmes, A. B. *Angewandte Chemie-International Edition* **1998**, *37*, 402-428.

(41) Greenham, N. C.; Friend, R. H.; Bradley, D. D. C. *Advanced Materials* **1994**, *6*, 491-494.

(42) Sheats, J. R.; Antoniadis, H.; Hueschen, M.; Leonard, W.; Miller, J.; Moon, R.; Roitman, D.; Stocking, A. *Science* **1996**, *273*, 884-888.

(43) Greenham, N. C.; Moratti, S. C.; Bradley, D. D. C.; Friend, R. H.; Holmes, A. B. *Nature* **1993**, *365*, 628-630.

(44) Hughes, G.; Bryce, M. R. *Journal Of Materials Chemistry* **2005**, *15*, 94-107.

(45) Kulkarni, A. P.; Tonzola, C. J.; Babel, A.; Jenekhe, S. A. *Chemistry Of Materials* **2004**, *16*, 4556-4573.

(46) Agrawal, A. K.; Jenekhe, S. A. *Macromolecules* **1993**, *26*, 895-905.

(47) Fink, R.; Frenz, C.; Thelakkat, M.; Schmidt, H. W. *Macromolecules* **1997**, *30*, 8177-8181.

(48) Jandke, M.; Strohriegl, P.; Berleb, S.; Werner, E.; Brutting, W. *Macromolecules* **1998**, *31*, 6434-6443.

(49) Karastatiris, P.; Mikroyannidis, J. A.; Spiliopoulos, I. K.; Kulkarni, A. P.; Jenekhe, S. A. *Macromolecules* **2004**, *37*, 7867-7878.

(50) Tonzola, C. J.; Alam, M. M.; Bean, B. A.; Jenekhe, S. A. *Macromolecules* **2004**, *37*, 3554-3563.

(51) Wang, C. S.; Kilitziraki, M.; MacBride, J. A. H.; Bryce, M. R.; Horsburgh, L. E.; Sheridan, A. K.; Monkman, A. P.; Samuel, I. D. W. *Advanced Materials* **2000**, *12*, 217-222.

(52) Thelakkat, M.; Schmidt, H. W. *Polymers For Advanced Technologies* **1998**, *9*, 429-442.

(53) Heidenhain, S. B.; Sakamoto, Y.; Suzuki, T.; Miura, A.; Fujikawa, H.; Mori, T.; Tokito, S.; Taga, Y. *Journal Of The American Chemical Society* **2000**, *122*, 10240-10241.

(54) Sakamoto, Y.; Suzuki, T.; Miura, A.; Fujikawa, H.; Tokito, S.; Taga, Y. *Journal Of The American Chemical Society* **2000**, *122*, 1832-1833.

(55) Adachi, C.; Tsutsui, T.; Saito, S. *Applied Physics Letters* **1990**, *56*, 799-801.

(56) Antoniadis, H.; Inbasekaran, M.; Woo, E. P. *Applied Physics Letters* **1998**, *73*, 3055-3057.

(57) Tokuhisa, H.; Era, M.; Tsutsui, T. *Advanced Materials* **1998**, *10*, 404-407.

(58) Tokuhisa, H.; Era, M.; Tsutsui, T.; Saito, S. *Applied Physics Letters* **1995**, *66*, 3433-3435.

(59) Brown, A. R.; Bradley, D. D. C.; Burroughes, J. H.; Friend, R. H.; Greenham, N. C.; Burn, P. L.; Holmes, A. B.; Kraft, A. *Applied Physics Letters* **1992**, *61*, 2793-2795.

(60) Schulz, B.; Bruma, M.; Brehmer, L. *Advanced Materials* **1997**, *9*, 601-613.

(61) Wang, C. S.; Kilitziraki, M.; Palsson, L. O.; Bryce, M. R.; Monkman, A. P.; Samuel, I. D. W. *Advanced Functional Materials* **2001**, *11*, 47-50.

(62) Lee, D. W.; Kwon, K. Y.; Jin, J. I.; Park, Y.; Kim, Y. R.; Hwang, I. W. *Chemistry Of Materials* **2001**, *13*, 565-574.

(63) Wu, F. I.; Reddy, D. S.; Shu, C. F.; Liu, M. S.; Jen, A. K. Y. *Chemistry Of Materials* **2003**, *15*, 269-274.

(64) Grice, A. W.; Bradley, D. D. C.; Bernius, M. T.; Inbasekaran, M.; Wu, W. W.; Woo, E. P. *Applied Physics Letters* **1998**, *73*, 629-631.

(65) List, E. J. W.; Guentner, R.; de Freitas, P. S.; Scherf, U. *Advanced Materials* **2002**, *14*, 374-378.

(66) Kulkarni, A. P.; Kong, X. X.; Jenekhe, S. A. *Journal Of Physical Chemistry B* **2004**, *108*, 8689-8701.

(67) Panozzo, S.; Vial, J. C.; Kervella, Y.; Stephan, O. *Journal Of Applied Physics* **2002**, *92*, 3495-3502.

(68) Uckert, F.; Setayesh, S.; Mullen, K. *Macromolecules* **1999**, *32*, 4519-4524.

(69) Uckert, F.; Tak, Y. H.; Mullen, K.; Basser, H. *Advanced Materials* **2000**, *12*, 905-908.

(70) Grem, G.; Leditzky, G.; Ullrich, B.; Leising, G. *Synthetic Metals* **1992**, *51*, 383-389.

(71) Grem, G.; Leditzky, G.; Ullrich, B.; Leising, G. *Advanced Materials* **1992**, *4*, 36-37.

(72) Remmers, M.; Neher, D.; Gruner, J.; Friend, R. H.; Gelinck, G. H.; Warman, J. M.; Quattrocchi, C.; dosSantos, D. A.; Bredas, J. L. *Macromolecules* **1996**, *29*, 7432-7445.

(73) Huber, J.; Mullen, K.; Salbeck, J.; Schenk, H.; Scherf, U.; Stehlin, T.; Stern, R. *Acta Polymerica* **1994**, *45*, 244-247.

(74) Gruner, J.; Hamer, P. J.; Friend, R. H.; Huber, H. J.; Scherf, U.; Holmes, A. B. *Advanced Materials* **1994**, *6*, 748-752.

(75) Gruner, J.; Wittmann, H. F.; Hamer, P. J.; Friend, R. H.; Huber, J.; Scherf, U.; Mullen, K.; Moratti, S. C.; Holmes, A. B. *Synthetic Metals* **1994**, *67*, 181-185.

(76) Bliznyuk, V. N.; Carter, S. A.; Scott, J. C.; Klarner, G.; Miller, R. D.; Miller, D. C. *Macromolecules* **1999**, *32*, 361-369.

(77) Klarner, G.; Davey, M. H.; Chen, W. D.; Scott, J. C.; Miller, R. D. *Advanced Materials* **1998**, *10*, 993-997.

(78) Klarner, G.; Lee, J. I.; Davey, M. H.; Miller, R. D. *Advanced Materials* **1999**, *11*, 115-119.

(79) Kreyenschmidt, M.; Klaerner, G.; Fuhrer, T.; Ashenhurst, J.; Karg, S.; Chen, W. D.; Lee, V. Y.; Scott, J. C.; Miller, R. D. *Macromolecules* **1998**, *31*, 1099-1103.

(80) Ohmori, Y.; Uchida, M.; Muro, K.; Yoshino, K. *Japanese Journal Of Applied Physics Part 2-Letters* **1991**, *30*, L1941-L1943.

(81) Friend, R. H.; Gymer, R. W.; Holmes, A. B.; Burroughes, J. H.; Marks, R. N.; Taliani, C.; Bradley, D. D. C.; Dos Santos, D. A.; Bredas, J. L.; Logdlund, M.; Salaneck, W. R. *Nature* **1999**, *397*, 121-128.

(82) Hamaguchi, M.; Fujii, A.; Ohmori, Y.; Yoshino, K. *Synthetic Metals* **1997**, *84*, 557-558.

(83) Ohmori, Y.; Tada, N.; Fujii, A.; Ueta, H.; Sawatani, T.; Yoshino, K. *Thin Solid Films* **1998**, *331*, 89-95.

(84) Yoshida, M.; Tada, N.; Fujii, A.; Ohmori, Y.; Yoshino, K. *Synthetic Metals* **1997**, *85*, 1259-1260.

(85) Setayesh, S.; Marsitzky, D.; Mullen, K. *Macromolecules* **2000**, *33*, 2016-2020.

(86) Grimsdale, A. C.; Leclère, P.; Lazzaroni, R.; Mackenzie, J. D.; Murphy, C.; Setayesh, S.; Silva, C.; Friend, R. H.; Mullen, K. *Advanced Functional Materials* **2002**, *12*, 729-733.

(87) Jacob, J.; Zhang, J. Y.; Grimsdale, A. C.; Mullen, K.; Gaal, M.; List, E. J. W. *Macromolecules* **2003**, *36*, 8240-8245.

(88) Jacob, J.; Sax, S.; Piok, T.; List, E. J. W.; Grimsdale, A. C.; Mullen, K. *Journal Of The American Chemical Society* **2004**, *126*, 6987-6995.

(89) Setayesh, S.; Grimsdale, A. C.; Weil, T.; Enkelmann, V.; Mullen, K.; Meghdadi, F.; List, E. J. W.; Leising, G. *Journal Of The American Chemical Society* **2001**, *123*, 946-953.

(90) Neher, D. *Macromolecular Rapid Communications* **2001**, *22*, 1366-1385.

(91) Xia, C. J.; Advincula, R. C. *Macromolecules* **2001**, *34*, 5854-5859.

(92) Bradley, D. D. C.; Grell, M.; Grice, A.; Tajbakhsh, A. R.; O'Brien, D. F.; Bleyer, A. *Optical Materials* **1998**, *9*, 1-11.

(93) Kulkarni, A. P.; Jenekhe, S. A. *Macromolecules* **2003**, *36*, 5285-5296.

(94) Zeng, G.; Yu, W. L.; Chua, S. J.; Huang, W. *Macromolecules* **2002**, *35*, 6907-6914.

(95) Miteva, T.; Meisel, A.; Knoll, W.; Nothofer, H. G.; Scherf, U.; Muller, D. C.; Meerholz, K.; Yasuda, A.; Neher, D. *Advanced Materials* **2001**, *13*, 565-567.

(96) Craig, M. R.; de Kok, M. M.; Hofstraat, J. W.; Schenning, A.; Meijer, E. W. *Journal Of Materials Chemistry* **2003**, *13*, 2861-2862.

(97) Biczok, L.; Berces, T.; Marta, F. *Journal Of Physical Chemistry* **1993**, *97*, 8895-8899.

(98) Müllen, K., Wegner, G. *Electronic Materials:The Oligomer Approach*; Wiley-VCH: Weinheim, 1998.

(99) Garnier, F.; Horowitz, G.; Peng, X. H.; Fichou, D. *Advanced Materials* **1990**, *2*, 592-594.

(100) Xu, B.; Fichou, D.; Horowitz, G.; Garnier, F. *Advanced Materials* **1991**, *3*, 150-153.

(101) Horowitz, G.; Peng, X. Z.; Fichou, D.; Garnier, F. *Journal Of Applied Physics* **1990**, *67*, 528-532.

(102) Garnier, F.; Horowitz, G.; Fichou, D. *Synthetic Metals* **1989**, *28*, C705-C714.

(103) Fichou, D.; Horowitz, G.; Nishikitani, Y.; Garnier, F. *Synthetic Metals* **1989**, *28*, C723-C727.

(104) Katz, H. E.; Bao, Z. N.; Gilat, S. L. *Accounts Of Chemical Research* **2001**, *34*, 359-369.

(105) Tour, J. M. *Accounts Of Chemical Research* **2000**, *33*, 791-804.

(106) Klaerner, G.; Miller, R. D. *Macromolecules* **1998**, *31*, 2007-2009.

(107) Lee, S. H.; Tsutsui, T. *Thin Solid Films* **2000**, *363*, 76-80.

(108) Simpson, C. D.; Wu, J. S.; Watson, M. D.; Mullen, K. *Journal Of Materials Chemistry* **2004**, *14*, 494-504.

(109) Adam, D.; Schuhmacher, P.; Simmerer, J.; Haussling, L.; Siemensmeyer, K.; Etzbach, K. H.; Ringsdorf, H.; Haarer, D. *Nature* **1994**, *371*, 141-143.

(110) Dotz, F.; Brand, J. D.; Ito, S.; Gherghel, L.; Mullen, K. *Journal Of The American Chemical Society* **2000**, *122*, 7707-7717.

(111) Watson, M. D.; Fechtenkotter, A.; Mullen, K. *Chemical Reviews* **2001**, *101*, 1267-1300.

(112) Stabel, A.; Herwig, P.; Mullen, K.; Rabe, J. P. *Angewandte Chemie-International Edition In English* **1995**, *34*, 1609-1611.

(113) Iyer, V. S.; Wehmeier, M.; Brand, J. D.; Keegstra, M. A.; Mullen, K. *Angewandte Chemie-International Edition In English* **1997**, *36*, 1604-1607.

(114) Wu, J. S.; Grimsdale, A. C.; Mullen, K. *Journal Of Materials Chemistry* **2005**, *15*, 41-52.

(115) Herwig, P.; Kayser, C. W.; Mullen, K.; Spiess, H. W. *Advanced Materials* **1996**, *8*, 510-&.

(116) van de Craats, A. M.; Warman, J. M.; Mullen, K.; Geerts, Y.; Brand, J. D. *Advanced Materials* **1998**, *10*, 36-+.

(117) van de Craats, A. M.; Stutzmann, N.; Bunk, O.; Nielsen, M. M.; Watson, M.; Mullen, K.; Chanzy, H. D.; Sirringhaus, H.; Friend, R. H. *Advanced Materials* **2003**, *15*, 495-499.

(118) Tracz, A.; Jeszka, J. K.; Watson, M. D.; Pisula, W.; Mullen, K.; Pakula, T. *Journal Of The American Chemical Society* **2003**, *125*, 1682-1683.

(119) Pisula, W.; Menon, A.; Stepputat, M.; Lieberwirth, I.; Kolb, U.; Tracz, A.; Sirringhaus, H.; Pakula, T.; Mullen, K. *Advanced Materials* **2005**, *17*, 684-689.

(120) http://home.ku.edu.tr/~aserpenguzel/phys313.html.

(121) Dimitrakopoulos, C. D.; Malenfant, P. R. L. *Advanced Materials* **2002**, *14*, 99-117.

(122) Newman, C. R.; Frisbie, C. D.; da Silva, D. A.; Bredas, J. L.; Ewbank, P. C.; Mann, K. R. *Chemistry Of Materials* **2004**, *16*, 4436-4451.

(123) Veres, J.; Ogier, S.; Lloyd, G.; de Leeuw, D. *Chemistry Of Materials* **2004**, *16*, 4543-4555.

(124) Pogantsch, A.; Wenzl, F. P.; List, E. J. W.; Leising, G.; Grimsdale, A. C.; Mullen, K. *Advanced Materials* **2002**, *14*, 1061-1064.

(125) Pogantsch, A.; Wenzl, F. P.; Scherf, U.; Grimsdale, A. C.; Mullen, K.; List, E. J. W. *Journal Of Chemical Physics* **2003**, *119*, 6904-6910.

(126) Ego, C.; Grimsdale, A. C.; Uckert, F.; Yu, G.; Srdanov, G.; Mullen, K. *Advanced Materials* **2002**, *14*, 809-811.

(127) Wiesler, U. M.; Berresheim, A. J.; Morgenroth, F.; Lieser, G.; Mullen, K. *Macromolecules* **2001**, *34*, 187-199.

(128) Morgenroth, F.; Berresheim, A. J.; Wagner, M.; Mullen, K. *Chemical Communications* **1998**, 1139-1140.

(129) Spiliopoulos, I. K.; Mikroyannidis, J. A. *Journal Of Polymer Science Part A-Polymer Chemistry* **2002**, *40*, 1449-1455.

(130) Bunz, U. H. F. *Chemical Reviews* **2000**, *100*, 1605-1644.

(131) Sato, T.; Jiang, D. L.; Aida, T. *Journal Of The American Chemical Society* **1999**, *121*, 10658-10659.

(132) Englert, B. C.; Smith, M. D.; Hardcastle, K. I.; Bunz, U. H. F. *Macromolecules* **2004**, *37*, 8212-8221.

2 Dendronised Polymers-Introducing Bulk

2.1 Introduction

In Section 1 the incorporation of bulky substituents pendant to the main chain was discussed in relation to the improvement in colour stability of poly(phenylene) based materials. It has been shown that the introduction of these substituents minimises undesirable long wavelength emission resulting from aggregation of polymer chains.[1,2] Among the choices possible as side chains, a shape persistent oligo-phenylene dendron is one that is desirable.

2.1.1 Dendrimers

Dendrimers are monodisperse, highly branched macromolecules that are typically 1-10 nm in size, and carry a multiplicity of functional groups at their periphery.[3] They possess a globular shape that is a result of the internal structure, in which all bonds emerge radially from a central core, or focal point, with repeat units that contain a branching point and are arranged in a regular, branching pattern.[3] Dendritic architectures are one of the most observed topologies, with innumerable examples of these patterns found throughout the natural world.[4] It is not known for certain why this obviously successful topology is used for so many functions, however it may be the structure type that provides the best interface for energy and nutrient extraction and distribution, and information storage and retrieval.[4] Therefore this topology, so clearly favoured by evolution, is an attractive basis for designing functional materials for a variety of applications.

2.1.2 Dendronised Polymers

The choice of the core of the dendrimer can greatly affect the overall topology of the final globular molecule, although most dendrimers tend to fill all available space above a certain generation. If one selects as core a linear polymer, then one obtains a dendronised polymer. By combining the properties of dendrimers and linear

polymers, it is possible to produce covalently constructed, cylindrically shaped molecules with a diameter of a few nanometres and a length of a few hundred nanometres.[5]

Many different classes of molecules have been used in dendronised polymers, both in the chain and dendron, including siloxane based polymers and polymers based on poly(styrene) with amide, ester and ether dendrons. [5-11] Dendronised conjugated polymers have also been synthesised. Schlüter and co-workers synthesised PPP's with fourth generation dendrons utilising Suzuki polycondensation of a macromonomer.[12,13]

2.1.3 Dendronised poly(fluorene)-separating the conjugated main chains

Poly(fluorene) has been utilised as the core of dendronised polymers.[1,2,14] In addition to polymers that incorporated Fréchet dendrons, oligo-phenylene based dendrons have been used to shield the polymer backbone.[2,14] These phenylene dendrimers are both shape persistent and chemically stable, hence better suited to shielding the backbone.[2] The rationale behind the synthesis of the dendronised poly(fluorene) was to produce a blue emitting EL polymer that did not form aggregates, in an attempt to fabricate stable OLED's. As discussed in Section 1, the net effect of dendronisation was to produce a more stable blue emitting EL device.[1,2]

The synthesis of the dendronised poly(fluorene) was undertaken utilising the macromonomer approach, *ie* the synthesis of a dendronised monomer that is polymerised. Attempts to prepare a precursor polymer for subsequent dendronisation were unsuccessful, due to the inability to polymerise the di-ethynyl monomer.[2] The synthesis of the dendronised poly(fluorene) is shown in Scheme 2.1.

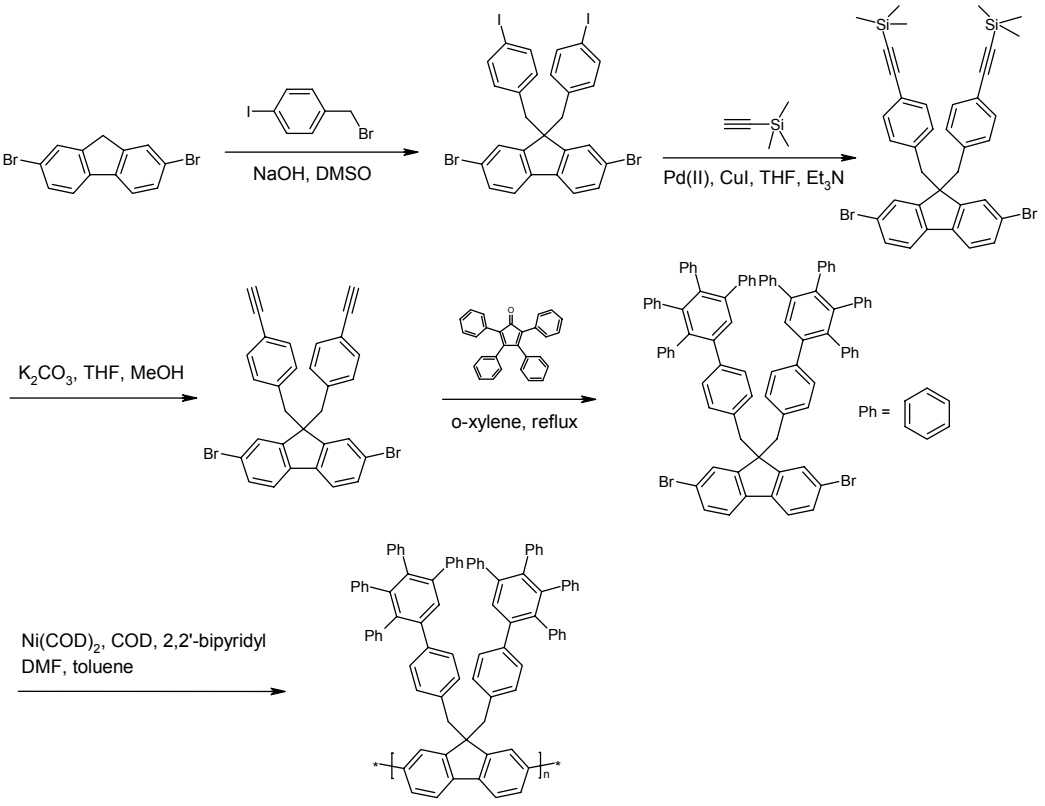

Scheme 2.1. Synthetic route to dendronised poly(fluorene).

The selective Hagihara-Sonogashira coupling of trimethylsilylacetylene with the diiodoaryl substituted fluorene, followed by the deprotection of the acetylene moieties and subsequent Diels-Alder reaction gave the macromonomer in a good overall yield.[2] The macromonomer was polymerised under Yamamoto conditions to result in a dendronised polymer with a number average molecular weight, M_n, of 4.6 x 10^4 $gmol^{-1}$.[2] Differential Scanning Calorimetry (DSC) results show the polymer exhibits only one phase transition at 248°C, a glass transition, and no liquid crystalline phase.[2] As a liquid crystalline phase is observed for poly(dialkylfluorene), the results indicate that the rigid tetraphenylbenzene units effectively suppress the organisation of the polymer chain. The aggregation suppressing effects of the phenylene dendrons was also investigated by modelling and X-ray crystallography of the monomer, and X-ray diffraction experiments of the polymer.[2]

The dendronised polymer was incorporated into an OLED. The observed blue EL has an emission maximum at 420 nm, similar to poly(dialkylfluorene), and a turn

on voltage of 4 V. The device was found to have a maximum luminance of 400 cdm^{-2}, and a η_{pow} of 0.16 lmW^{-1}.[2] The device was operated under an inert argon atmosphere, and so no lifetime data was reported. As the luminance and electrical characteristics of the dendronised polymer is comparable to poly(dialkylfluorene) derivatives, the addition of dendrons to the polymer suppresses aggregation without adversely affecting the properties of the poly(fluorene) backbone.

The benzyl linkages of the dendronised polymer are potential sites for oxidation, therefore could introduce an oxygenated functionality into the polymer. The synthesis of an analogous dendronised polymer without the benzyl linkage was achieved, as shown in Scheme 2.2.[2]

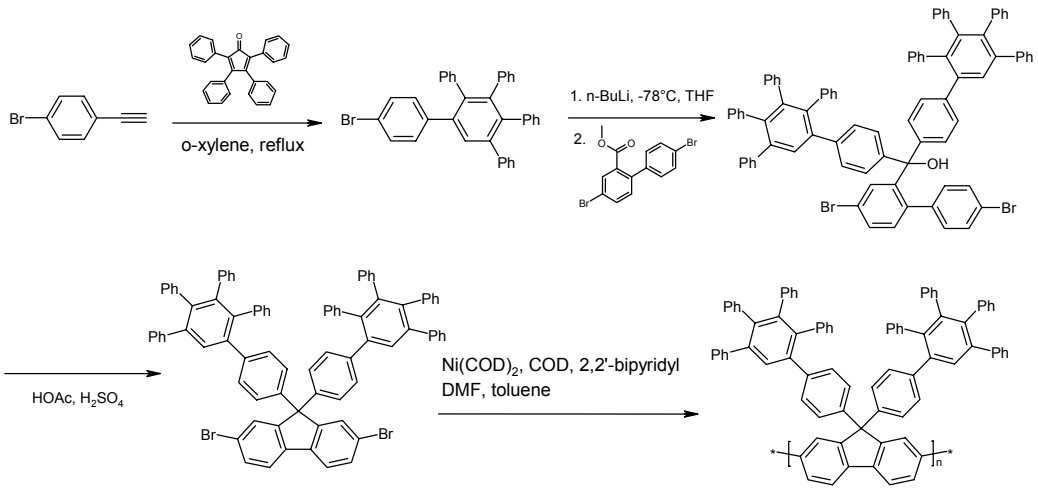

Scheme 2.2. Synthetic route to dendronised poly(fluorene) without benzylic linkages.

The brominated dendron was prepared by the Diels-Alder reaction of a tetraphenylcyclopentadienone with a 4-bromophenylacetylene. Lithiation and addition of the dendron to 4,4'-dibromobiphenyl-2-carboxylate, with a subsequent ring closure yielded the benzylic-free macromonomer. The polymerisation of the macromonomer was carried out in an analogous manner to the previous macromonomer.[2] The dendronised polymer had a weight average molecular weight, M_w, of 6.3 x 10^4 $gmol^{-1}$, polydispersity, D, of 1.28, and no phase transition was observed in the DSC up to 250 °C.[2]

The dendronised poly(fluorene) was incorporated as the active material into an OLED, and again gave an EL spectrum comparable to poly(dialkylfluorene) with an emission maximum at 420 nm.[1] The device had a power efficiency of 0.06 lmW^{-1}, a turn-on voltage of 6 V and a maximum luminance of 380 cdm^{-2}.[1] Continuous operation under high stress conditions resulted in a degradation of the emission properties, however to a lesser extent when compared to other poly(fluorene) OLED's.[1,2] Time-resolved PL measurements revealed that the dendrons suppress exciton migration, and so the chance of an exciton drifting to a ketonic defect site is low and hence the long wavelength emission is reduced.[1,15]

A novel and improved synthetic route to dendronised poly(fluorenes) is proposed, which allows for the synthesis of functionalised dendronised polymers. The synthetic technique is modified and applied to the indenofluorene monomer unit to yield the first dendronised poly(indenofluorene). An additional polymer backbone type, PPE, is also synthesised with oligo-phenylene dendrimers attached. The synthesis and characterisation of the range of dendronised conjugated polymers is presented with discussion in the following section.

2.2 Results and Discussion

2.2.1 Dendronised poly(fluorene)

For the ready synthesis of a variety of dendronised macromonomers, a divergent synthetic route is most appealing, *ie* the dendron is built out from the core. For synthetic ease, a common intermediate that can be easily reacted to yield the desired macromonomer is required. The synthetic route to the common intermediate used in this study is shown in Scheme 2.3. The drawbacks to adopting a divergent approach are surmounted since the reactions involved with the dendrimer formation, *ie* the terminal acetylene generation and subsequent Diels-Alder reaction, proceed in high yields and generates products that are easily purified.

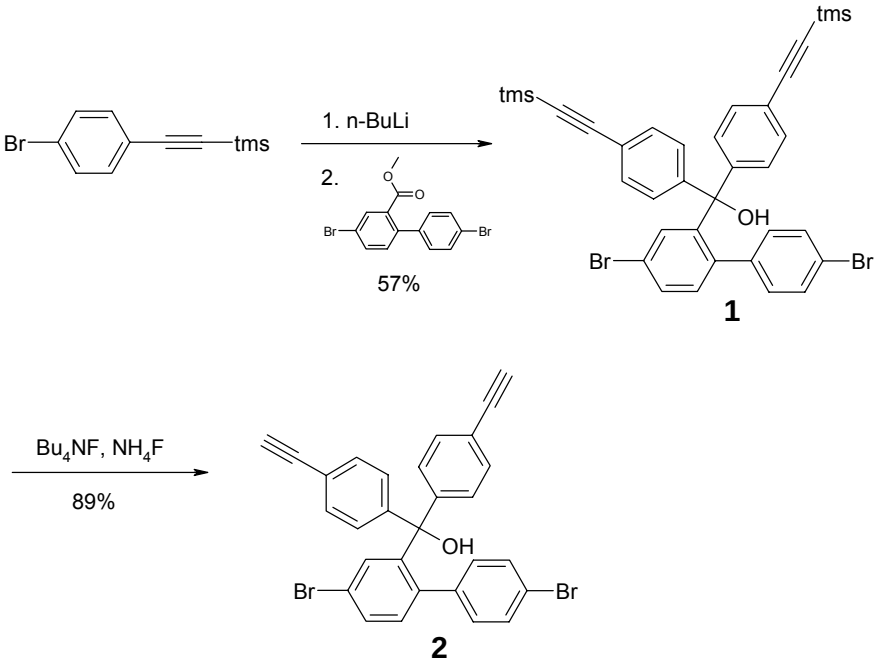

Scheme 2.3. Synthetic route to bis-acetylene intermediate, 2.

The synthesis of **2** is an adaptation of the previous synthetic route to dendronised poly(fluorene) that does not contain benzylic linkages.[2] Instead of the aryl lithium addition of the preformed dendron to the monomer unit, (4-bromo-phenylethynyl)-trimethylsilane is coupled to methyl 4,4'-dibromobiphenyl-2-

carboxylate to yield **1**. The trimethylsilane protecting groups can be easily removed by treatment with tetrabutylammonium fluoride, to give the common intermediate **2**.

The dendronised macromonomer is formed by a Diels-Alder reaction of a tetraphenylcyclopentadienone with **2**, followed by the Lewis or Brønsted acid-promoted ring closure to give the fluorene moiety. The resulting macromonomer **3** is the same as the dendronised monomer previously described.[2]

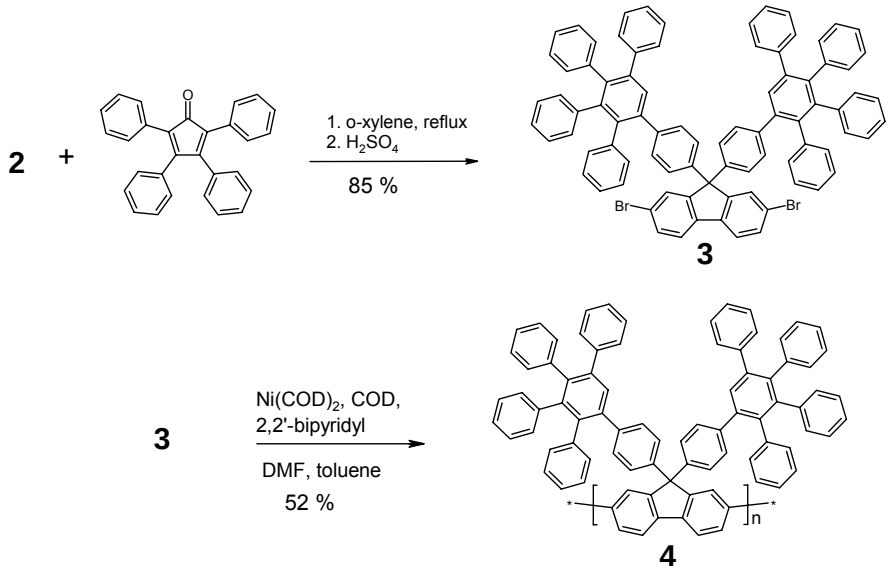

Scheme 2.4. Synthetic route to first generation dendronised poly(fluorene), 4.

The polymerisation of **3** was performed via a Yamamoto polymerisation using literature procedures, to afford the dendronised polymer **4**, with a yield of 60%. GPC analysis of **4** shows a M_n of 9.9 x 10^3 gmol^{-1}, M_w of 1.8 x 10^4 gmol^{-1}, and a D of 1.8 against PS standard, and a M_n of 7.4 x 10^3 gmol^{-1}, M_w of 1.1 x 10^4 gmol^{-1}, and a D of 1.6 against PPP standard. This corresponds to a degree of polymerisation of about 10 units.

The GPC results of rigid rod polymers such as poly(tetrahydropyrene) and poly(fluorene) are known to be inaccurate.[16,17] In the GPC column, rigid rod polymers behave similarly to larger molecular weight examples of the more flexible calibration polymers. The comparison of M_n values of poly(dioctylfluorene) obtained from GPC and from light scattering experiments determined that GPC overestimates the size of

the polymer by a factor of 2.7.[17] Due to the increasing influence of the dendron units on the overall nature of the polymer, one can assume that the GPC results of the dendronised poly(fluorenes) overestimate the size of the polymer by an even larger extent. The choice of polymer standard can yield M_n values that are more accurate, with PPP the most suitable for accurate M_n estimates of polyphenylene based materials, while PS is the more commonly used in the literature. Realising the values of M_n obtained from GPC may have a high uncertainty for the polymers in this section, the characterisation technique is useful for comparison of materials of a similar class. The M_n, M_w and D values, measured against PS and PPP, of the dendronised polymers in this section will be presented for comparison.

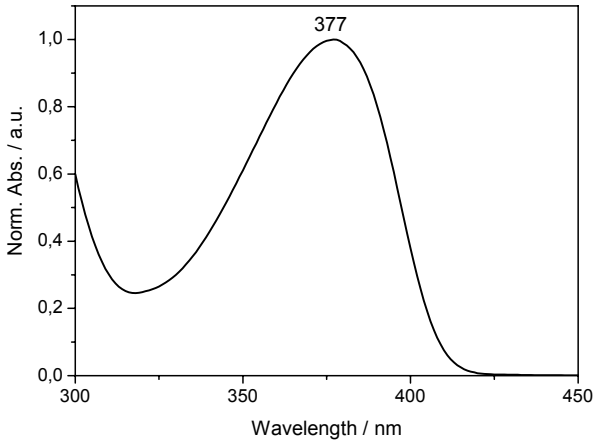

a.

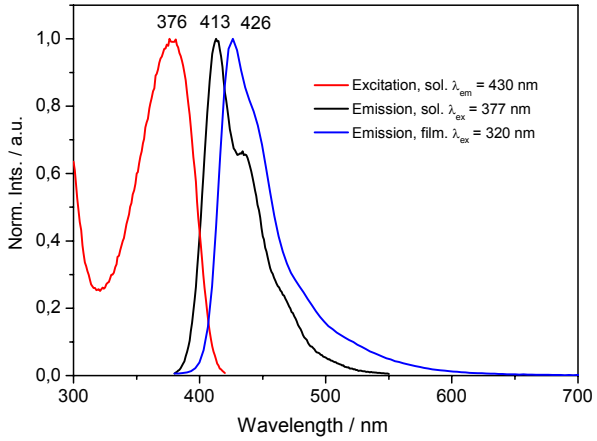

b.

Figure 2.1. Optical properties of 4 in THF and thin film. a. UV-vis absorption spectrum of 4. b. Excitation (λ_{em} = 430 nm), solution (λ_{ex} = 377 nm) and thin film emission (λ_{ex} = 320 nm) spectra of 4.

The spectroscopic characteristics of **4** are shown in Figure 2.1. The dendronised polymer **4** shows a broad absorption with a maximum absorption at 377 nm. The emission spectrum of **4** in solution (λ_{ex} = 377 nm) displays a vibronic fine structure with two bands at 413 nm and 434 nm.

The emission characteristics of a material in an OLED are best estimated by the solid state emission spectrum. Thin films were prepared on a glass substrate, which was cleaned by washing with THF in an ultrasonic bath. Films were prepared by drop casting from 2 $mgmL^{-1}$ solutions of the polymer, which were allowed to dry in the air whilst protected from atmospheric dust.

The thin film emission spectra of **4**, Figure 2.1, is bathochromically shifted compared to the solution spectrum with an emission maximum at 426 nm, and a tail into longer wavelengths. The absorption and emission maxima of **4** are similar to the those for a poly(dialkylfluorene), which suggests that the bulky groups at the 9-position do not affect the torsion angle of the conjugated backbone.

Ideally, the molecular weight of the dendronised polymers should be as large as possible to impart good processability while retaining solubility. The Yamamoto polymerisation is not restricted to aryl bromides, and can also be extended to include other functionalities such as aryl chlorides.[18,19] While the polymerisation of aromatic chlorides is known, to the best of our knowledge there are no available systematic studies on the choice of halide on the molecular weight of the products of Yamamoto polymerisations. Hence to investigate the effect of halide on the polymerisation reaction, the chloro analogue of **3** was synthesised as shown in Scheme 2.5.

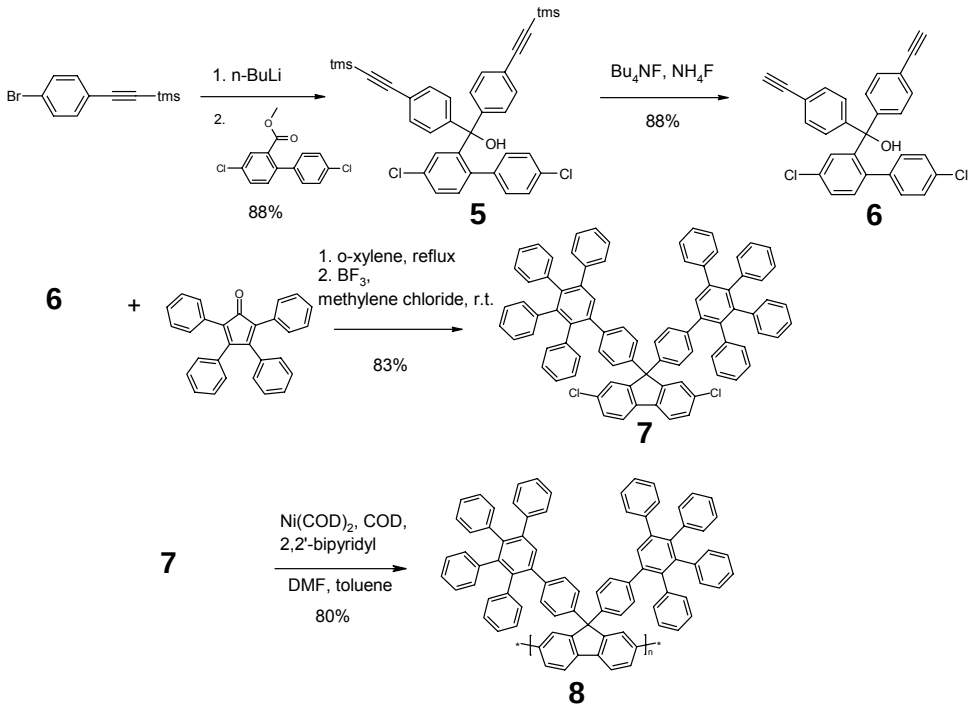

Scheme 2.5. Synthetic route to first generation dendronised poly(fluorene), 8.

The synthesis of the monomer **7** is essentially identical to that of **3**. The Yamamoto polymerisation of **7** to give **8** afforded a high molecular weight material in a good yield of 80%. GPC analysis of **8** shows a M_n of 3.2 x 10^4 $gmol^{-1}$, M_w of 8.7 x 10^4 $gmol^{-1}$, and a D of 2.7 against PS standard, and a M_n of 2.1 x 10^4 $gmol^{-1}$, M_w of 4.5 x 10^4 $gmol^{-1}$, and a D of 2.1 against PPP standard. In comparison with the previously reported polymer (M_w = 6.3 x 10^4 $gmol^{-1}$, PS standard), prepared via a different synthetic route, polymer **8** has a higher molecular weight.[2] Thermogravimetric analysis (TGA) shows **8** has thermal stability up to 450°C.

The polymerisation of the di-chloro dendronised macromonomer **7** thus gives a higher molecular weight material than the polymerisation of the di-bromo derivative **3**. It is known that aryl chlorides are generally less reactive than aryl bromides and iodides (Cl < Br < I), and so one would expect aryl chlorides would yield lower molecular weight polymers compared to aryl bromides. The increase in molecular weight for **8** may be a result of the stability of the aryl halide bond. The aryl chloride bond is stronger than the aryl bromide, and so may be less susceptible to dehalogenation at the relatively high reaction temperatures and times required for

Yamamoto polycondensations. This decrease in dehalogenated side product would cause an increase in the molecular weight of the polymer.

The absorption, excitation and emission spectra of **8** are presented in Figure 2.2. The dendronised polymer **8** shows a broad absorption with a maximum absorption at 382 nm, which is slightly red-shifted compared to **4**. The emission spectrum of **8** in solution (λ_{ex} = 382 nm) matches that of the lower molecular mass polymer **4**. This suggests that **4** is longer than the effective conjugation length for emission, but not for absorption. These have been estimated for poly(dialkylfluorene) to be 6 and 12 fluorene units respectively.[20]

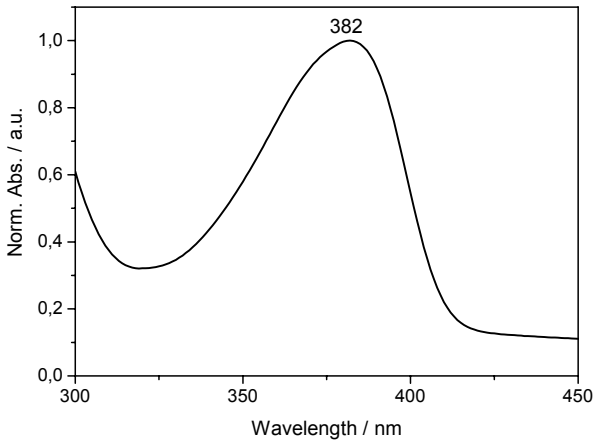

a.

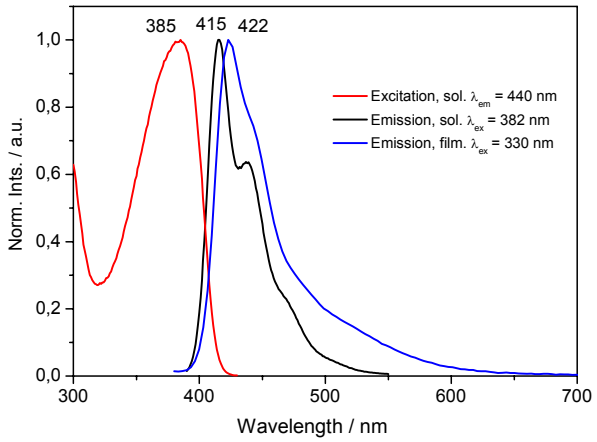

b.

Figure 2.2. Optical properties of 8 in THF and thin film. a. UV-vis absorption spectrum of 8. b. Excitation (λ_{em} = 440 nm), solution (λ_{ex} = 382 nm) and thin film emission (λ_{ex} = 330 nm) spectra of 8.

From the common intermediates **2** and **6**, a range of dendronised polymers can be synthesised as a result of the easy functionalisation of a tetraphenylcyclopentadienone. The dibromotetraphenylcyclopentadienone, **9**, can be prepared from dibromobenzildiketone and diphenylacetone in a Knoevenagel condensation, Equation 4.[21] The dibromo tetraphenylcyclopentadienone can be easily functionalised using standard cross coupling chemistry such as Hagihara-Sonigashira to introduce a triple bond or palladium catalysed Buchwald type coupling to introduce an amino function.[22-24]

Equation 4. Synthetic route to dibromo tetraphenylcyclopentadienone, 9.

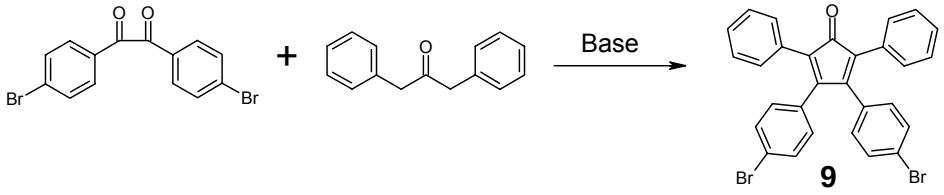

The importance of balanced hole and electron injection was discussed in Section 1.3.1, with most OLED's fabricated in a multilayer fashion incorporating hole and electron transport materials. Triarylamine derivatives have been recognised as effective hole transport materials (HTM) in OLED's.[25,26] Triarylamines have been used in blends with poly(dialkylfluorenes) as HTM in OLED's, however the device stability was affected due to phase separation.[27] The hole transporting moieties have been covalently attached to polymers as endcapping units, which limits the charge carrier properties to the polymer chain ends.[28,29] Triarylamine has also been introduced at the 9-position of poly(fluorene), where the substituent both suppresses aggregation and improves hole-injection[30]. The synthesis of poly[9,9-bis(triphenylamine)fluorene] is shown in Scheme 2.6.

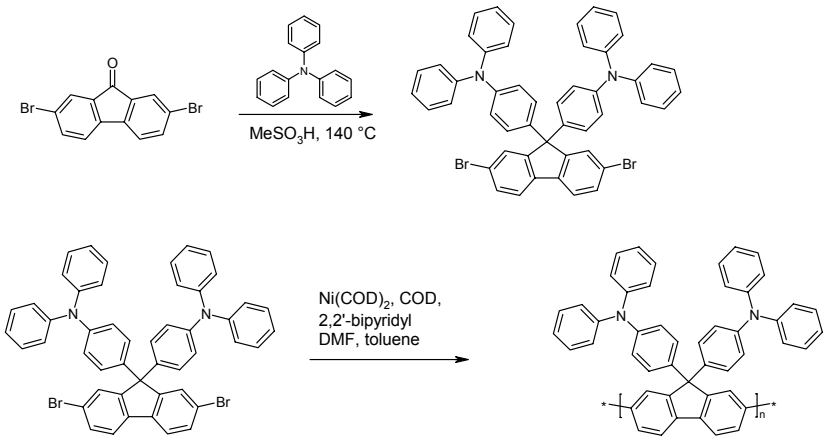

Scheme 2.6. Synthesis of poly(9,9-bis(triphenylamine)fluorene).

Poly(9,9-bis(triphenylamine)fluorene) has two arylamine substituents per repeat unit. In order to increase the ratio of HTM units per repeat unit, the monomer for a dendronised analogue with four amine substituents per unit was synthesised. It is envisioned that the resulting polymer will benefit from dendronisation in terms of the shielding of the main chains to prevent aggregation, and from the high concentration of charge injection and transporting moieties on the polymer. The synthesis of the arylamine substituted monomer and subsequent polymerisation is shown in Scheme 2.7.

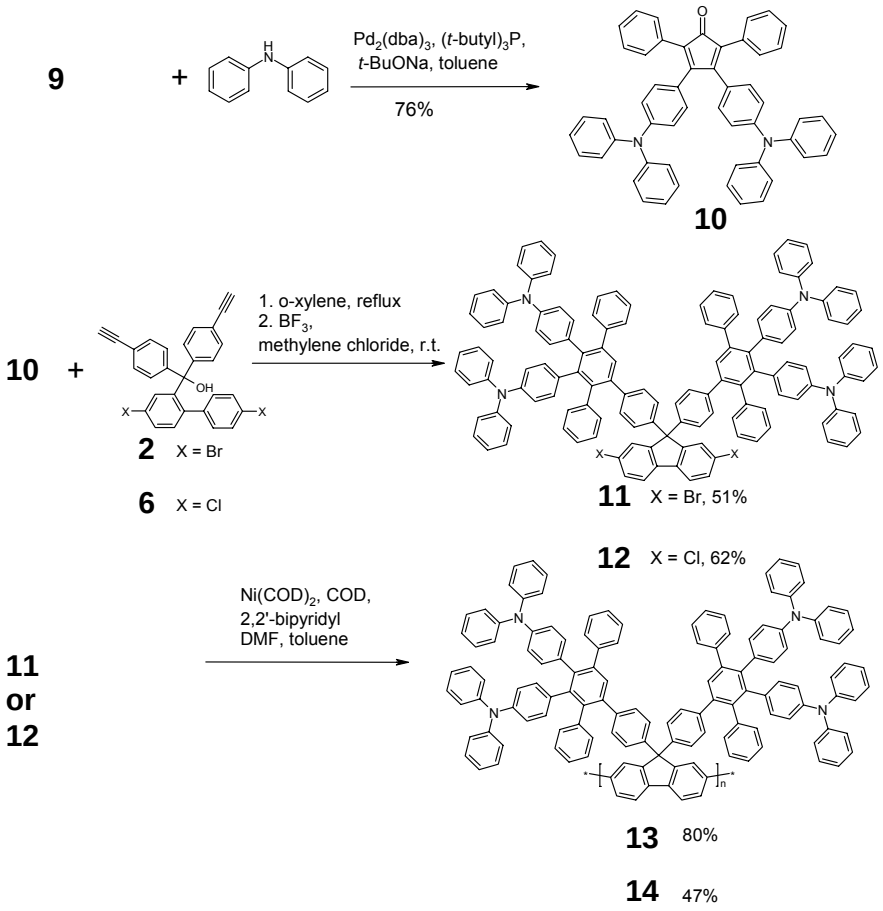

Scheme 2.7. Synthetic route to phenylamine dendronised poly(fluorene), 13 and 14.

The substituted tetraphenylcyclopentadienone **10** was synthesised according to literature procedures.[23] The Diels-Alder addition of **10** with **2**, followed by a BF_3 ring closure gave the monomer **11** in 51% yield. **12** was synthesised from **6** by an analogous route with a 62% yield. Both **11** and **12** were polymerised under Yamamoto conditions to generate **13** and **14** respectively. The GPC results are tabulated in Table 1.1. The polymerisation of the dibromo monomer resulted in short oligomer formation, while the polymerisation of **14** yielded a higher molecular weight material. This corresponds to a degree of polymerisation of approximately 2 and 10 for **13** and **14** respectively. The substituted dendronised fluorene monomers **11** and **12** have a much lower solubility than the unsubstituted monomers **7** and **3**, and this low solubility may explain the poor molecular weights of these materials. The effect of solubility on the polymerisation of dendronised monomers will be discussed later. TGA of **13** shows an initial weight loss of 10% at 350°C, with the main decomposition occurring at 500°C. TGA indicates **14** is thermally stable up to 500°C.

Table 1.1. GPC data for 13 and 14 in THF.

Polymer	Standard	Mn / $gmol^{-1} \times 10^3$	Mw / $gmol^{-1} \times 10^3$	D
13	PS	3.8	5.4	1.4
	PPP	3.1	4.0	1.3
14	PS	17	31	1.9
	PPP	12	19	1.6

The UV-vis absorption spectra and photoluminescence spectra of **13** and **14** are shown in Figure 2.3 and Figure 2.4 respectively. Figure 2.3 illustrates that both **13** and **14** have a broad absorption with a maximum of 307 nm and a shoulder at approximately 380 nm. The major absorption at 307 nm is due to the arylamine dendrons on the polymer, while the shoulder at 380 nm is from the polyphenylene backbone of the material. Figure 2.3b demonstrates **14** has a stronger relative absorption at 380 nm, due to the increased molecular weight, and so conjugation, of the polymer.

Figure 2.4a illustrates **13** in solution has a broad featureless emission (λ_{ex} = 308 nm) with a maximum at 414 nm. The thin film emission of **13** (Figure 2.4a) shows significant emission at long wavelengths. Figure 2.4b demonstrates **14** in solution (λ_{ex} = 379 nm) displays a vibronic fine structure with two bands at 415 nm and 436 nm. The thin film emission of **14**, Figure 2.4b, is shifted bathochromically compared to the solution emission spectrum. The increased long wavelength emission from the thin film emission of **13** compared to **14** can be attributed to the low molecular weight and polydispersity of **13**. This allows for better packing, as the oligomers π-systems can interact as the backbone is short, and this aggregation leads to an increase in the low energy emission bands.

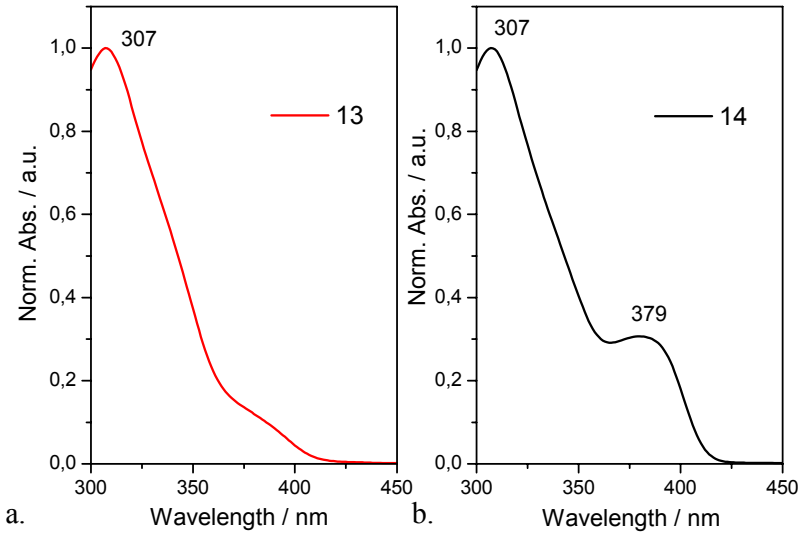

Figure 2.3. Absorption spectra of a. 13 and b. 14 in THF.

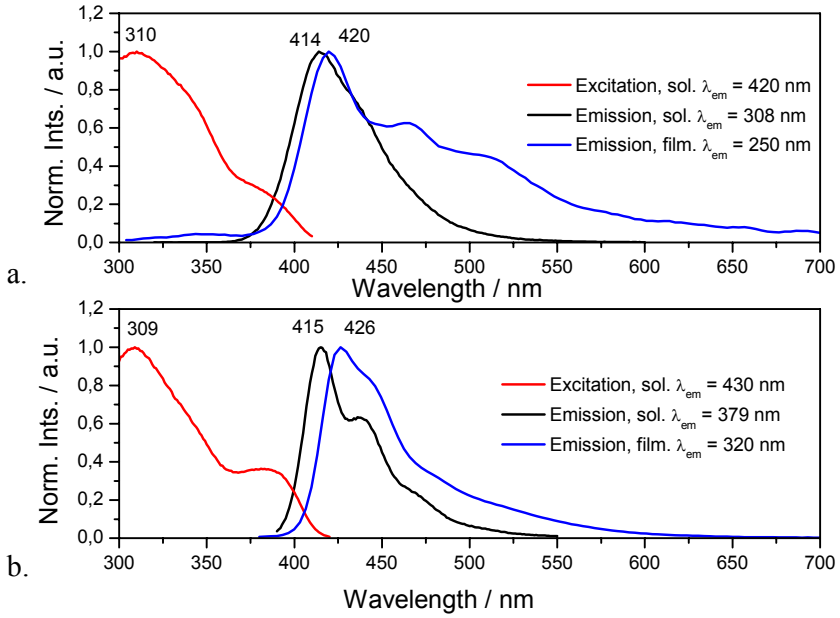

Figure 2.4. Photoluminescence data of 13 and 14. a. Excitation (λ_{em} = 420 nm), solution (λ_{ex} = 308 nm) and thin film emission (λ_{ex} = 250 nm) spectra of 13. b. . Excitation (λ_{em} = 430 nm), solution (λ_{ex} = 379 nm) and thin film emission (λ_{ex} = 320 nm) spectra of 14.

The GPC results indicate that the polymerisation afforded low molecular weight oligomers from the dibromo monomer, approximately 2-3 units, and higher molecular weight oligomers from the dichloro monomer, approximately 10 units. Experience has

demonstrated that the Yamamoto polymerisation yields the best molecular weights when the reaction is carried out in concentrated solutions. For the polymerisation of both **11** and **12** large amounts of solvent were required, with concentrations of 0.022 M and 0.026 M respectively, and required heating to get into solution. To determine whether the low solubility of the monomers results in the low molecular weights of the materials, a monomer with solubilising alkyl chains on the periphery of the arylamine was synthesised, Scheme 2.8.

The Buchwald coupling of **9** with bis-[4-(1,1,3,3-tetramethylbutyl)-phenyl]-amine yielded the substituted tetraphenylcyclopentadienone **15**, with a yield of 57%. The low yield is a result of the difficulties in purifying the product of the reaction from the arylamine reactant. The Diels-Alder addition of **15** with **2**, followed by a BF_3 ring closure gave the monomer **16** in 69% yield. The Yamamoto polymerisation of **16** to give **17** proceeded with a yield of 37%. The low yield of the polycondensation reaction can be attributed in part to the low scale on which the reaction was carried out, and in part to loss of material on work up. The monomer **16** was found to be more soluble than the unsubstituted monomers **11** and **12**, and was used in the polymerisation with a concentration of 0.045 M.

GPC analysis of the substituted phenylamine dendronised poly(fluorene) **17** has a M_n of 3.5 x 10^4 $gmol^{-1}$, M_w of 1.8 x 10^5 $gmol^{-1}$, and a D of 5.2 against PS standard, and a M_n of 2.4 x 10^4 $gmol^{-1}$, M_w of 8.5 x 10^4 $gmol^{-1}$, and a D of 3.5 against PPP standard. The polymerisation of the more soluble, substituted phenyl amine monomer **16** proceeds to a much higher degree compared to the unsubstituted material. This suggests that it is the solubility of the material that limits the polymerisation to form **13** and **14**.

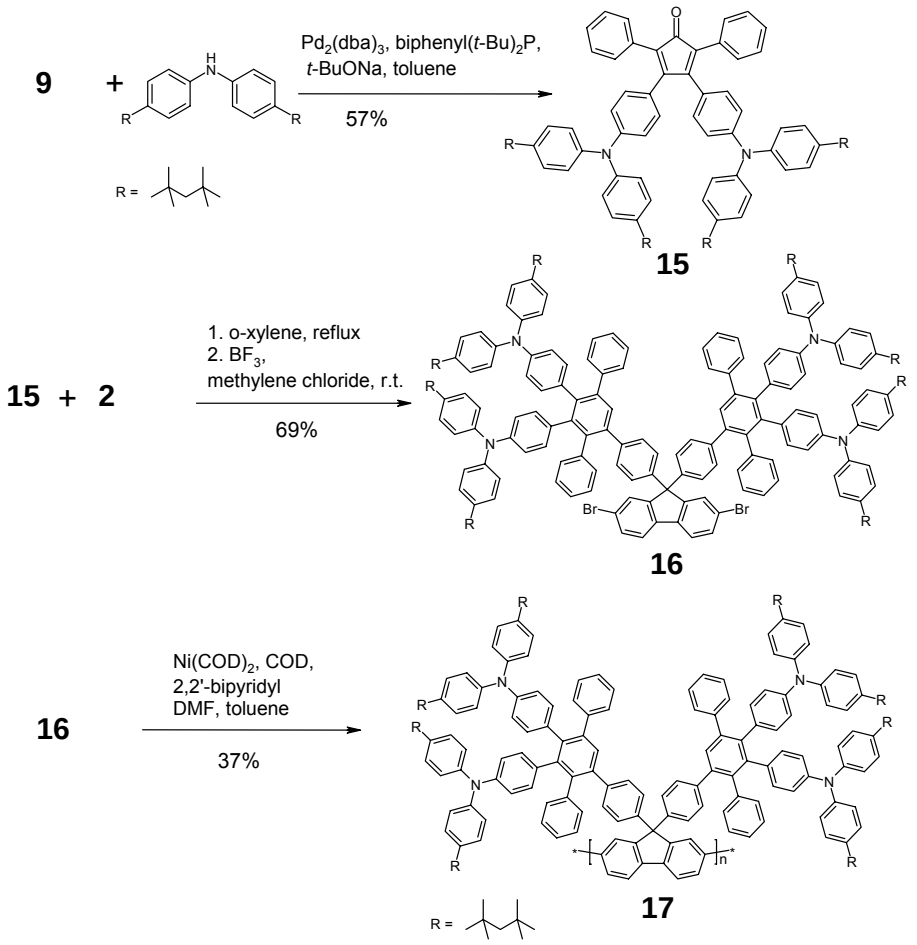

Scheme 2.8. Synthetic route to substituted phenylamine dendronised poly(fluorene), 17.

The UV-vis absorption spectrum, the excitation and emission spectra of **17** in solution and thin film are presented in Figure 2.5. Figure 2.5a demonstrates a broad absorption with a maximum at 312 nm and a shoulder at 384 nm. The shoulder at 384 nm corresponds to an absorption by the poly(fluorene) backbone, while the broad absorption is from the dendronised sidechain. The emission spectrum of **17** in solution (λ_{ex} = 312 nm) displays a vibronic fine structure with two bands at 418 nm and 442 nm. The thin film emission spectrum (λ_{ex} = 320 nm) is bathochromically shifted compared to the solution spectrum with an emission maximum at 423 nm, and a tail into longer wavelengths. The long wavelength emission is more pronounced for **17** than for the unsubstituted **4**. The emission maximum of **17** in solution is red-shifted compared to **13** and **14**, due to the increased molecular weight of this material.

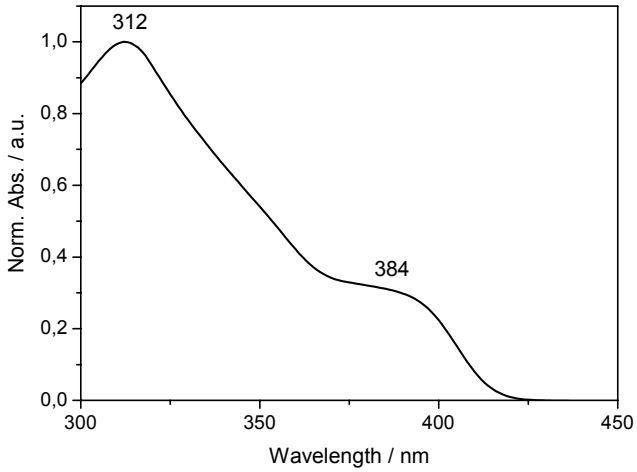

a.

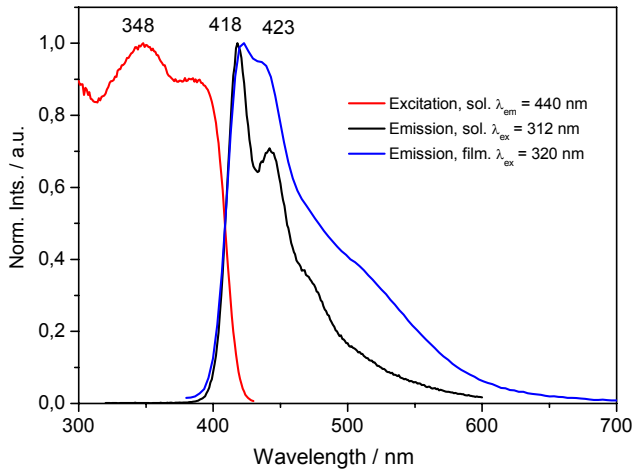

b.

Figure 2.5. Optical properties of 17 in THF and thin film. a. UV-vis absorption spectrum of 17. b. Excitation (λ_{em} = 440 nm), solution (λ_{ex} = 312 nm) and thin film emission (λ_{ex} = 320 nm) spectra of 17.

Cyclic voltammetry (CV) was measured on a film of **17** deposited on a carbon electrode in CH_3CN/ClO_4 with a platinum counter electrode and a silver quasi-reference electrode, calibrated against ferrocene-ferrocenium. The voltamograms are presented in Figure 2.6.

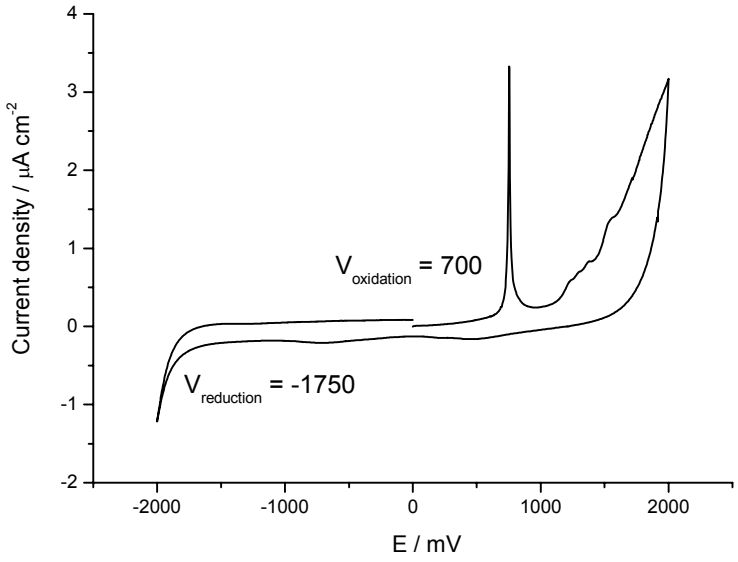

a.

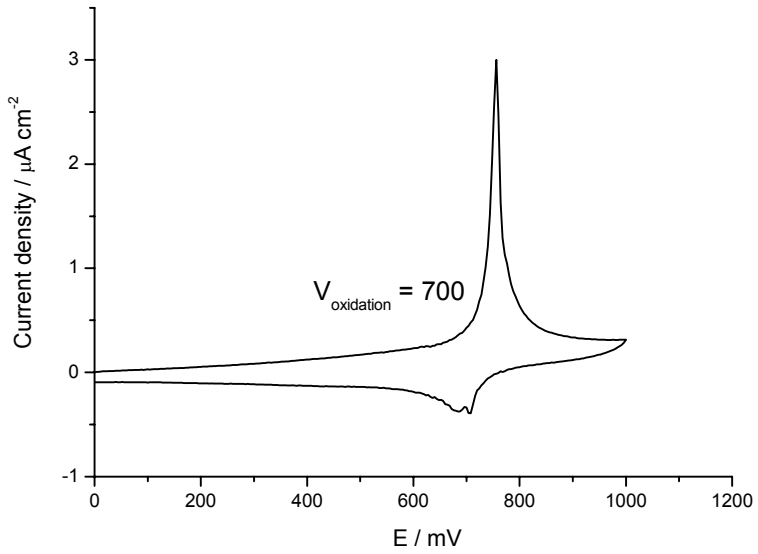

b.

Figure 2.6. Cyclic voltamogram of thin film of 17. a. Full plot. b. Oxidation. Onset voltage of oxidation and reduction is shown.

The onset voltage of oxidation for **17** in thin film is 0.7 V, and the reduction onset voltage is -1.75 V. From the reduction and oxidation potential, the IP (HOMO) and EA (LUMO) can be estimated.[31] The vacuum energy level of the ferrocene/ferrocenium standard is accepted as –4.8 eV. The ferrocene/ferrocenium redox couple was measured at 0.4 V in the experimental setup used for these

experiments. This results in a work function for our silver quasi-reference electrode of 4.4 eV. Adding the onset voltages of oxidation and reduction to the calculated vacuum energy level of the reference electrode (-4.4 eV) gives the IP and EA of the thin film, respectively.

The calculated IP and EA values for **17** are -5.1 eV and -2.65 eV respectively, with a bandgap of 2.45 eV. The optical bandgap, as defined by the absorption onset of 420 nm, is 2.95 eV, which is significantly higher than the electrochemical bandgap. The HOMO and LUMO levels for poly(dioctylfluorene) have been measured electrochemically at –5.8 eV and –2.12 eV respectively.[32] For poly(fluorene) the electrochemical bandgap was found to be higher than the optical bandgap, while the optical and electrochemical bandgaps of poly(9,9-bis(triphenylamine)fluorene) were similar.[30,32] The difference in optical and electrochemical bandgap values for **17** may be due to an inaccurately measured value of the LUMO. One would not expect that the LUMO of **17** would be 0.53 eV lower than for poly(dioctylfluorene).[32] If the LUMO of **17** is calculated from the optical band gap and the IP, a value of -2.15 eV is obtained. This is much closer to the LUMO level of poly(dioctylfluorene).[32]

In terms of an OLED, the barrier to injection of holes from the anode (*eg* ITO, ionisation energy of 4.7-5.0 eV) and electrons from the cathode (eg Ca, work function of 2.9 eV) is an important consideration in the device construction. The comparison of the HOMO and LUMO levels of poly(dioctylfluorene) and **17** with the energy levels of ITO and Ca is presented schematically in Figure 2.7. The figure clearly demonstrates that the barrier to electron and hole injection to the polymer layer is reduced for **17** compared with poly(dioctylfluorene).

The value for the IP for poly(9,9-bis(triphenylamine)fluorene) is -5.34 eV, which means that **17** is a better hole transporting material by comparison.[30] This is not surprising, as there is twice the density of triarylamine units per fluorene in **17** compared to poly(9,9-bis(triphenylamine)fluorene). The results from the electrochemical experiments support the hypothesis that functionalised dendrons pendant to the polymer chain can improve the characteristics of the material, due to the increased concentration of the active moiety.

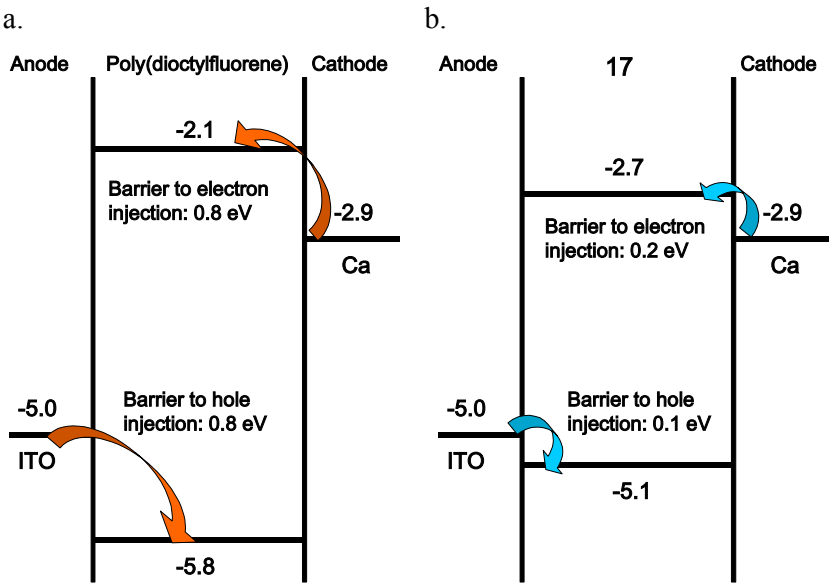

Figure 2.7. Schematic representation of barriers to electron and hole injection for a. poly(dioctylfluorene) and b. 17. Energy levels calculated from electrochemical data.

Figure 2.6b shows the oxidation of **17** to be irreversible. This suggests that there is some chemical change in the species upon oxidation. The oxidation of triphenyl amine is known to lead to the formation of a radical cation, which then dimerises as shown in Scheme 2.9.[25] The formation of dimers is not normally observed for *p*-substituted triphenyl amines.[25,33,34] *p*-Bromo aniline has been observed to form a dicationic dimer, however the evolution through to the neutral dimer species is not observed as it would yield an energetically unfavourable bromine cation.[35] In the case of the substituted arylamine moiety of **17**, the dimerisation and neutralisation would result in a tertiary carbocation, which is more favourable. This would explain the fact that the oxidation cycle of **17** is not reversible, as the oxidation of the arylamine moieties results in dimerisation, albeit at a lower rate than for unsubstituted arylamines.

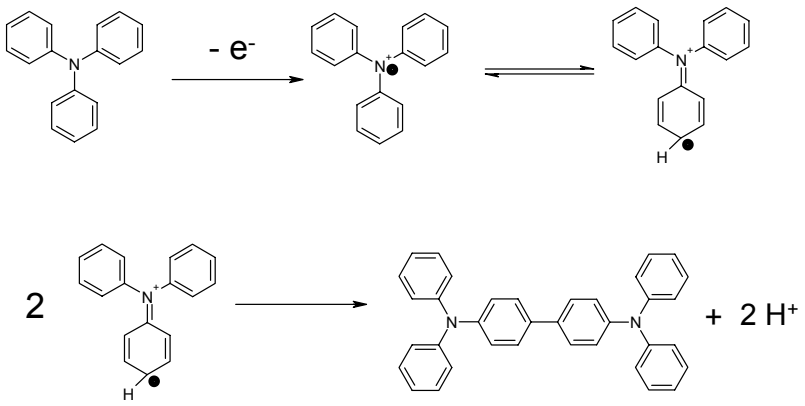

Scheme 2.9. Formation of radical cation and subsequent dimerisation of triphenyl amine.

The electroluminescent properties of **17** were investigated by our collaborator, Dr Emil List (Christian-Doppler Laboratory, Technische Universität Graz, Graz, Austria). To test the stability of **17**, the thin film absorption and emission spectra were recorded after heating the films in air. Thin films of **17** were prepared on a quartz substrate by spincoating from 4 gL^{-1} solution in $CHCl_3$. The film was heated in air for 30 minutes then the spectra were recorded. The temperature was increased in increments of 30°C starting from 30°C, up to 210°C. The absorption and emission spectra of thermally degraded films of **17** are presented in Figure 2.8.

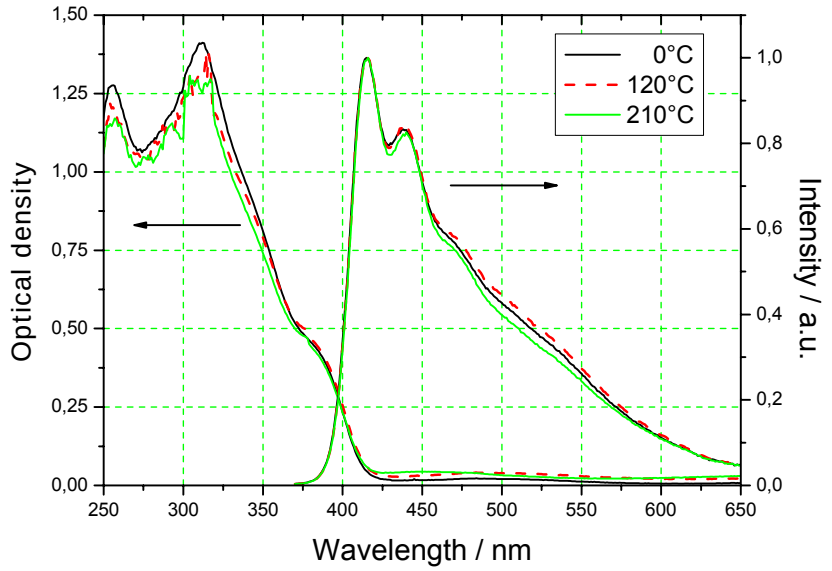

Figure 2.8. Absorption and emission spectra of 17 after thermal degradation in air.

Figure 2.8 illustrates the thermal stability of films of **17**. After 30 minutes of heating in air at 210°C, the absorption and emission spectra remain unchanged. The spectral stability of **17** in the solid state is promising for the preparation of spectrally stable OLED's.

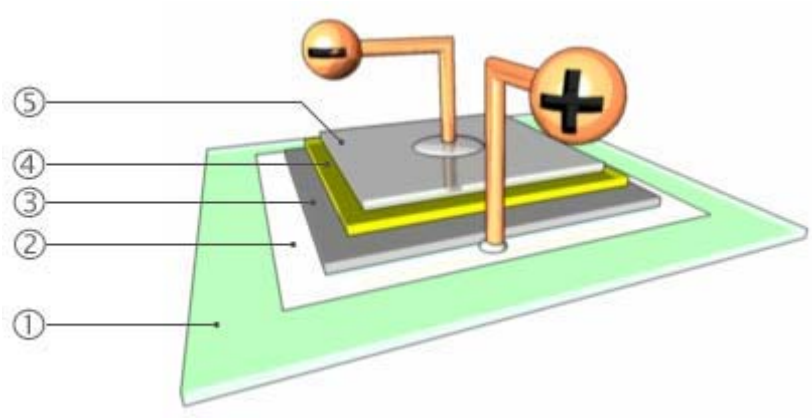

Figure 2.9. Device architecture used in the EL experiments. 1. Transparent substrate. 2. Hole injecting anode (ITO). 3. Hole transporting layer (PEDOT/PSS). 4. 17. 5. Electron injecting cathode (Ca/Al).

The electroluminescent properties of **17** were tested by incorporating the polymer into a device, using the architecture shown in Figure 2.9. The ITO covered substrate was etched using oxygen plasma, then the PEDOT/PSS layer was subsequently applied by spincoating then heated at 150°C for two hours in a vacuum. **17** was deposited by spincoating in the argon box to prevent oxidation and heated at 150°C for two hours in a vacuum. The cathode was vacuum deposited to give a 10 nm thick Ca layer covered with a 100 nm thick aluminium layer.

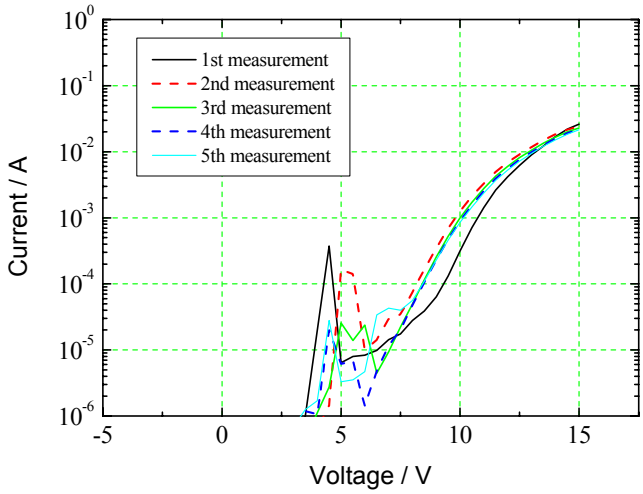

a.

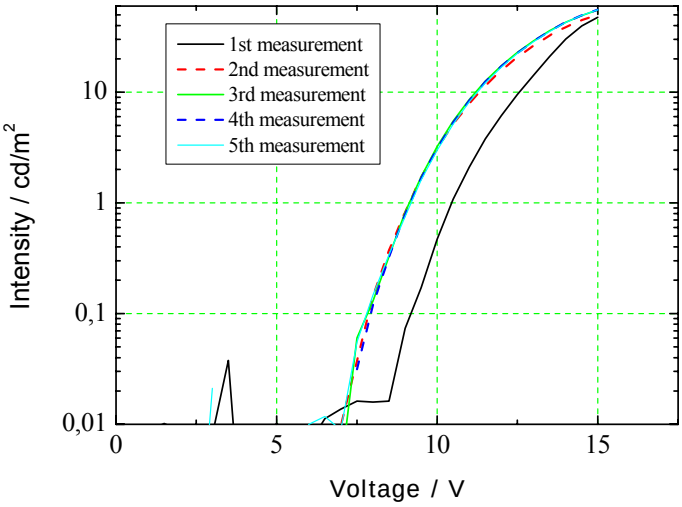

b.

Figure 2.10.a. Current-Voltage characteristics of OLED of 17, measured 5 times. b. Intensity-Voltage characteristics of OLED of 17, measured 5 times.

Figure 2.10 displays the current-voltage and intensity-voltage characteristics of the OLED with **17** as the active layer. The device was found to have a turn-on voltage of 7-8 V, as determined from Figure 2.10b. A maximum luminance of 50 cdm^{-2} was obtained for the device, at 15 V. This low luminance, coupled with the low current, is not indicative of good device performance. Figure 2.11 illustrates the time dependent current and intensity characteristics of the device. Both the current and intensity values of the OLED lost a large fraction of intensity in the first 100 seconds of

operation, before reaching a plateau. The poor device characteristics are attributed to inhomogeneous film forming of the PEDOT/PSS layer in the fabrication process.

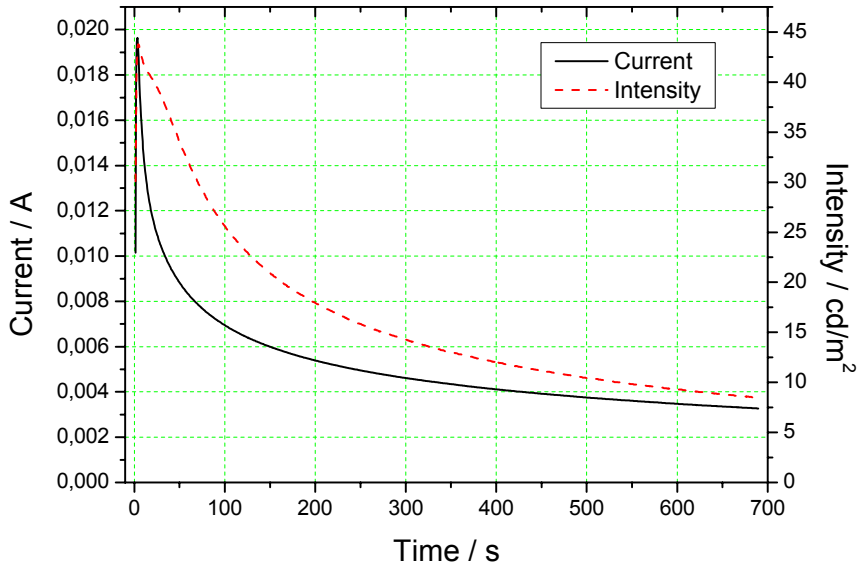

Figure 2.11. Time dependent intensity and current plots of OLED, with device run at a constant 14 V.

The time dependent EL spectra of **17** are presented in Figure 2.12. The device has a maximum emission at 415 nm, with a shoulder at 435 nm. Initially two additional shoulders can be observed at 570 nm and 640 nm, which disappear on further operation. This long wavelength emission is not attributed to defect formation or the formation of aggregates for several reasons. The synthetic route to **17** would make the formation of fluorenone moieties unlikely, and the structure of **17** should inhibit excimer formation. Also, the low energy emission usually found for poly(fluorene) based OLED's is a broad peak with a maximum at 530 nm. The presence of the two shoulders at 570 nm and 640 nm can not be explained at this time. The spectra in Figure 2.12 demonstrate that **17** possesses good spectral stability in a device, with no long wavelength emission arising after 16 minutes of operation at 14 V.

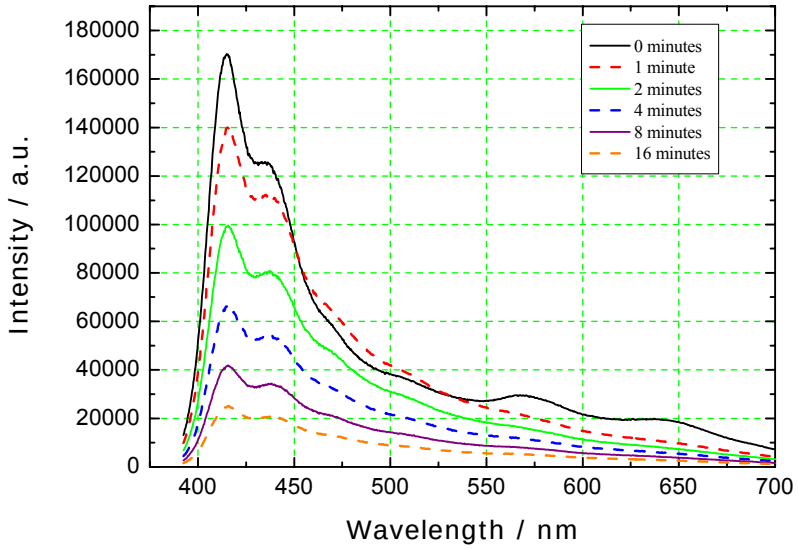

a.

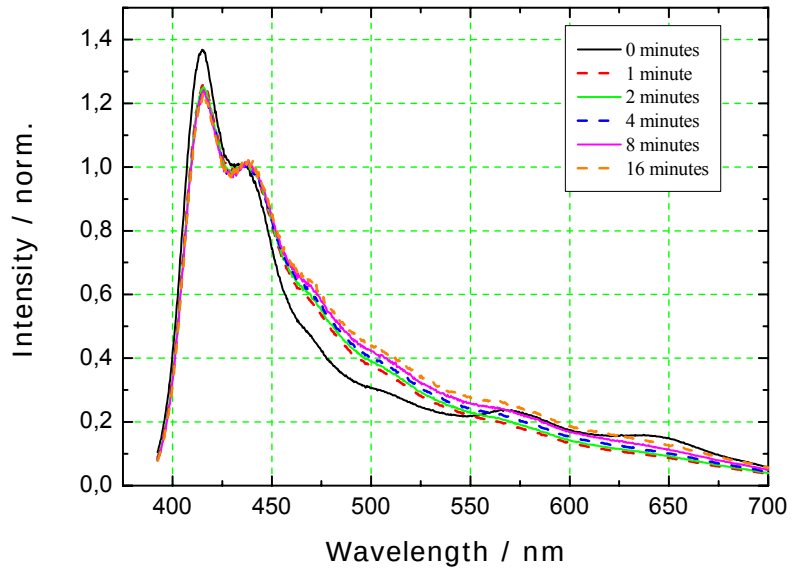

b.

Figure 2.12. Time dependent EL spectra of the emitted light after different periods of time, with a permanent loading of 14V a. Absolute intensities b. Normalised to the 0-1 peak (435 nm).

The spectral stability of **17** is a very promising aspect of the material. The thermal degradation studies undertaken in air show no spectral change, up to 210°C for 30 minutes. In addition, the EL spectrum of **17** in an OLED does not exhibit the long wavelength emission at 530 nm common for poly(fluorene) based devices. With further optimisation of the device construction, the performance of devices based on **17** should improve. The current-voltage and intensity-voltage properties of the EL devices are not good, and a significant proportion of the current and light intensity is lost in the first seconds of operation. This is attributed to the PEDOT/PSS hole-transporting layer however, and not to **17**. It was noted previously that the deposited films of PEDOT/PSS were inhomogeneous. Improvements in this layer alone should greatly improve the device. The initial EL studies of **17** demonstrate that the polymer may hold promise as the active material in a blue OLED.

The consequence of separating the polymer backbone by introducing dendrimers is a decrease in the long wavelength emission in the EL spectrum.[1] In order to probe the effect of the spatial distance on the EL properties of a material, polymers with differing size of the dendrons are required. Towards this end, the second generation dendronised fluorene macromonomer was synthesised. The synthetic route to the dibromo and dichloro macromonomers is shown in Scheme 2.10. The synthesis of the second generation consists of a deprotection and further Diels-Alder reaction to form the second generation dendron. The synthesis is an extension of the general route to the dendronised fluorene, and proceeded as expected. Contrary to expectations, however, was the relatively low solubility of the second generation monomer. This low solubility of the monomer may be detrimental the polymerisation to yield a second generation dendronised poly(fluorene).

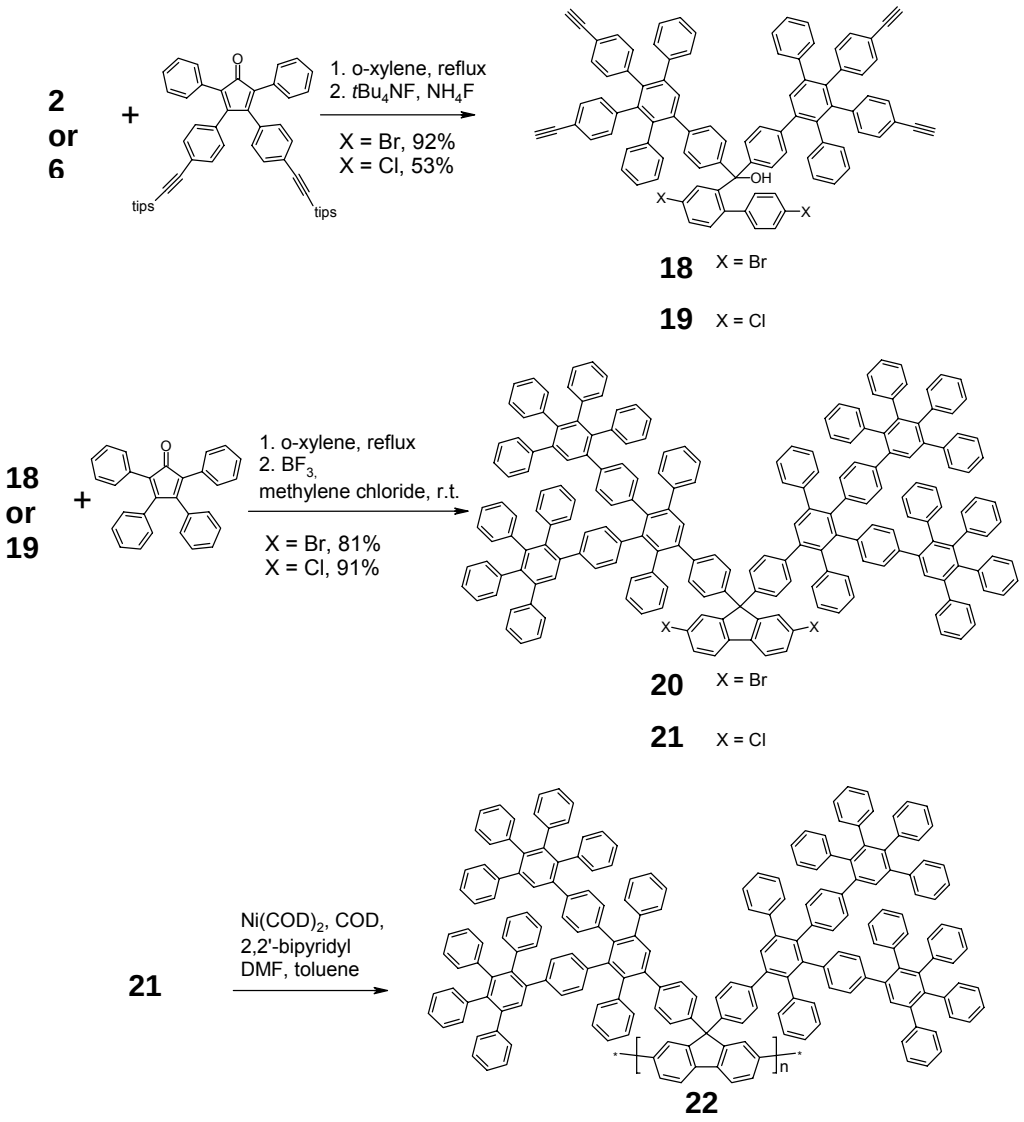

Scheme 2.10. Synthetic route to second generation dendronised poly(fluorene), 22.

The dichloro macromonomer **21** was polymerised using the Yamamoto procedure to generate polymer **22**. GPC analysis of **22** shows a M_n of 6.8 x 10^3 $gmol^{-1}$, M_w of 9.4 x 10^3 $gmol^{-1}$, and a D of 1.4 against PS standard, and a M_n of 5.2 x 10^3 $gmol^{-1}$, M_w of 6.7 x 10^3 $gmol^{-1}$, and a D of 1.3 against PPP standard. As the molecular weight of the repeat unit is 2599 $gmol^{-1}$, only oligomers were formed in the polymerisation reaction. As the chloro monomer is expected to give higher molecular weight polymers compared to the bromo monomer, only **21** was polymerised. The low molecular weight of the polymer is not unexpected however, as the solubility of the monomer is low, 0.019 M, similar to the arylamine substituted monomers **11** and **12**. TGA shows **22** to be thermally stable up to 400°C.

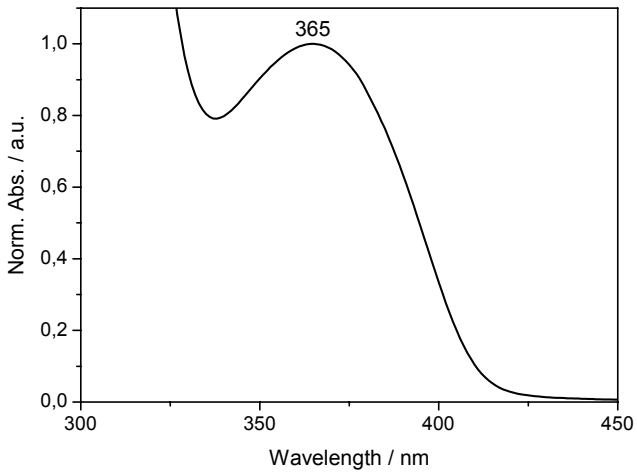

a.

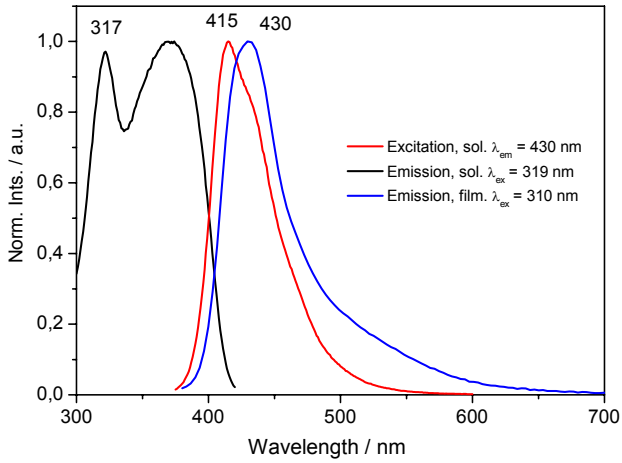

b.

Figure 2.13. Optical properties of 22 in THF and thin film. a. UV-vis absorption spectrum of 22. b. Excitation (λ_{em} = 430 nm), solution (λ_{ex} = 319 nm) and thin film emission (λ_{ex} = 310 nm) spectra of 22.

The UV-vis absorption spectrum, the excitation and emission spectra in solution and thin film of **22** are presented in Figure 2.13. The absorption maximum of **22**, 365 nm, demonstrates a hypsochromic shift compared to the first generation dendronised polymer, due to the low molecular weight of the material. The emission spectrum of **22** in solution (λ_{ex} = 319 nm) displays a broad, featureless emission with a maximum at 415 nm. The thin film emission spectrum (λ_{ex} = 310 nm) is bathochromically shifted compared to the solution spectrum with an emission maximum at 430 nm, and a tail into longer wavelengths.

Marsitzky et al. reported the synthesis of Fréchet dendron substituted poly(fluorene) up to the third generation, using Yamamoto polymerisation conditions.[14] In order to obtain polymers of higher molecular weight, the second and third generation polymerisation reactions were carried out in a much higher concentration than commonly reported in the literature.[14] Even with the increased concentration of monomer, the polymerisation only yielded low molecular weight third generation polymer, which was attributed by the authors to be due to the steric crowding of the reactive site.[14] The phenylene dendronised fluorene monomers mentioned previously do not exhibit the solubility to be able to proceed with the Yamamoto polymerisation at such concentrations. These dendrimers do not have the inherent flexibility and back-bending ability of the Fréchet dendrons, and so will not inhibit the reactivity of the halide due to steric crowding. Rather, the low solubility of the materials is the limiting characteristic of the phenylene dendronised fluorene polymerisations. The authors also prepared copolymers of the dendronised fluorene, and this approach will be discussed later.[14]

2.2.2 Dendronised poly(indenofluorene)-towards a better blue

The dendronisation of poly(fluorene) yielded a material that proved to have better colour stability, compared to the parent poly(fluorene), as the active material in an OLED.[2] In order to obtain a material that emits light at a wavelength to which the eye is more sensitive and possess high colour stability, the dendronisation of poly(indenofluorene) was undertaken. The synthetic route to the dendronised indenofluorene polymer is analogous to that of fluorene and is presented in Scheme 2.11.

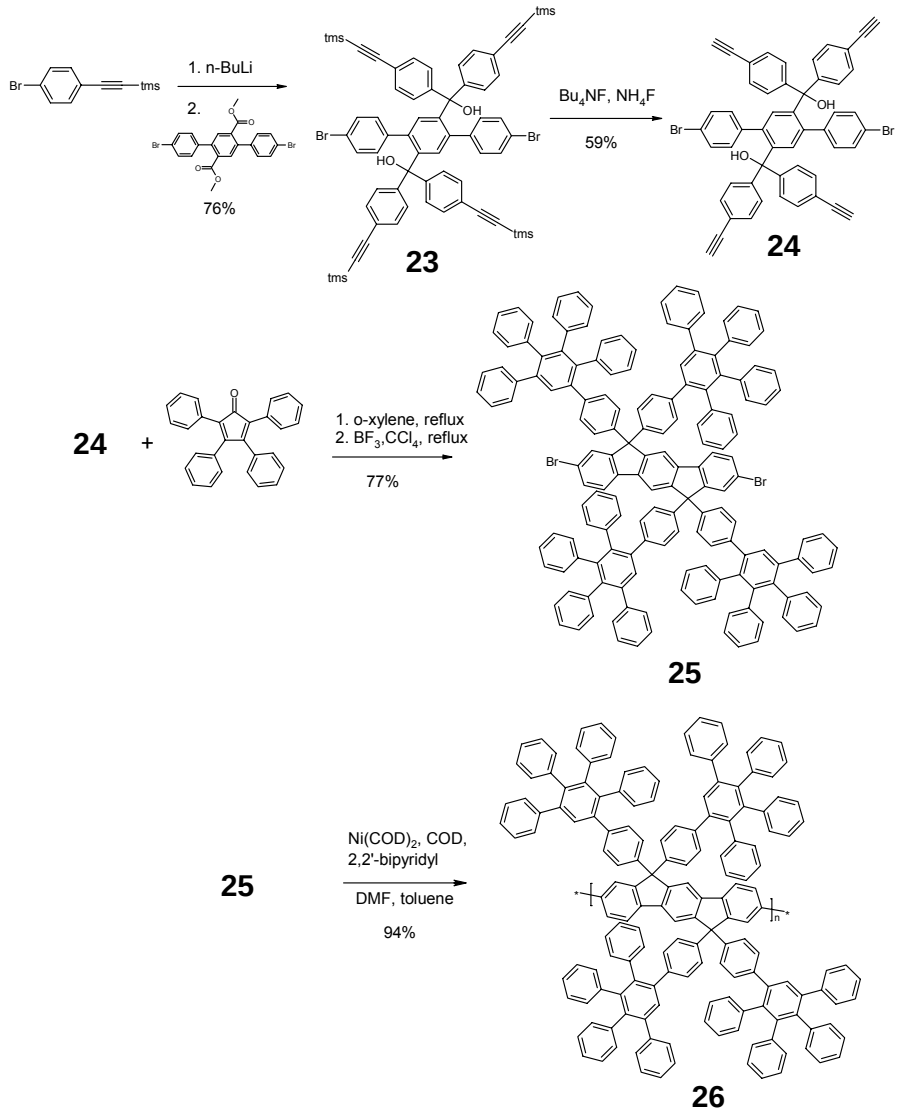

Scheme 2.11. Synthetic route to dendronised poly(indenofluorene), 26.

The synthesis of the monomer **25** differed from the synthesis of the dendronised fluorene analogues in that the Friedel-Crafts ring closure reaction required the use of refluxing CCl_4, as opposed to methylene chloride at room temperature. This was due to the low solubility of the monomer in chlorinated solvents at room temperature, which led to its precipitation from solution before complete ring closure was achieved. The polymerisation of **25** to yield **26** using Yamamoto procedures proceeded with a yield of 94%. GPC analysis of **26** shows a M_n of 3.2 x 10^3 $gmol^{-1}$, M_w of 6.9 x 10^3 $gmol^{-1}$, and a D of 2.2 against PS standard, and a M_n of 2.8 x 10^3 $gmol^{-1}$, M_w of 5.0x 10^3 $gmol^{-1}$, and a D of 1.8 against PPP standard. This corresponds

to a degree of polymerisation of only 1-2 monomer units. We attribute this low molecular weight due to the very low solubility of the monomer. TGA shows **26** is thermally stable up to 450°C.

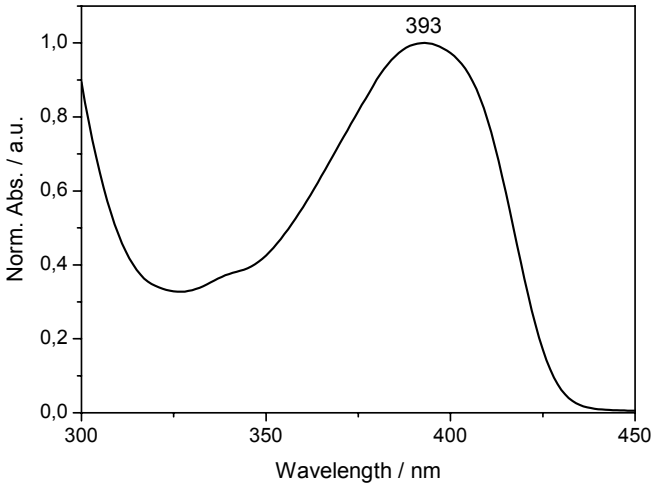

a.

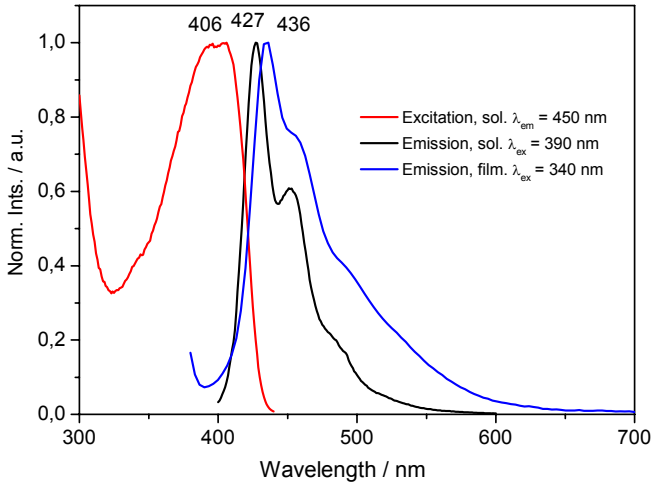

b.

Figure 2.14. Optical properties of 26 in THF and thin film. a. UV-vis absorption spectrum of 26. b. Excitation (λ_{em} = 450 nm), solution (λ_{ex} = 390 nm) and thin film emission (λ_{ex} = 340 nm) spectra of 26.

The UV-vis absorption spectrum, the excitation and emission spectra in solution and thin film of **26** are presented in Figure 2.14. Figure 2.14a displays an absorption maximum at 393 nm. The emission spectrum of **26** in solution (λ_{ex} = 390 nm) displays a vibronic fine structure with two bands at 427 nm and 451 nm. The thin film

emission spectrum (λ_{ex} = 340 nm) shows an emission maximum at 436 nm, and a tail into longer wavelengths. Alkylated poly(indenofluorene) has an absorption maximum at 416 nm, and an emission spectrum (λ_{ex} = 390 nm) which exhibits vibronic fine structure with two bands at 432 nm and 479 nm.[36] The dendronised poly(indenofluorene) has absorption and emission spectra which are shifted to higher energies than the alkylated poly(indenofluorene). This hypsochromic shift can be attributed to the low molecular weight of the material.

2.2.3 Dendronised copolymers

The synthesis of dendronised polymers presented previously, with the exception of the first generation dendronised poly(fluorene) (**4** and **8**) and the alkyl substituted arylamine dendronised poyl(fluorene) (**17**), gave relatively low molecular weight materials. This oligomer formation could potentially be a result of steric interactions between successive repeat units, or more probably due to the solubility of the materials. In either scenario, the insertion of alkylated monomer units into the polymer backbone should increase the molecular weight of the materials, either by separating the distance between successive dendron units or by solubilising the polymer chain. This approach has been used previously for Fréchet-type dendronised fluorene materials, where an increase in molecular weight was observed for the co-polymers of the dendronised materials compared to the homo polymer.[14] With this in mind, copolymers of **12**, **21** and **26** were synthesised via a Suzuki polymerisation. The synthesis of the copolymers is presented in Scheme 2.12.

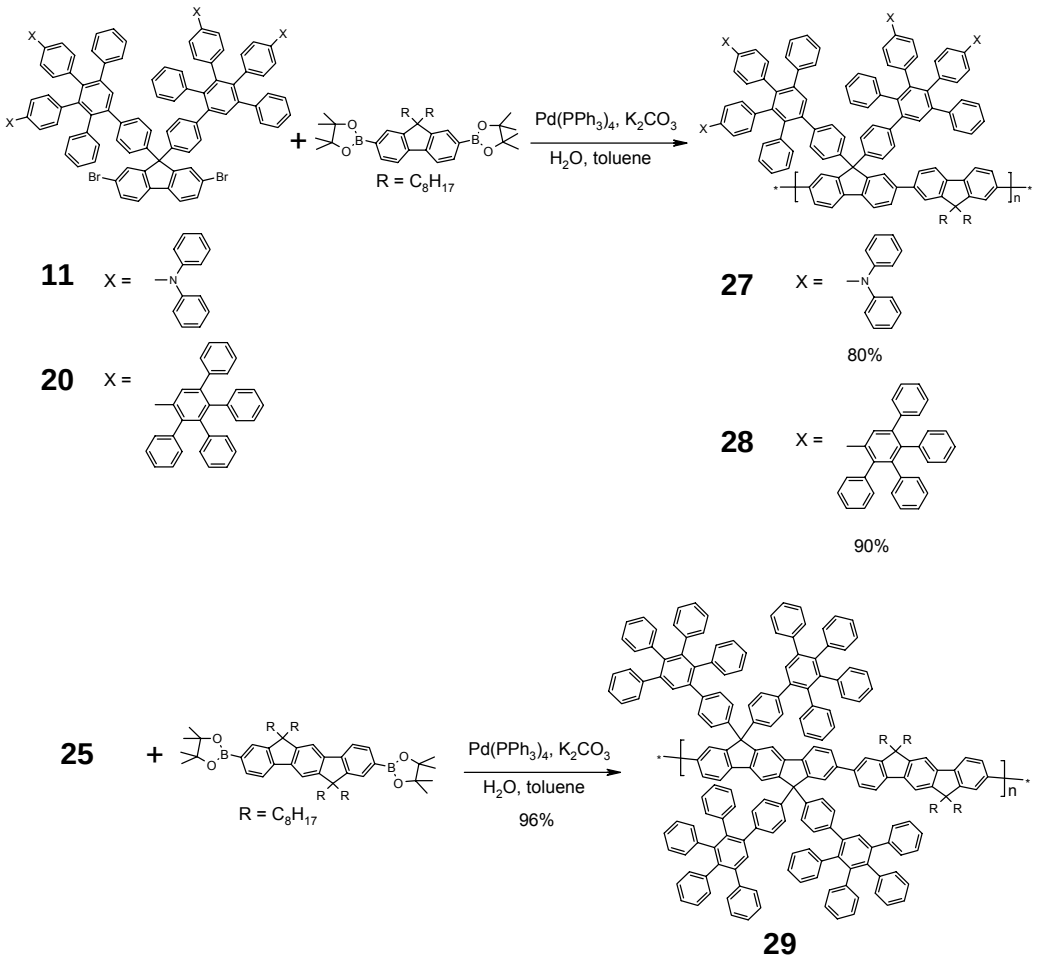

Scheme 2.12. Synthetic route to copolymers 27,28 and 29.

In order to maintain a regular backbone structure, **11** and **20** were copolymerised with the diboronic ester of 9,9-dioctylfluorene, while **25** was copolymerised with the diboronic ester of 6,6,12,12-tetraoctylindenofluorene. The molecular weight data for **27**, **28**, and **29** is presented in Table 1.2. The molecular weights of the co-polymers are not improved with respect to the appropriate homo-polymers. While the co-polymer approach was successful for the Fréchet-type dendronised fluorene materials, which are highly soluble, the phenylene dendronised fluorene and indenofluorene materials do not yield high molecular weight co-polymeric materials.[14] This is likely due to the low solubility of the dendronised monomers, as the more soluble substituted monomer, **16**, does yield a polymeric material.

Table 1.2. GPC data for 28, 29, and 30 in THF.

Polymer	Standard	Mn / $gmol^{-1} \times 10^3$	Mw / $gmol^{-1} \times 10^3$	D
27	PS	3.2	6.9	2.1
	PPP	2.7	5.0	1.8
28	PS	4.7	7.4	1.6
	PPP	3.8	5.4	1.4
29	PS	1.9	3.6	1.9
	PPP	1.7	2.8	1.6

The TGA shows **27** has an initial weight loss of 10% at 350°C, with further decomposition at 450°C, while **28** is thermally stable up to 400°C. **29** has an initial weight loss of 5% at 250°C, and further decomposition at 500°C.

The UV-vis absorption spectra of the dendronised copolymers, **27**, **28**, and **29**, are presented in Figure 2.15. The absorption spectrum of **27** is similar to that of the homopolymer of the arylamine substituted dendronised fluorene, with an absorption maximum at 308 nm and a shoulder at 375 nm. Similarly, the absorption spectrum of **28** is similar to that of the second generation fluorene homopolymer, with an absorption maximum at 364 nm. The hypsochromic shift in absorption maximum when compared with poly(dioctylfluorene), is caused by the low molecular weight of the material. The absorption spectrum of **29** shows a narrow band with a maximum at 353 nm, and a broad absorption band with a maximum at 393 nm.

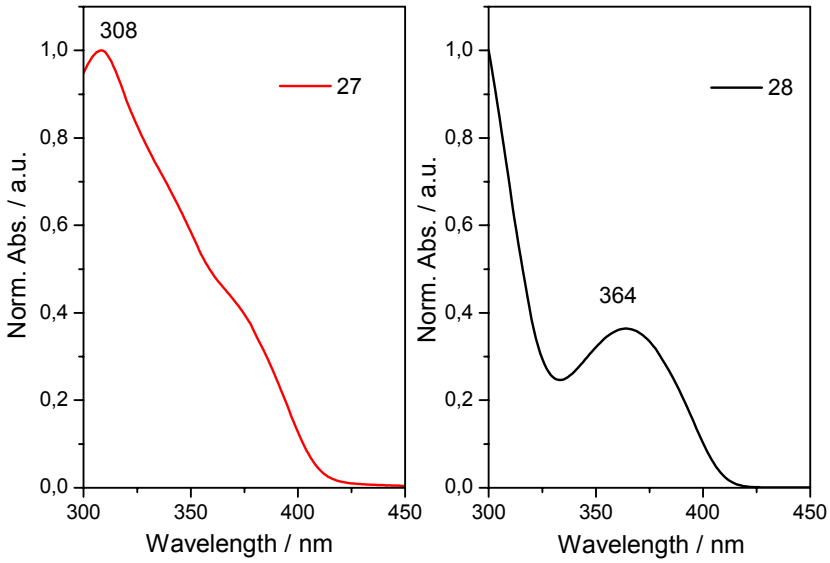

a. b.

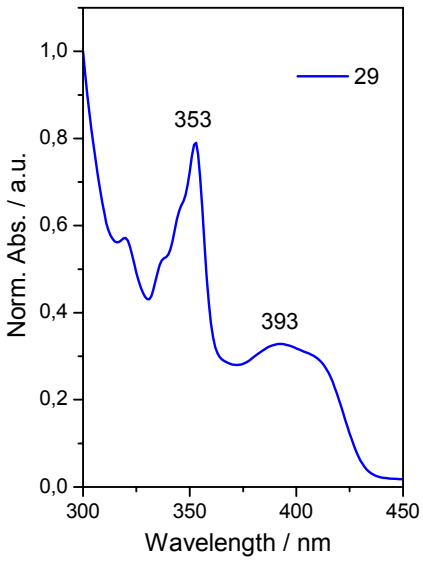

c.

Figure 2.15. UV-vis absorption spectra of dendronised copolymers in THF. a. UV-vis absorption spectrum of 27. b. UV-vis absorption spectrum of 28. c. UV-vis absorption spectrum of 29.

Figure 2.16 displays the UV-vis absorption spectra of the two components of the copolymer **29**, the dialkylindenofluorene and the dendronised monomer **25**. When the spectrum in Figure 2.15c is compared to the spectra in Figure 2.16, the major absorption band in Figure 2.15c at 353 nm is due to the absorption of a monomer unit,

especially the dendronised indenofluorene unit **25**. As described previously, **25** exhibits poor solubility in common solvents and was retained with the polymer mixture even after Soxhlet extraction. The smaller absorption band in Figure 2.15c at 393 nm is from the oligomers formed in the polymerisation reaction.

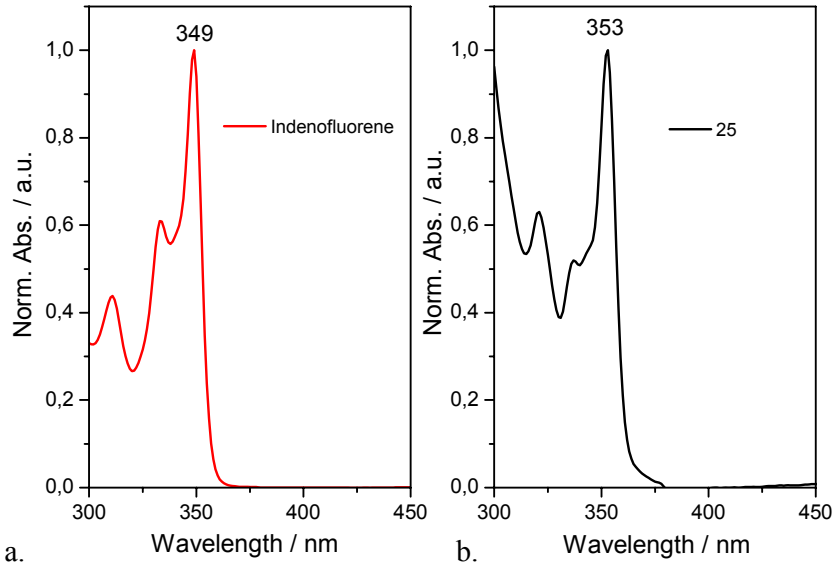

Figure 2.16. UV-vis absorption spectra of the two components of copolymer 29. a. Spectrum of dialkylindenoflourene in THF. b. Spectrum of 25 in THF.

The photoluminescence spectra of **27**, **28** and **29** are presented in Figure 2.17. The emission spectrum of **27** in solution (λ_{ex} = 308 nm) displays a vibronic fine structure with two bands at 417 nm and 434 nm. The thin film emission spectra (λ_{ex} = 340 nm) shows an emission maximum at 423 nm, and a tail into longer wavelengths. The emission spectra of **27** are similar to the spectra of the homopolymer **14**, indicating the optical properties of the copolymer are dominated by the fluorene backbone. The emission spectrum of **28** in solution (λ_{ex} = 364 nm) displays an emission maximum at 418 nm with a shoulder at 433 nm. The thin film emission spectrum (λ_{ex} = 320 nm) shows a broad emission with a maximum at 423 nm, and a tail into longer wavelengths that is similar to the dilute solution emission spectrum of **28**. The emission spectrum of **28** is also similar to that of **22**. The emission spectrum of **29** in solution (λ_{ex} = 353 nm) displays a vibronic fine structure with two bands at 432 nm and 455 nm. The thin film emission spectrum (λ_{ex} = 340 nm) displays an

emission maximum at 436 nm, and a tail into longer wavelengths. The homopolymer **26** exhibits a relatively more intense emission in the longer wavelength region of the spectrum in comparison with **29**. This may be due to better packing for the homopolymer when compared to the copolymer.

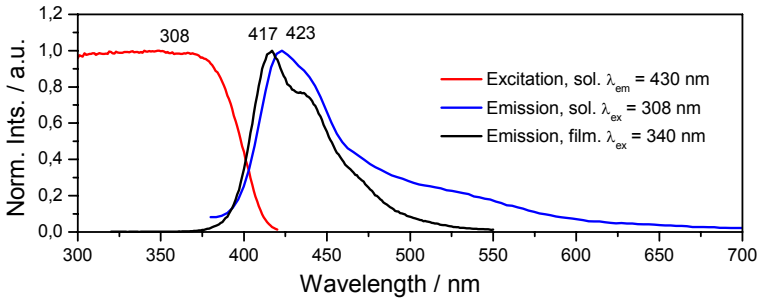

a.

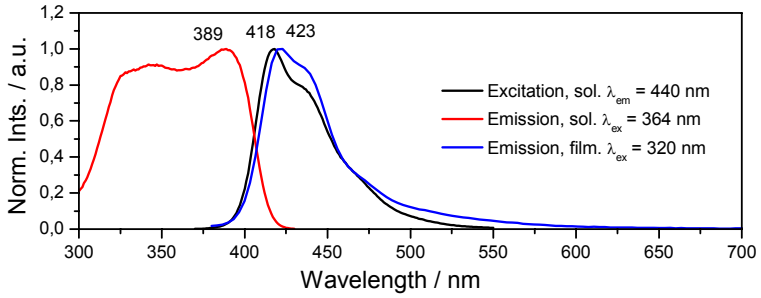

b.

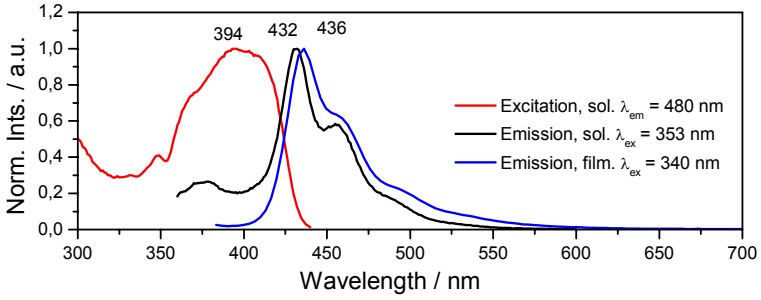

c.

Figure 2.17. The photoluminescence data of 27, 28 and 29 in THF and thin film. a. Excitation (λ_{em} = 430 nm), solution (λ_{ex} = 308 nm) and thin film emission (λ_{ex} = 340 nm) spectra of 27. b. Excitation (λ_{em} = 440 nm), solution (λ_{ex} = 364 nm) and thin film emission (λ_{ex} = 320 nm) spectra of 28. c. Excitation (λ_{em} = 480 nm), solution (λ_{ex} = 353 nm) and thin film emission (λ_{ex} = 340 nm) spectra of 29.

2.2.4 Dendronised PPE-shielding the rigid, linear chain

As previously mentioned, PPE is a promising material for OLED applications, however exhibits a broad, bathochromically shifted emission in the solid state. This has been attributed to aggregation effects, and hence the attachment of oligo-phenylenes dendrons to the rigid, linear polymer should yield a material suitable for use in OLED's. The synthesis of the dendronised PPE is presented in Scheme 2.13.

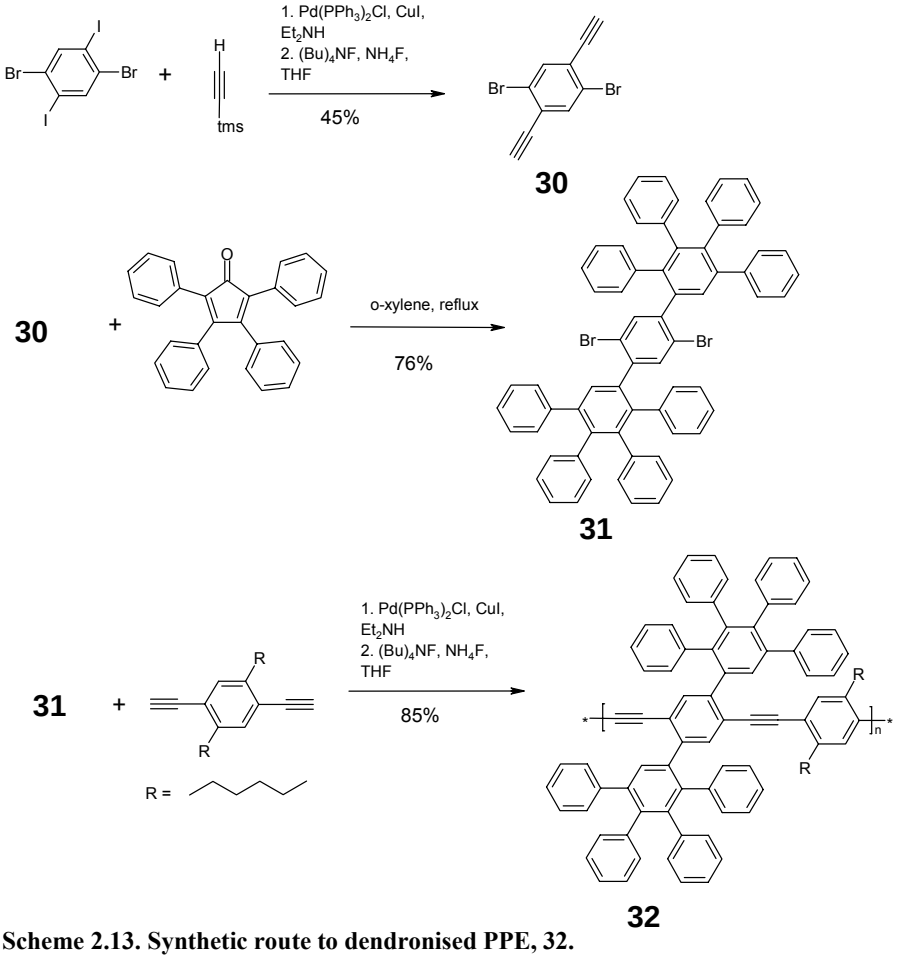

Scheme 2.13. Synthetic route to dendronised PPE, 32.

The selective Hagihara coupling of trimethylsilyl acetylene with 1,4-diiodo-2,5-dibromobenzene, and subsequent deprotection gave **30** in a 45% yield. The low yield of the reaction is due to the further reaction of trimethylsilyl acetylene with the aryl bromide, and the resulting purification of the desired product from this side product. The Diels-Alder addition of **30** to tetraphenylcyclopentadienone gives the dendronised monomer **31**, which was poorly soluble in common organic solvents at

room temperature. **31** was polymerised with 2,5-dihexyl-1,4-diethynylbenzene using Hagihara techniques to yield the dendronised PPE, **32**. **32** required heating for extended periods in order to get the material into solution. GPC analysis, PS standard, demonstrates **32** has a M_n of 670 $gmol^{-1}$, M_w of 980 $gmol^{-1}$, with a D of 1.5. TGA shows **32** is thermally stable up to 350°C. The MALDI-TOF mass spectrum of **32** confirms the major product to be the starting material, with only a small amount of oligomers observed.

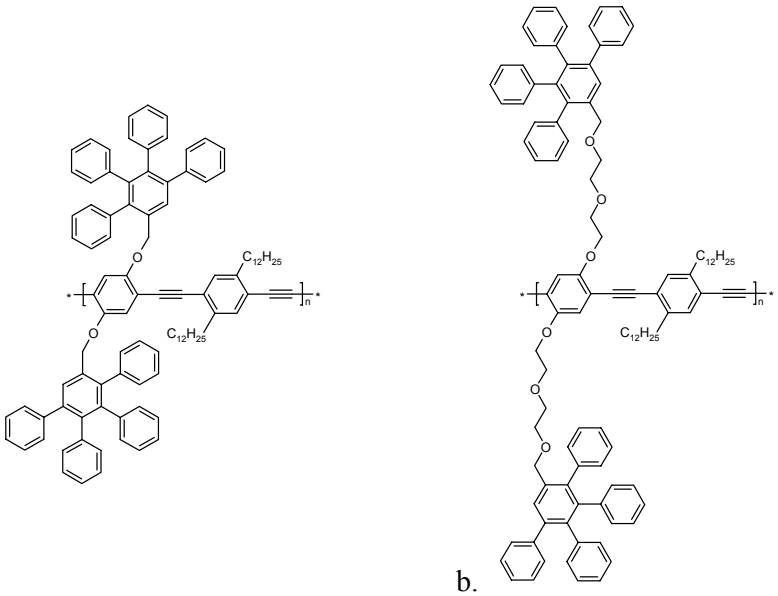

a. b.

Figure 2.18. Structure of dendronised PPE with a. small linker and b. long linker.[37]

Bunz and co-workers have recently published the synthesis and properties of dendronised PPE's.[37] They describe a synthetic scheme similar to that presented in Scheme 2.13, however a flexible spacer is incorporated between the tetraphenyl benzene dendron and the dihalo benzene backbone unit of the PPE. [37] The authors found that the monomer with the shortest spacer between the dendrons and the backbone gave the lowest molecular weight polymer, and that the optical properties of this material are blue-shifted compared to dialkyl substituted PPE's.[37] The longer spacer between the dendron and backbone may inhibit the packing ability of the material, making it more soluble. The reason for the hypsochromic shift is an increased twist in the main chain and an insulation of the chains from each other.[37]

This indicates that the dendrons have a strong influence on the conformational freedom of the polymer chain.[37]

Monomer **31** does not contain a flexible spacer, and the tetraphenyl benzene dendron is ortho to the aryl bromine. This suggests that the initial step of the catalytic polymerisation cycle, the oxidative addition of the aryl bromide to palladium (0), is hindered sterically. This steric hindrance, and the low solubility of the stiff spacerless monomer, inhibits the polymerisation of **31**.

The absorption and photoluminescence characteristics of **32** are displayed in Figure 2.19. The dendronised polymer **32** demonstrates a broad absorption with a maximum absorption at 386 nm. The emission spectrum of **32** in solution (λ_{ex} = 386 nm) displays a broad emission with an emission maximum at 435 nm. The material could not be deposited as a satisfactory film for the thin film emission spectrum to be obtained.

Literature values for the spectroscopic properties of dialkyl substituted PPE's are comparable with the values obtained for **32**. For example, poly(dioctylphenylene ethynylene) has a solution absorption maximum at 384 nm, and an emission maximum of 425 nm, with a shoulder at 440 nm.[38] This comparison suggests that oligomer formation has occurred in the polymerisation reaction to give a material with some PPE character; the relatively low solubility of the material accounts for the observed GPC values.

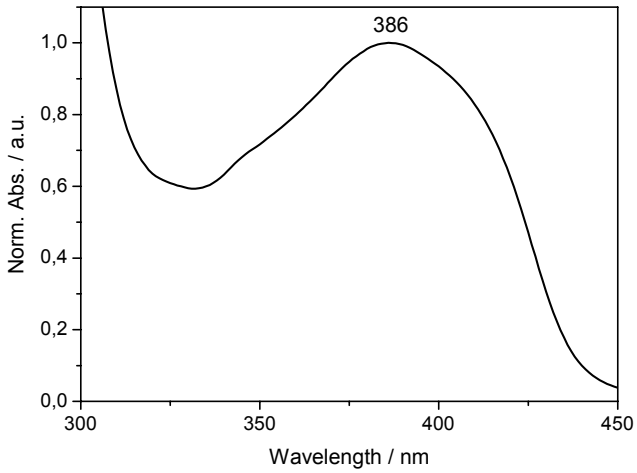

a.

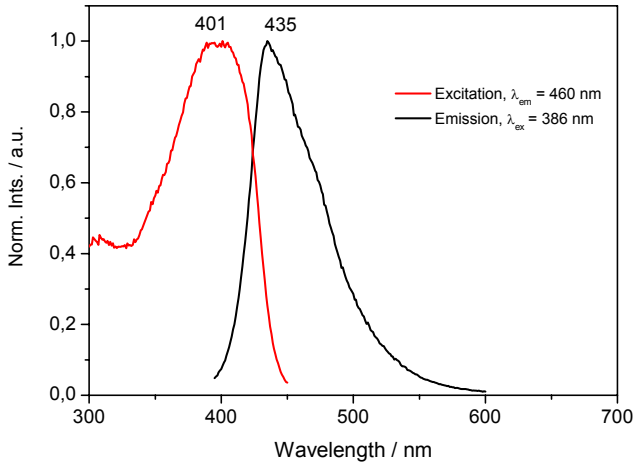

b.

Figure 2.19. Optical properties of 32 in THF. a. UV-vis absorption spectrum of 32. b. Excitation (λ_{em} = 460 nm) and solution (λ_{ex} = 386 nm) spectra of 32.

2.3 Conclusion

One approach that has been shown in the past to be successful in improving the colour stability of poly(fluorene) based OLED's is the dendronisation of the conjugated polymer.[2] A novel and improved synthesis of dendronised poly(fluorene) was developed. The reported synthesis utilised a divergent approach where two convenient building blocks, **2** and **6**, can be transformed into a range of dendronised fluorene monomers by selection of an appropriate tetraphenylcyclopentadienone.

The same first-generation dendronised poly(fluorene) was synthesised from two different macromonomers; with either bromide or chloride as the functional group. The comparison of the molecular weights of the dendronised polymer synthesised in this study, in addition to the literature reports, indicated that the polymerisation of dichloride macromonomers yields polymers of a higher molecular weight. The improved molecular weight is attributed to the higher stability of the C-Cl bond, minimizing any undesirable dehalogenation during polymerisation.

The synthesis of dendronised macromonomers containing moieties to improve charge injection and transport was described. The concept of using oligo-phenylene dendrimers to not only shield the polymer backbone but also as the framework to which a higher concentration of functional groups can be attached, was envisioned to enhance OLED performance. From the two diethynyl intermediates, the fluorene macromonomers with four arylamine substituents were synthesised. The Yamamoto polycondensation of these macromonomers did not yield high molecular weight materials, although the polymer obtained from the dichloride monomer was of a higher molecular weight than from the dibromide. The low molecular weight of the materials was attributed to the low solubility of the arylamine substituents. To test this hypothesis, a related macromonomer with solubilising alkyl chains on the arylamine moieties was synthesised. The polymerisation of this monomer yielded a material of a comparably higher molecular weight, indicating the effect of solubility on the polymerisation of oligo-phenylene dendronised fluorenes. The electrochemical analysis of thin films of the functionalised dendronised polymer show that the barrier for electron and hole injection is indeed improved by the incorporation of the

arylamine units, compared to poly(dioctylfluorene) and poly(9,9-bis(triphenylamine)fluorene).[30,32]

The functionalised dendronised polymer was incorporated into an OLED as the active material. The unoptimised device exhibited poor current-voltage and intensity-voltage characteristics, and lost a large portion of intensity in the first 100 seconds of operation. The spectral stability of films degraded at 210°C in air demonstrates the thermal stability of the polymer. The absence of the low energy band after device operation makes the polymer worthy of further investigation. Further optimisation and characterisation of the material is ongoing.

As a result of the divergent synthetic route described, the synthesis of the second generation dendronised fluorene macromonomer was easily achieved. This was anticipated to result in a dendronised polymer with increased shielding of the polymer backbone, to give an active material with improved colour stability, and to improve the solubility of the material. While the synthesis of the macromonomer was easily achieved, the Yamamoto polycondensation did not proceed to give high molecular weight materials. Contrary to expectations, the higher generation fluorene was not more soluble than the first generation dendronised fluorene. The low solubility was attributed to the low molecular weight of the polymer.

The improvement in colour stability of the dendronised poly(fluorene) based OLED's implies that a similar enhancement of properties can be achieved for poly(indenofluorene) based materials. Utilising a modified synthetic approach, the dendronised indenofluorene monomer was synthesised. Once more, the solubility of the dendronised monomer was lower than that of the alkyl substituted monomer. The polymerisation of the dendronised indenofluorene macromonomer yielded low molecular weight materials, which was attributed to the low solubility of the monomer.

As the solubility of the dendronised materials was considered the primary reason for the inability to obtain high molecular weight materials, copolymers of the arylamine and second generation dendronised fluorene and dendronised indenofluorene were synthesised. However, the solubility of the dendronised

monomers was so poor that the dialkyl fluorene and tetraalkyl indenofluorene comonomer units did not impart enough solubility to yield polymeric materials.

The aggregation of PPE's in thin film, and the subsequent bathochromic shift in the emission, inhibits the use of these materials as the active component in OLED's. In order to suppress this aggregation, the dendronisation of PPE was presented. Again the oligo-phenylene dendrons did not impart solubility, and the Hagihara polymerisation did not proceed to yield polymeric material.

The solubility of the dendronised macromonomers synthesised in this study was reasoned to be the cause for the low molecular weight materials. As the Yamamoto polymerisation generally works best when carried out at a high concentration, the polycondensation reaction was limited by the large amounts of solvent needed to fully dissolve the monomers. Single molecule oligo-phenylene dendrimers are generally soluble in common organic solvents.[21,22,24] The solubility is a result of the amorphous quality of the solid due to poor packing of the dendrimer units, which allows for simple solvation of the molecules. This implies that the monomers described in the beforementioned study have the ability to pack well. The reason for the favourable packing abilities could be the core shape of the dendrimers, *ie* the fluorene and indenofluorene units, which allows for more efficient packing.

The solubility of a dendronised macromonomer has been shown to improve when alkyl chains are attached to the periphery, demonstrated by the alkyl substituted arylamine dendronised fluorene. tetraphenylcyclopentadienone's substituted with alkyl chains are known.[39-41] In future, the synthetic route to dendronised macromonomers should include the use of alkyl substituted tetraphenylcyclopentadienone's. While this would require more synthetic steps to obtain the substituted tetraphenylcyclopentadienone's, as opposed to the commercially available unsubstituted tetraphenylcyclopentadienone, the added solubility appears to be a requirement for the synthesis of reasonably high molecular weight materials.

While the presence of pendant dendrons on poly(fluorene) has been shown to improve device characteristics of OLED's previously, extension of the concept to

other polymer systems has not been successful due to problems in obtaining high molecular weight materials.[2] Yamamoto polymerisation of di-chloro monomers has been shown to give polymers of higher molecular weight than di-bromo monomers, but even here the solubility of the materials precludes very high masses.

2.4 References

(1) Pogantsch, A.; Wenzl, F. P.; List, E. J. W.; Leising, G.; Grimsdale, A. C.; Mullen, K. *Advanced Materials* **2002**, *14*, 1061-1064.

(2) Setayesh, S.; Grimsdale, A. C.; Weil, T.; Enkelmann, V.; Mullen, K.; Meghdadi, F.; List, E. J. W.; Leising, G. *Journal Of The American Chemical Society* **2001**, *123*, 946-953.

(3) Frechet, J. M. J. *Journal Of Polymer Science Part A-Polymer Chemistry* **2003**, *41*, 3713-3725.

(4) Tomalia, D. A.; Frechet, J. M. J. *Journal Of Polymer Science Part A-Polymer Chemistry* **2002**, *40*, 2719-2728.

(5) Zhang, A. F.; Shu, L. J.; Bo, Z. S.; Schluter, A. D. *Macromolecular Chemistry And Physics* **2003**, *204*, 328-339.

(6) Grayson, S. K.; Frechet, J. M. J. *Chemical Reviews* **2001**, *101*, 3819-3867.

(7) Grayson, S. M.; Frechet, J. M. J. *Macromolecules* **2001**, *34*, 6542-6544.

(8) Schluter, A. D. *Comptes Rendus Chimie* **2003**, *6*, 843-851.

(9) Shu, L. J.; Schluter, A. D.; Ecker, C.; Severin, N.; Rabe, J. P. *Angewandte Chemie-International Edition* **2001**, *40*, 4666-4669.

(10) Kim, C.; Kang, S. *Journal Of Polymer Science Part A-Polymer Chemistry* **2000**, *38*, 724-729.

(11) Ouali, N.; Mery, S.; Skoulios, A.; Noirez, L. *Macromolecules* **2000**, *33*, 6185-6193.

(12) Bo, Z. S.; Schluter, A. D. *Macromolecular Rapid Communications* **1999**, *20*, 21-25.

(13) Bo, Z. S.; Schluter, A. D. *Chemistry-A European Journal* **2000**, *6*, 3235-3241.

(14) Marsitzky, D.; Vestberg, R.; Blainey, P.; Tang, B. T.; Hawker, C. J.; Carter, K. R. *Journal Of The American Chemical Society* **2001**, *123*, 6965-6972.

(15) Pogantsch, A.; Wenzl, F. P.; Scherf, U.; Grimsdale, A. C.; Mullen, K.; List, E. J. W. *Journal Of Chemical Physics* **2003**, *119*, 6904-6910.

(16) Kreyenschmidt, M.; Uckert, F.; Mullen, K. *Macromolecules* **1995**, *28*, 4577-4582.

(17) Grell, M.; Bradley, D. D. C.; Long, X.; Chamberlain, T.; Inbasekaran, M.; Woo, E. P.; Soliman, M. *Acta Polymerica* **1998**, *49*, 439-444.

(18) Morin, J. F.; Leclerc, M. *Macromolecules* **2001**, *34*, 4680-4682.

(19) Morin, J. F.; Leclerc, M. *Macromolecules* **2002**, *35*, 8413-8417.

(20) Klaerner, G.; Miller, R. D. *Macromolecules* **1998**, *31*, 2007-2009.

(21) Morgenroth, F.; Reuther, E.; Mullen, K. *Angewandte Chemie-International Edition In English* **1997**, *36*, 631-634.

(22) Morgenroth, F.; Berresheim, A. J.; Wagner, M.; Mullen, K. *Chemical Communications* **1998**, 1139-1140.

(23) Qu, J. Q.; Pschirer, N. G.; Liu, D. J.; Stefan, A.; De Schryver, F. C.; Mullen, K. *Chemistry-A European Journal* **2004**, *10*, 528-537.

(24) Wiesler, U. M.; Berresheim, A. J.; Morgenroth, F.; Lieser, G.; Mullen, K. *Macromolecules* **2001**, *34*, 187-199.

(25) Thelakkat, M. *Macromolecular Materials And Engineering* **2002**, *287*, 442-461.

(26) Tang, C. W.; Vanslyke, S. A. *Applied Physics Letters* **1987**, *51*, 913-915.

(27) Sainova, D.; Miteva, T.; Nothofer, H. G.; Scherf, U.; Glowacki, I.; Ulanski, J.; Fujikawa, H.; Neher, D. *Applied Physics Letters* **2000**, *76*, 1810-1812.

(28) Chen, J. P.; Klaerner, G.; Lee, J. I.; Markiewicz, D.; Lee, V. Y.; Miller, R. D.; Scott, J. C. *Synthetic Metals* **1999**, *107*, 129-135.

(29) Miteva, T.; Meisel, A.; Knoll, W.; Nothofer, H. G.; Scherf, U.; Muller, D. C.; Meerholz, K.; Yasuda, A.; Neher, D. *Advanced Materials* **2001**, *13*, 565-567.

(30) Ego, C.; Grimsdale, A. C.; Uckert, F.; Yu, G.; Srdanov, G.; Mullen, K. *Advanced Materials* **2002**, *14*, 809-811.

(31) Neher, D. *Macromolecular Rapid Communications* **2001**, *22*, 1366-1385.

(32) Janietz, S.; Bradley, D. D. C.; Grell, M.; Giebeler, C.; Inbasekaran, M.; Woo, E. P. *Applied Physics Letters* **1998**, *73*, 2453-2455.

(33) Dapperheld, S.; Steckhan, E.; Brinkhaus, K. H. G.; Esch, T. *Chemische Berichte* **1991**, *124*, 2557-2567.

(34) Nelson, R. F.; Adams, R. N. *Journal Of The American Chemical Society* **1968**, *90*, 3925-&.

(35) Larumbe, D.; Moreno, M.; Gallardo, I.; Bertran, J.; Andrieux, C. P. *Journal Of The Chemical Society-Perkin Transactions 2* **1991**, 1437-1443.

(36) Setayesh, S.; Marsitzky, D.; Mullen, K. *Macromolecules* **2000**, *33*, 2016-2020.

(37) Englert, B. C.; Smith, M. D.; Hardcastle, K. I.; Bunz, U. H. F. *Macromolecules* **2004**, *37*, 8212-8221.

(38) Bunz, U. H. F. *Chemical Reviews* **2000**, *100*, 1605-1644.

(39) Loi, S.; Wiesler, U. M.; Butt, H. J.; Mullen, K. *Macromolecules* **2001**, *34*, 3661-3671.

(40) Iyer, V. S.; Yoshimura, K.; Enkelmann, V.; Epsch, R.; Rabe, J. P.; Mullen, K. *Angewandte Chemie-International Edition* **1998**, *37*, 2696-2699.

(41) Wu, J. S.; Watson, M. D.; Tchebotareva, N.; Wang, Z. H.; Mullen, K. *Journal Of Organic Chemistry* **2004**, *69*, 8194-8204.

3 Electron transporting materials

3.1 Introduction

Most conjugated polymers are p-type conductors, and so the injection of holes and electrons in an OLED is not balanced. This imbalance of charge carrier injection results in reduced device performance. As there are relatively few examples of n-type polymer in literature, there is an increasing need to develop new classes of n-type materials. [1-3]

Novel n-type conducting polymers can also be used as an active material in other types of optoelectronic devices such as solar cells. When solar radiation is converted into electrical power, the reverse process of an OLED, the device is called a solar cell. The photovoltaic process involves absorption of a photon, charge separation and charge migration to the electrodes. Practically all photovoltaic devices incorporate a pn-junction in semiconductor, across which a photovoltage is formed.[4] The synthesis of novel n-type polymers can contribute to the field of organic solar cells. These have the same advantages over inorganic solar cells that were mentioned in Section 1, namely cost, processability and potential for chemical functionalisation.

The synthesis and characterisation of two varieties of n-type polymers are presented. The synthesis of oxadiazole containing polymers is undertaken by two routes. The first is a novel synthesis of a previously reported oxadiazole containing monomer; the second is a variation of a previously published synthetic route to yield a novel monomer. The second type of electron transporting polymer discussed is the fluorenone-based polymer. The novel synthesis of the first soluble poly(fluorenone) and the subsequent characterisation are presented in the following section.

Results and Discussion

3.1.1 Oxadiazole containing poly(fluorene)

Prior to the publication of Jen *et al.*, the synthesis of the fluorene monomer bearing oxadiazole substituents at the 9-position was attempted via a different route. The oxadiazole functionality was initially generated and then attached to 4,4'-dibromobiphenyl-2-carboxylate via aryl lithium addition. The novel synthetic route to the oxadiazole fluorene monomer, and subsequent polymerisation, is shown in Scheme 3.1.

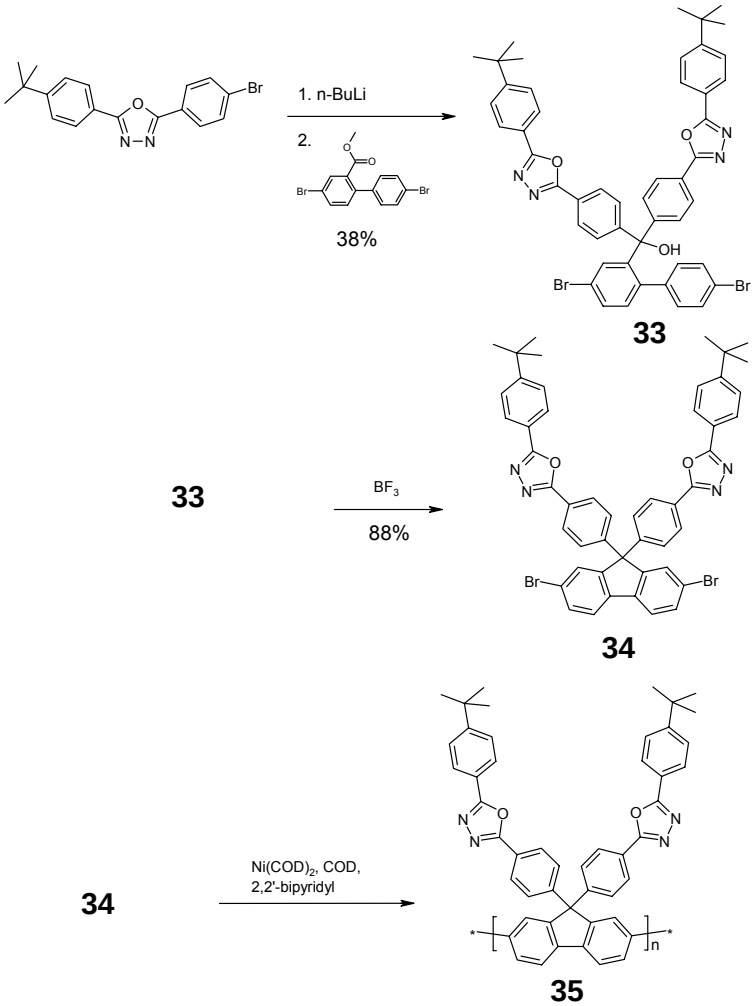

Scheme 3.1. Synthetic route to oxadiazole containing poly(fluorene), 35.

The oxadiazole aryl lithium addition to the methyl ester function to form **33** proceeded with a yield of 38%, the low yield in part due to complications in the purification of the material. The BF_3 ring closure proceeded in high yield, to afford **34** at 88%. The Yamamoto polymerisation of **34** only gave low molecular weight materials as a consequence of the low solubility of the monomer. The GPC analysis of **34** shows a M_n of 6.5 x 10^3 g mol^{-1}, M_w of 1.8 x 10^4 g mol^{-1}, and a D of 2.8 against a PS standard, and a M_n of 5.1 x 10^3 g mol^{-1}, M_w of 1.2 x 10^4 g mol^{-1}, and a D of 2.3 against a PPP standard. This corresponds to a degree of polymerization of about 7 units (calculated from the M_n against PPP standard). The suspicion of the low solubility of the oxadiazole unit is further illustrated by the low molecular weight of the copolymer of **34** with dioctylfluorene, a M_n of 1.3 x 10^4 g mol^{-1} against a PS standard.[5]

As the poor solubility of the oxadiazole substituted fluorene was thought to be the primary cause for the observed low molecular weight of the homopolymer **35**, a monomer unit with a long alkyl chain as a solubilising group on the oxadiazole was prepared. The synthesis of a more soluble analogue of the bromooxadiazole in Scheme 3.1 was deemed to be less preferable than the modified synthesis of Jen *et al*.[5] The synthesis of the soluble oxadiazole containing fluorene monomer and its subsequent polymerisation is shown in Scheme 3.2.

In addition to the synthesis discussed above, in a slightly different approach to the same monomer, dibromo fluorene was first used in a nucleophilic substitution reaction with 4-fluorobenzonitrile.[5] This approach reduced the synthesis of the monomer by one step. The purification of the dibenzonitrile substituted fluorene **36** was difficult and involved washing with methylene chloride, which resulted in a low yield of 13% for the reaction. The reaction of **36** with sodium azide to form the bistetrazole substituted fluorene proceeded quantitatively to give **37**. Coupling of **37** with 4-decylbenzoic acid chloride afforded the oxadiazole containing monomer **38**, in 83% yield. The Yamamoto polymerisation of **38** gave the homopolymer **39** in an isolated yield of 33%.

The polymer **39** is only sparingly soluble in organic solvents. The GPC analysis of the THF soluble fraction of **39** shows a M_n of 1.6 x 10^4 g mol^{-1}, M_w of 3.9 x 10^4 g

mol^{-1}, and a D of 2.4 against PS standard, and a M_n of 1.2 x 10^4 g mol^{-1}, M_w of 2.3 x 10^4 g mol^{-1}, and a D of 2.0 against PPP standard. This corresponds to a degree of polymerisation of 17 units.

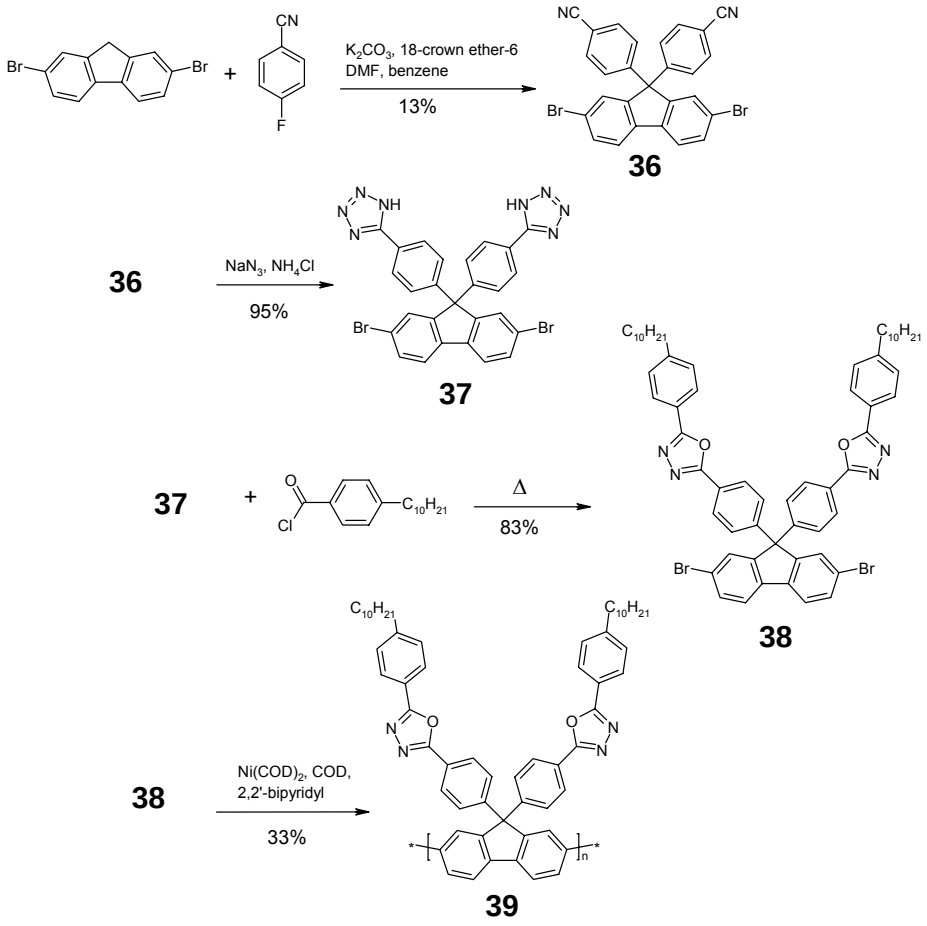

Scheme 3.2. Synthetic route to oxadiazole substituted poly(fluorene), 39.

The absorption and photoluminescence spectra of **39** are presented in Figure 3.1. **39** in solution exhibits a broad absorption with a maximum at 389 nm, corresponding to the π-π* transition of the poly(fluorene) backbone. The additional absorption at shorter wavelengths with a maximum at 303 nm is due to the oxadiazole sidechains, as literature reports of oxadiazole molecules such as 2,5-di-(4-*t*-butylphenyl)-1,3,4-oxadiazole show an absorption maximum of 298 nm.[5] The emission spectrum of **39** (λ_{ex} = 300 nm) in solution shows photoluminescence from the poly(fluorene) backbone exclusively, with a maximum emission at 408 nm, and no contribution from the oxadiazole moiety. The thin film emission maximum is 426

nm, and has a significant shoulder 550 nm. The spectroscopic characteristics of **39** are comparable with the published results of Jen *et al.*

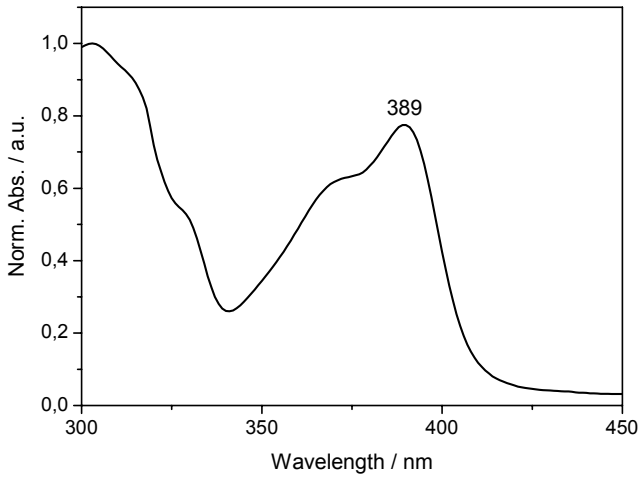

a.

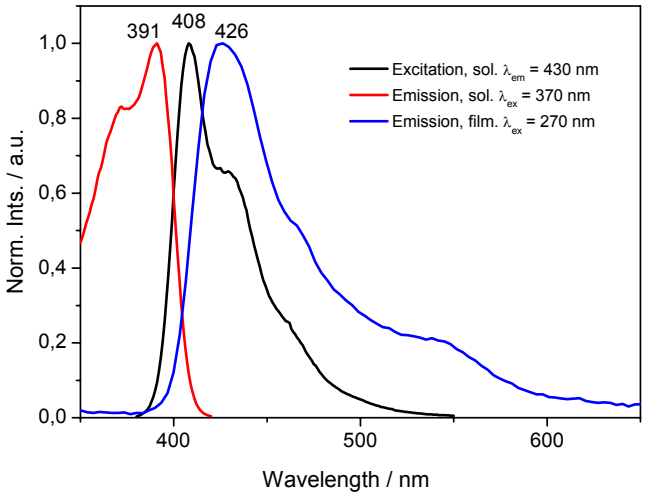

b.

Figure 3.1. Optical properties of 39 in THF and thin film. a. UV-vis absorption spectrum of 39. b. Excitation (λ_{em} = 430 nm), solution (λ_{ex} = 370 nm) and thin film emission (λ_{ex} = 300 nm) spectra of 39.

The thin film obtained from a filtered solution of **39** was not of a high quality, which we attribute to be due to the low solubility of the polymer. In order to be the active material in a device, high quality films in the order of 100 nm are needed. Due to the low solubility of **39**, this material was not incorporated into an OLED.

3.1.2 Soluble Poly(fluorenone)

Poly(fluorenone) is an insoluble material due to the rigid planar nature of the monomer and the strong dipole interactions that exits in the solid state. In order to prepare a soluble poly(fluorenone) analogue, a substituent that inhibits the stacking must be introduced. However, the position best suited for substitution on the fluorene unit, C-9, is blocked by the ketone. In order to overcome this problem, a fluorenone substituted at the 4 position was synthesised. The 4 position was selected as the substitution point as this is the next reactive position for electrophillic aromatic substitution, after 2 and 7.

The first synthetic route to a soluble poly(fluorenone) began with the Sandmeyer conversion of a commercially available 4-aminofluorenone to the corresponding iodo material, **40**. The bromination of **40** was attempted, however the presence of the ketone function requires the use of strong brominating conditions. Use of N-bromo succinimide in sulphuric acid resulted in a reaction mixture that contained mono-, di-, tri- and tetra substitution products. In order to be able to apply mild bromination techniques, **40** was reduced with hypophosphoric acid and iodine to 4-iodofluorene. Bromination using copper bromide on alumina of 4-iodofluorene did not proceed cleanly, and gave a mixture of products that included the oxidised monobromo fluorene and the product without an iodide. This mixture of products could not be purified satisfactorily, and as such, an alternate synthetic route was developed.

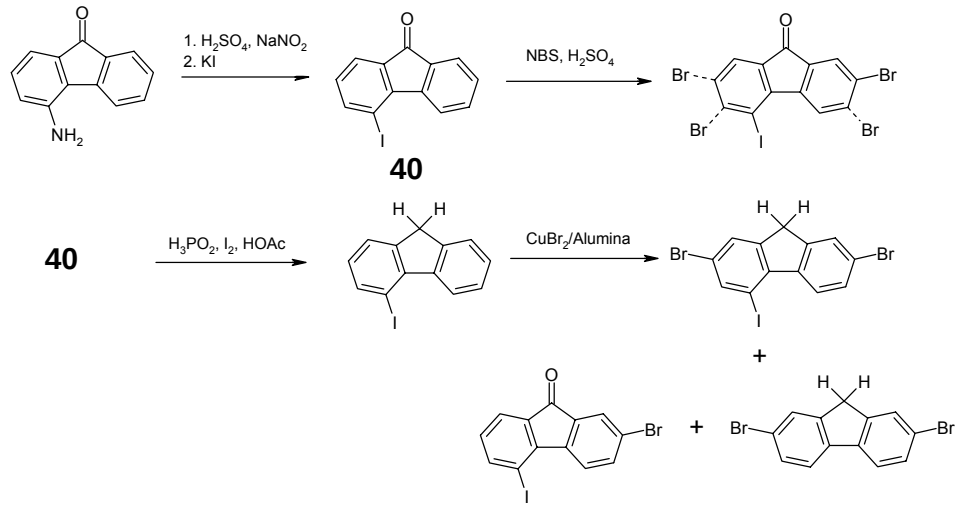

Scheme 3.3. First synthetic route to soluble poly(fluorenone).

As the bromination of either the fluorene or fluorenone units was unsuccessful, a synthetic scheme where the commercial starting material already contains the bromo functions was developed. The synthesis, and subsequent polymerisation, of the 4-dendronised 9-fluorenone monomer is shown in Scheme 3.4.

2,7-dibromofluorene was nitrated according to literature procedures, then reduced to the amino substituted fluorene **41** using tin and hydrochloric acid, the Clemmensen reduction, with a yield of 87%.[6] The amino functionality was converted using a Sandmeyer reaction to give the 2,7-dibromo-4-iodofluorene **42** in 70% yield, which was oxidised to the corresponding fluorenone **43**, with a yield of 87%. Selective Hagihara-Sonogashira cross coupling of **43** with trimethylsilyl acetylene, followed by the deprotection of the trimethylsilyl with potassium carbonate, afforded **44** in a yield of 68%. A Diels-Alder reaction of **44** with a dialkyl substituted tetraphenylcyclopentadienone yielded the tetraphenylbenzene substituted dibromofluorenone monomer **45**, in 68% yield. The long dove-tail alkyl chain was selected as the substituent on the dendrimer as it has been shown previously to dramatically increase the solubility of materials.[7,8] **45** was polymerised under Yamamoto conditions to yield **46**.

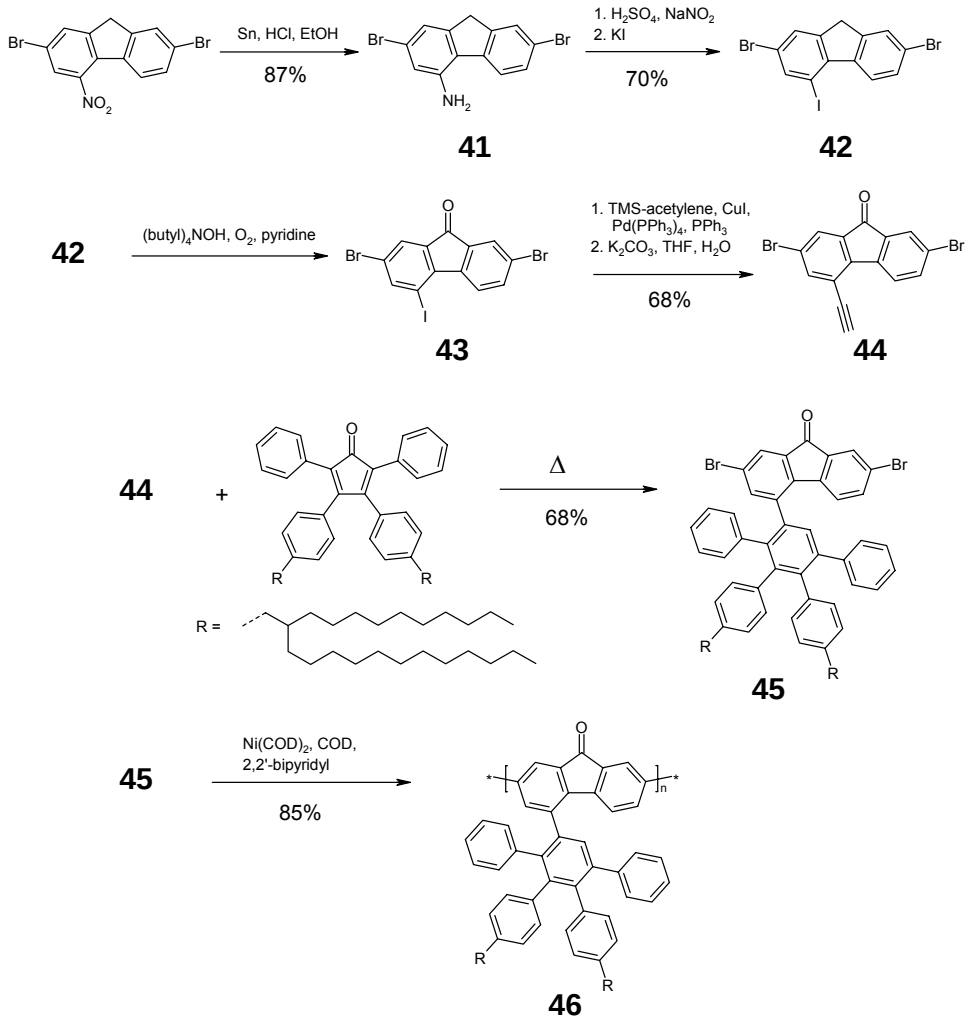

Scheme 3.4. Synthetic route to dendronised poly(fluorenone), 46.

The dendronised poly(fluorenone) is soluble in common organic solvents such as toluene and THF. GPC analysis of **46** shows a M_n of 4.10 x 10^4 g mol^{-1}, M_w of 1.50 x 10^5 g mol^{-1}, and a D of 3.50 against PS standard, and a M_n of 2.70 x 10^4 g mol^{-1}, M_w of 7.00 x 10^4 g mol^{-1}, and a D of 2.60 against PPP standard. This corresponds to a degree of polymerisation of 22 units. TGA indicates that **46** has good thermal stability up to 400 °C. The DSC analysis shows that **46** has an amorphous structure with no phase transition between –100°C and 350°C, due to the bulky tetraphenylbenzene substituents on the polymer.

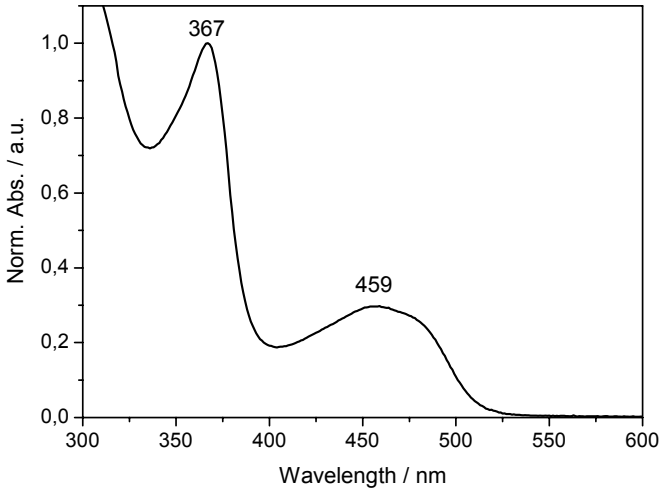

a.

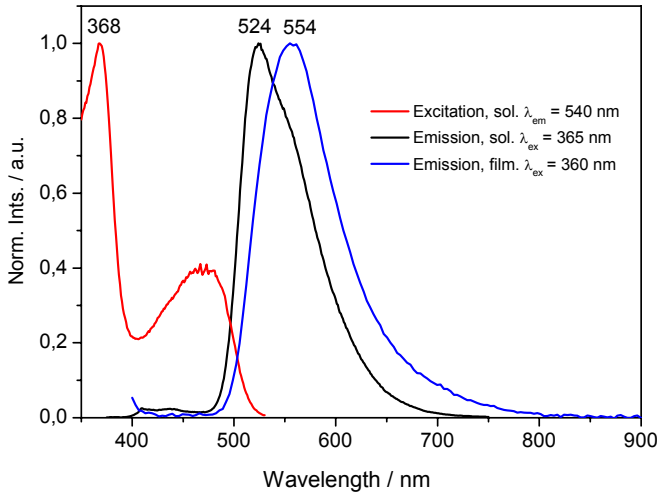

b.

Figure 3.2. Optical properties of 46 in THF and thin film. a. UV-vis absorption spectrum of 46. b. Excitation (λ_{em} = 540 nm), solution (λ_{ex} = 365 nm) and thin film emission (λ_{ex} = 360 nm) spectra of 46.

The absorption and photoluminescence spectra of **46** are presented in Figure 3.2. The dendronised poly(fluorenone) shows an absorption spectrum, Figure 3.2a, with a maximum at 367 nm corresponding to the polyphenylene conjugated backbone, and another transition band at 459 nm from the n-π* transition of the ketone.[9]

The ketone n-π* transition is symmetry forbidden, however Figure 3.2 shows a relatively strong absorption when compared to the absorption at 367 nm. The

absorption spectrum of the monomer **45** shows a much weaker absorption for this n-π* transition, which is hypsochromically shifted to 418 nm. The low energy and increased intensity of this absorption is due to the interactions with the delocalised π-system.[9]

Figure 3.2b shows the excitation and emission spectra of **46** in solution (λ_{ex} = 365 nm) and solid state (λ_{ex} = 360 nm). **46** has a broad featureless emission, with a maximum at 524 nm in solution, and 554 nm in solid state. This corresponds to an emission from the ketone moiety, indicating efficient energy transfer from the conjugated backbone to the ketone.

In order for **46** to be considered an ETM it must show a reversible reduction, with an appropriate reduction potential.[3] CV was measured on a film of **46** deposited on a carbon electrode in CH_3CN/ClO_4 with a platinum counter electrode and a silver quasi-reference electrode, calibrated against ferrocene-ferrocenium. The cyclic voltamograms of **46** are presented in Figure 3.3. **46** shows an oxidation onset at 1.4 V, and a reduction onset at -1.45 V. The method to transform the oxidation and reduction onset values to the IP and EA values respectively was discussed in Section 2. If the work function of silver is taken to be 4.4 eV, the IP and EA values of **46** are found to be at -5.8 eV and -2.95 eV respectively.[10] For comparison, the EA of poly(fluorenone) from a precursor polymer was found to be at –3.3 eV, when measured by cyclic voltammatry.[9] The electrochemical band gap of **46** is then calculated to be 2.85 eV. The optical band gap, as calculated by the onset of absorption at 525 nm, is calculated to be 2.36 eV. The electrochemical bandgap is significantly larger than the optical bandgap, by approximately 0.5 eV. This is not unprecedented, as the electrochemical bandgap of poly(dioctylfluorene) was also found to be higher than the optical bandgap, by 0.75 eV.[11] It has been found that redox reactions on thin films generally occur at higher oxidation and reduction potentials than in solution, which would explain the higher values for the electrochemical bandgap, measured on thin films.[12]

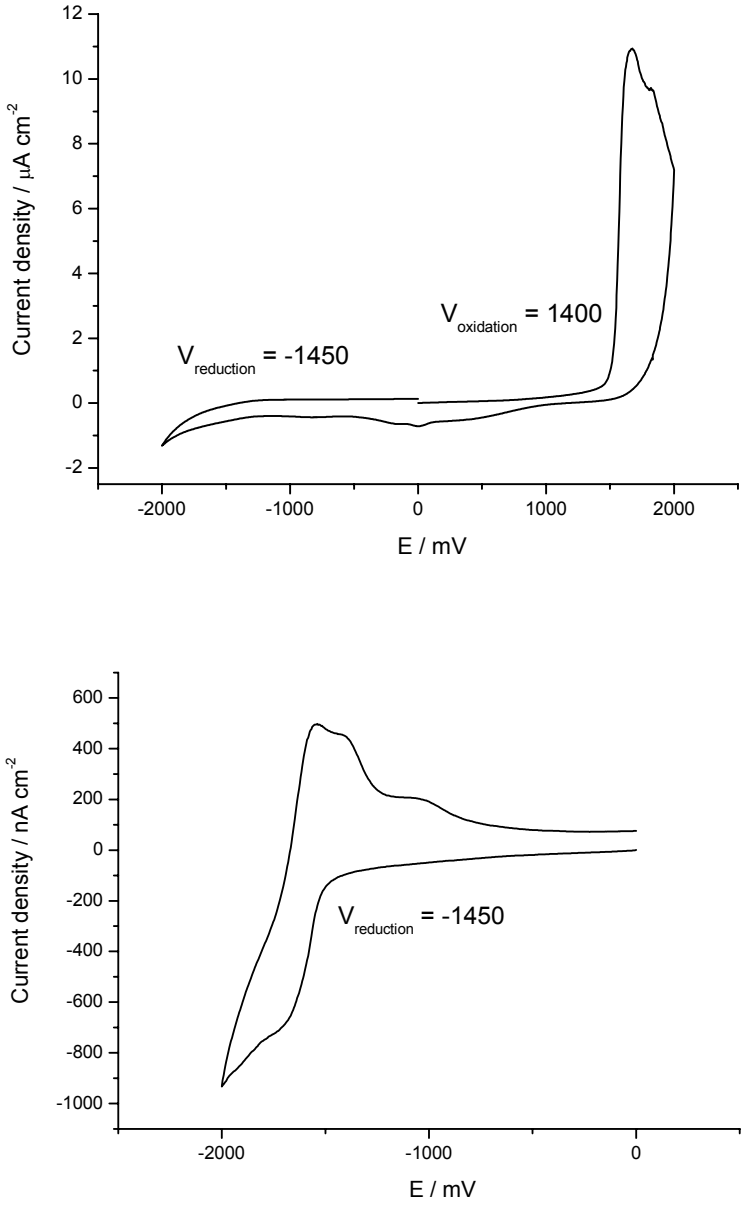

Figure 3.3. Cyclic voltamogram of thin film of 46. a. Full plot. b. Reduction. Onset voltage of oxidation and reduction is shown.

The CV of **46** was measured for direct comparison with the previously reported EA levels of poly(fluoreneone). A more sensitive and precise method to measure of the reduction potential of a material is differential pulse voltammetry.[13] These advantages arise from the ease with which the signal can be separated from the background. The differential pulse voltamogram of **46** is presented in Figure 3.4.

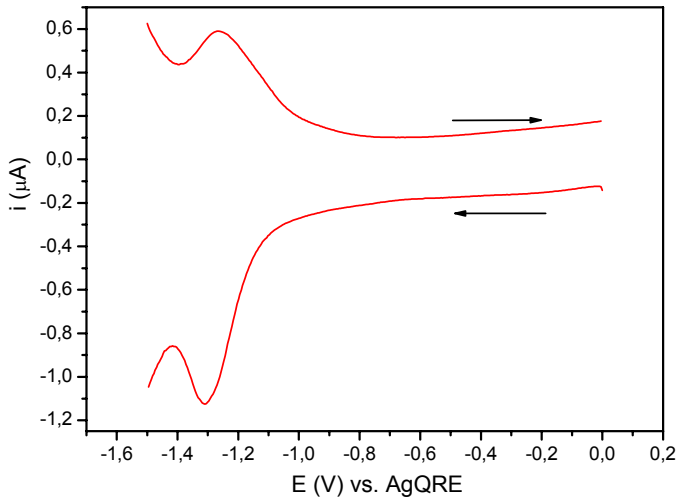

Figure 3.4. Differential pulse voltammogram (reduction) of 46 vs AgQRE (film on gold, 0.1 M $TBAClO_4$ in Acetonitrile).

The differential pulse voltammogram exhibited a reversible reduction with a reduction potential of -1.29 V vs AgQRE for **46**. Using the ferrocene/ferrocenium standard, the silver quasi reference electrode was measured to have a work function of 4.33 eV. This leads to an EA of -3.04 eV for **46**. While it is more appropriate to compare the CV results of the poly(fluorenone) prepared by the precursor route with the CV results of **46**, the differential pulse voltammogram yields more accurate values for the EA of the material.[9] The LUMO level of poly(fluorenone), obtained from a precursor polymer, was found to be at –3.3 eV, when measured by cyclic voltammatry.[9] This means that **46** is not as easy to reduce compared to the unsubstituted poly(fluorenone). This could be due to the dendronised side chain on **46** where the alkyl chains and phenyl groups shield the ketone moiety, making it less susceptible for reduction. **46** is still a better electron acceptor when compared to other prevalent ETM such as PBD, which has a LUMO level of –2.4 eV.[14] While PBD exhibits good electron mobility, the electron injection barrier is high, *ie* 1.3 eV for a magnesium cathode (Φ = -3.7 eV), compared to 0.66 eV for **46**.[14] Other electron deficient polymers that have been used in the past as the ETM lack redox stability. The cyano substituted PPV, CN-PPV, has been successfully used as the ETM in an OLED, but shows an irreversible reduction.[15,16]

The mobility of material is used to describe the relationship between the drift velocity of the charge carrier, electrons or holes, and an applied electric field. One technique to measure the mobility of a material is by the time-of-flight (TOF) method. In a typical experimental setup, the material is filled between two quartz plates that are covered by semitransparent aluminium electrodes.[17,18] The thickness of the cells is in the order of 10-30 μm, and must be accurately known.[17,18] Pulsed laser irradiation into the absorption band of the material leads to the creation of electron-hole pairs.[17,18] Importantly, the penetration depth of the laser pulse is less than 1 μm, and so the charge carrier pairs are only formed close to one electrode.[17,18] Depending on the polarity of the electric field, either holes or electron charge carrier packets drift across the sample cell to the opposite electrode, causing a displacement currents that are measured in an external circuit.[17,18] The transient time of the charge carrier packets is taken from the stepped decay nature of the current versus time plots.[17,18] The mobility of the charge carriers, μ, in $cm^2V^{-1}s^{-1}$, is derived from the sample cell thickness, l, transient time, t_T, and the applied voltage, V, as shown in Equation 3.1.[17,18] Generally, the measurement of electron mobility is considered more difficult than the measurement of hole mobility due to difficulties in removing oxygen from the sample, which acts as a trapping site.[17]

Equation 3.1. Charge carrier mobiltiy as function of transient time and electric field.

$$\mu = l^2 t_T^{-1} V^{-1}$$

The technique of TOF requires relatively thick films, of the order of tens of microns, in order for the penetration depth of the laser pulse to be less than 5% of the film thickness. This is important for the production of charge carrier packets that traverse the entire, known thickness of the films. The motivation for the synthesis of **46** was to produce an n-type material that possessed high electron mobility. In order to establish this, the TOF measurement was attempted on **46**.

Films of **46** were deposited onto prepared ITO substrates by drop casting from a filtered, saturated toluene solution. Two samples were prepared; a thick sample of approximately 10 μm, and a thin sample of about 1 μm. Subsequently, an aluminium

electrode was deposited by vacuum sublimation through a mask. The aluminium cathode that was deposited on the 1 μm thick sample of **46** desorbed, and the sample was discarded. The 10 μm sample was arranged in the experimental set up, and irradiated under a bias (YAGNd laser, 3rd harmonic. λ_{ex} = 355 nm). The bias was ramped from 0 V to 300 V, however no current signal was observed. There are a number of possible reasons for the lack of signal. The deposited film was inhomogeneous to the eye, which would make the TOF measurement difficult to obtain. Also, the excess roughness from the film may result in deep energy trapping sites in the film. Another reason for the lack of signal could be the lack of percolation pathways between the created excitons and the aluminium electrodes. Lastly, the electron-hole pairs may not have formed in the experiment.

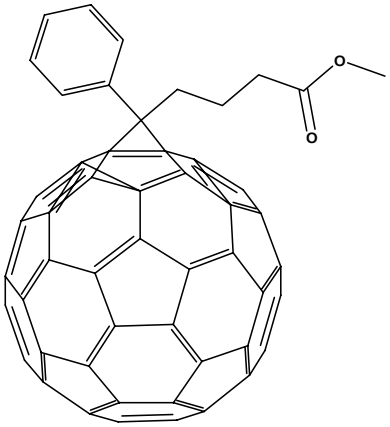

Figure 3.5. Structure of PCBM.

Organic photovoltaic devices have the potential to be a major source of energy in the future, and recently has been the subject of much research.[19-21] The opposite of an OLED, a solar cell requires the absorption of a photon, charge separation, and charge transport to the electrodes, as shown in Figure 3.6.[19] This means the active materials must have a high absorption over a wide range of the solar spectrum, the HOMO and LUMO values of the donor and acceptor materials must be correctly aligned and the active materials must have good charge carrier mobility.[19] **46** was incorporated into a simple organic solar cell with (6,6)-phenyl-C61-butyric acid methyl ester (PCBM), Figure 3.5, in order to test the basic photovoltaic properties of the material. PCBM is widely and successfully used as the acceptor material in solar cells, with polymeric compounds usually incorporated as the donor material.[19,22] In

order to test the material properties of **46**, not the acceptor properties, the polymer was included as the donor material in a solar cell with the proven acceptor PCBM. From the schematic energy level diagram presented in Figure 3.6 it can be seen that the energy levels of **46** and PCBM match well. Figure 3.2 demonstrates that **46** has an absorption up to 500 nm, and so covers a large section of the solar spectrum. In subsequent studies it is envisaged that a polymer-only solar cell will be fabricated, with **46** as the acceptor and another polymeric donor such as poly(carbazole). The solar cell was fabricated as a bulk heterojunction solar cell, where photo-induced electron transfer occurs in an interpenetrating donor and acceptor network.[19]

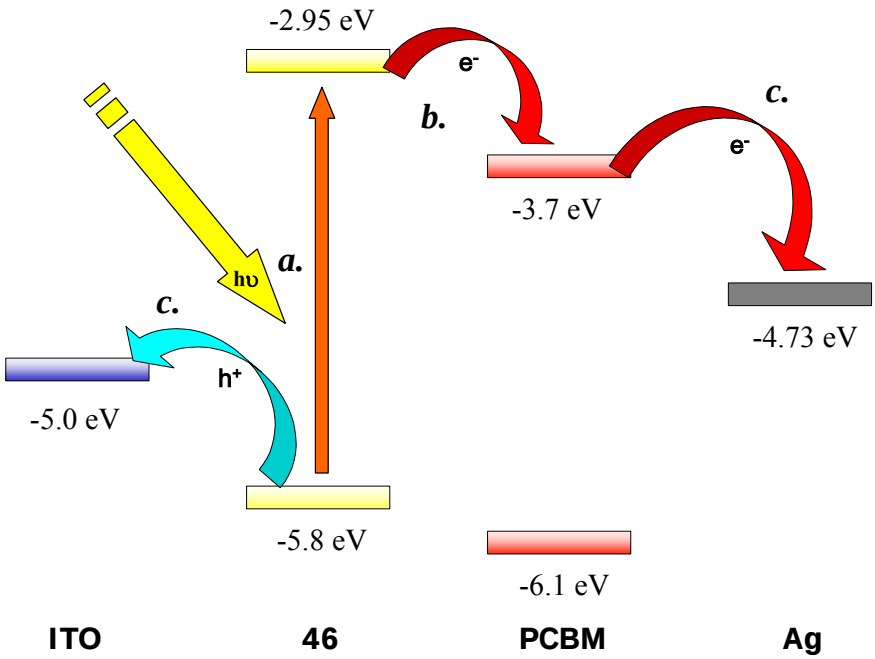

Figure 3.6. Schematic diagram of energy levels of ITO, 46, PCBM and silver. The processes of the photovoltaic effect are also shown schematically. a. absorption of a photon b. charge separation c. charge transport to the electrodes.

The photovoltaic devices were fabricated by spin coating films of the active materials, 1:1 by weight, onto ITO substrates pre-treated with acetone and isopropanol in an ultrasonic bath, followed by cleaning for 10 minutes with oxygen plasma. A 100 nm thick silver cathode was subsequently evaporated through a mask. The effective area of the device was approximately 6 mm^2, defined by the overlap of the etched ITO and the cathode, which was accurately measured by an optical microscope. A tungsten-halogen lamp was employed as the light source, supplying

monochromatic light from 300 nm to 800 nm through a TRIAX 180 monochromator. Incident light intensity was determined by a calibrated silicon diode. The maximum intensity was 6 Wm^{-2} at ca. 600 nm. Devices were tested under a nitrogen atmosphere.

Two solutions of **46** were spin coated onto the ITO substrates, a 15 mg mL^{-1} chloroform solution and a 5 mg mL^{-1} 1,1,2,2-tetrachloroethane solution. The 1,1,2,2-tetrachloroethane solution was filtered through a 0.45 micron syringe filter before being spin coated onto the substrates. Although the chloroform solution appeared to be fully dissolved, this solution physically could not be filtered through the syringe filter, and was spin coated without filtering. As a result, the prepared film did not appear homogeneous. A silver electrode was deposited on the polymer covered substrates, and the organic photovoltaic devices were tested using the testing setup described above.

Both of the device configurations, *ie* with films prepared from a filtered tetrachloroethane solution and from an unfiltered chloroform solution, did not show any photovoltaic behaviour. The current-voltage curves exhibited short circuit behaviour, where the plot is a straight line through the origin. This indicates the photovoltaic devices were just resistors in the circuit, and did not produce any photocurrent. These results were attributed to the film forming behaviour of **46**. The short circuit behaviour of the devices is indicative of the formation of pin holes or a thin film of the active materials. A lack of solubility of the polymer meant that it is not known how much of the polymeric material was filtered from the solution that was spin coated. The thin film produced from the filtered solution and the inhomogeneous film prepared from the unfiltered chloroform solution were not of a high enough quality for use in an organic solar cell. The current-voltage characteristics of the cells are attributed to the poor film quality.

For future photovoltaic experiments, **46** must exhibit better film forming behaviour. The preparation of high quality films requires that the solution be of a high enough concentration, and that the solutions can be filtered, to yield homogeneous films of the material of the correct thickness.

While the emission characteristics of thin films of **46** could be determined, the characterisation of the charge carrier mobility by TOF and the photovoltaic performance in a solar cell could not be obtained. The reason for this inability to observe these two physical processes has been attributed to the poor film forming abilities of **46**. While the material is soluble enough for spectroscopic studies, high concentration homogeneous solutions could not be achieved. Especially for TOF measurements, which require films in the order of ten of microns, the low concentration solutions could not be transferred into high quality films of the thickness required. As such, for the complete characterisation and utilisation of **46** as an ETM, a more soluble polymer must be produced. One possible solution to this problem would be to introduce more and larger solubilising alkyl groups to the periphery of the dendrimer, or to introduce a larger generation dendrimer onto the fluorenone unit to further reduce the π-stacking of the repeat units. The tetradecyl decyl alkyl groups of **46** are already very large and are well known to be good solubilising groups for materials with a tendency to aggregate. In Section 2 it was demonstrated that an increase in dendrimer generation does not necessarily translate into an increase in solubility.[7,8] A more practical solution would be to limit the molecular weight of the polymer. This could be achieved with the addition of a calculated amount of a monofunctionalised end-capping material. It is envisioned that a lower molecular weight material would be more soluble than the polymer produced without the addition of an end-capping agent. This synthesis is currently being undertaken.

3.2 Conclusion

In the hope of improving the processability and performance of current oxadiazole based electron transporting materials, two oxadiazole containing poly(fluorene) products have been synthesised and characterised. An alternate synthetic route has been developed for the synthesis of an oxadiazole containing fluorene monomer, using an aryl lithium approach. The polymer obtained from the Yamamoto polycondensation of this monomer yielded a material that is only sparingly soluble. The synthetic method can be applied to other systems, such as the ladder-type pentaphenylene mentioned in Section 1, substituting the four aryl groups with oxadiazole to give a monomer that includes functionalities for electron transport and solubility.[23]

In order to increase the solubility of the oxadiazole containing polymers, the synthesis of a monomer with larger alkyl groups was performed, using the previously reported literature method.[5] The Yamamoto polycondensation of this more soluble monomer resulted again in a material that is only sparingly soluble. The film forming properties of the polymer was not satisfactory enough to warrant the inclusion of this material in an OLED. The solubility of oxadiazoles, which has been previously commented on, is an issue in the synthesis of polymers containing oxadiazoles for optoelectronic applications.[24] The synthesis of oxadiazoles bearing groups that impart greater solubility, such as branched long alkyl chains, is one possible solution for the problems of processability of oxadiazole containing polymers. Another option is the dilution of the oxadiazole moiety with more soluble components, for example in a copolymer, however the electronic properties of the diluted oxadiazole may not be as attractive as more oxadiazole rich materials.

A novel route to soluble poly(fluorenone) has been described. This new method eliminates the need for undesirable protection and deprotection steps in the synthesis of the fluorenone polymer. As poly(fluorenone) is an insoluble material, an alkyl substituted tetraphenyl benzene group has been attached to the 4-position of the fluorenone monomer. This dendronised side group allows for the synthesis of a soluble poly(fluorenone) with a M_n of 2.7 x 10^4 $gmol^{-1}$ against PPP. The absorption

spectrum of the poly(fluorenone) shows an absorption from the ketone moiety as well as the poly(fluorene) backbone. A broad emission from the ketone group is observed in film and solution, indicating efficient energy transfer from the backbone to the ketone moiety.

The CV data of soluble poly(fluorenone) shows it has a LUMO level of –2.95 eV, while the differential pulse voltammogram indicates a LUMO level of –3.04 eV. This EA is not as good as the value obtained for the unsubstituted poly(fluorenone), due to the presence of the alkyl substituted oligo-phenylene dendrimer. Soluble poly(fluorenone) is a better electron acceptor than other widely used ETM's such as PBD, which has a LUMO level of –2.4 eV.[14] This represents a decreased barrier to electron injection of about 0.6 eV. Also, soluble poly(fluorenone) shows a reversible reduction, unlike some ETM's such as CN-PPV. [15,16]

An initial attempt to obtain the electron mobility of the polymer using TOF measurements was unsuccessful. The failure to obtain high quality films of the thickness required for TOF measurements may have meant that the electron mobility could not be determined. While it is inherently more difficult to measure TOF results from a conjugated polymer than from a discotic material, more effort is needed to provide a material that can form high quality films of the desired thickness.The soluble poly(fluorenone) was incorporated into organic photovoltaic devices as the donor polymer. The devices did not demonstrate any photocurrent behaviour, only short curcuit current-voltage curves. This is attributed to the poor film forming behaviour of the polymer.

The synthesis of a soluble poly(fluorenone), a novel electron transporting material, is an important achievement towards organic optoelectronic devices. To gain a better understanding of the effectiveness of this material, the electron mobility must be measured. The material could not form satisfactory thick films for TOF measurements. Attempts to test the polymer in a photovoltaic device were likewise unsuccessful due to the film forming behaviour. While the polymer appears to be dissolved completely in a number of solvents, the synthesis of a polymer of a lower molecular weight may result in a material that can be tested fully and incorporated into optoelectronic devices. The synthesis of the lower molecular weight polymer by

addition of end-capping units is currently being undertaken. As the number of electron transporting materials is low, compared to hole transporting materials, this polymer has the potential to be useful for applications such as OLED's and photovoltaic devices.

3.3 References

(1) Mitschke, U.; Bauerle, P. *Journal Of Materials Chemistry* **2000**, *10*, 1471-1507.

(2) Hughes, G.; Bryce, M. R. *Journal Of Materials Chemistry* **2005**, *15*, 94-107.

(3) Kulkarni, A. P.; Tonzola, C. J.; Babel, A.; Jenekhe, S. A. *Chemistry Of Materials* **2004**, *16*, 4556-4573.

(4) Goetzberger, A.; Hebling, C.; Schock, H. W. *Materials Science & Engineering R-Reports* **2003**, *40*, 1-46.

(5) Wu, F. I.; Reddy, D. S.; Shu, C. F.; Liu, M. S.; Jen, A. K. Y. *Chemistry Of Materials* **2003**, *15*, 269-274.

(6) Price, D. W.; Tour, J. M. *Tetrahedron* **2003**, *59*, 3131-3156.

(7) Kastler, M.; Pisula, W.; Wasserfallen, D.; Pakula, T.; Mullen, K. *Journal Of The American Chemical Society* **2005**, *127*, 4286-4296.

(8) Pisula, W.; Kastler, M.; Wasserfallen, D.; Pakula, T.; Mullen, K. *Journal Of The American Chemical Society* **2004**, *126*, 8074-8075.

(9) Uckert, F.; Setayesh, S.; Mullen, K. *Macromolecules* **1999**, *32*, 4519-4524.

(10) Neher, D. *Macromolecular Rapid Communications* **2001**, *22*, 1366-1385.

(11) Janietz, S.; Bradley, D. D. C.; Grell, M.; Giebeler, C.; Inbasekaran, M.; Woo, E. P. *Applied Physics Letters* **1998**, *73*, 2453-2455.

(12) Meerholz, K.; Gregorius, H.; Mullen, K.; Heinze, J. *Advanced Materials* **1994**, *6*, 671-674.

(13) Kissinger, P. T., Heineman, W.R. *Laboratory Techniques in Electroanalytical Chemistry*; Marcel Dekker, Inc.: New York, 1996.

(14) Pommerehne, J.; Vestweber, H.; Guss, W.; Mahrt, R. F.; Bassler, H.; Porsch, M.; Daub, J. *Advanced Materials* **1995**, *7*, 551-554.

(15) Cervini, R.; Li, X. C.; Spencer, G. W. C.; Holmes, A. B.; Moratti, S. C.; Friend, R. H. *Synthetic Metals* **1997**, *84*, 359-360.

(16) Greenham, N. C.; Moratti, S. C.; Bradley, D. D. C.; Friend, R. H.; Holmes, A. B. *Nature* **1993**, *365*, 628-630.

(17) Adam, D.; Closs, F.; Frey, T.; Funhoff, D.; Haarer, D.; Ringsdorf, H.; Schuhmacher, P.; Siemensmeyer, K. *Physical Review Letters* **1993**, *70*, 457-460.

(18) Adam, D.; Schuhmacher, P.; Simmerer, J.; Haussling, L.; Siemensmeyer, K.; Etzbach, K. H.; Ringsdorf, H.; Haarer, D. *Nature* **1994**, *371*, 141-143.

(19) Brabec, C. J.; Sariciftci, N. S.; Hummelen, J. C. *Advanced Functional Materials* **2001**, *11*, 15-26.

(20) Brabec, C. J.; Sariciftci, S. N. *Monatshefte Fur Chemie* **2001**, *132*, 421-431.

(21) Coakley, K. M.; McGehee, M. D. *Chemistry Of Materials* **2004**, *16*, 4533-4542.

(22) Al-Ibrahim, M.; Roth, H. K.; Zhokhavets, U.; Gobsch, G.; Sensfuss, S. *Solar Energy Materials And Solar Cells* **2005**, *85*, 13-20.

(23) Jacob, J.; Sax, S.; Piok, T.; List, E. J. W.; Grimsdale, A. C.; Mullen, K. *Journal Of The American Chemical Society* **2004**, *126*, 6987-6995.

(24) Schulz, B.; Bruma, M.; Brehmer, L. *Advanced Materials* **1997**, *9*, 601-613.

4 Indenofluorene based materials

4.1 Introduction

Poly(indenofluorene) was introduced in Section 1 as a conjugated polymer whose emission maximum shows a bathochromic shift compared to poly(fluorene), due to the extended planarisation. [1,2] This makes poly(indenofluorene) a 'better' blue emitting material compared to poly(fluorene), which emits too near the violet part of the visible spectrum. The emitting characteristics of indenofluorene based materials, coupled with the relatively small quantity of research into this material compared with fluorene, makes indenofluorene a desirable building block for novel conjugated materials.

While oligomers of fluorene are easily synthesised, there has been no success in the preparation of oligomers of indenofluorene previously. The preparation of a monofunctionalised indenofluorene moiety by a novel synthetic route is presented. This synthetic route does not involve the separation of mixtures of mono- and difunctionalised indenofluorene units, which has been shown previously to be difficult. The monofunctional building block is used to produce a dimer and trimer of indenofluorene. These are the first examples of small, well-defined, linear materials such as this. The further functionalisation of the dimer is also described.

In order to fully understand the role of defect structures in the unwanted long wavelength emission in poly(indenofluorene) based OLED's, the synthesis of a model defect structure is presented. The spectroscopic analysis of this defect in solution and in blended films with a poly(indenofluorene) is discussed in detail.

4.2 Results and Discussion

4.2.1 Oligomers of indenofluorene

The synthesis of a fluorene trimer is trivial as 2-bromofluorene is commercially available. From this monofunctionalised material fluorene oligomers can be synthesised by a step-by-step process. The challenge in synthesising oligoindenofluorene is the synthesis of the analogous monofunctionalised building block.

Initially, previous members of the group attempted the monobromination of indenofluorene via $CuBr_2$/alumina or molecular bromine, Equation 4.1. However, this reaction only resulted in an inseparable mixture of the nonbrominated, mono- and dibrominated products. The desired product could not be separated from the other materials to a satisfactory extent by column chromatography or recrystallisation.

Equation 4.1. Unsuccessful attempts at monobromination of indenofluorene.

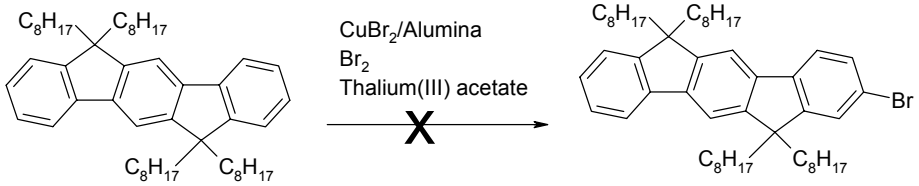

A more exotic bromination technique was also applied. Thallium(III) acetate has been used previously as a catalyst for the monobromination of *p*-terphenyl in the 4 position.[3] As indenofluorene is a bridged terphenyl, it was anticipated that the same technique could be used for the monobromination of this substrate. This bromination was not successful, and again a mixture of unreacted, mono- and dibrominated substrate was obtained.

Various attempts to monobrominate indenofluorene were not successful, so in order to overcome this difficulty, an alternate approach was undertaken. Instead of trying to monofunctionalise an indenofluorene molecule, the concept was to react a dibromoindenofluorenefluorene only once. It was know from previous work in the

group that 2,7-dibromofluorene can be monolithiated, and used to form a trimethylsilyl or boronic ester derivative, Equation 4.2. It was envisaged that the monolithiated indenofluorene could be used to form the required building blocks for the synthesis of indenofluorene oligomers.

Equation 4.2. Synthetic route to monobromo monotrimethylsilyl fluorene.

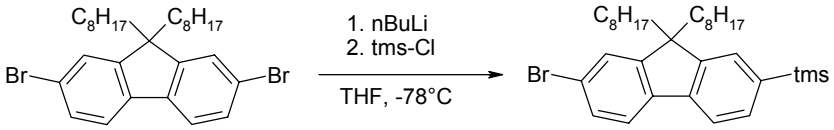

The approach undertaken was to try and form the monobromo monotrimethylsilyl indenofluorene, which was predicted to be separable from the starting material and two time reacted product, Scheme 4.1. Addition of 1 equivalent of nBuLi and trimethylsilyl chloride afforded a mixture of the starting material and bis-trimethylsilyl indenofluorene by FD MS. The desired monoreacted product was not observed at all.

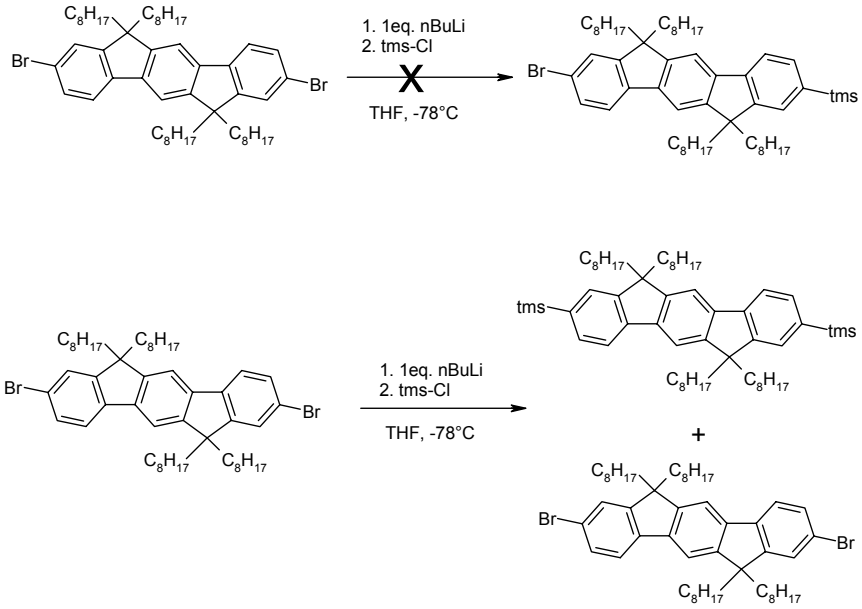

Scheme 4.1. Proposed synthetic route to monobromo monotrimethylsilyl indenofluorene, and the products obtained from the reaction.

As the undesired formation of the dianion was observed in the reaction, the synthesis was repeated with diethyl ether as the solvent. The less polar solvent should be less effective in stabilising the dianion, and so the bis-trimethylsilyl product should

not be formed. After the reaction however, only the starting material was observed. A 3.5 excess of n-BuLi was added, and the reaction left to warm to room temperature, but no reaction was observed.

Attempts to heterofunctionalise indenofluorene either by the monobromination of the indenofluorene moiety or by the monoreaction of dibromoindenofluorene were unsuccessful. Therefore a new strategy was formulated, where an intermediate is monofunctionalised before the indenofluorene moiety is formed. This requires a novel synthetic route to indenofluorene.

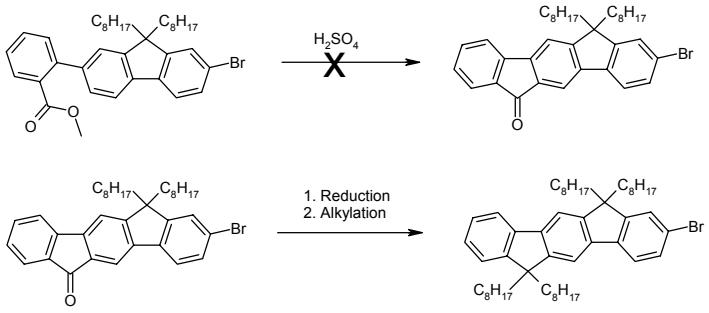

Scheme 4.2. Synthetic route to monobromoindenofluorene monoketone.

A potential route to monobromoindenofluorene is through the reduction and subsequent alkylation of monobromoindenofluorene monoketone, shown in Scheme 4.2. The synthesis of benzoic acid methyl ester substituted fluorene was successful, however the following step could not be driven to completion. The sulphuric acid ring closure to give the monoketone indenofluorene afforded a mixture of the desired product, sulphonated products and the de-esterification of the starting material. As the yield of this reaction was very low, especially since two additional synthetic steps were required to reach the monobromoindenofluorene, this approach was abandoned.

The debilitating step in the previous synthetic route was the ring closure to form the ketone. It would also be synthetically desirable to shorten the synthetic route, as many steps are required to prepare the benzoic acid methyl ester substituted fluorene in addition to the subsequent reaction steps. An alternate synthetic scheme with a reduced number of reaction steps is shown in Scheme 4.3.

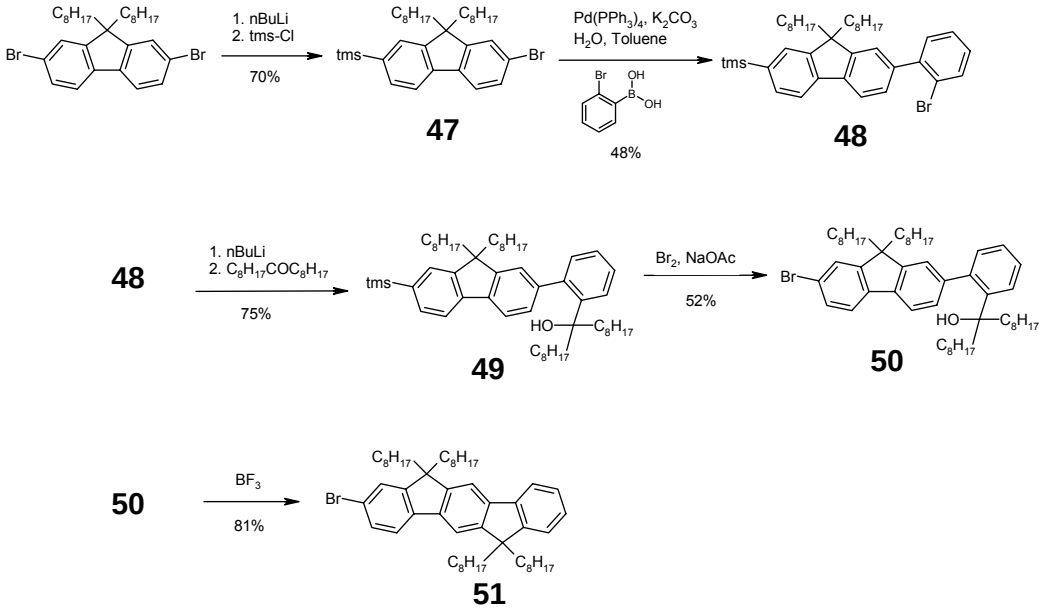

Scheme 4.3. Synthetic route to monobromoindenofluorene.

The Suzuki cross coupling reaction of the trimethylsilyl monobromofluorene, **47**, with 2-bromo-benzene boronic acid afforded the 2-bromobenzene substituted fluorene **48**. Care must be taken to avoid the product from further reacting to form higher oligomers, however the product was isolated with a yield of 48%. The aryl lithium addition of **48** to 9-heptadecanone gave the tertiary alcohol **49**, with a yield of 75%. Following the conversion of the trimethylsilyl group to a bromide, the Friedel-Crafts ring closure afforded the desired intermediate, monobromoindenofluorene (**51**), with a 81% yield.

51 was characterised by ^{1}H, ^{13}C and COSY NMR and FD MS. The ^{1}H and ^{13}C NMR spectra of **51** are shown in Figure 4.1. The aromatic region of the ^{1}H NMR spectrum in Figure 4.1a is complicated due to the desymmetrisation of **51**. The ^{13}C NMR spectrum of **51** provides the best structural proof of the synthesis of the monobrominated indenofluorene. The aromatic region of the spectrum shows 18 different carbon atoms, and two benzylic carbons in the molecule at 55.55 and 55.19 ppm. The NMR and FD MS data supports the structure of **51** to be as shown in Scheme 4.3.

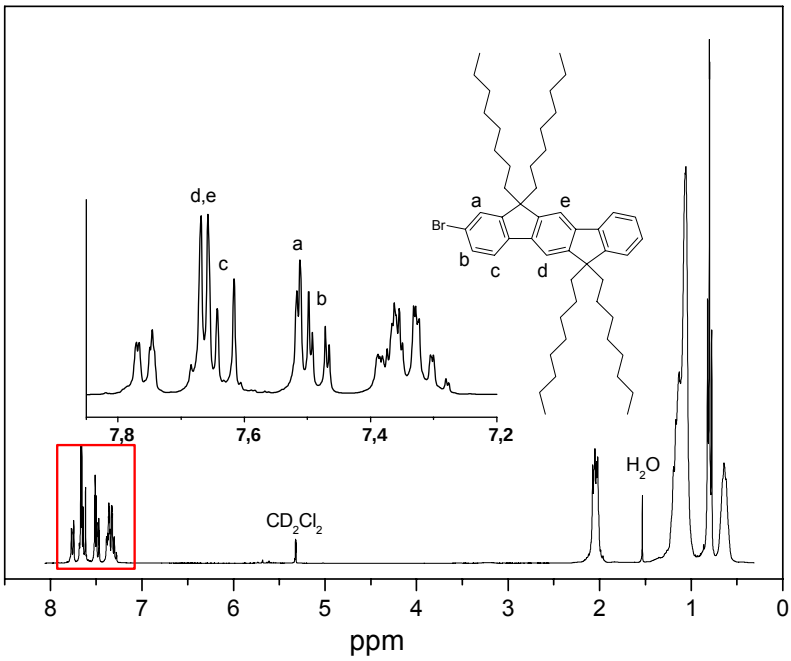

a.

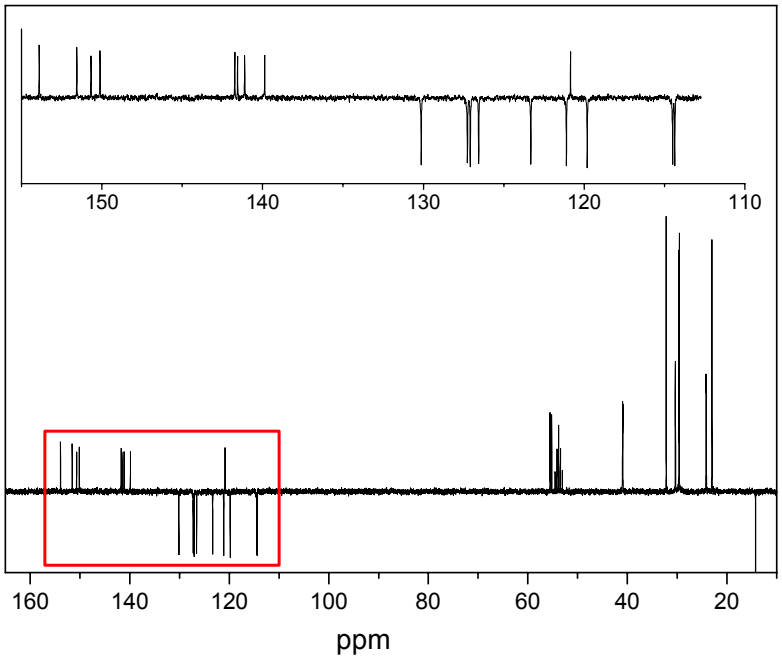

b.

Figure 4.1. a. ^{1}H (300 MHz) and b. ^{13}C (75.46 MHz) NMR spectra of 51 in CD_2Cl_2.

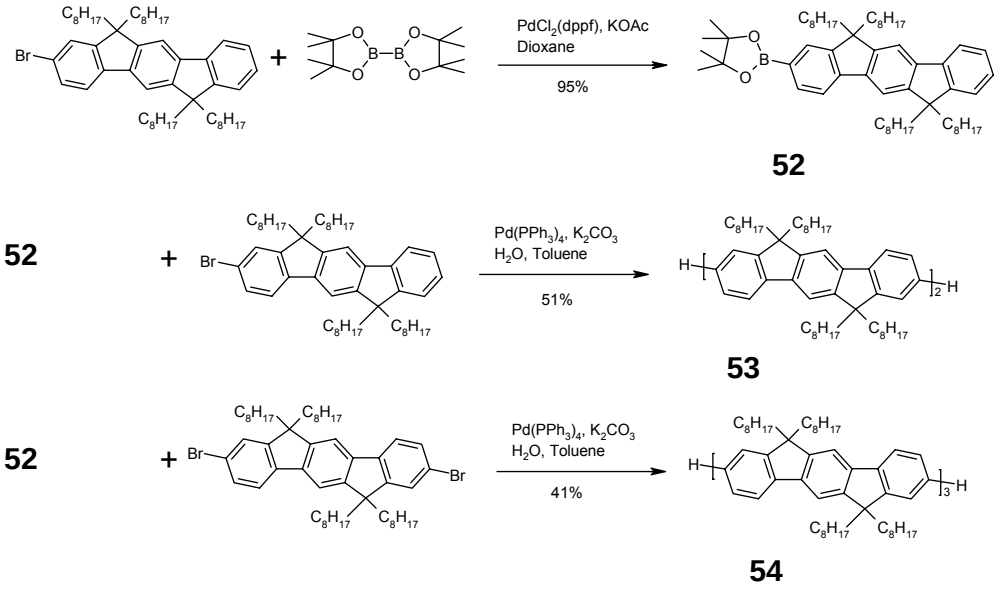

Scheme 4.4. Synthetic route to indenofluorene dimer and trimer, 53 and 54 respectively.

The synthesis of the indenofluorene dimer and trimer is shown in Scheme 4.4. The monobromoindenofluorene was converted to the corresponding boronic ester using the palladium catalysed Miyaura coupling, in 95% yield. The palladium catalysed method was utilised because the aryl lithium method for boronic ester synthesis did not afford the product in high yields. This was a result of the purification required for the aryl lithium method, which reduced the reaction yield.

The monoboronic ester of indenofluorene was coupled with either mono- or dibromoindenofluorene to give the indenofluorene dimer or trimer respectively. The relatively low yields for the Suzuki cross coupling of the indenofluorene units to form the oligomers is a result of the separation of the products from the excess starting materials by column chromatography. For both the dimer and trimer, there was a significant proportion of product slightly contaminated with excess starting materials and side products. The full removal of the unwanted materials required the loss of some of the target material.

The synthesis of the indenofluorene dimer and trimer required the careful purification of the oligomers using column chromatography. This suggests that the random synthesis technique could be applied to the preparation of indenofluorene

oligomers, as oligomers of different sizes could be separated and purified. This would eliminate the need to synthesise the monobromoindenofluorene by the long synthetic strategy illustrated in Scheme 4.3. However, the majority of the products from the cross coupling reaction were the target material, and its purification was not trivial. We assume the separation of an even mixture of many oligomers of indenofluorene would be very difficult.

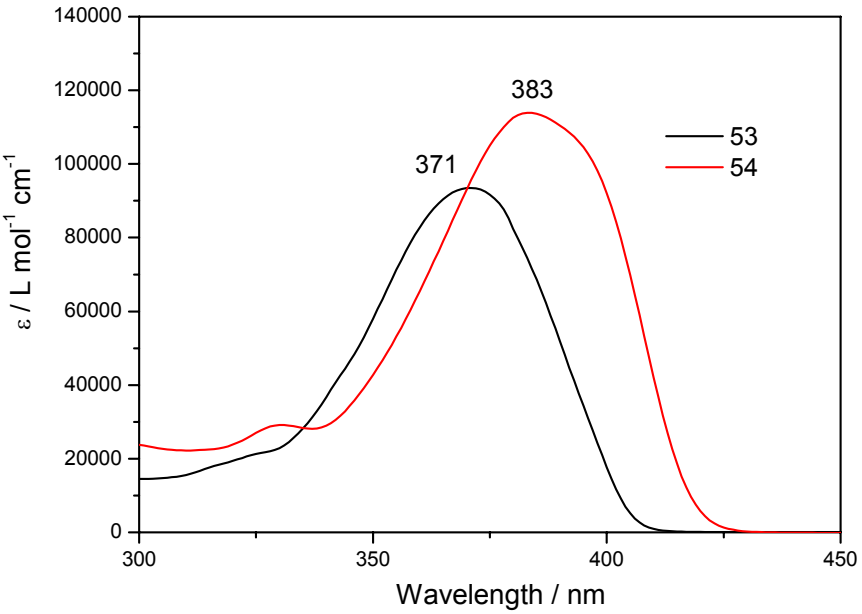

Figure 4.2. UV-vis absorption spectra of 53 and 54 in THF.

The absorption spectra of **53** and **54** in solution are shown in Figure 4.2. Both the indenofluorene dimer and trimer show a broad featureless absorption in THF. The absorption maximum of the trimer, **54**, shows a bathochromic shift of 12 nm compared to the absorption maximum of the dimer, **53**, which is expected. The maximum extinction coefficient (ε) of **54**, 1.39 x 10^5 $Lmol^{-1}cm^{-1}$, is larger than that of **53**, 9.35 x 10^4 $Lmol^{-1}cm^{-1}$.

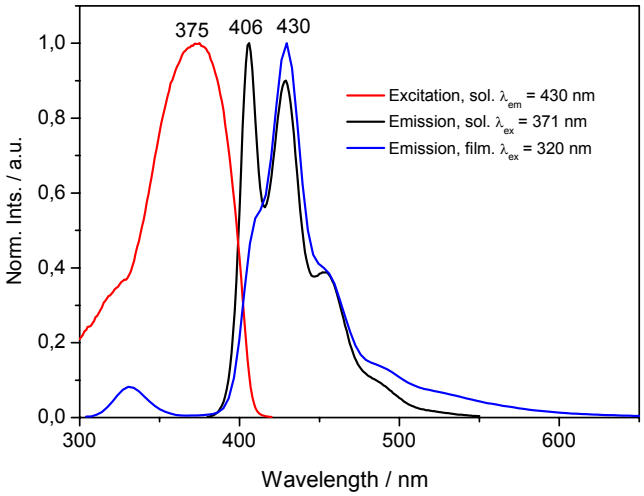

a.

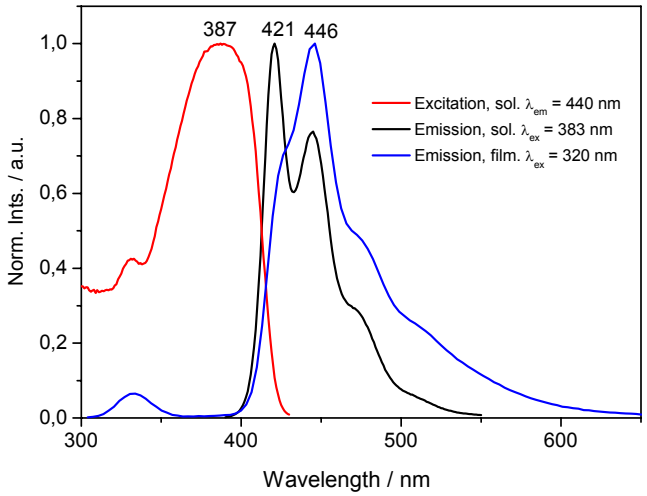

b.

Figure 4.3. Photoluminescence data of 53 and 54. a. Excitation (λ_{em} = 430 nm), solution (λ_{ex} = 371 nm) and thin film emission (λ_{ex} = 320 nm) spectra of 53. b. Excitation (λ_{em} = 440 nm), solution (λ_{ex} = 383 nm) and thin film emission (λ_{ex} = 320 nm) spectra of 54.

The solution and solid state excitation and emission spectra of **53** and **54** are presented in Figure 4.3. The solution emission spectra of both the dimer (λ_{ex} = 371 nm) and trimer (λ_{ex} = 383 nm) exhibit a vibronic fine structure. The emission maximum of **54**, 421 nm, shows a bathochromic shift when compared to the emission of **53**, 406 nm. This difference of 15 nm is consistent for these materials on going from a dimer to a trimer. The thin film emission maxima of **53** and **54** is at the same wavelength as the shoulder peaks of the solution emission spectra. We attribute the

change in relative intensity of the two peaks in the thin film emission spectra of **53** and **54** to be due to self absorption.

The morphological structure, or solid state packing behaviour, of **53** and **54** was investigated by DSC, polarizing optical microscopy (POM) and 2-dimensional wide-angle X-ray diffraction (2D-WAXS). The molecular dynamics of **53** and **54** was investigated by dielectric spectroscopy. These experiments were performed in conjunction with our collaborator, Prof. G. Floudas (University of Ioannina, Department of Physics, 451 10 Ioannina, Greece). The DSC traces from the second heating cycle for the indenofluorene monomer (without bromide functionalities), **53** and **54** are presented in Figure 4.4.

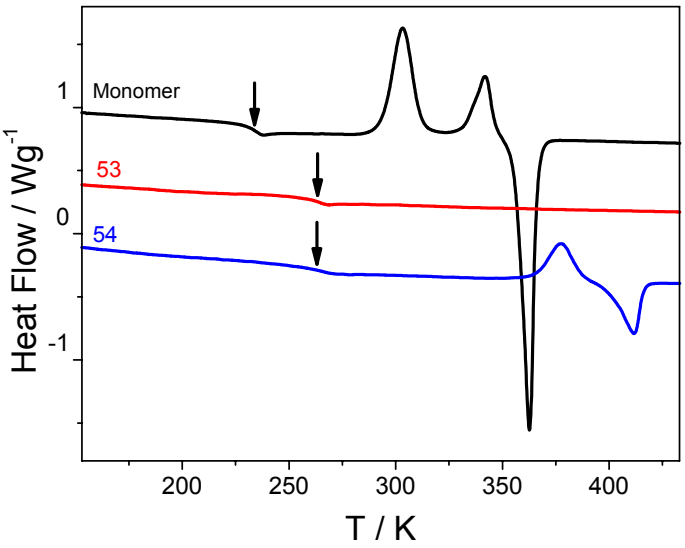

Figure 4.4. DSC traces of the indenofluorene monomer, 53 and 54, obtained during the second heating run with a rate of 10 Kmin^{-1}. The vertical arrows give the respective glass transition temperatures.

In all traces presented in Figure 4.4, a clear step in the specific heat can be seen at the respective glass transition temperature (T_g) with values of 231, 258 and 261 K for the monomer, **53** and **54**, respectively. The heat capacity step (Δc_P) has values comparable to the corresponding oligofluorenes, *i.e.* for the **53** Δc_P=0.39 Jg^{-1}K^{-1} as compared to 0.34 Jg^{-1}K^{-1} for the dimer of fluorene.[4] In addition, the IF monomer and

trimer traces during the second heating runs contain exothermic and endothermic peaks characteristic of mesophases/cold crystallization and melting. For the monomer two exothermic peaks appear at 303 and 342 K followed by a subsequent melting at 363 K. For the trimer, organization and melting occur at 378 and 411 K, respectively.

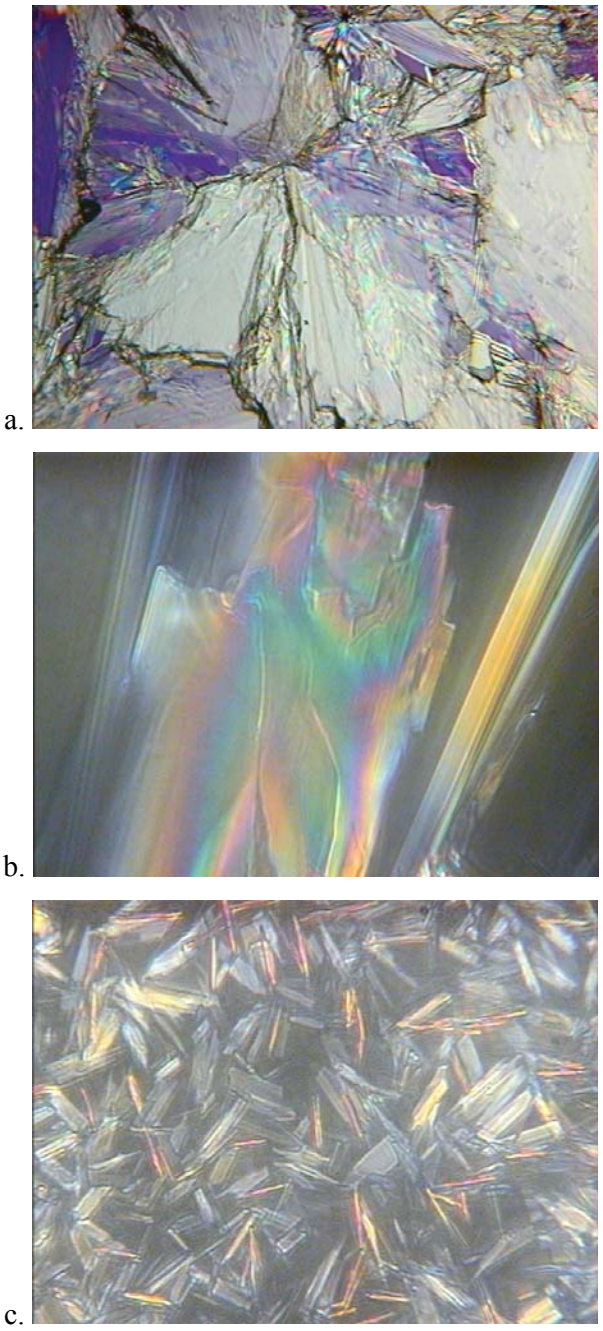

Figure 4.5. POM images of a. indenofluorene monomer (313 K) b. 53 (373 K) c. 54 (423 K).

The POM images of the indenofluorene monomer, **53** and **54** are shown in Figure 4.5. Such periodic structures are typical for liquid crystalline phases. The interferences are due to variations of the optical axis of portions of the phase with respect to the direction of the electric field vector of light and the colour originates from a spatial periodicity in the order of the wavelength of light. Thread-like lines and singular points connected by intersecting black stripes (known as Schlieren texture) are normally observed for nematic liquid crystals, whereas fan-shaped and mosaic textures for smectic phases. The images of the three IF oligomers are distinctly different from the corresponding oligofluorenes and suggest smectic mesophases.[4] For the monomer in particular, the image shown suggests a smectic A phase.

To identify the exact morphologies the 2-dimensional wide-angle X-ray (2D-WAXS) patterns of macroscopically oriented samples were investigated. The samples were prepared by filament extrusion using a home-built extruder. The material is heated to a phase at which it is deformable, and extruded as a thin fibre, 0.7 mm diameter, by a constant rate motion of a piston in a cylinder. Under such conditions, the materials are well orientated, with the longest dimension of the material orientated in the direction of extrusion.

2D-WAXS diffraction patterns were obtained from the monomer, **53** and **54** using the X-ray beam with a pinhole collimation and a 2-dimensional detector (Siemens A102647) with 1024x1024 pixels. A double graphite monochromator for the Cu Kα radiation (λ=0.154 nm) was used. The sample-to-detector distance was 7.3 cm. Measurements were made from macroscopically oriented cylindrical filaments with a diameter of 0.7 mm. All patterns were recorded with a vertical orientation of the filament axis and the X-ray beam perpendicular to the filament. The 2D-WAXS images of **53** and **54** are shown in Figure 4.6 and Figure 4.7, respectively. The scattered intensity distributions were integrated along the equatorial and meridional axis and the resulted intensities are presented as a function of the scattering wave vector $q=(4\pi/\lambda)\sin\theta$, where 2θ is the scattering angle.

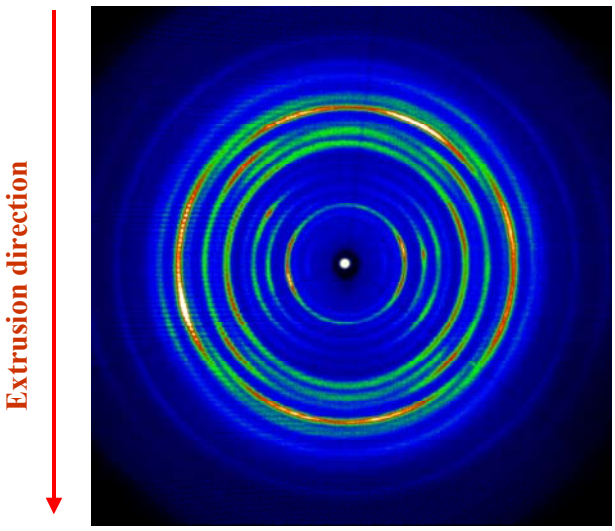

a.

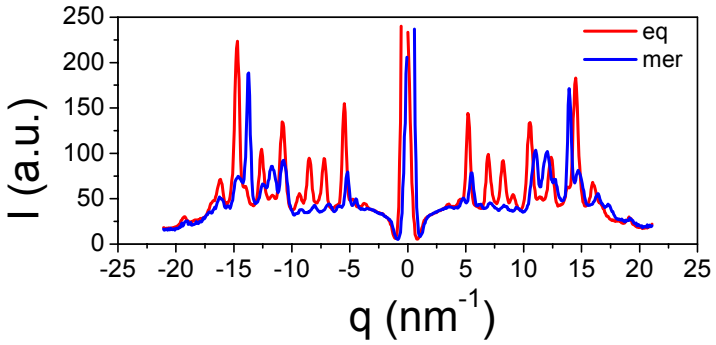

b.

Figure 4.6. a. 2D-WAXS diffraction pattern from a fibre of 53 taken at T=298 K (the fibre was extruded at 298 K). The vertical arrow gives the orientation of the fiber axis. b. Equatorial and meridional scattered intensity distributions.

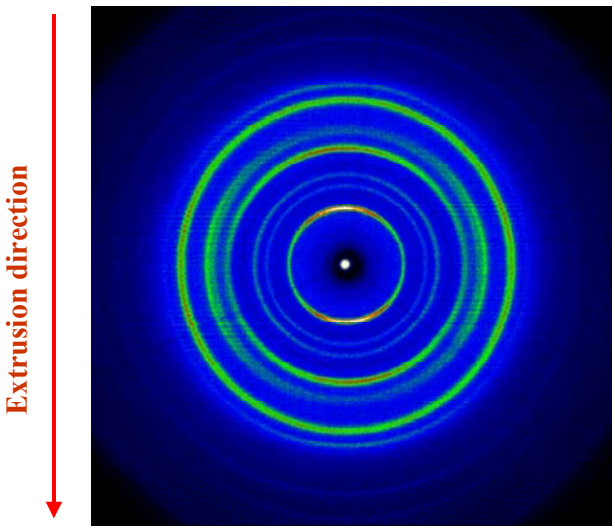

a.

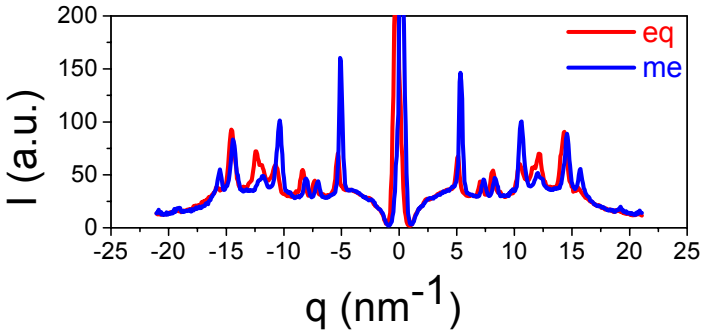

b.

Figure 4.7. a. 2D-WAXS diffraction pattern from a fibre of 54 taken at T=403 K (the fibre was extruded at 333 K). The vertical arrow gives the orientation of the fiber axis. b. Equatorial and meridional scattered intensity distributions.

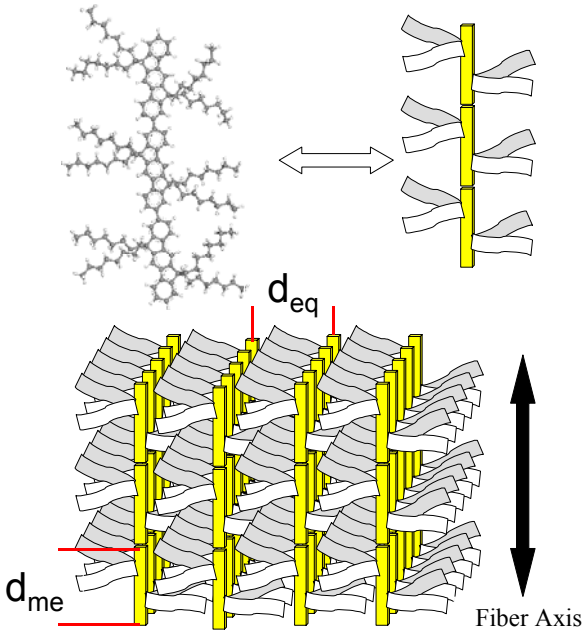

Figure 4.8. Schematic diagram of the structure of the extruded fibre of 54.

The 2D-WAXS patterns from the oriented fibres of **53** and **54** display some similarities but also some differences. The 2D-WAXS of **54** will be discussed first. Figure 4.7 shows the pattern of **54**, a 2D-WAXS pattern consisting of intense meridional low-angle reflections and of some less intense equatorial reflections. The periodicity along the extrusion direction corresponds to the intramolecular repeat distance (d_{me}). This periodicity is attributed to the main chain repeat unit (monomer) with a characteristic length of d_{me}=1.17 nm at 403 K is good agreement with the calculated monomer length of 1.09 nm. The first intense equatorial reflection is attributed to the lateral periodicity between the supramolecular assemblies with an interlayer period of d_{eq}~0.88 nm. The latter suggests that the spacing between the self-assembled backbone layers is controlled by the length of side chains. The remaining equatorial reflections corresponding to d = 0.52, 0.44 and 0.33 nm, with relative positions $1:3^{1/2}:4^{1/2}:7^{1/2}$ with respect to the low-angle reflection, suggest a hexagonal packing of the backbone layers. These findings for the structure in the trimer are summarized in a highly schematic way in Figure 4.8. Figure 4.8 depicts a 3D arrangement of the trimer in the oriented fibre state. The rigid parts of the trimer stack on each other forming layers aligned parallel to the fibre axis. The flexible aliphatic

side-chains fill the space between the backbones and effectively control the lateral distance.

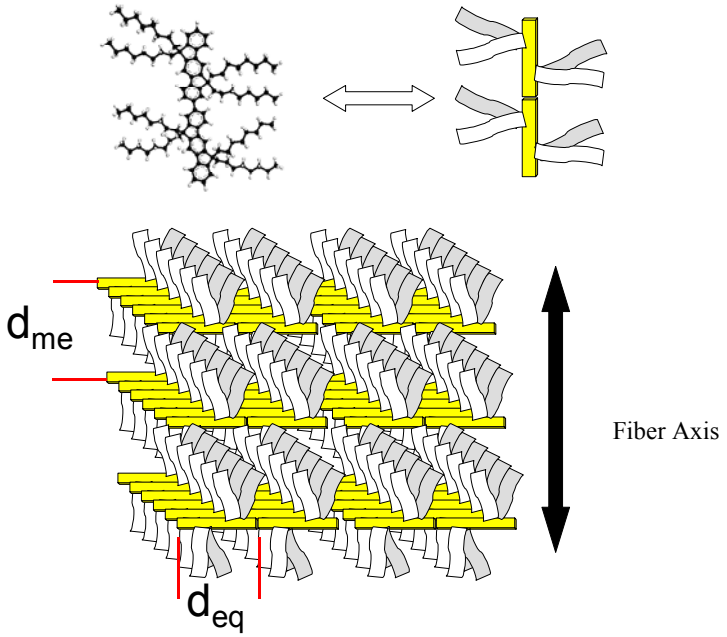

Figure 4.9. Schematic diagram of the structure of the extruded fibre of 53.

The WAXS pattern for **53**, Figure 4.6, has similar reflections to those of **54** in Figure 4.7 with respect to their positions, but rotated by 90^0. The intense equatorial low-angle reflection (d_{eq}=1.2 nm) has the same periodicity as the intense trimer meridional reflection suggesting that the backbone repeat unit is now along the equator (*i.e.* in the horizontal direction), thus perpendicular to the fibre axis. This turn in the orientation in the dimer structure results from the similarity in the lengths of the backbone and side-chains in their fully extended conformation. During fibre formation there is competition for orientation along the extrusion direction, with the longer length to be preferentially along the fibre axis. For **54**, the longer length is clearly the backbone and orients along the extrusion direction, Figure 4.8. In the case of **53**, the dominating length dimension of the unit changes from the backbone to the side chains, which gives rise to the observed rotation of the whole structure, Figure 4.9. As expected the monomer 2D-WAXS pattern, not shown here, shows the same orientation as the dimer.

Overall, the observed 2D-WAXS patterns reflect the spatial segregation of the immiscible aromatic and aliphatic parts of the oligomers driven by the intermolecular cohesive forces favouring π-stacking of the aromatic segments and the entropically driven conformations of the flexible side-chains. Likewise, the orientation of these structures with respect to the extrusion direction, results from a competition between the backbone and side-chain lengths.

The relaxation dynamics of soft matter, e.g. polymeric materials, is characterized by a large frequency range, from 10^{-6} Hz to 10^{10} Hz.[5] Dielectric spectroscopy, DS, the measurement of dielectric properties, comprises this range. It is based on the interaction of an external field with the electric dipole moment of the sample. The fluctuations of local electrical fields are measured, which are connected to the dynamics on a molecular scale. The T_g is the temperature at which the amorphous domains of a polymer take on the characteristic properties of the glassy state-brittleness, stiffness, and rigidity. As the polymer is heated to the T_g, the solid, glassy polymer begins to soften and flow. One method to measure the T_g is to investigate the molecular motion using DS. The T_g of **53** and **54** were measured by DS and compared to the T_g results presented in Figure 4.4. These results are also compared to the values of the T_g of fluorene based oligomers and polymers.

The temperature dependent relaxation times for the α-process (which is the freezing at the T_g) and the ionic conductivity of the indenofluorene monomer, **53**, **54** and the indenofluorene polymer are presented in Figure 4.10 as an Arrhenius representation. The strong conductivity of the polymer restricts measurement over a broader temperature range.

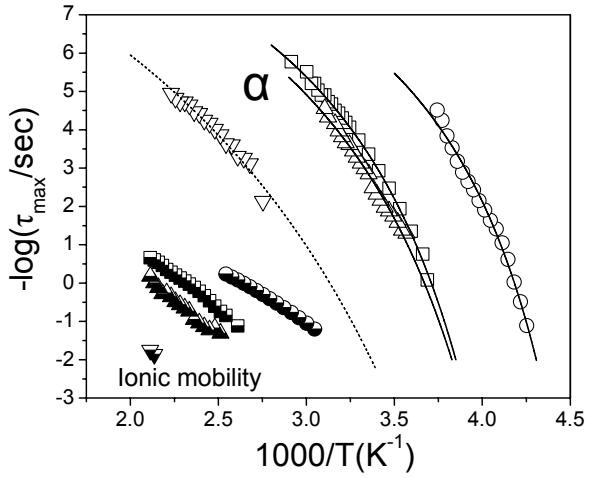

Figure 4.10. Arrhenius relaxation map for the different processes in the IF monomer (circles), 53 (squares), 54 (up triangles) and polymer (down triangles). The different symbols correspond to the α-process (open symbols) and the process due to the ionic mobility (half-filled symbols).

The Tg can be calculated from the plot in Figure 4.10, and is defined as the temperature with a relaxation time $\tau \sim 10^2$ s.[4] The T_g as a function of degree of polymerisation, n, obtained from the DS and DSC experiments are compared in Figure 4.11. No T_g value for the polymer could be obtained from the DSC experiments. The n dependent T_g values for dioctylfluorene based oligomers and polymers are included for comparison.[4] Figure 4.11 illustrates the good agreement between the T_g obtained by the two different methods. The high uncertainty of the polymer T_g is due to the larger extrapolation used to obtain the value from Figure 4.10. The data points in Figure 4.11 can be fitted according to the Fox equation, Equation 4.3, where T_g^{∞} is the T_g at infinite molecular weight and A is a constant (~62±12).[4]

Equation 4.3. Relationship between the number of repeat units (n) and T_g, the Fox equation. T_g^{∞} is the T_g at infinite molecular weight and A is a constant.

$$T_g = T_g^{\infty} - \frac{A}{n}$$

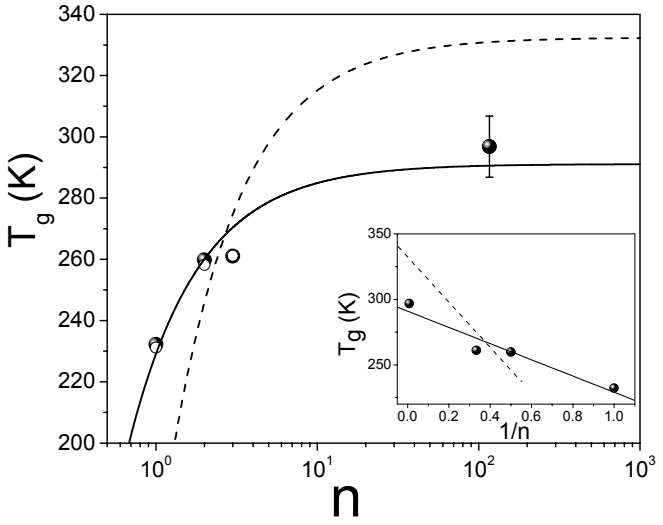

Figure 4.11. Dependence of T_g on the number of repeat units (n) obtained from DS (at $\tau=10^2$ s) (filled circles) and DSC (heating rate of 10 K/min)(open circles). The corresponding data from the oligofluorenes (dashed line) are also included for comparison. The lines are fits according to the Fox equation (see text). In the inset, the T_g values from DS are plotted as a function of 1/n.

The plot in Figure 4.11 clearly demonstrates that for oligomers above trimer, the fluorene based materials have a T_g higher than the corresponding indenofluorene materials. The T_g^{∞} of poly(fluorene) is found to be higher, ~332 K, compared to the T_g^{∞} of poly(indenofluorene), 291±9 K, suggesting that poly(indenofluorene) has a higher backbone flexibility. This is surprising, as it is expected that the more rigid backbone structure of indenofluorene would lead to a more rigid polymer. This situation may be a result of the side chains of the materials, of which indenofluorene has twice as much per unit compared to fluorene. The rigid backbone of indenofluorene, which acts to raise the T_g, may be in competition with the side chains that can increase the main chain mobility, and could lead to a lower T_g.

4.2.2 Dye end-capped indenofluorene oligomers-straightening the linker

One important parameter for the effectiveness of OLED's is the conformation adopted by the active molecules.[6] One method to realise the conformation of polymers is to study the orientation and conformation of single oligomer molecules in films. This can be achieved using single molecule spectroscopy (SMS), which can elucidate the orientation of a molecule from the conformational dependency of the spectra, polarisation information and from simulations of spectra.[7-11] The merit of SMS is that it does not require ensemble averaging, which is found in standard spectroscopic techniques.[12,13] Thus SMS yields insight into complex fluctuation phenomena that cannot be observed using standard techniques.

The easiest method to detect and study a single molecule is by the measurement of the fluorescence of a small sample volume, in which no more than one molecule can be excited by the incoming laser and be imaged onto the detector.[12] The easiest way to achieve this reduction in the number of target molecules is to have a dilute bulk sample, to which the exciting laser essentially selects a single molecule. This laser spatial selection is most often achieved optically.[12] The use of confocal microscopy, where the same lens is used for excitation and collection with a pinhole to limit the active area of the detector, allows for the relatively easy acquisition of data with a low signal-to-noise ratio.[12-14]

SMS can elucidate the relative orientation of fluorescent dyes in multichromophoric systems in a matrix. Initially, by varying the polarisation of the excitation the dipole orientation of a stationary molecule flat on the surface was measured.[15] The technique was used on a dye end-capped fluorene trimer, Figure 4.12, in 2002.[6] Importantly, the authors demonstrated that the technique could be applied to randomly oriented systems, with respect to the sample plane.[6] This was possible as a result of the analysis of histograms presenting the projection of the angle between both chromophores into the plane of the excitation light, and by comparison with simulation results.[6]

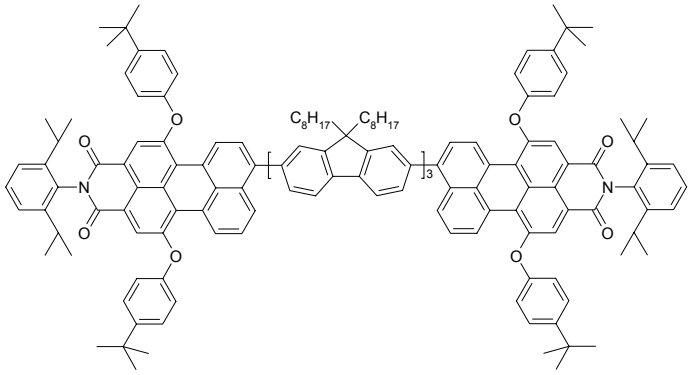

Figure 4.12. Structure of dye end-capped fluorene trimer.

Intramolecular energy transfer was observed, which the authors ascribe to Förster-transfer.[6] A Förster-radius of 5.4 nm was calculated for the structure shown in Figure 4.12, where the distance between the chromophores was calculated to be 4.3 nm.[6] More interestingly, the angle between the dye dipoles was determined to be 114°, indicating the trimer is banana shaped, with the fluorene alkyl groups pointing to the same side, Figure 4.13.[6]

The fluorene molecule has an inherent angle between the 2 and 7 position. There are other phenylene based oligomers that do not have such a bend and have substitution points at the end of the oligomer that are co-linear. One such material is indenofluorene. To investigate the orientation of the dipoles of two chromophores held in a co-linear arrangement, perylene dye was attached to the ends of the indenofluorene oligomers, **53** and **54**.

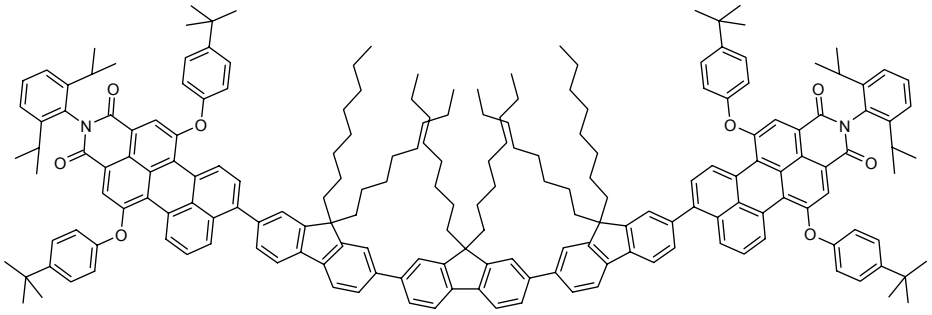

Figure 4.13. Bent structure of dye end-capped fluorene trimer.

The synthesis of the dye end-capped indenofluorene dimer and trimer is shown in Scheme 4.5. The indenofluorene oligomers, **53** and **54**, can be brominated easily with the mild brominating agent copper bromide on alumina to give the functionalised dimer and trimer, **55** and **56** respectively. The palladium catalysed Suzuki cross coupling reaction of the indenofluorene oligomers with the boronic ester of a perylene monoimide affords the dye end-capped oligomers, **57** and **58**.

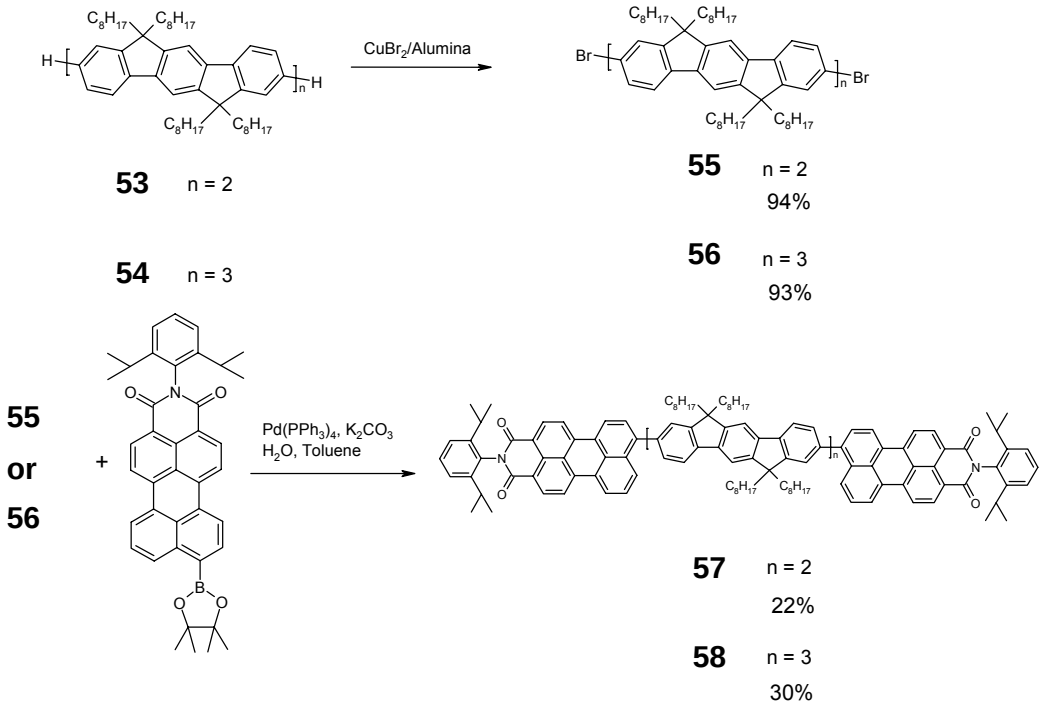

Scheme 4.5. Synthetic route to dye end-capped indenofluorene dimer, 57, and trimer, 58.

Perylene was chosen as the low band gap chromophore due to its exceptional light fastness, high chemical stability and high photoluminescence quantum yield.[16] A side product of the cross coupling reaction is the monobromo perylene monoimide. While this is the precursor to the dye boronic ester, it was not present before the Suzuki reaction was commenced. This bromide exchange afforded a material that cannot be separated from the desired product using column chromatography. **57** was purified by repeated precipitation into hexane from methylene chloride, and characterised by FD MS, ^{1}H and ^{13}C NMR. This however resulted in the loss of a significant amount of the desired product, hence the low yield of the reaction at 22%.

The same precipitation technique was applied to the dye end-capped trimer **58**, but this material could not be purified, and the bromo-dye side product was still present.

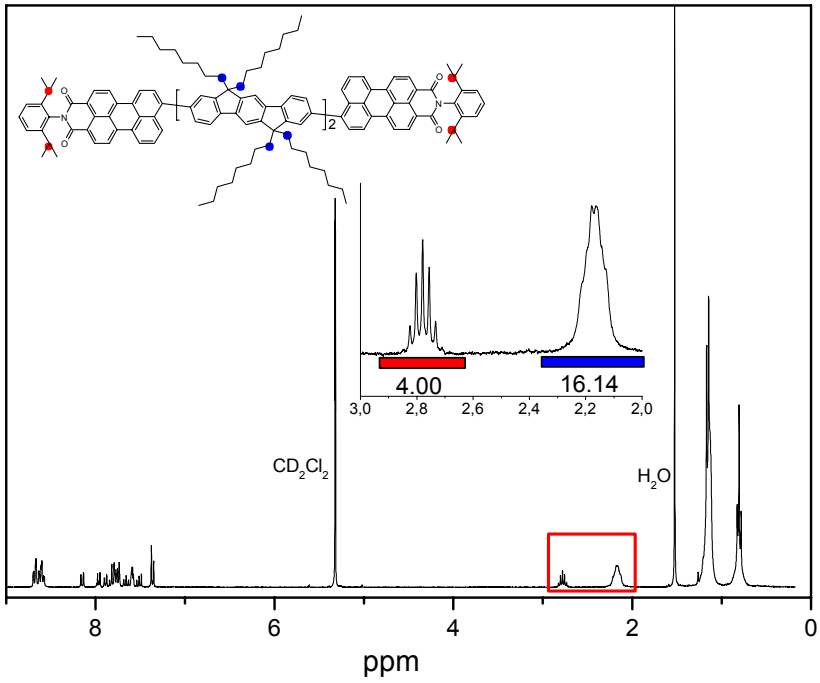

Figure 4.14. ^{1}H NMR spectra of 57 in CD_2Cl_2, 300 MHz.

The ^{1}H NMR spectrum of **57** in CD_2Cl_2 is presented in Figure 4.14. The number and splitting of the aromatic signals is that which would be expected for **57**. The insert of Figure 4.14 shows the integration of the two protons labelled in the structure, and shows the correct ratio between the 4 isopropyl protons on the dye moieties and the 16 protons next to the benzylic position on the indenofluorene oligomer. The ^{1}H NMR spectrum of **57** is proof of the purity of the compound, and that the side product was removed successfully.

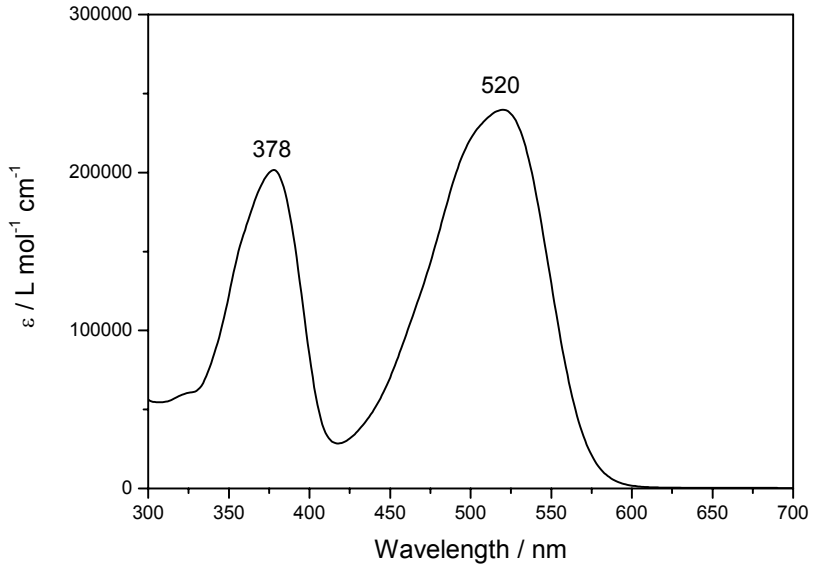

a.

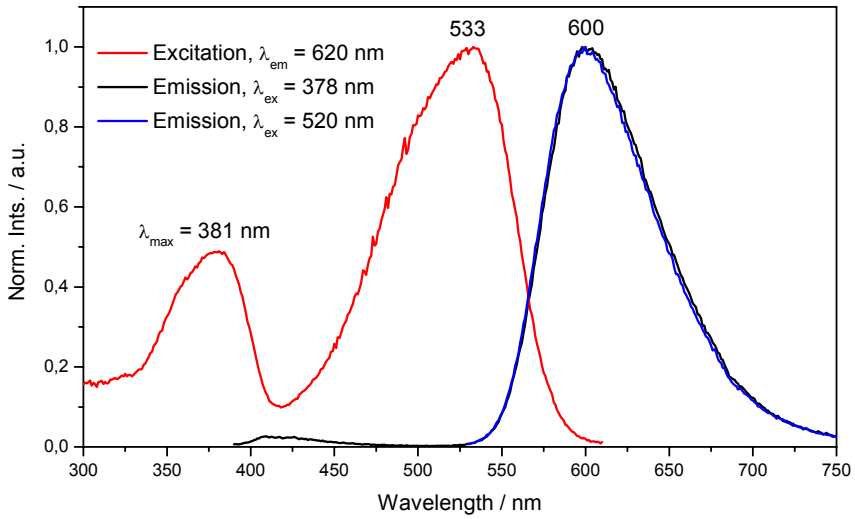

b.

Figure 4.15. Optical properties of 57 in THF. a. UV-vis absorption spectrum of 57. b. excitation (λ_{em} = 620 nm) and emission (λ_{ex} = 378 nm, 520 nm) spectra of 57.

The absorption and photoluminescence spectra of **57** are presented in Figure 4.15. The UV-vis absorption spectrum of **57** shows two featureless absorptions with maxima at 378 nm and 520 nm, which correspond to absorption from the indenofluorene dimer and perylene dye respectively.

Figure 4.15b shows the emission spectra of **57** excited at 378 nm and 520 nm. When the molecule is excited with 520 nm light, into the absorption profile of the dye, a broad emission from the dye with a maximum at 600 nm is observed. When the indenofluorene part of the molecule is excited with 378 nm light, efficient Förster energy transfer is observed. Only a small fraction of the absorbed energy is emitted from the indenofluorene moiety, at approximately 410 nm, and mostly emission from the dye is observed. This is in accord with previously studied molecules incorporating perylene dye and poly(fluorene).[16]

The rate constant of exciton transfer from the donor to the acceptor chromophores, k_{DA}, is the related to the spectral overlap of the emission spectrum of the donor, f_D, and the absorption spectrum of the acceptor, A_A.[16] The relationship is shown in Equation 4.4.

Equation 4.4. Relationship between the exciton transfer rate constant, k_{DA}, and the spectral overlap of the emission of the donor, f_D, and the absorption of the acceptor, A_A.

$$k_{DA} \propto \int_0^\infty f_D(\bar{\nu}) A_A(\bar{\nu}) d\bar{\nu}$$

For efficient energy transfer between the chromophores the emission of **53** must overlap with the absorption of the perylene dye. The two spectra are presented in Figure 4.16. The overlap of the emission and absorption spectra of 53 and the perylene dye is not perfect, with the emission spectrum having a maximum of 406 nm and the absorption spectrum a maximum at 488 nm. Qualitatively however, the emission and absorption spectra do overlap to quite an extent. This would allow for a reasonably fast exciton transfer between the indenofluorene backbone and the perylene acceptor. This transfer is not 100% efficient however, as emission from the indenofluorene dimer can be observed at 410 nm.

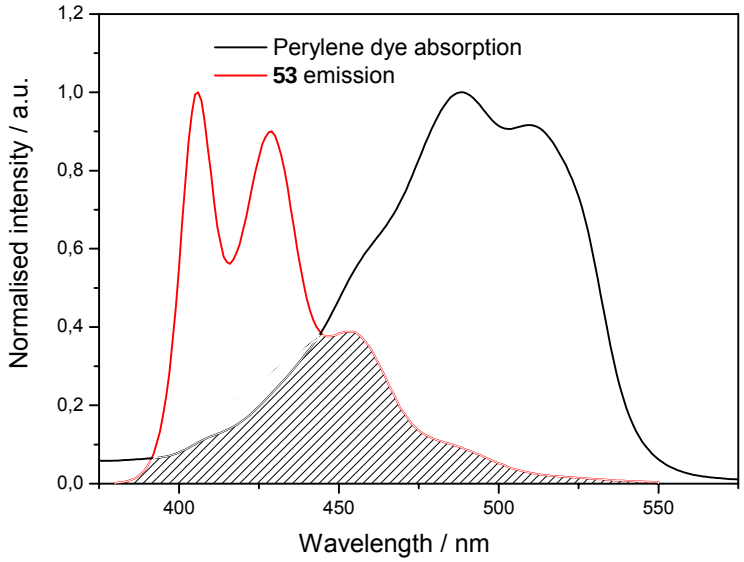

Figure 4.16. Normalised emission spectrum of 53 and absorption spectrum of perylene dye, demonstrating the spectral overlap (shaded area).

The dye end-capped indenofluorene dimer, **57**, has been sent to our collaborators for SMS. In addition to the relative orientation of the chromophores, it is hoped that the SMS investigation will yield additional information on the Förster energy transfer processes that occur in single molecules of **57**.[6,17]

4.2.3 Indenofluorene monoketone

In the literature synthesis of poly(tetraalkylindenofluorene), the indenofluorene molecule is alkylated by treatment with n-BuLi then alkyl bromide, and repeated to afford the tetraalkyl indenofluorene, Scheme 4.6. There is the possibility for the reaction to not go to completion, and that some monoalkylated bridge-head positions remain. These positions are susceptible to oxidation, as described in Section 1, to give the ketonic defect structure shown in Scheme 4.6.

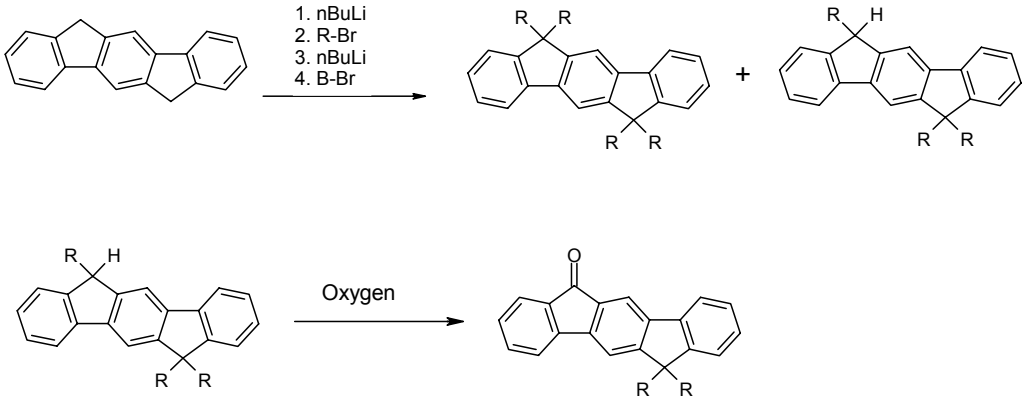

Scheme 4.6. Full and partial alkylation of indenofluorene, and subsequent oxidation of tri-alkyl indenofluorene.

In order to test whether this ketone moiety is responsible for the long wavelength emission in poly(indenofluorene) based OLED's, the potential defect structure was synthesised. The synthesis of the indenofluorene monoketone is presented in Scheme 4.7.

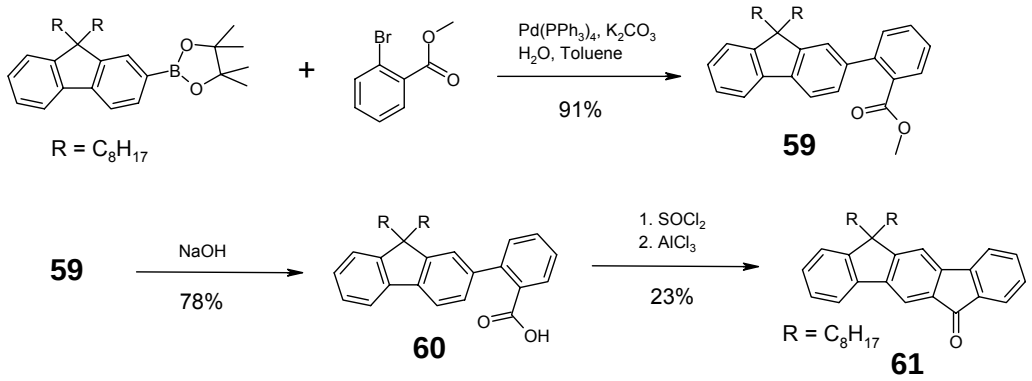

Scheme 4.7. Synthetic route to indenofluorene monoketone.

The synthesis of the indenofluorene monoketone is a variation of the attempted synthesis of monobromoindenofluorene, Scheme 4.2. The palladium catalysed Suzuki cross coupling reaction to afford 2-(9,9-dioctyl-fluorene)-benzoic acid methyl ester (**59**) proceeded with a 91% yield.

The ring closure to form the ketone moiety was the limiting step in the synthetic route shown in Scheme 4.2. To assist in the ring closure, the methyl ester was deprotected to afford the corresponding carboxylic acid, **60**, in 78% yield. The ring closure was attempted using a range of various Lewis and Brønsted acids such as triflic acid, sulphuric acid, methane sulphonic acid and boron triflouride. The ring closure reactions using these reagents were not successful, and afforded either the starting material or sulphonated products. The successful ring closure was achieved by the intramolecular Friedel-Crafts acylation of the acid chloride derivative of **60**. The reaction afforded the target indenofluorene monoketone with a 23% yield in 2 steps. The low yield of the two reactions is due to incomplete ring closure, either due to the presence of water during the Friedel-Crafts reaction or incomplete conversion of the acid to the acid chloride.

The ^{1}H NMR spectrum of **61** in CD_2Cl_2 is presented in Figure 4.17. The important feature to note is the two singlet peaks marked in red at 7.97 ppm and 7.55 ppm, both with an integration of one proton. If the Friedel-Crafts ring closure reaction had occurred at the other possible position there would be no singlet peaks in the ^{1}H NMR spectrum. The splitting pattern and integration of the aromatic region of the

spectrum in Figure 4.17, together with FDMS, strongly supports the structure of **61** as shown in Scheme 4.7.

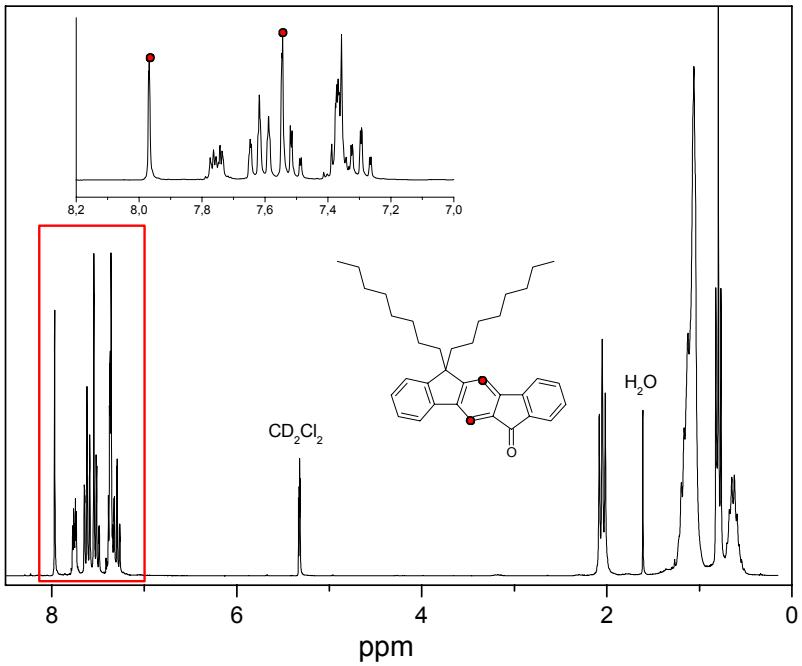

Figure 4.17. ^{1}H spectrum of 61 in CD_2Cl_2, 300 MHz.

CV was measured on a 1 mM methylene chloride solution of **61** with a platinum counter electrode and a silver quasi-reference electrode, calibrated against ferrocene-ferrocenium. The complete and reduction cyclic voltamogram are presented in Figure 4.18. **61** shows an oxidation onset at 1.4 V, and a reduction onset at -1.25 V. The method to transform the oxidation and reduction onset values to the IP and EA values respectively was discussed in Section 2. If the work function of silver is taken to be 4.4 eV, the IP and EA values of **61** are found to be at -5.8 eV and -3.15 eV respectively.[18] This results in an electrochemical bandgap of 2.65 eV. Figure 4.18b demonstrates the reversible reduction of **61** in solution, with an EA of -3.15 eV. As mentioned in Section 3, a material that is reversibly reducible with a low EA such as **61** could be used as an ETM.

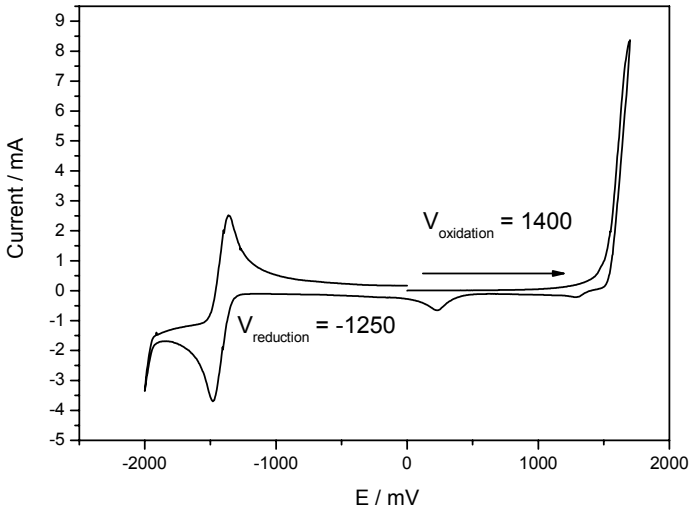

a.

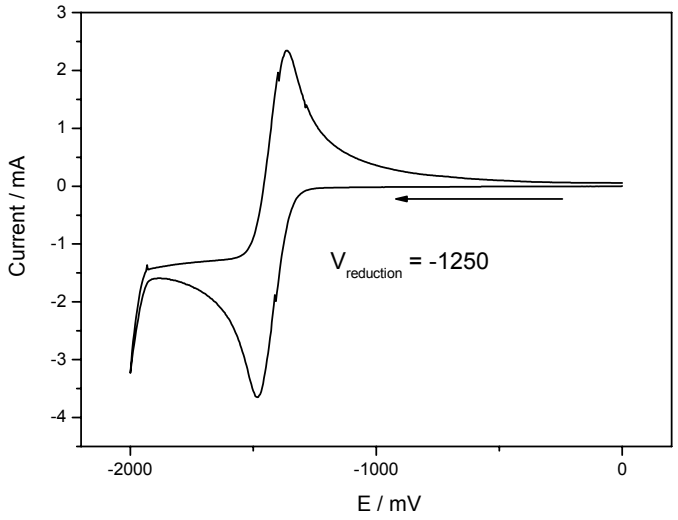

b.

Figure 4.18. Cyclic voltamogram of methylene chloride solution of 61. a. Full plot. b. Reduction. Onset voltage of oxidation and reduction is shown.

The absorption spectra of **61** in toluene, chloroform and acetonitrile is presented in Figure 4.19. The indenofluorene monoketone **61** exhibits an absorption maximum at 327 nm, 328 nm and 329 nm in acetonitrile, toluene and chloroform respectively. Figure 4.19b shows **61** has an additional absorption at longer wavelengths, with an absorption maximum of 427 nm. This low energy transition is due to the symmetry forbidden π-n* transition of the carbonyl group.[19]

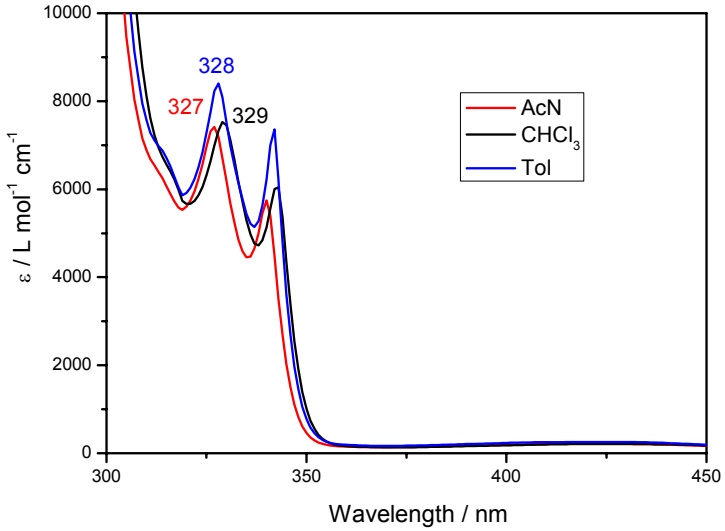

a.

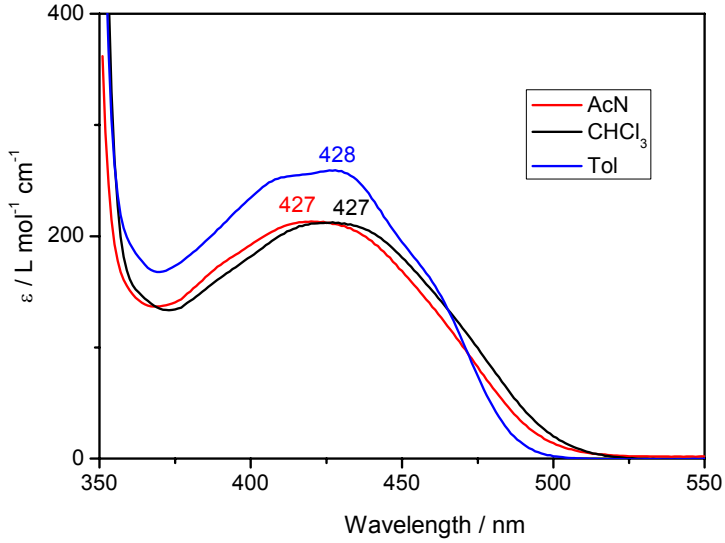

b.

Figure 4.19. a. UV-vis absorption spectra of 61 in acetonitrile (AcN), chloroform ($CHCl_3$) and toluene (Tol). b. Spectrum from 350 nm to 550 nm.

The solvent dependent photoluminescence spectra of **61** in acetonitrile, chloroform and toluene are shown in Figure 4.20. In all solvents **61** exhibits a broad emission with emission maxima greater than 500 nm. The emission maximum of **61** in the non-polar solvent toluene is 527 nm, compared to an emission maximum of 560 nm and 568 nm for solutions of **61** in acetonitrile and chloroform respectively, more polar solvents. The lower energy emission of **61** from acetonitrile and chloroform,

compared to the non-polar solvent toluene, is due to the stabilisation of the charge transfer excited state by the polar solvents. This results in a lower energy emission.

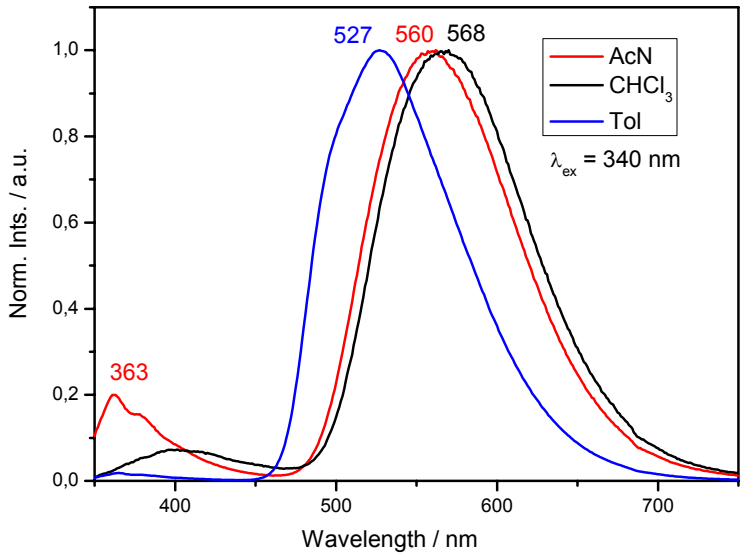

Figure 4.20. Photoluminescence emission spectra of 61 in acetonitrile (AcN), chloroform ($CHCl_3$) and toluene (Tol) (λ_{ex} = 340 nm).

The long wavelength emission of poly(indenofluorenes) is a broad peak with a maximum of 565 nm.[1,20] A direct comparison of the emission maxima of **61** with previously described poly(indenofluorenes) indicates that a ketone defect could be the source of the low energy emission.

The solvatochromism of poly(monoalkylfluorene), *ie* the absence of the long wavelength emission in methylene chloride, was discussed in Section 1 as proof of the defect emission, as more polar solvents increase the rate of non-radiative decay by solvent quenching.[21] While the emission maximum of **61** is solvent dependant, there is no observed reduction in the emission intensity of the long wavelength emission due to solvent quenching. This does not preclude ketone defects to be the source of long wavelength emission in poly(indenofluorenes) however, as the two systems are fundamentally different. In the case of the solvatochromism of poly(monoalkylfluorene), there are a small number of ketone defects spread throughout a polymer chain, while every molecule of **61** has the ketone embedded.

To further investigate the nature of the long wavelength emission in indenofluorene based materials, the emission spectra of **61** in toluene was obtained at a variety of concentrations. For poly(monoalkylfluorene), the observed emission maxima are not concentration dependant.[21] This is seen as an argument against the role of aggregate or excimer formation in the low energy emission, as the formation of excimers or aggregates should increase with concentration. The concentration dependant emission spectra of **61** are presented in Figure 4.21a, with the lowest three concentration plots expanded in Figure 4.21b.

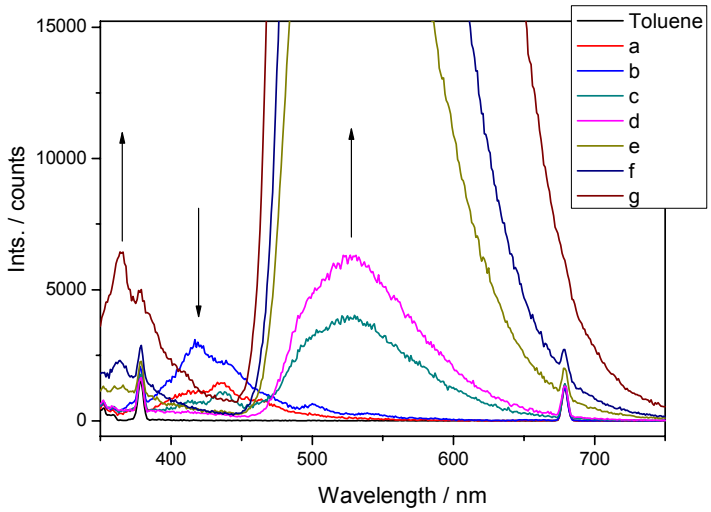

a.

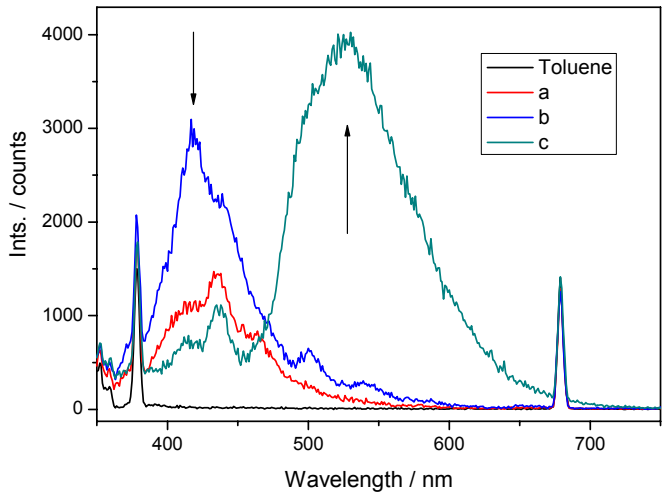

b.

Figure 4.21. Concentration dependant emission spectra of 61 in toluene: a 7.7 x 10^{-9} M (red), b 1.5 x 10^{-8} M (blue), c 7.7 x 10^{-7} M (dark cyan), d 1.5 x 10^{-6} M (pink), e 7.7 x 10^{-6} M (dark yellow), f 1.5 x 10^{-5} M (navy), g 7.7 x 10^{-5} M (wine). The solvent emission is also included (black).

Figure 4.21 demonstrates the emission spectrum of **61** is concentration dependant, with three bands of importance indicated, at 364 nm, 418/435 nm and 527 nm. At the lowest concentrations, there is an emission band at 418 nm and 435 nm. As the concentration of **61** increases, this emission first increases (plot b) then decreases (plot c). With the diminishing emission at 418 nm there is a corresponding increase in the emission at 527 nm, and then the emission at 364 nm can be observed when the concentration of the solution gets above 7.7 x 10^{-6} M (plot e).

The concentration dependant nature of the emission spectra of **61** can be explained in terms of the formation of dimers, driven by the strong dipole interactions of the carbonyl groups. It is known that upon aggregation, a splitting of the emissive energy level takes place.[22] At very low concentrations, in the case for **61** below 15 nM, the molecules in solution are isolated. So as the concentration of **61** increases from plot a to plot b, the intensity of the emission at 418 nm and 435 nm increases. At higher concentrations, 0.77 μM, **61** forms dimers and a band at 527 nm is observed, while the emission at 418 nm decreases. Above 7.7 μM a third band is observed at 364 nm, which increases with concentration.

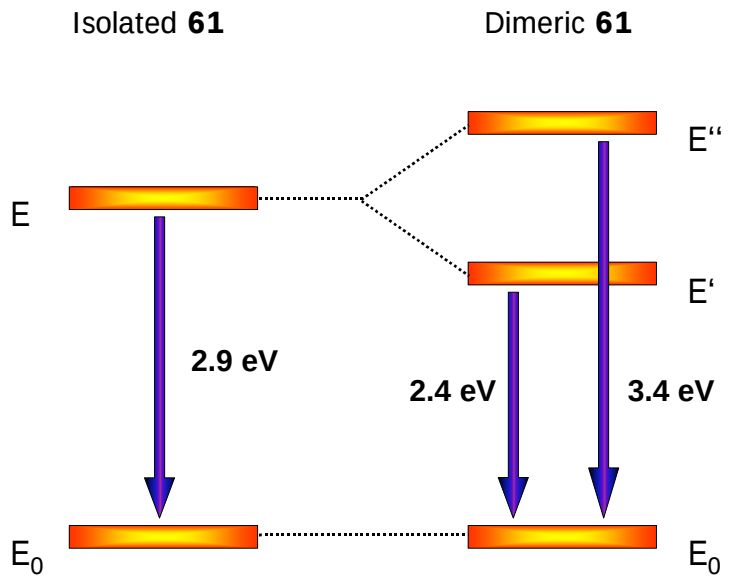

Figure 4.22. Schematic representation of the proposed exciton band splitting for 61. The emission values are given in eV (2.9 eV, 435 nm; 2.4 eV, 527 nm; 3.4 eV, 364 nm).

Figure 4.22 illustrates the proposed exciton band splitting.[22] The emission maximum of a single molecule of **6**1 in toluene is taken to be the band at 435 nm, this corresponds to an energy of 2.9 eV. As the dimers form with increasing concentration, the exciton band splitting results in two new emission energies.[22] Depending on the exact symmetry conditions of the higher (E") and lower (E') energy levels, their radiative coupling to the ground state is determined.[22] First the lower energy emission at 2.4 eV, 527 nm, appears, followed by the higher energy emission at 3.4 eV, 363 nm. The emission energy of the isolated molecules of **61** is halfway between the split bands. The fact that the lower energy emission of **61** at 527 nm is the most intense observed implies that the symmetry-activated component of the excimer is the low energy level. However, further increasing the concentration of **61** results in the activation of the high energy band, possibly due to changes in the symmetry conditions following the formation of larger excimer aggregates.

In order to elucidate whether the dimerisation of **61** occurs in the ground state, aggregate formation, or in the excited state, excimer formation, the concentration dependent absorption spectra was obtained. No concentration dependent change in the absorption spectra was observed at high concentrations. At very low concentrations the signal to noise ratio was too high, resulting in unsatisfactory spectra.

The emission of isolated molecules of **61** is hypothesised to be 435 nm. The emission for an indenofluorene monomer is at approximately 370-380 nm. The bathochromic shift of the emission of **61** compared to the emission of an indenofluorene monomer can be attributed to the electronic effect of the carbonyl group, which may lower the LUMO level of **61**. The presence of two bands at 418 nm and 435 nm can not be explained at this time.

61 is a model for the potential cause of the long wavelength emission observed in poly(indenofluorene) based OLED's, a monoketone defect. The interaction between this model dopant and a poly(indenofluorene) was investigated using time-resolved photoluminescent spectroscopy by our collaborator, Dr P.E. Keivanidis (MPIP-Mainz, Ackermannweg 10, D-55128 Mainz, Germany).

From the time-resolved emission data of various poly(indenofluorene) materials with different pendant groups, it was found that the spectrum of the polymer with the aryl-ocytl side chain (PAOIF) does not possess the spectral features that would be indicative of significant amounts of the ketone defect on the polymer backbone.[23] Therefore, PAOIF can be considered as an appropriate host compound for the guest defect molecule **61**. Blends of PAOIF and **61** at various guest concentrations were spin coated onto glass substrates, to give films of a thickness of approximately 60 nm.[23] In solid state the process of energy transfer from host to guest is 3-dimensional and faster than the on-chain energy transfer, and so the fact the guest is not covalently bound to the host does not affect the conclusions of the experiment.[23,24]

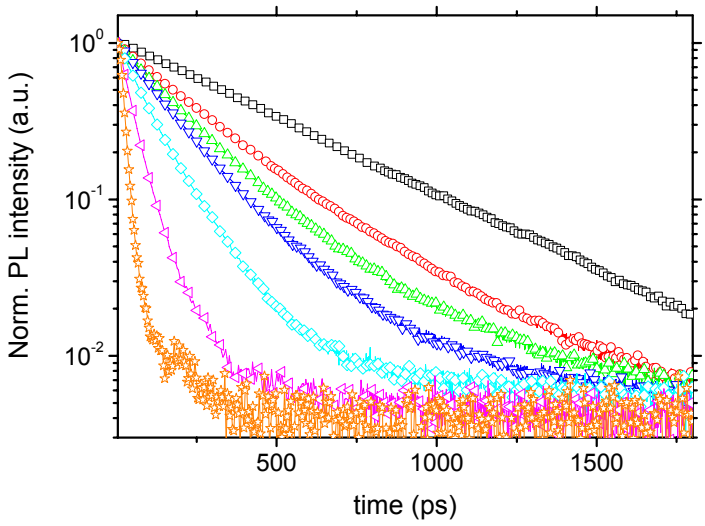

Figure 4.23. Room temperature normalised transient decays of singlet emission (PAOIF emission maximum) monitored for thin films on glass substrate, of blends consisting of PAOIF with increased 61 content: 0 wt% 61 film (circles), 0.03 wt% 61 film (up-triangles), 0.1 wt% 61 film (down-triangles), 0.3 wt% 61 film (diamonds), 1 wt% 61 film (tilted triangles), 4.5 wt% 61 film (stars). λ_{ex} = 390 nm (3.18 eV), p= 10^{-5} mbar. For comparison the normalized transient decay of singlet emission 0 wt% 61 in degassed 2-methyltetrahydrofuran (MTHF) solution (squares) is depicted.

The normalised single decay transients obtained for the variously doped PAOIF films is presented in Figure 4.23.[23] Figure 4.23 shows that as the concentration of guest molecule increases in the host matrix, the singlet emission from the polymer decays more rapidly. From the decay of the fluorescence, the lifetime values of PAOIF with varying amounts of **61** can be determined. From these lifetime values at various concentrations of the quencher **61**, [Q], a Stern-Volmer plot can be

constructed, according to the equation shown in Equation 4.5.[23] τ^0 and τ are the lifetime values for PAOIF in the absence and presence of the quencher **61**, and k_q represents the quenching rate of the emission.

Equation 4.5. Stern-Volmer equation.

$$\frac{\tau^0}{\tau} = 1 + \tau^0 k_q [Q]$$

The Stern-Volmer plot of **61** doped PAOIF at two temperatures is presented in Figure 4.24. The observed linearity of the plot indicates a homogeneous mixing of the guest in the host films in the doping concentration range used in this experiment.[23] The reduction of the PAOIF singlet emission is attributed to a dynamic quenching process that arises from the excitation energy transfer from host to guest.[23] Figure 4.24 inset shows a parallel reduction in the cw-PL fluorescence intensity and lifetime for increasing concentrations of **61**. This concomitant decrease in combination with the linear Stern-Volmer plot excludes the formation of a non-fluorescent excimer between PAOIF and **61**.[23]

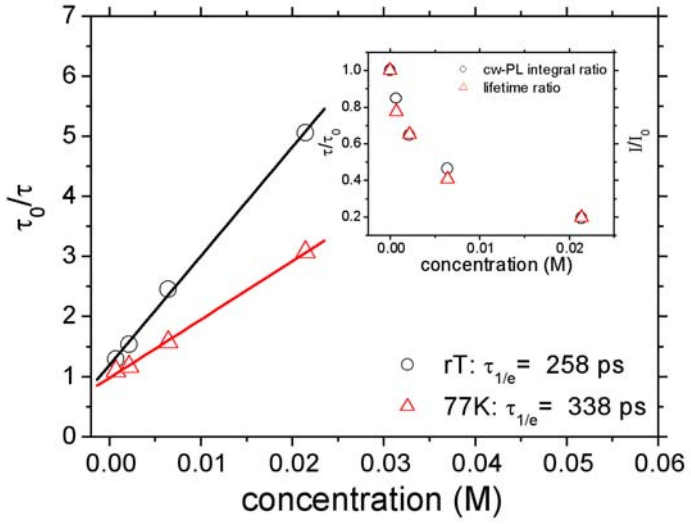

Figure 4.24. Stern-Volmer plot of PAOIF singlet emission for films of blends consisting of PAOIF with increased 61 content at room temperature (circles) and 77 K (triangles). Solid lines are linear fits to the data. λ_{ex} = 390 nm (3.18 eV), p= 10^{-5} mbar. Inset: comparison of the relative decrease in lifetime (triangles) and continuous-wave PL (cw-PL) singlet intensity (circles) of PAOIF as film with increased 61 content. Intensity ratios correspond to PL integral ratios determined from spectral integration of obtained cw-PL spectra.

Based on the Stern-Volmer formalism, the quenching rates, k_q, of energy transfer can be deduced. From the linear fit of Figure 4.24, the quenching rate at room temperature and 77K was found to be 7.05 x 10^{11} $M^{-1}s^{-1}$ and 2.88 x 10^{11} $M^{-1}s^{-1}$, respectively.[23] The values for the rate constant can be transformed into the energy transfer time, τ_{ET}, at a given concentration using the equation shown in Equation 4.6. The values for the singlet PL lifetime values and energy transfer times are tabulated in Table 4.1.

Equation 4.6. Energy transfer time as a function of guest concentration and quenching rate constant.

$$\tau_{ET} = \left([Q] k_q \right)^{-1}$$

The calculated energy transfer times were found to be in the order of picoseconds. So at room temperature, with a 0.3wt% concentration of **61**, the quenching of an exciton will take place within 220 ps. This is comparable to the observed radiative lifetime for pristine films of PAOIF.[23] From these results it can be hypothesised that the concentration of quenchers, or defect ketone sites, in a polymer matrix should be less than 0.3wt% for the desired colour stable emission. At lower concentrations, the rate for the singlet emission becomes higher than the rate of energy transfer to the quenching sites.

Table 4.1. Singlet lifetime date with doping concentration of 61 in PAOIF films. Singlet lifetime of PAOIF was determined from data presented in Figure 4.23. The calculated times from energy transfer from PAOIF to 61 are presented. The density of the polymer film was taken as 1 g/cm^3.

61 doping content / wt%	[Q] / mmolL^{-1}	Singlet PL lifetime value τ / ps	Energy transfer time τ_{ET} / ps
0	0	258	-
0.03	0.70	200	2029
0.1	2.14	168	663
0.3	6.43	105	221
1	21.41	51	66

The decrease in quenching rate at lower temperatures is consistent with previous reports of a thermally activated component in the energy transfer rate from a polymeric host to a guest molecule.[25] The energy transfer is described as a two-step process where the diffusion of the photoexcitons within the polymer is followed by energy transfer to the dopant.[25] At lower temperatures the diffusion process is slowed, leading to a reduction in the observed energy transfer rate. As a result, the doping experiment can only elucidate information regarding an observed quenching rate k_q, a product of the rate of Förster-type energy transfer and the rate of exciton migration.[23]

4.2.3.1 Tetraphenylene diketone.

After the successful synthesis of indenofluorene monoketone, the synthetic strategy was applied to a different system. The synthetic route to a tetraphenylene diketone is shown in Scheme 4.8.

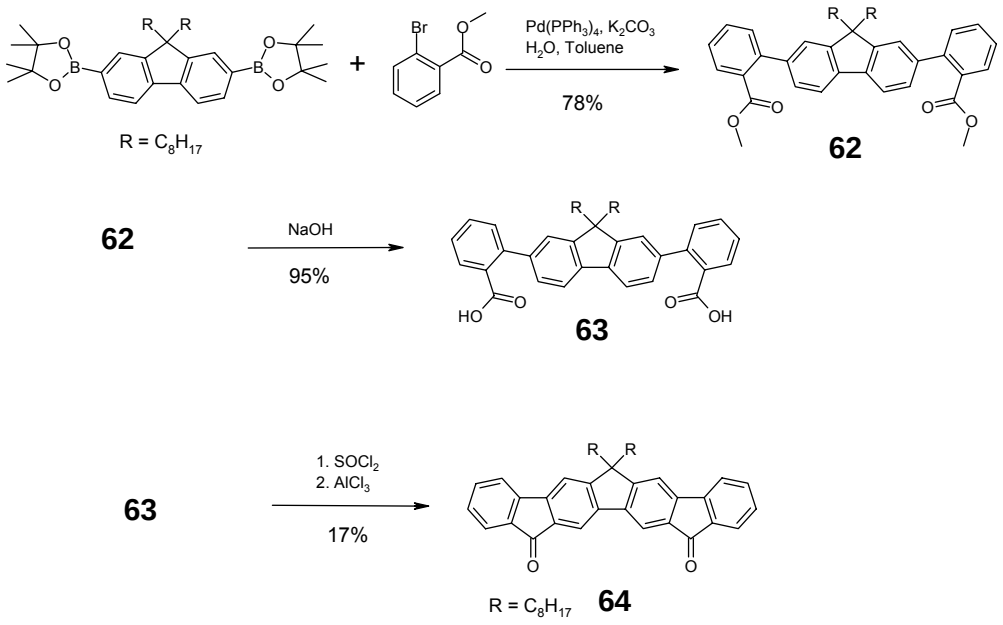

Scheme 4.8. Synthetic route to tetraphenylene diketone, 64.

The synthesis of **64** is analogous to the synthetic route to form **61**, except a bis-boronic ester of fluorene is used in the first Suzuki cross coupling reaction. This palladium catalysed reaction proceeded with a yield of 78%, to give the dimethyl ester

62. The deprotection of the methyl ester functionalities to afford the di-acid **63** proceeded with a yield of 95%. The conversion of the carboxylic acids to the corresponding acid chloride, and the subsequent Friedel-Crafts acylation to afford the tetraphenylene diketone, **64**, proceeded with a yield of 17%.

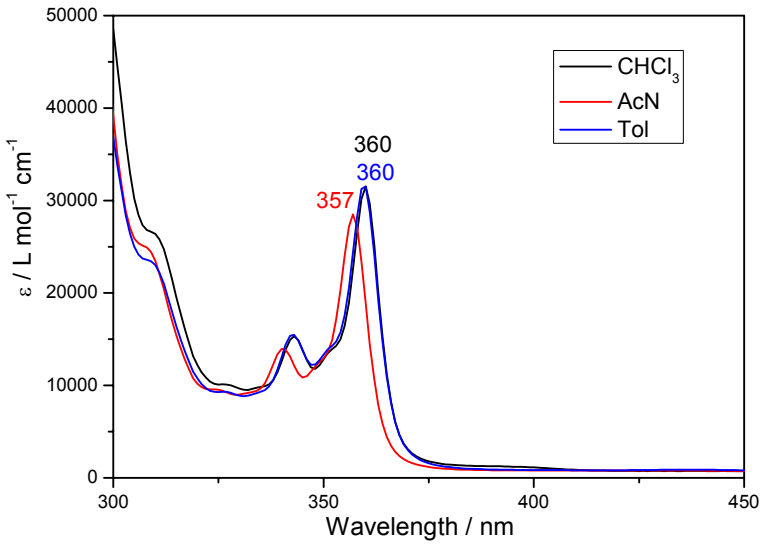

a.

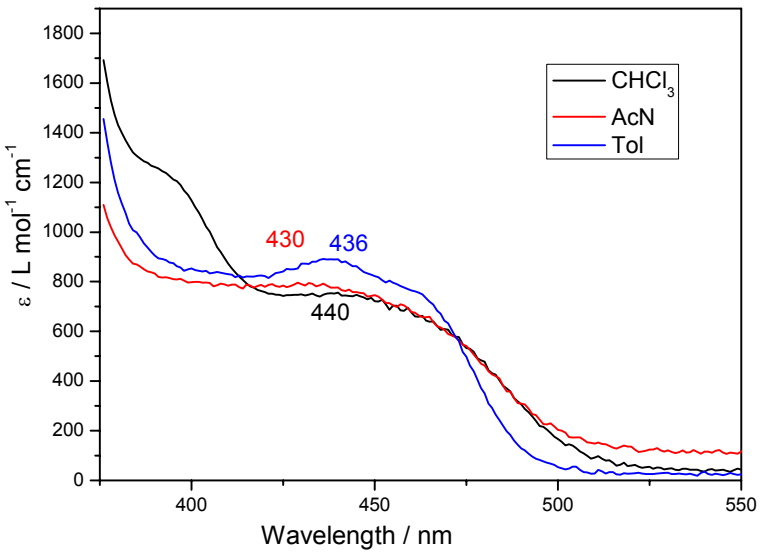

b.

Figure 4.25. a. UV-vis absorption spectra of 64 in acetonitrile (AcN), chloroform ($CHCl_3$) and toluene (Tol). b. Spectrum from 375 nm to 550 nm.

The UV-vis absorption spectrum of **64** in acetonitrile, chloroform and toluene is presented in Figure 4.25. **64** exhibits an absorption maximum at 360 nm in chloroform and toluene, and 357 nm in acetonitrile. The absorption maxima are bathochromically shifted compared to the absorption maxima of **61** in Figure 4.19, due to the extended conjugation of the tetraphenylene compared to the indenofluorene aryl structure. Figure 4.25b shows the absorption spectrum from 375 nm to 550 nm. The weak absorption, which we attribute to the two carbonyl groups of **64**, can be seen with a maximum absorption at 430 nm, 436 nm and 440 nm for acetonitrile, toluene and chloroform respectively.

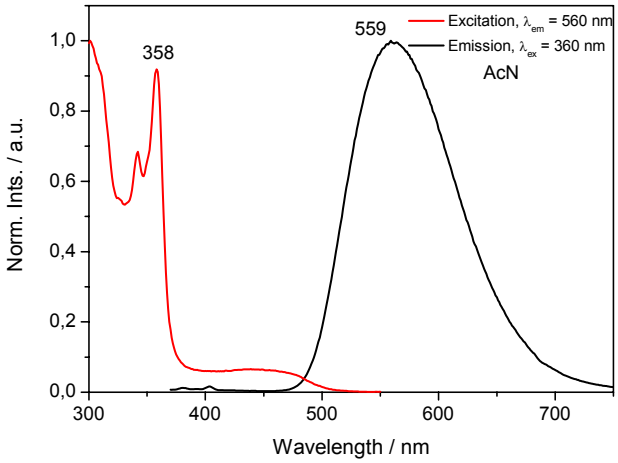

a.

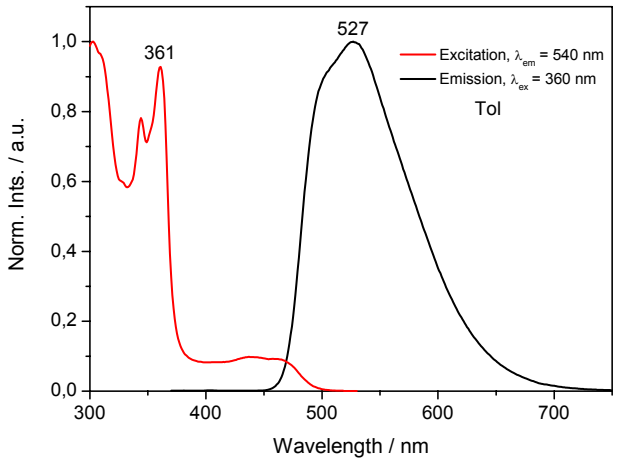

b.

Figure 4.26. Excitation and emission spectra of 64 in a. Acetonitrile (λ_{em} = 560 nm, λ_{ex} = 360 nm) b. Toluene (λ_{em} = 540 nm, λ_{ex} = 360 nm).

The excitation and emission spectra of **64** are presented in Figure 4.26. Figure 4.26a and b show **64** has a broad emission with a maximum at 559 nm in acetonitrile and 527 nm in toluene. The emission maximum of **64** is the same as the emission maximum of **61** in the same solvents. This is expected, as the carbonyl π*-n emitting transition is not affected by the length of the conjugated phenylene unit. In Figure 4.21 it was demonstrated that the emission of **61** at 530 nm is due to excimer formation. The similarity of the polarity dependence of the spectra of **61** and **64** can be explained in terms of an intermolecular charge transfer process within the excimer. In both cases the carbonyl moieties drive the formation of aggregates. The intermolecular charge transfer excited state of the excimer is stabilised by the polar solvents, hence emission in acetonitrile is at a lower energy than from toluene.

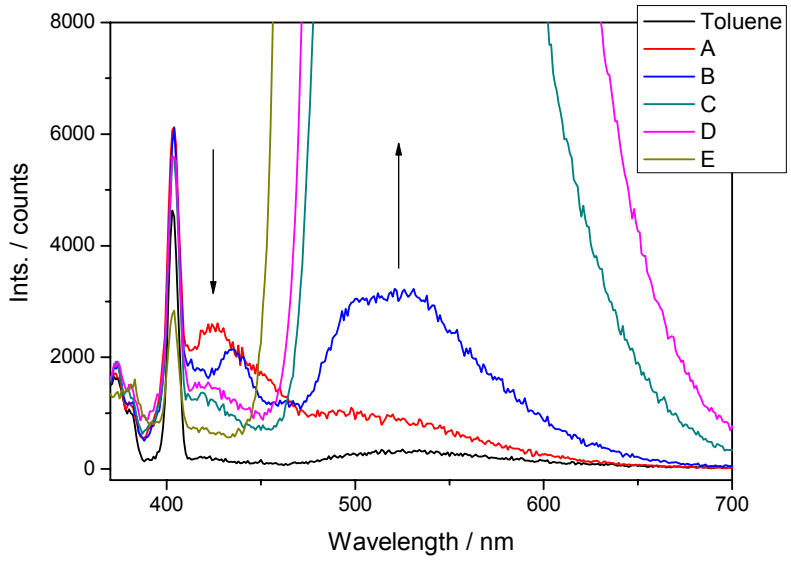

Figure 4.27. Concentration dependant emission spectra of 64 in toluene: a 7.1 x 10^{-9} M (red), b 3.5 x 10^{-8} M (blue), c 3.5 x 10^{-7} M (dark cyan), d 7.1 x 10^{-7} M (pink), e 3.5 x 10^{-5} M (dark yellow). The solvent emission is also included (black).

The concentration dependent emission spectra of **64** in toluene are presented in Figure 4.27. Similar to the emission spectra in Figure 4.21, the low concentration, less than 35 nM, solutions show a reduced emission from the 527 nm band, and the appearance of a band at 425 nm. As the concentration increases, the band at 425 nm decreases, and the band at 527 nm increases. In contrast to the low concentration

emission spectra of **61**, even at the lowest concentration, 7.1 nM, of **64** a significant emission from 527 nm can be observed. As **64** contains two carbonyl moieties per molecule, the dipole interactions between two molecules is expected to be stronger. As a result, the concentration at which the solution of **64** is not aggregating would be lower. In Figure 4.21, increasing concentration resulted in the appearance of two bands, whereas only the band at 527 nm can be observed in the case of **64**. This may be a result of the symmetry of the excimer. Depending on the relative symmetry of the dipoles, the transition from the higher or lower state can be allowed or disallowed.[22] It may be that the symmetry of the individual carbonyl groups in excimers of **64** results in the low energy splitting level having an allowed transition to the ground state, but not the high energy level.

4.3 Conclusion

An efficient synthetic route to monofunctionalised indenofluorene has been developed. This is a very valuable synthon for the synthesis of well defined oligomers of indenofluorene. Monobromoindenofluorene was prepared and used in the synthesis of a novel indenofluorene dimer and trimer. The morphological structure of these well-defined linear molecules was studied by DSC, POM and 2D-WAXS. POM images of the two oligomers indicate that semectic mesophases formed in the various temperature regimes used in these experiments. The 2D-WAXS images of the two oligomers demonstrate clearly the different alignment of the dimer and trimer in an extruded fibre relative to the extrusion direction. The trimer orientates with the rigid aromatic backbone aligned with the extrusion direction whereas the dimer aligns with the aromatic backbone perpendicular to the extrusion direction, due to the increasing influence of the alkyl chains in the competition to align along the extrusion direction.

The indenofluorene oligomers can be further functionalised, and so the facile synthesis of perylene dye end-capped indenofluorene dimer was performed. The emission spectrum of this material showed efficient energy transfer from the indenofluorene backbone to the perylene dye. The rate of Förster energy transfer was discussed in terms of the spectral overlap of the emission of the donor, **53**, and the absorption of the acceptor, perylene monoimide. This material is currently being studied utilising SMS by our collaborators.

In order to probe the basis of the long wavelength emission of OLED's prepared from poly(indenofluorene), an indenofluorene monoketone was synthesised. The compound exhibited absorption only from the indenofluorene backbone, and emission from a low energy band. This broad, long wavelength emission is spectrally similar to the undesired emission form indenofluorene based OLED's. The observed solvatochromism of **61** suggests that a charge transfer excited state is formed, however it has not been elucidated whether it is intermolecular or intramolecular charge transfer. Concentration dependent PL studies of **61** demonstrated this low energy emission is markedly different at very low concentrations, less than 15 nM. We attribute this to be evidence of the formation of excimers, and the emission at long

wavelengths to be due to band splitting of the excited energy levels of the excimer. To investigate the relationship between the emission of a poly(indenofluorene) and the possible defect structure, films of PAOIF and **61** were studied using time-resolved PL spectroscopy. Variation of the concentration of the quencher, **61**, and analysis of the decay curves of the PAOIF emission using Stern-Volmer formulism, the rate constant of quenching was found to be 7.05 x 10^{11} $M^{-1}s^{-1}$ at room temperature. Further analysis shows that the concentration of quencher must be less than 0.3wt% in a device in order for the rate of host emission to be greater than the rate of quenching.

The conclusion from the quenching and concentration dependent emission experiments can be summarised as follows. The emission from poly(indenofluorene) materials is quenched with the introduction of the proposed defect structure **61**, accompanied by the appearance of an emission band at low energies. This low energy emission corresponds spectrally with the observed undesirable long wavelength emission in poly(indenofluorene) based OLED's. The emission spectrum of **61** is found to be concentration dependent, but at very low concentrations. Taken together, the experimental results lead to the hypothesis that the unwanted emission from poly(indenofluorene) based OLED's is due to excimer emission from polymer defects, where excimer formation is driven by the strong dipole interactions of the ketone defects. While this hypothesis adds to the knowledge of the nature of the low energy emission, it doesn't alter the approaches for limitation of the unwanted emission in poly(indenofluorene) based devices, namely separation of the backbone and the limiting of ketone formation.

As an extension of the indenofluorene monoketone, a tetraphenylene diketone was synthesised by an analogous route. This material had an absorption maximum from the phenylene backbone shifted bathochromically compared to the indenofluorene, due to the extended phenylene moiety. The emission maxima from the carbonyl moieties was the same as for the indenofluorene monoketone, indicating the carbonyl groups are unaffected by the length of the phenylene backbone. A similar solvent and concentration dependence in emission was observed for the tetraphenylene diketone as for the indenofluorene monoketone.

4.4 References

(1) Grimsdale, A. C.; Leclère, P.; Lazzaroni, R.; Mackenzie, J. D.; Murphy, C.; Setayesh, S.; Silva, C.; Friend, R. H.; Mullen, K. *Advanced Functional Materials* **2002**, *12*, 729-733.

(2) Setayesh, S.; Marsitzky, D.; Mullen, K. *Macromolecules* **2000**, *33*, 2016-2020.

(3) McKillop, A.; Taylor, E. C.; Bromley, D. *Journal Of Organic Chemistry* **1972**, *37*, 88-&.

(4) Papadopoulos, P.; Floudas, G.; Chi, C.; Wegner, G. *Journal Of Chemical Physics* **2004**, *120*, 2368-2374.

(5) Hedvig, P. *Dielectric Spectroscopy of Polymers*; Akadémiai Kiadó: Budapest, 1977.

(6) Jackel, F.; De Feyter, S.; Hofkens, J.; Kohn, F.; De Schryver, F. C.; Ego, C.; Grimsdale, A.; Mullen, K. *Chemical Physics Letters* **2002**, *362*, 534-540.

(7) White, J. D.; Hsu, J. H.; Fann, W. S.; Yang, S. C.; Pern, G. Y.; Chen, S. A. *Chemical Physics Letters* **2001**, *338*, 263-268.

(8) Hofkens, J.; Vosch, T.; Maus, M.; Kohn, F.; Cotlet, M.; Weil, T.; Herrmann, A.; Mullen, K.; De Schryver, F. C. *Chemical Physics Letters* **2001**, *333*, 255-263.

(9) Yu, J.; Hu, D. H.; Barbara, P. F. *Science* **2000**, *289*, 1327-1330.

(10) Stracke, F.; Blum, C.; Becker, S.; Mullen, K.; Meixner, A. J. *Chemical Physics Letters* **2000**, *325*, 196-202.

(11) Betzig, E.; Chichester, R. J. *Science* **1993**, *262*, 1422-1425.

(12) Tamarat, P.; Maali, A.; Lounis, B.; Orrit, M. *Journal Of Physical Chemistry A* **2000**, *104*, 1-16.

(13) Xie, X. S.; Trautman, J. K. *Annual Review Of Physical Chemistry* **1998**, *49*, 441-480.

(14) Funatsu, T.; Harada, Y.; Tokunaga, M.; Saito, K.; Yanagida, T. *Nature* **1995**, *374*, 555-559.

(15) Ying, L. M.; Xie, X. S. *Journal Of Physical Chemistry B* **1998**, *102*, 10399-10409.

(16) Ego, C.; Marsitzky, D.; Becker, S.; Zhang, J. Y.; Grimsdale, A. C.; Mullen, K.; MacKenzie, J. D.; Silva, C.; Friend, R. H. *Journal Of The American Chemical Society* **2003**, *125*, 437-443.

(17) Izquierdo, M. A.; Bell, T. D. M.; Habuchi, S.; Fron, E.; Pilot, R.; Vosch, T.; De Feyter, S.; Verhoeven, J.; Jacob, J.; Mullen, K.; Hofkens, J.; De Schryver, F. C. *Chemical Physics Letters* **2005**, *401*, 503-508.

(18) Neher, D. *Macromolecular Rapid Communications* **2001**, *22*, 1366-1385.

(19) Kulkarni, A. P.; Kong, X. X.; Jenekhe, S. A. *Journal Of Physical Chemistry B* **2004**, *108*, 8689-8701.

(20) Jacob, J.; Zhang, J. Y.; Grimsdale, A. C.; Mullen, K.; Gaal, M.; List, E. J. W. *Macromolecules* **2003**, *36*, 8240-8245.

(21) Scherf, U.; List, E. J. W. *Advanced Materials* **2002**, *14*, 477-487.

(22) Pope, M., Swenberg, C. *Electronic Processes in Organic Crystals and Polymers*; Oxford University Press: New York, 1999.

(23) Keivanidis, P. E.; Jacob, J.; Oldridge, L.; Sonar, P.; Carbonnier, B.; Baluschev, S.; Grimsdale, A. C.; Mullen, K.; Wegner, G. *Chemphyschem* **2005**, *6*, 1650-1660.

(24) Beljonne, D.; Pourtois, G.; Shuai, Z.; Hennebicq, E.; Scholes, G. D.; Bredas, J. L. *Synthetic Metals* **2003**, *137*, 1369-1371.

(25) List, E. J. W.; Creely, C.; Leising, G.; Schulte, N.; Schluter, A. D.; Scherf, U.; Mullen, K.; Graupner, W. *Chemical Physics Letters* **2000**, *325*, 132-138.

5 Defect bypass-bridging the gap between columns

5.1 Introduction

In terms of the usability of a material as the active component in an OFET, the charge carrier mobility is the one characteristic that most limits the performance of OFET's when compared to silicon based transistors.[1-3] The charge carrier mobility in a device can be influenced by many factors including the inherent nature of the material, the interfacial barriers and in the case of discotic materials, the homogeneous alignment. Due to entropy considerations, no perfectly aligned layer of a discotic material such as HBC is allowed.[4] Defects are formed in every film, and act as a barrier to the overall mobility of a device.[4] One possible solution to this problem of defect structures is to provide an alternate pathway for the charges to migrate towards the drain electrode. Normal charge carrier movement in HBC is one-dimensional along the axis of the stacked columns. With the introduction of a conjugated linker between two columns of HBC, the possibility of intercolumn charge carrier movement is introduced. This should allow for the charge carriers to sidestep the defect structures and migrate to the drain electrode with a high mobility. The synthesis of a novel HBC dimer linked by a conjugated indenofluorene moiety is described in the following, and the discussion of the characterisation presented.

5.2 Results and Discussion

5.2.1 Superindenofluorene

The by-pass molecule must contain HBC anchor groups for insertion into the HBC columns, and a conjugated spacer to allow charge to flow from one HBC to the other. One previously published HBC dimer is the superfluorene, a fluorene molecule where the two benzene rings are substituted with HBC, shown in Scheme 5.1.[5] While this material is not suitable for use as a by-pass molecule due to the small distance between the HBC discs, the synthesis of the superfluorene could be modified to prepare an appropriate material.

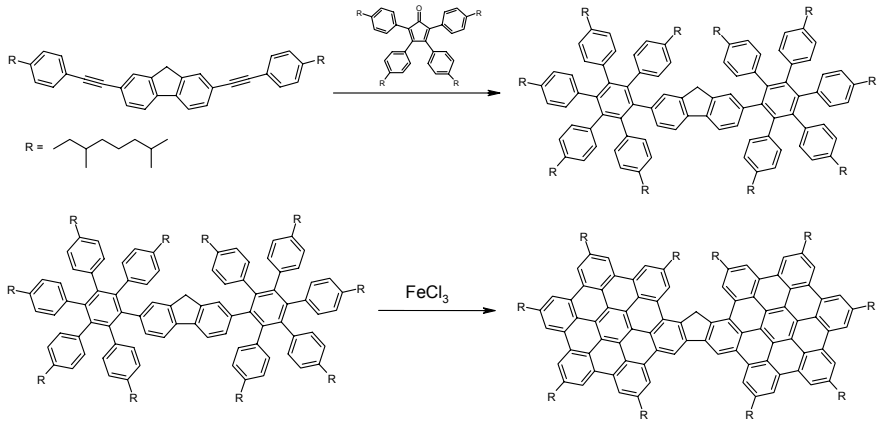

Scheme 5.1. Synthetic route to superfluorene.

While the π-interaction of the aromatic core of HBC's leads to the self-assembly into columnar structures, it is the choice of side chains that determines the spatial arrangement of the columns. As a result of the cylindrical symmetry, the most common arrangement of liquid crystal HBC columns is the hexagonal organisation.[6] The side chains on the periphery of the core adopt an arrangement that usually involves the intercalation of chains between the adjacent cores.[6] As such, the steric effects of the side chains, such as length and branching, greatly effects the packing distances between adjacent HBC columns. Naked HBC, *ie* without any side chains, has a hexagonal unit cell parameter, a_{hex}, of 1.28 nm.[6] One of the largest value of a_{hex} recorded has been found to be 3.37 nm, over 2.6 times as large, for the branched alkyl

chain 3,7,11,15-tetramethyl hexadecane.[6] The hexagonal packing of HBC columns with different side chains is shown schematically in Figure 5.1.

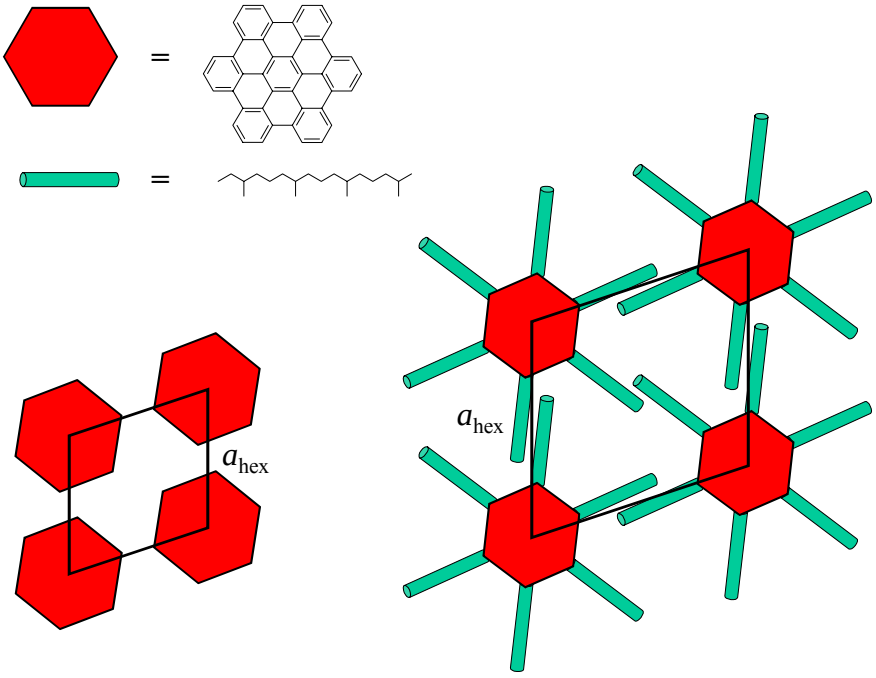

Figure 5.1. Schematic representation of two examples of hexagonal lattice arrangements of HBC based materials.

The possible values for the a_{hex} of the liquid crystal phase of HBC ranges from 1.28 nm to 3.37 nm.[6] The proposed linker must be conjugated and have a length of approximately the correct distance. It is also assumed that the relative orientation of the two HBC units at the end of the linker will also be important. In order to lock the HBC units into the same plane, a completely fused structure may be beneficial. Figure 5.2 displays the proposed bypass molecule structure, superindenofluorene. The distance between the centres of the two HBC cores in an unsubstituted superindenofluorene was calculated by means of Spartan for Windows (AM1 of ground state) to be 1.8 nm, within the range of the HBC a_{hex} values.[6]

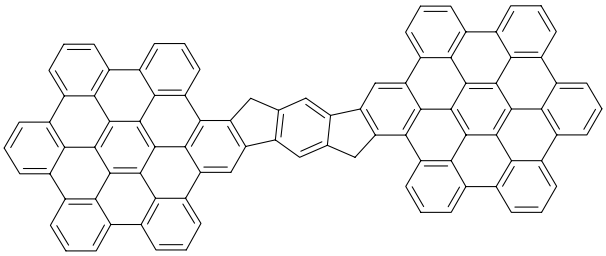

Figure 5.2. Structure of unsubstituted superindenofluorene.

In order to separate the HBC discs by an appropriate distance, the synthesis of a superindenofluorene-based material was proposed. However, unsubstituted bridgehead carbons in superindenofluorene would be susceptible to oxidation. In order to render this oxidation irrelevant, the indenofluoren-6,12-dione was selected as the linker for the molecule. The synthesis of the superindenofluorene diketone is presented in Scheme 5.2.

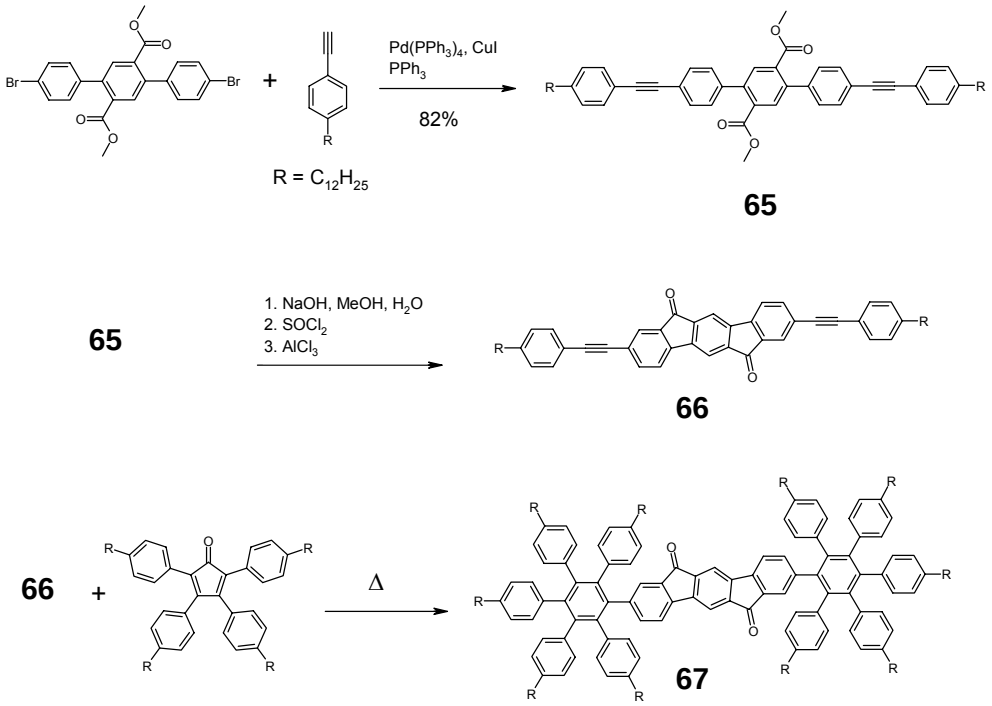

Scheme 5.2. Synthetic route to dendronised indenofluorene diketone, 67.

The Hagihara-Sonogashira palladium catalysed cross coupling reaction of a dibromoterphenyl dimethyl ester with *p*-bromo dodecylbenzene gave the di-ethynyl terphenyl, **65** in 82% yield. The methyl ester functionalities were converted to the

corresponding acid and then to the acid chloride. This was then transformed into the indenofluorene diketone, **66**, via a Friedel-Crafts acylation. Previous attempts to prepare unsubstituted indenofluorene diketone were unsuccessful due to the low solubility of the material. It was envisaged that the long alkyl phenyl groups in **66** would help to solubilise the material, however **66** was also insoluble and uncharacterised. The next step in the synthetic route, Diels-Alder cycloaddition of **66** with tetra-alkylphenyl cyclopentadienone (C_{12}Cp), was attempted with the insoluble **66** anticipating that the dendronised material **67** will be soluble. The reaction was attempted using microwave heating, at 250°C, with diphenyl ether as the solvent in a sealed tube. Heating using microwave radiation allows the direct heating of the substrates, not the solvents, and therefore increases the rate of the reaction. This heating method was anticipated to solubilise **66** enough so that the reaction can occur, to yield a more soluble product in **67**. However, with extended reaction times and increased heating **67** could not be formed, due to the insoluble starting material.

An alternate synthetic route was attempted. The Diels-Alder reaction is first before the formation of the diketone, as this should result in a soluble dendronised material. The substituted dendrons should prevent the strong dipoles of the planar indenofluorene diketone from stacking, and so the diketone should be soluble. The alternate synthetic route towards **67** is shown in Scheme 5.3.

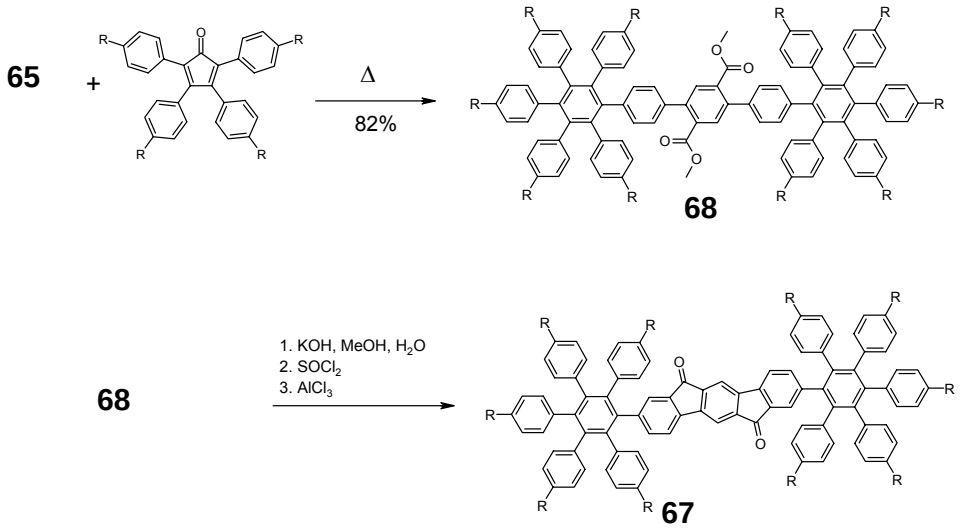

Scheme 5.3. Alternate synthetic route to dendronised indenofluorene diketone, 67.

The Diels-Alder cycloaddition of **65** with $C_{12}Cp$ was carried out under microwave heating conditions in a sealed tube. A 2.6 molar equivalent of $C_{12}Cp$ was used in order to drive the reaction to completion, however the reaction still required extended heating times of up to 16 hours to obtain a complete conversion of **65** to the product, **68**. The excess $C_{12}Cp$ could be removed from the desired product with careful column chromatography. The dendronised diester was soluble in common organic solvents, and could be characterised by NMR and mass spectroscopy. The conversion of the ester functionalities to the diacid with potassium hydroxide proceeded quantitatively, and characterised by the loss of the methyl ester peak in the ^1H NMR spectrum. However, the conversion of the carboxylic acid groups to the corresponding acid chloride and subsequent Friedel-Crafts acylation did not yield the desired product **67**. No product was observed in the crude mass spectra, or after an attempted purification by column chromatography. It is possible that the $AlCl_3$ could cleave the alkyl chains in the reaction, however no assignable peaks for such an event were found in the mass spectra.[7]

As the intermediate compound **67** could not be obtained, an alternate target material was designed for use as a by-pass molecule in HBC based OFET's. Originally the indenofluorene diketone was chosen as the linker part of the by-pass molecule due to the planar structure, which was envisaged to be most suited to slot into HBC columns. As the linker part of the by-pass molecule is not actually in the columnar structure, rather in the area between the HBC columns where the soft alkyl chains of the HBC molecules can adopt a suitable conformation to accommodate the substituents of the linker part, tetraalkyl-indenofluorene was chosen as the linker for a by-pass molecule. The previous problems of solubility with the indenofluorene diketone can thus be avoided. The synthesis of a super tetraalkyl-indenofluorene is presented in Scheme 5.4.

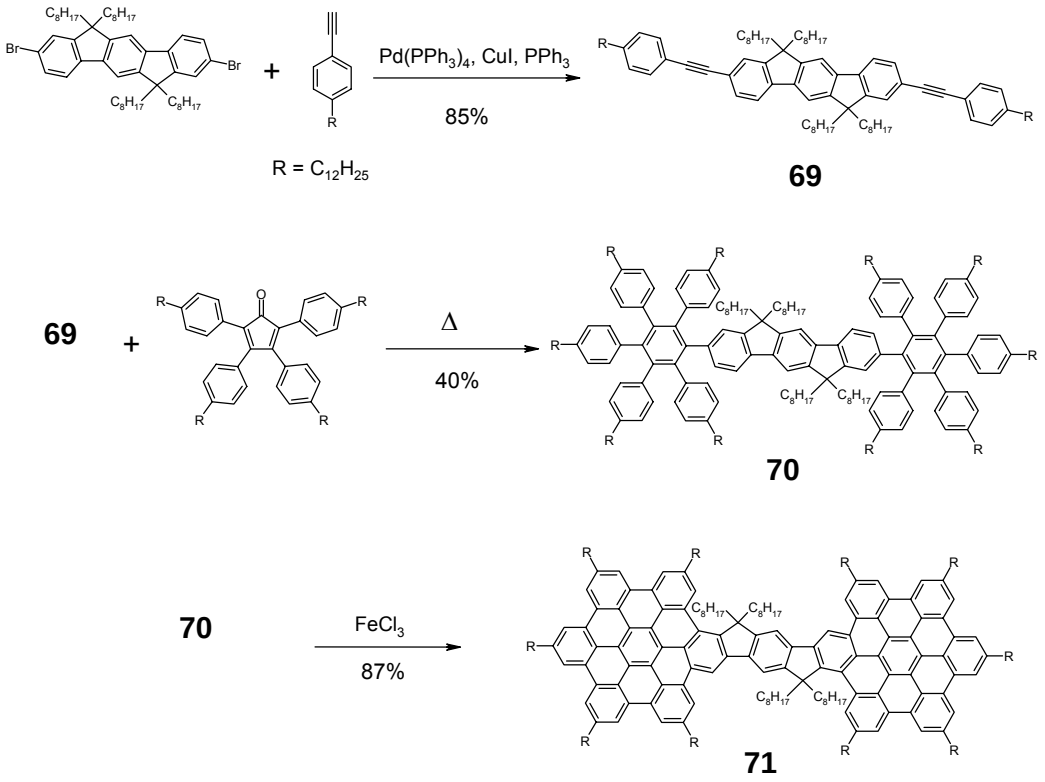

Scheme 5.4. Synthetic route to super tetraalkyl-indenofluorene, 71.

The palladium catalysed Hagihara-Sonogashira coupling of tetraoctyl dibromo indenofluorene with *p*-bromo dodecylbenzene afforded the di-ethynyl indenofluorene **69**, in an 85% yield. Similar to the synthesis of **68**, the Diels-Alder cycloaddition of **69** with C_{12}Cp was carried out in a microwave reactor in a sealed container, at 270°C, with a 3.3 molar equivalent of C_{12}Cp. The reaction required the high temperature and molar equivalent in order to completely consume all the starting material. **70** was purified by repeated column chromatography, however the material could not be obtained completely pure. By FD MS some dealkylation had occurred, which could not be separated from the desired product, and a satisfactory ^{1}H NMR could not be obtained. The cyclodehydrogenation of **70** was carried out on the impure product.

The oxidative cyclodehydrogenation of **70** was carried out using $FeCl_3$ in an 87% yield. The first attempt to planarise **70** was carried out with a 24 molar equivalent of $FeCl_3$, 1 per hydrogen. The MALDI-TOF MS of the product of this reaction shows incomplete ring closure. The reaction was repeated with an increased amount of $FeCl_3$, 120 molar equivalent or 5 per hydrogen. When an increased

stoichiometry of $FeCl_3$ was used, chlorination becomes more prevalent. The MALDI-TOF MS of **71** from the second reaction mixture is shown in Figure 5.3.

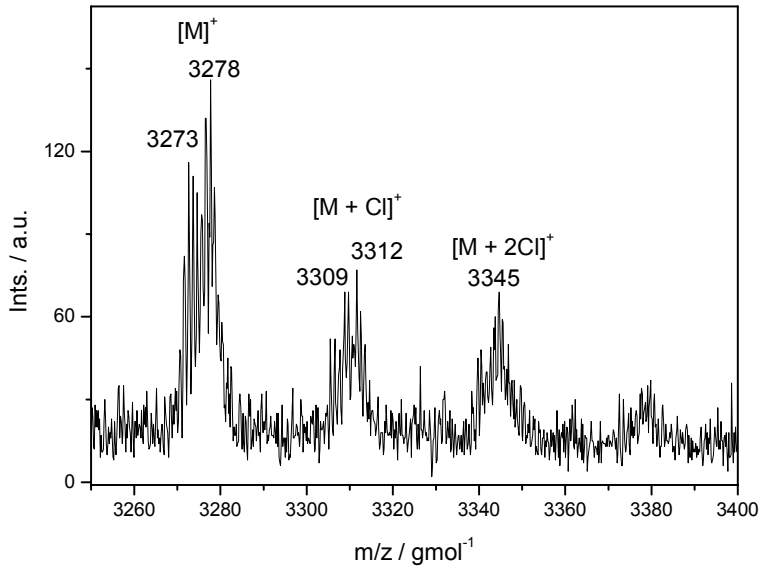

Figure 5.3. MALDI-TOF MS of 71, from a TCNQ matrix.

The calculated mass for the target material **71** is 3275.5 $gmol^{-1}$. Figure 5.3 illustrates two important features. First, the sets of peaks at 3278 $gmol^{-1}$ show that the ring closure reaction did not go to completion. Second, the peaks at higher molecular weights correspond to chlorinated products. Unfortunately, in order to drive the reaction to completion more $FeCl_3$ should be added to the reaction mixture, however this would result in more chlorination. This problem could not be solved. The inability to fully ring close **70** is further demonstrated by the spectroscopic properties of the impure **71**.

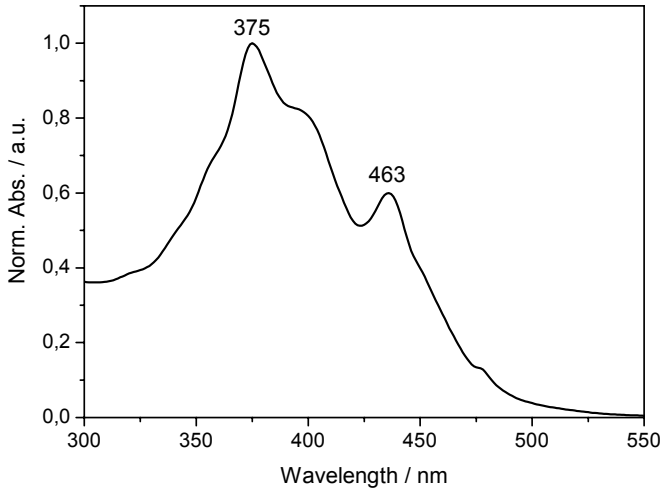

a.

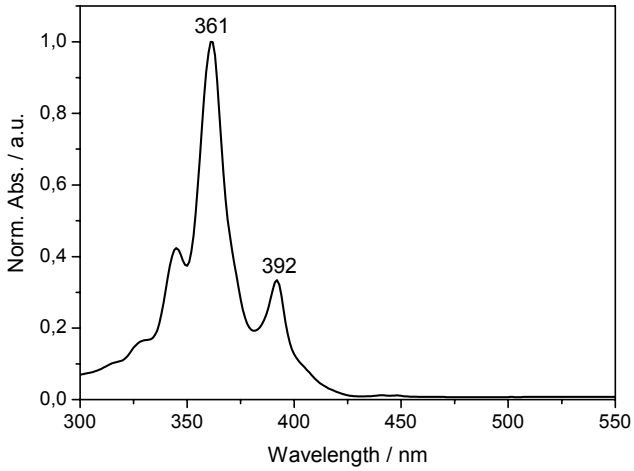

b.

Figure 5.4. UV-vis absorption spectrum of a. 71 in THF and b. hexa(ethylhexyl)HBC in THF.

The UV-vis absorption of **71** and a representative HBC, hexa(ethylhexyl)HBC, is shown in Figure 5.4. The UV-vis absorption spectrum of HBC shows a sharp, featured absorption with a maximum at 361 nm, and peaks at 345 nm and 392 nm. The absorption spectrum of **71** is broader than that of HBC, with a maximum at 375 nm and a peak at 463 nm. The maximum absorption of **71** shows a bathochromic shift compared to HBC, indicating a possible extended conjugation of the HBC moiety. This may correspond to a partially ring closed material where one HBC moiety has been formed in plane with the indenofluorene, but not both. A schematic representation of the extended planar section of the molecule that may correspond to

the absorption maximum is shown in Figure 5.5. It is possible that chlorination occurs at the sites for cyclodehydrogenation, which would prevent complete cyclisation of the material.

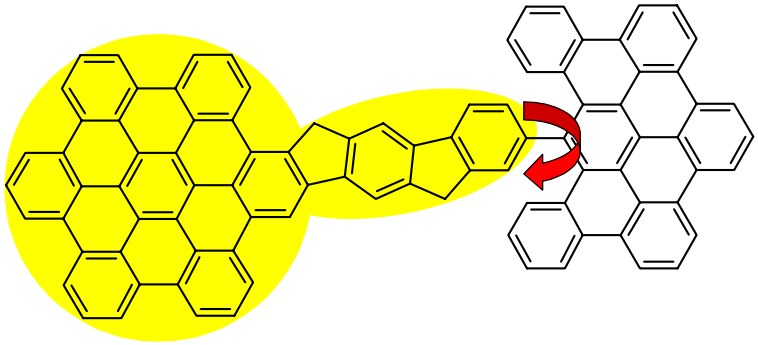

Figure 5.5. Schematic representation of partially ring closed superindenofluorene. Yellow shading represents planarised section of molecule. Red arrow indicates the possible break in conjugation due to incomplete dehydrogenation. Alkyl substituents omitted for clarity.

The peak at 436 nm in Figure 5.4, of which there is no corresponding peak in the spectrum of HBC, may correspond to the fully planarised system of the product. The extended conjugation of the planarised HBC dimer should result in a significant bathochromic shift with respect to the absorption spectrum of a single HBC.

Attempts to prepare a superindenofluorene were unsuccessful due to the insolubility of the indenofluorene diketone intermediate, the inability to perform the Friedel-Crafts acylation on the dendronised terphenyl diester, and the chlorination and incomplete ring closure of the tetraalkyl superindenofluorene. An alternate approach to prepare a by-pass molecule was designed, where the whole system is not fully fused.

5.2.2 HBC dimer-indenofluorene linker

The cyclodehydrogenation of **70** did not proceed to completion. Research in the group has investigated the ring closure to form higher analogues of HBC. This has shown that larger, more complicated structures are more difficult to ring close completely, compared to the synthesis of HBC. The coupling of a preformed HBC unit to a linker is an alternate approach that avoids this problem of ring closure.

Scheme 1.9 shows the Diels-Alder cycloaddition to form a HPB. In this case all the substituents were labelled equivalent, however this is not necessarily the case. Scheme 5.5 shows the synthesis of monobromo HBC from an asymmetrical tolane. This monofunctionalised HBC allows for the synthesis of a linked HBC dimer.

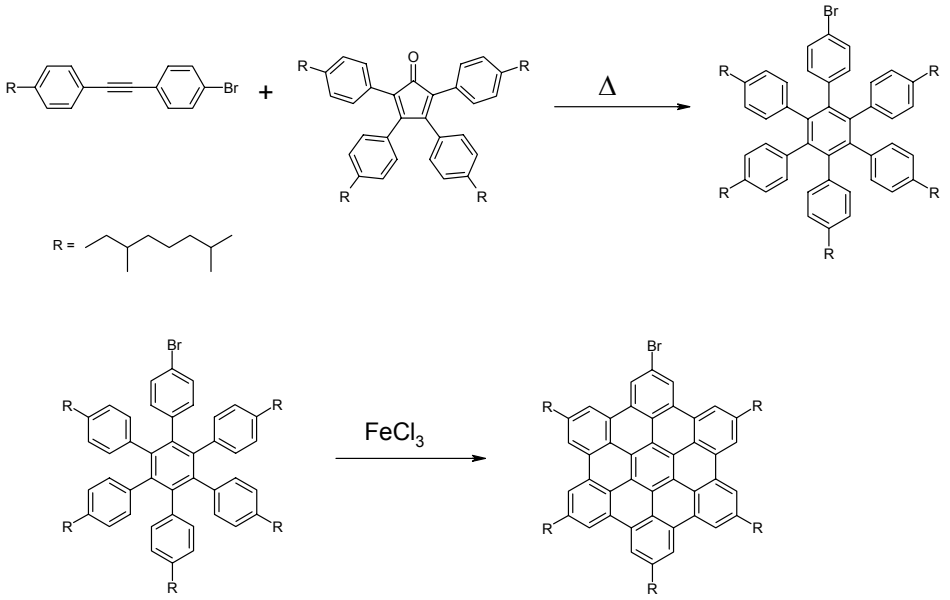

Scheme 5.5. Synthetic route to monobromo HBC.

The synthesis of an indenofluorene linked HBC dimer is presented in Scheme 5.6. Previous research has shown that the palladium catalysed Hagihara-Sonogashira coupling is a versatile reaction that proceeds in high yield for HBC derivatives.[8] For these reasons this reaction was selected as the coupling reaction to join the two HBC moieties to the indenofluorene linker. The previously proposed synthesis had a fully fused superindenofluorene as the target molecule. The synthesis presented in Scheme

5.6 results in a material that contains two acetylene units, which imparts rotational freedom on the molecule. This rotational freedom of the HBC units may be advantageous, considering the motivation of the synthesis of this material. The HBC columns in an OFET are not perfectly aligned, and contain defect structures.[4] The insertion of a molecule that has some degrees of freedom between two columns of HBC may be more likely compared to a rigid material, as the flexible molecule can adjust itself to fit in between the stacked HBC. The indenofluorene linked HBC dimer is also expected to be more soluble, which is also an important consideration.

The Hagihara-Sonogashira coupling of dibromoindenofluorene with trimethylsilyl acetylene, and subsequent deprotection proceeded with a yield of 68% to give **72**. The cross-coupling reaction of the indenofluorene bisacetylene with monobromo HBC was undertaken according to literature procedures.[8]

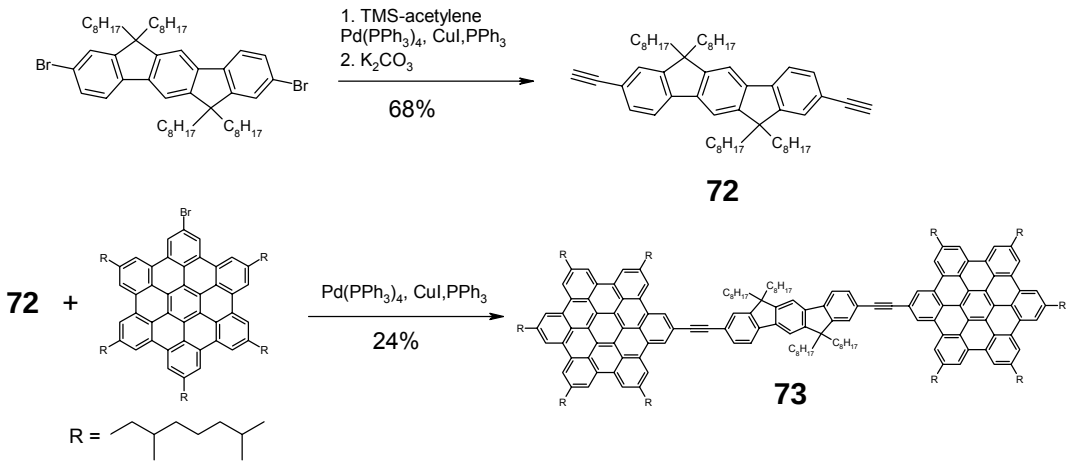

Scheme 5.6. Synthetic route to indenofluorene linked HBC dimer.

The MALDI-TOF MS of the crude product of the reaction indicated the presence of **73** and unreacted monobromo HBC, but not the one time reacted **72**. However, the purification of **73** was not trivial. The two elements of the product mixture had very different mobilities on TLC plates, however could not be separated by column chromatography. The HBC derivative was washed off with an eluent combination of petrol ether and methylene chloride (7:3), and then **73** was removed with THF. While a large amount of starting material was removed in this way, when the desired product was washed off the column there was still a significant amount of

HBC. The tendency of HBC to π-stack so effectively means that the starting material was sticking to the product on the column. No solvent mixture was found that could remove all the excess HBC from **73** by column chromatography.

The solubility of **73** is much less than monobromo HBC, only soluble in hot THF, xylene and toluene, and in CS_2. Attempts were made to purify **73** by recrystallisation using various solvent combinations such as THF/methanol or ethanol. However, the solubility of **73** was so poor that the product would crash out of solution with the HBC derivative. After numerous trials, it was found that the best method to obtain the material pure is to dissolve it in hot THF and then let the solution cool slowly to room temperature. The less soluble **73** would come out of the solution as a fine yellow powder. The target material 73 could be obtained spectroscopically pure after repeating the process three times.

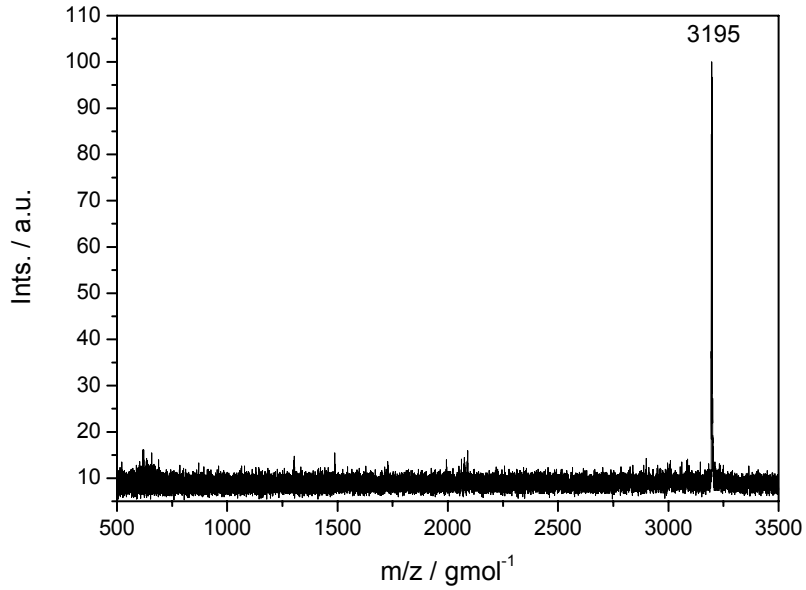

Figure 5.6. MALDI-TOF MS of 73, TCNQ matrix.

The MALDI-TOF mass spectrum of **73** from a TCNQ matrix is presented in Figure 5.6. The calculated molecular weight of **73** is 3195.15 g mol^{-1}, which is observed in Figure 5.6. The half reacted product would have a molecular weight of 1973.20 g mol^{-1}, and is not observed. The unreacted starting material or the mono-

bromo HBC (molecular weight of 1302.86 g mol^{-1}) which was difficult to remove, is also not observed.

The 300 MHz ^{1}H NMR spectrum of **73** in CS_2 is presented in Figure 5.7. A drop of CD_2Cl_2 was added for calibration purposes. The aromatic region of the spectrum shows the peaks corresponding to the 24 protons on the HBC from 8.5 ppm to 9.1 ppm, as expected for HBC protons. The multiplet from 8.0 ppm to 7.8 ppm, with an integration of 8 protons, corresponds to those from the indenofluorene linker. The black arrow in the inset of Figure 5.7 indicates the position of a peak from the mono-bromo HBC, which is absent in this purified material. A ^{13}C NMR spectrum could not be obtained for **73**.

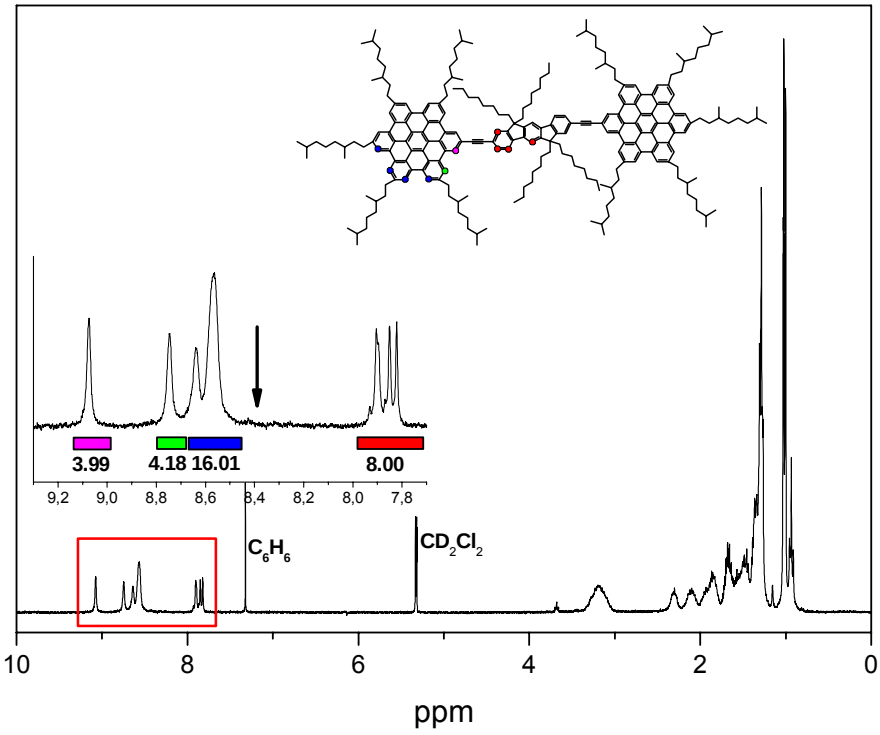

Figure 5.7. ^{1}H NMR spectra of 73 in CS_2 (small amount of CD_2Cl_2 added for calibration), 300 MHz. The inset displays the aromatic region of the spectrum, with a black arrow indicating the position of a mono-bromo HBC peak.

To aid in the assignment of the peaks in Figure 5.7, the ^{1}H COSY NMR, 500 MHz, spectrum of **73** in CS_2 was recorded. The spectrum is presented in Figure 5.8. The 500 MHz spectrum of **73** shows a splitting pattern of two doublets and two

singlets in the aromatic region, from 7.8 ppm to 7.9 ppm. The meta-coupling of the 'blue' doublet with the 'yellow' singlet allows for the assignment of those peaks as shown in Figure 5.8. The remaining 'red' doublet and 'green' singlet peaks must then be assigned as shown.

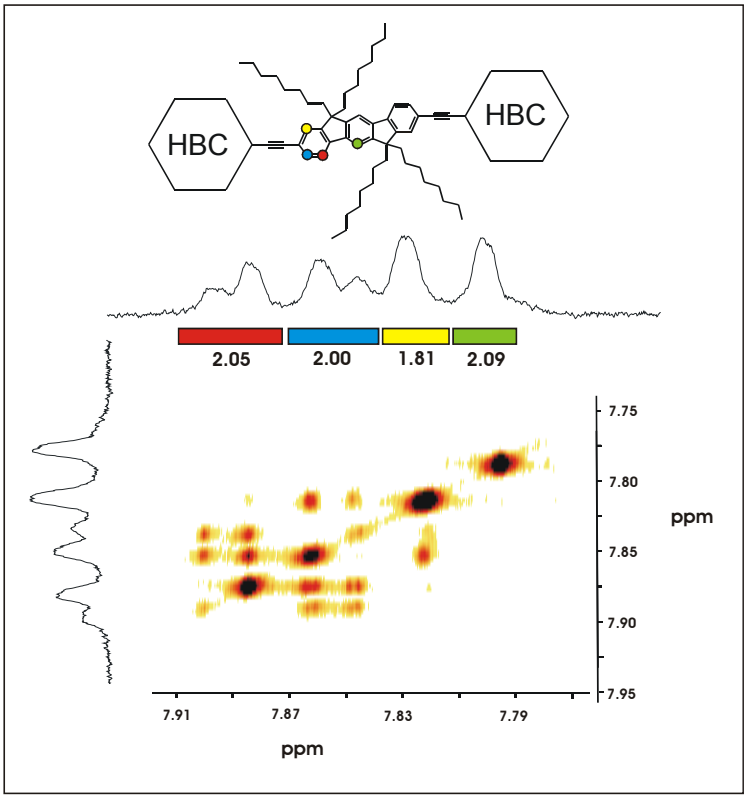

Figure 5.8. ^{1}H COSY NMR spectrum of 73 in CS_2 (small amount of CD_2Cl_2 added for calibration), 500 MHz.

The UV/vis absorption spectrum of **73** and hexa(ethylhexyl)HBC in THF is presented in Figure 5.9. Figure 5.9a demonstrates **73** has a broad absorption exhibiting vibronic fine structure, with an absorption maximum of 365 nm. The spectrum of **73** exhibits a bathochromic shift of 32 nm when compared to the hexa(ethylhexyl)HBC, Figure 5.9b. This is due to the extended conjugation through the triple bond and indenofluorene moiety of **73**. A previously prepared HBC dimer, the super biphenyl (two HBC molecules linked directly without a conjugated linker) does not exhibit such a bathochromic shift.[5] This is because of the orthogonal arrangement of the HBC moieties, which results in no orbital overlap and so no interaction between the HBC units. The triple bond between the HBC and the

indenofluorene moiety permits an orbital overlap regardless of the rotational arrangement of the units, and so allows for interaction between the HBC and the rest of the conjugated system. The absorption spectrum of **73** exhibits increased structure compared to the spectrum of hexa(ethylhexyl)HBC. This is a result of the decreased symmetry of **73**, which has C_{2h} symmetry, compared to the D_{6h} symmetry of HBC.

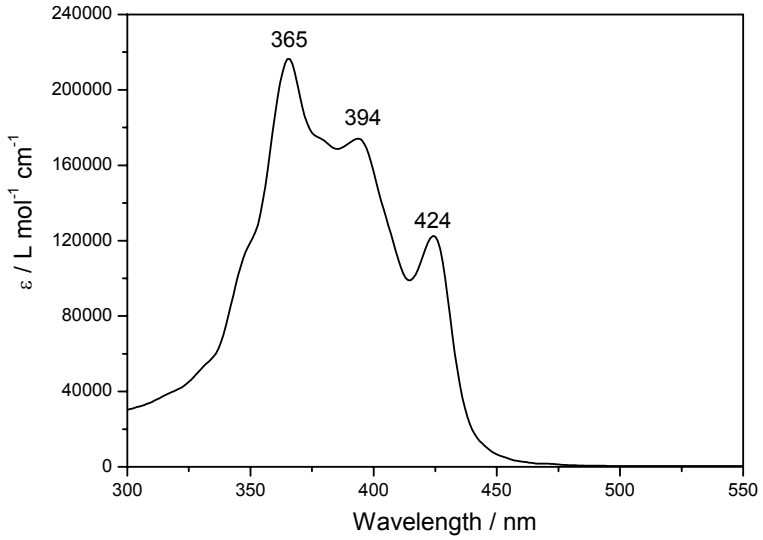

a.

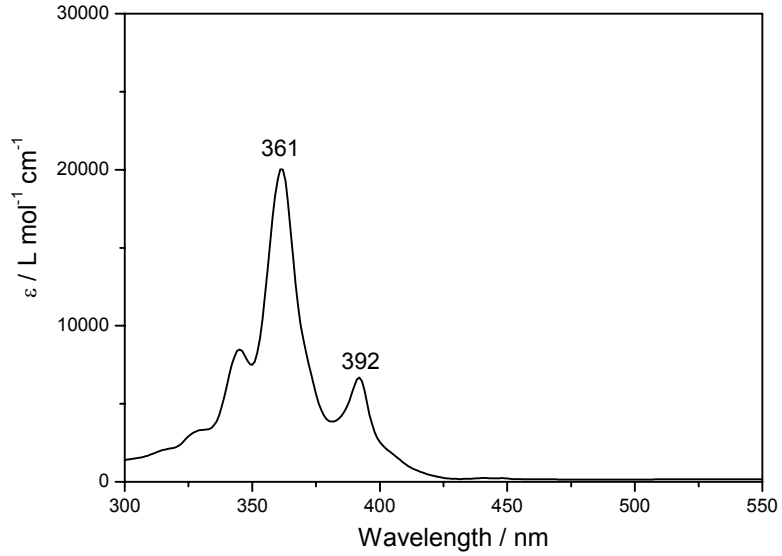

b.

Figure 5.9. UV/vis absorption spectrum of a. 73 and b. hexa(ethylhexyl)HBC in THF.

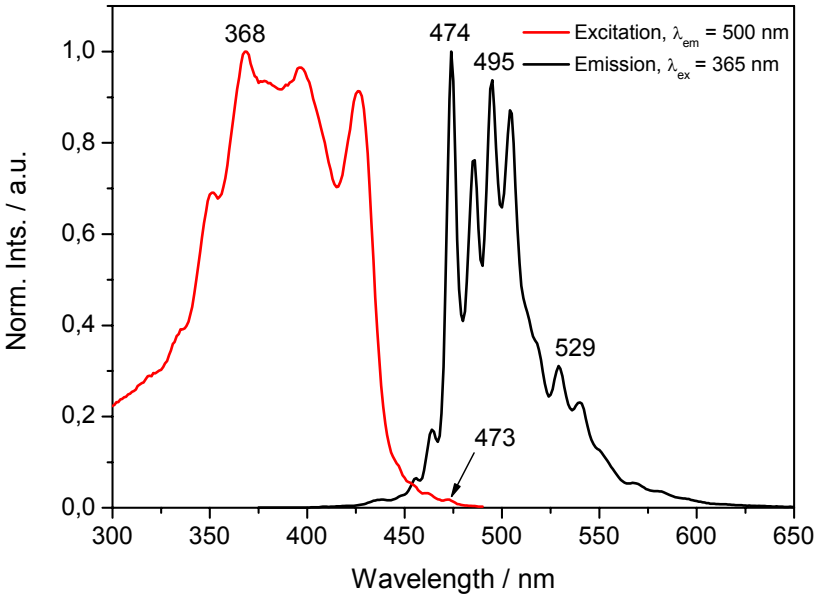

a.

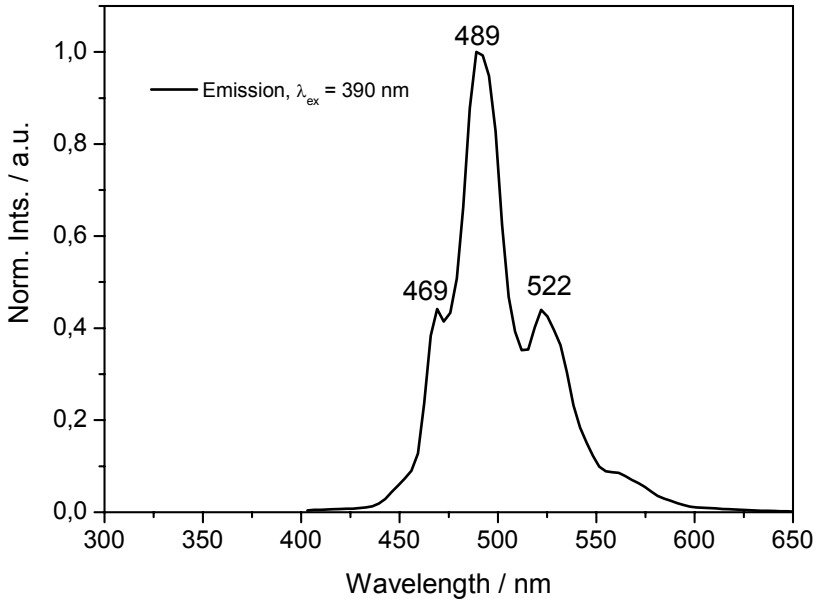

b.

Figure 5.10. a. Excitation, λ_{em} = 500 nm, and emission, λ_{ex} = 365 nm, spectra of 73 in THF. b. Emission spectrum of hexa(ethylhexyl)HBC in THF.

The excitation and emission spectra of **73** in THF and the emission spectrum of hexa(ethylhexyl)HBC in THF are presented in Figure 5.10. Figure 5.10a shows **73** has

an emission maximum at 474 nm, with vibrational fine structure. The excitation spectrum of **73** shows a maximum at 368 nm, however there is peak with low intensity visible at 473 nm. This corresponds to the symmetry forbidden transition of HBC, $S_{0\rightarrow1}$, which is not observed in the absorption spectrum in Figure 5.9a.[9] The emission at 474 nm is the corresponding transition, $S_{1\rightarrow0}$.[9] The transition is observable in both **73**, and HBC at 469 nm, due to Kasha's rule, which states that luminescence originates from the lowest excited state of a given spin multiplicity, *ie* $S_{1\rightarrow0}$.[10] The relative intensity of the transition is stronger for **73** than for HBC, due to the decreased symmetry of **73**, rendering the symmetry forbidden transition more allowed. This results in a Stokes shift of 1 nm. This small Stokes shift for **73** is due to the similar polarity characteristics of the ground and excited states. This reduces the solvent sphere rearrangement on transition to the excited state.

The emission spectrum of **73** has a bathochromic shift of 5 nm in comparison with HBC. This shift is smaller compared to the bathochromic shift observed for the absorption spectra in Figure 5.9. The small emission peaks at 464 nm and 456 nm are thermal bands, transitions from higher vibrational levels of the excited state to the ground state.

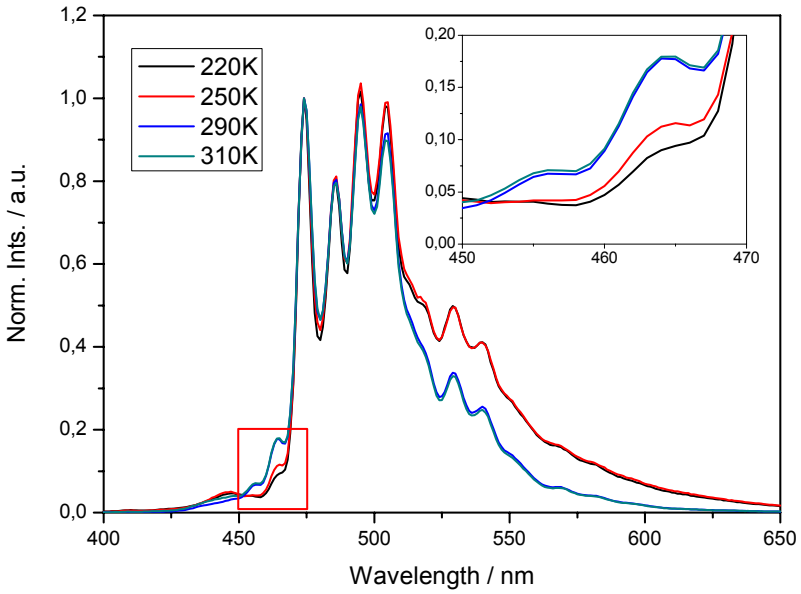

Figure 5.11. Normalised temperature dependent emission spectra of 73 in THF, λ_{ex} = 365 nm. The inset displays the emission region from 450 nm to 470 nm.

The temperature dependent emission spectra of **73** in THF are presented in Figure 5.11. The emission maximum of 474 nm is unaffected by temperature change. The inset of Figure 5.11 shows that the intensity of the emission of **73** at 464 nm and 456 nm decrease with decreasing temperature. This is expected for the thermal bands of a material, as the higher vibrational levels of the excited state are less populated at lower temperatures.

The packing behaviour of **73** in an extruded fibre was investigated using 2D-WAXS. The experimental set up is described in Section 4. The fibre of **73** was extruded at 100°C. The 2D-WAXS of **73**, and a schematic representation including the π-stacking distance of 0.35 nm, is presented in Figure 5.12. The extruded fibre of **73** exhibits intercolumnar organisation perpendicular to the extrusion direction, with the disc plane along the shearing direction. No tilting of the discs is observed, indicating all of the HBC cores are in the same plane.

The HBC cores of **73** form columnar structures that are arranged in a hexagonal fashion, with a unit cell parameter of 2.82 nm. The distance between the centres of the two HBC cores in **73** was calculated by means of Spartan for Windows (AM1 of ground state) to be 3.0 nm. This suggests that **73** does not stack as the whole molecule, *ie* dimers of HBC, rather that the HBC cores stack individually, to form a 3D network of **73**. The amorphous halo indicates that the side chains are disordered, which is not characteristic for a crystalline or highly ordered sample. It is not surprising that the 2D-WAXS of **73** does not exhibit high order, as the structure of the material may not be conducive to molecular packing. The indenofluorene linker may not be compatible with the alkyl side chains of the HBC and interfere with the packing behaviour. Similarly, the second HBC unit, and the intermolecular columnar structures it forms, may not be able to be adequately packed.

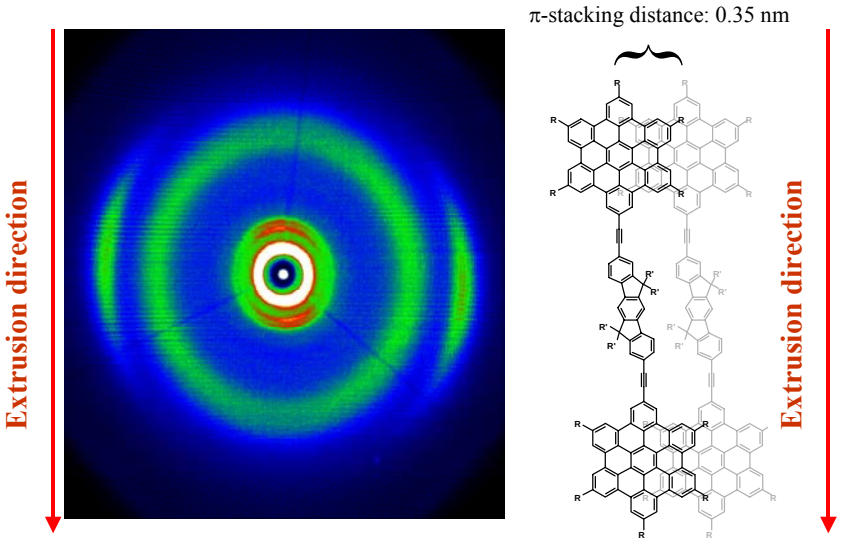

a.

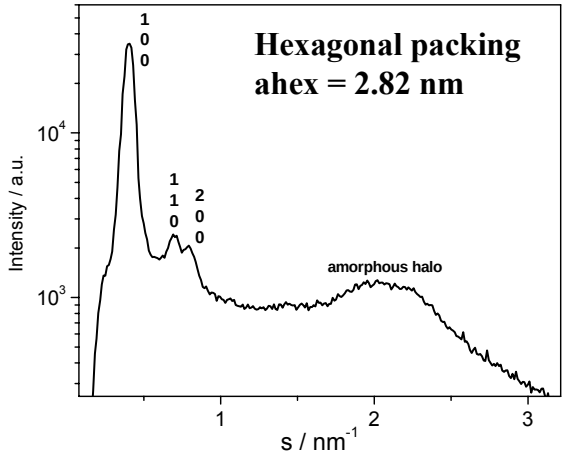

b.

Figure 5.12. a. 2D-WAXS of 73, and schematic representation of 73 in relation to extrusion direction. b. Equatorial reflection intensity distribution as a function of the scattering vectors.

The 2D-WAXS of HBC-C8, 2, the mono HBC with the same side chains as **73**, in the mesophase at 120°C is presented in Figure 5.13.[6] In contrast to the WAXS of **73** in Figure 5.12, Figure 5.13 shows that single HBC molecules form columns in the extrusion direction. This is the case for other discotic molecules, where the disc plane is organised perpendicular to the extrusion direction.[11,12] The columnar structures of HBC-C8,2 are also arranged in a hexagonal fashion, with a unit cell parameter of 2.64

nm. This parameter is smaller than the unit cell parameter of **73**, which suggests that the indenofluorene linker increases the distance between the HBC columns.

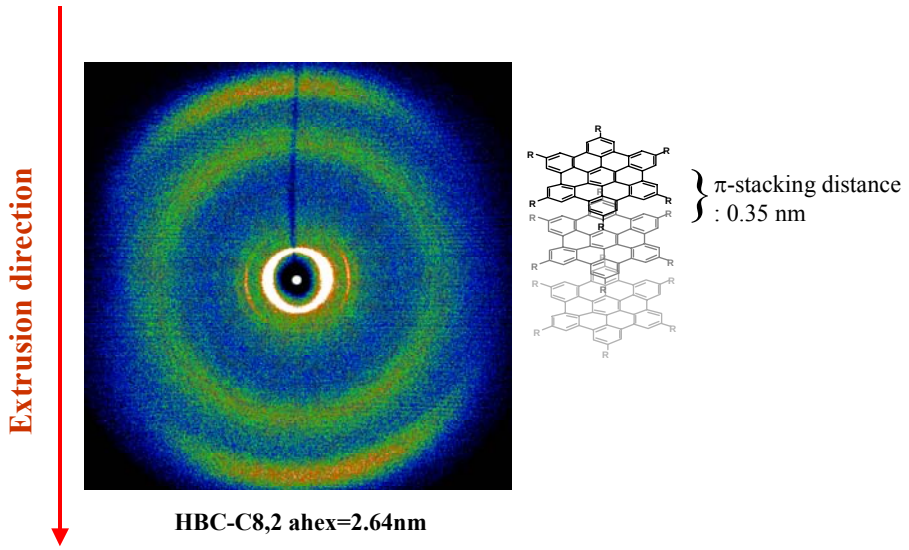

Figure 5.13. 2D-WAXS of HBC-C8, 2, and schematic representation of columns in relation to extrusion direction.

The rotation of the column axis of **73** compared to HBC-C8, 2 can be explained by much the same discussion as was presented in Section 4. As the fibre is extruded the molecules are forced to orientate, with the longer length axis of the material preferentially along the fibre axis. For HBC-C8, 2 at 120°C, the formation of columns dominates, so the cylindrical structures align with the extrusion direction. Alternately, in the case of **73** it is the single dimer that is the dominating length dimension, and this aligns along the extrusion direction. These two alternate factors, *ie* column formation and long dimer molecule, account for the rotated 2D-WAXS.

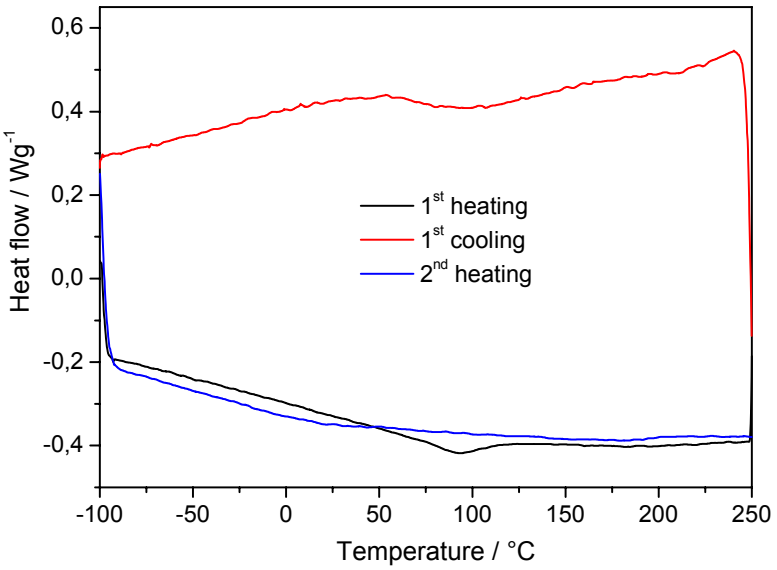

Figure 5.14. DSC traces of 73 obtained with a rate of 10 Kmin^{-1}.

The DSC traces of **73**, measured at a rate of 10 Kmin^{-1}, are presented in Figure 5.14. On the first heating and cooling scan a transition is observed at approximately 90°C, which could be a T_g. The transition is not observed in the second heating run. The first heating DSC trace of a compound is known to be affected by the history of the material. Additional factors such as trapped solvent and how the compound was collected can influence the first heating trace in the DSC. The phase behaviour was also investigated using POM. 3 mg of **73**, in the form of a powder, was deposited onto a clean glass substrate, and heated slowly.**73** did not exhibit any long range order under cross polarised illumination, and did not melt up to 300°C. Above 300°C, **73** turned black and decomposed. The DSC traces presented in Figure 5.14 and the POM investigations indicate that **73** forms an amorphous glassy phase, which persists up to the decomposition temperature.

The film forming behaviour of **73** was studied by POM, and the images are presented in Figure 5.15. Films were drop-cast onto a glass substrate from *o*-xylene and pyridine solutions, filtered through a 0.45 micron syringe filter. Figure 5.15a presents the POM images of a film of **73** drop-cast from *o*-xylene. The image illustrates that **73** has formed spherulitic structures on the glass substrate, evident

from the observed Maltese cross pattern. This indicates that **73** has formed ordered structures growing radially from the nucleation point. The spherulite structures for **73** are small, in the order of 2-3 μm, compared to the large structures formed by hexa-(2-decyltetradecyl) HBC, which are 200 μm in diameter.[13] The spherulites were found to be distributed throughout the film area.

a.

b.

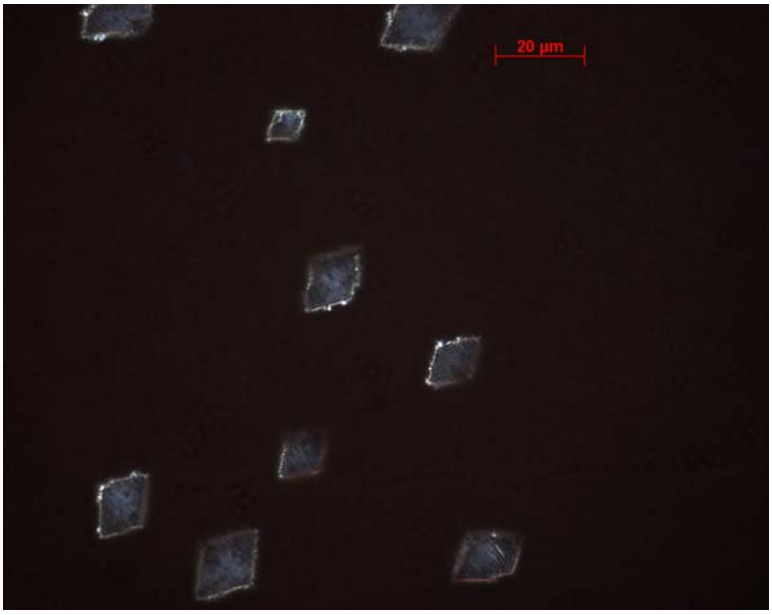

Figure 5.15. POM images of films of 73 drop-cast from a. *o*-xylene and b. pyridine.

Figure 5.15b shows the POM images of films of **73** drop-cast from pyridine. The image shows **73** forms rhombic structures when drop-cast from pyridine. These rhombic structures have dimensions of the order of 20 μm, and are also evenly distributed throughout the film area. The structures obtained from the pyridine solution do not exhibit the same degree of long range order as the films cast from *o*-xylene. This may indicate that the solvent, pyridine, has a large influence in the ordering of the structures.

The films of **73** drop-cast from solution were heated between 30°C and 125°C, at a rate of 5 $Kmin^{-1}$. When the films drop-cast from *o*-xylene were heated no change in the POM image was observed. The films were heated to 300°C, at which point the material decomposed. In contrast, the films prepared from the pyridine solution were observed to melt at 55°C. In the cooling cycle, some order in the films was observed at 50°C. This was not the same rhombic structures observed in the drop-cast films, rather local areas of order of an unknown origin. Although the boiling point of pyridine is 115°C, it can be assumed that some solvent is present after heating to 125°C. From the comparison with the films drop-cast from *o*-xylene, the pyridine molecules obviously play a role in the formation of ordered structures of **73**. The exact nature of this solvent interaction is not known at this time.

5.2.2.1 Mixing experiments

The motivation for the synthesis of the bypass molecule was to obtain a compound that would be a conjugated linker between two columns of HBC. The objective is to increase charge carrier mobility by allowing the current to flow around the unavoidable defects in the columns. In order for this situation to be possible, the dimer molecule must be compatible with the bulk HBC material and be homogeneously intermixed. In order to remove any effects caused by side chain interactions, the side chains of the dimer and single HBC materials used in the mixing investigations are the same.

In order for the DSC results to have any significance, **73** must be mixed homogeneously with the HBC. The approach utilised in this investigation was to use a ball mill to mechanically homogenise the two compounds. The two materials were accurately weighed into a metal cylinder and a ball bearing (diameter ~ 4 mm) was added. After the cylinder was sealed, it was agitated in a Retsch milling machine, at a frequency of 30 s^{-1}, for 30 minutes. The action of the ball in the chamber mechanically mixes the two compounds. The mixing behaviour of **73** with HBC-C8, 2 was investigated by DSC, to see what effect the incorporation of the dimer has on the thermal transitions of the HBC. The first and second heating run of various mixtures of the two components are presented in Figure 5.16.

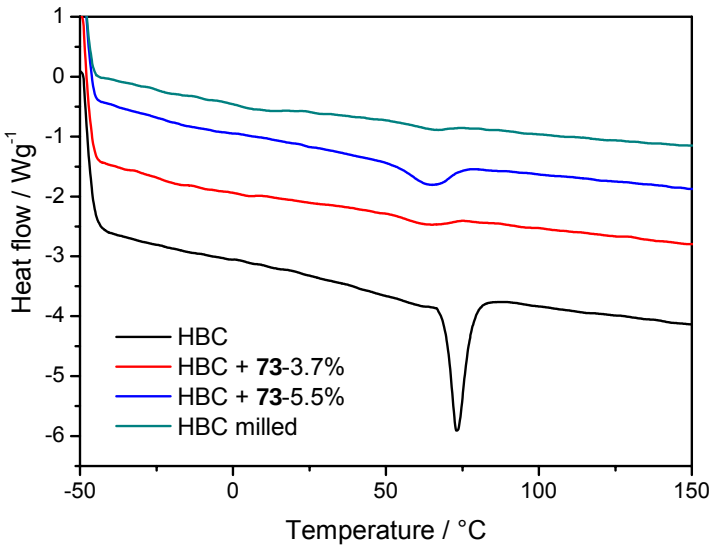

a.

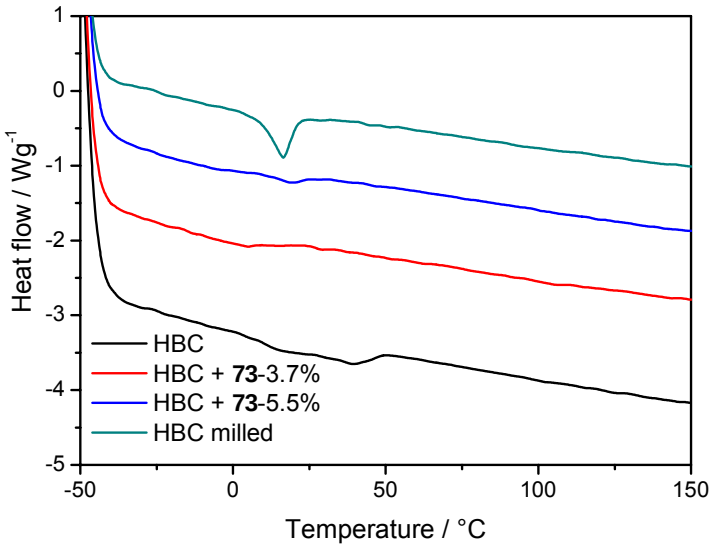

b.

Figure 5.16. DSC traces of HBC-C8, 2 before and after milling process, and with various proportions of 73. a. First heating b. Second heating. Obtained with a rate of 10 Kmin^{-1}.

On the first heating cycle, Figure 5.16a, HBC-C8, 2 shows a thermal transition at 73°C, which is attributed to a hexagonal ordered mesophase.[6] The DSC traces of the first heating run of the two mixtures exhibited a thermal transition at 64°C, which has a much lower intensity compared to the transition of HBC-C8, 2. The second heating does not show the same thermal transitions as the first heating. The DSC trace

of the second heating of HBC-C8, 2 exhibits a thermal transition at 40°C, which may be a T_g. No clear thermal transitions are observed for the DSC traces of the mixtures on the second heating. These DSC results are not conclusive. The action of ball milling could itself affect the phase transition behaviour of the samples. A sample of unmixed HBC-C8, 2 was ball milled under the same conditions. There is no thermal transition observed in the first heating cycle, however a phase transition at 16°C is seen in the second heating cycle. The results of the DSC mixing experiments do not demonstrate what the nature of the mixed materials is; however they do show that some kind of interaction is occurring. There is an obvious change in the DSC traces of the mixed materials compared with the pure materials, indicating that **73** is mixing with HBC-C8, 2 and changing the thermal properties of the material.

The mixing behaviour of **73** in an HBC matrix was also investigated by POM. Films of **73** and HBC-C8, 2 were drop cast on a glass substrate from CS_2 solutions of various concentrations. When the films were examined under cross polarisation, the images illustrated the aggregation of **73**, *ie* the films were not homogeneous. The substrate was heated to 200°C, into the mesophase, however the films did not exhibit any change due to the presence of **73**. The aggregates of **73** persisted as separate entities, while the bulk film showed the transitions that would be expected for pure HBC-C8, 2 films.[6]

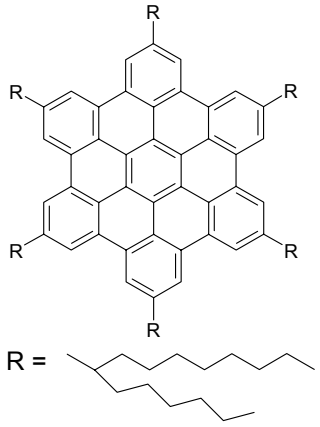

Figure 5.17. Structure of HBC-$C_{10,6}$.

The isotropisation temperature of HBC-C8, 2 is reported to be approximately 420°C.[6] The substrates were heated to 350°C in an attempt to mix the two phases of

the films, however no change was observed before the material decomposed. For **73** to be used as a bypass molecule between two HBC columns, it must be distributed evenly in the HBC. Films drop-cast from solution were observed to be inhomogeneous, with the low solubility of **73** presumably leading the dimer to come out of solution and aggregate before the bulk HBC. In order to circumvent this problem it was proposed that **73** be dissolved in an HBC that is isotropic at temperatures below the decomposition temperature. The HBC that was selected, HBC-$C_{10,6}$, is shown in Figure 5.17. HBC-$C_{10,6}$ isotropic above 90°C and forms a liquid crystal phase between 25°C and 90°C.[14] The intercolumnar arrangement of HBC-$C_{10,6}$ was investigated by powder X-ray scattering, which resulted in a complex diffractogram. The intercolumnar arrangement was proposed to be a lateral monoclinic, with intercolumnar distances ranging from 2.5 nm and 2.9 nm to 4.32 nm and 2.36 nm.[14] The distance between two columns of HBC-$C_{10,6}$ is in the same range as the calculated distance between the two HBC units in **73**.

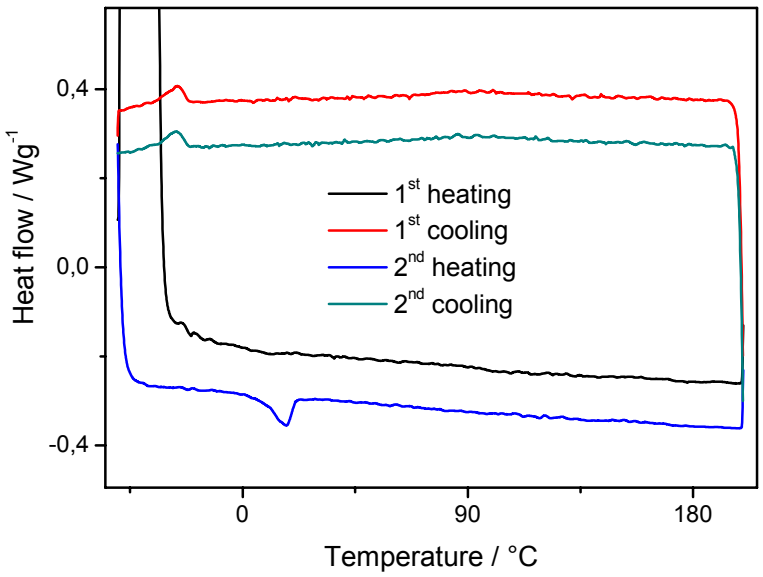

Figure 5.18. DSC traces of HBC-$C_{10,6}$ and 2.4% 73, obtained with a rate of 5 Kmin^{-1}. Material was heated to 200°C for one hour before the first heating cycle.

The DSC trace of a 2.4% mixture of **73** in HBC-$C_{10,6}$ is presented in Figure 5.18. The mixture was mixed in solution, the solvent removed, then the DSC pot was heated to 200°C for one hour. The mixture was then heated at 5 Kmin^{-1} from –50°C to

200°C and cooled back again, for two cycles. No transition was observed in the first heating cycle. A very small crystallisation is observed at –26°C for both cooling cycles, while a very small melting is observed on the second heating cycle at 17°C. No isotropisation transition is observed on either cycle, heating or cooling. Even though the material was heated to 200°C before the first cycle was obtained, no melting was observed in the first heating cycle. The reason for this is that the sample was cooled to –50°C rapidly before the first heating cycle, and so could not crystallise, resulting in the lack of melting transition. In the hope of gaining a better understanding of the mixing behaviour of the two materials, the POM images were obtained.

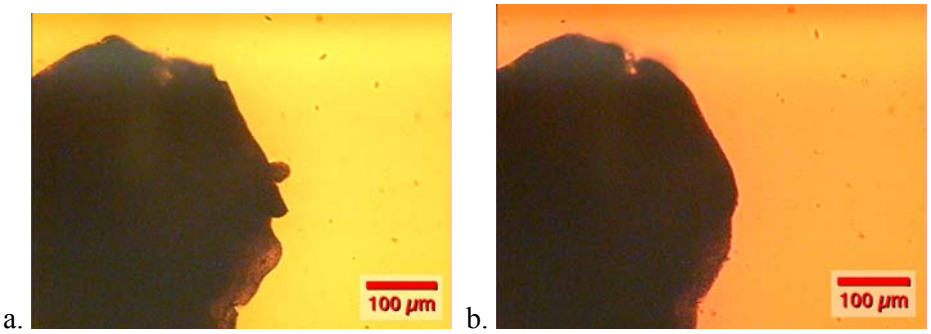

Figure 5.19. Image of 73 dissolved in HBC-$C_{10,6}$. a. At 190°C, t = 0. b. At 190°C, t = 10 min.

In order to test the ability of HBC-$C_{10,6}$ to dissolve **73**, a 0.1 mg grain of the dimer was placed on 4.7 mg of HBC-$C_{10,6}$ on a glass substrate. The material was heated to 190°C and held at that temperature for 10 minutes. The images of the particle in HBC-$C_{10,6}$ at 190°C before and after the 10 minutes holding period is shown in Figure 5.19. The particle was observed to soften and the edges of the particle can be seen to be dulled, however the particle remained intact. Continued heating for an additional hour did not allow for the particle of **73** to completely dissolve. The sample was cooled at a rate of 5 $Kmin^{-1}$. The POM images of **73** cooled to 123°C, 115°C and 110°C are presented in Figure 5.20.

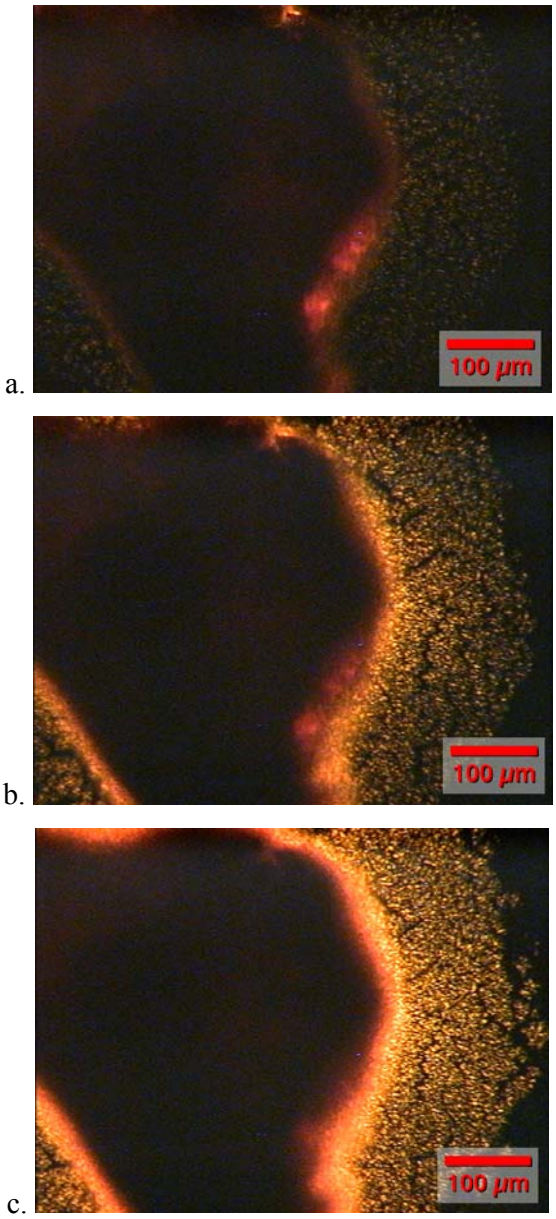

Figure 5.20. POM images of 73 particle in HBC-$C_{10,6}$ on cooling from 190°C, at a rate of 5 $Kmin^{-1}$, at a. 123°C b. 115°C and c. 110°C.

Figure 5.20a illustrates the start of the ordering process of the mixture of HBC-$C_{10,6}$ and **73** on cooling to 123°C. This transition into an ordered phase from the isotropic phase occurred at a higher temperature for the mixture than for the pure HBC. Also, the order is only observed in the region directly next to the particle of **73**. The bulk of the sample became ordered when cooled to 95°C. This suggests that **73** is dissolving to a small extent, but is not mobile enough to migrate a large distance in the conditions used in this experiment. The nature of the ordered structures formed

below 123°C is not known at this time. The order could be due to an interaction between **73** and HBC-$C_{10,6}$, *eg* **73** acts as a nucleation site or binds the HBC columns, or the observed structure could be due to **73** alone. The mixture was reheated to 200°C between two glass substrates and was observed while under shear. The particle of **73** was not fully mixed with HBC-$C_{10,6}$ under shearing conditions, however it softened and spread slightly on the substrate. Upon cooling, the same ordering transitions were observed at 123°C and 95°C as for the sample without shear.

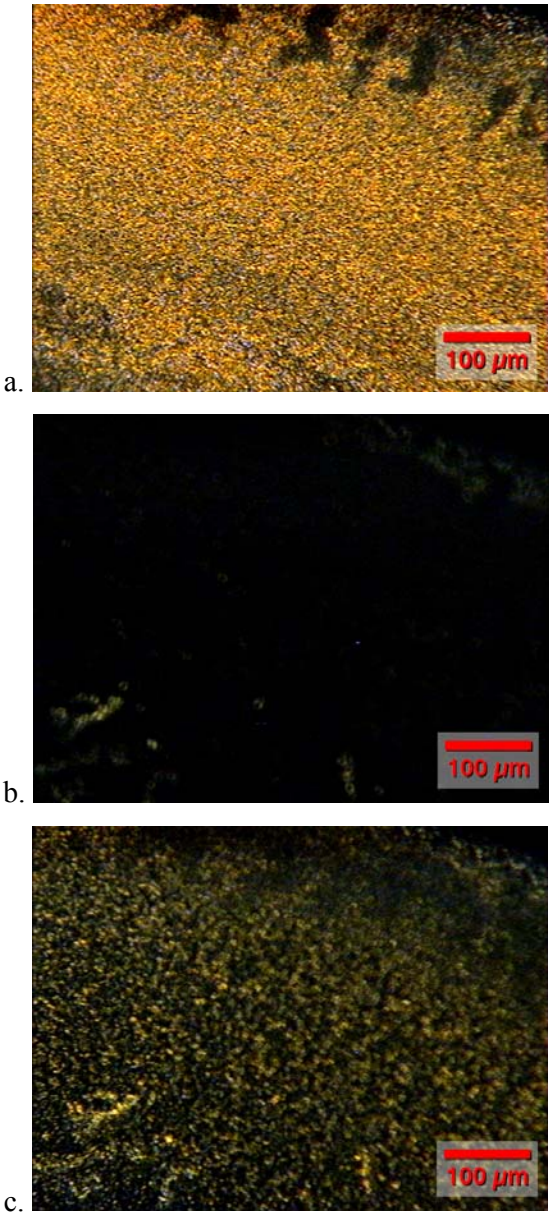

Figure 5.21. POM images of drop cast film of 73 and HBC-$C_{10,6}$ at a. 30°C b. heating to 200°C c. cooled to 125°C. (Rate of 5 $Kmin^{-1}$).

73 was not completely dissolved in HBC-$C_{10,6}$ with heating up to 200°C, however some incorporation of **73** into the HBC matrix was observed. In order to have a more evenly mixed sample on the substrate before the heating experiment, drop cast films of **73** and HBC-$C_{10,6}$ in CS_2 were prepared. Two drop cast films were prepared, with 9.1% and 19.5% of **73** in HBC-$C_{10,6}$. The observed films were not homogeneous and contained particulate material in the centre of the drop cast film, which was attributed to the formation of **73** aggregates. The substrates were heated at a rate of 5 $Kmin^{-1}$ from 30°C to 200°C and back again. On heating to 200°C the bulk of the material became isotropic, however a small amount of ordered material was still observed in the POM image, Figure 5.21b. On cooling the amount of ordered material increased slowly, until approximately 125°C when a phase transition was observed for the bulk of the material, Figure 5.21c. The same affects were observed for the films with both concentrations of **73**.

The mixing experiments have shown that **73** can be incorporated in some way into an HBC matrix. In order to get homogeneous mixing of **73** with an HBC material it is necessary to select an HBC with an isotropisation temperature below the decomposition temperature of the materials. Although mixing of HBC and **73** has been observed, as shown by the different temperatures for the transition from isotropic to mesophasic state, there was no complete mixing. The presence of some ordered structures at 200°C, Figure 5.21b, demonstrates that some of the aggregates of **73** are not dissolved in the HBC. While it can be said that there is some interaction between **73** and the HBC matrix, the nature of the interaction can not be further elucidated at this time.

To test the concept of the bypass molecule, a measurement of charge carrier mobility is needed. **73** is currently being incorporated into a device, with the aim of measuring the TOF mobilities. The concept of TOF has been discussed in Section 3. The TOF device fabrication of discotic materials with low isotropisation temperatures such as HBC is different than for those described previously. Polyester beads of a specific diameter are sandwiched between two etched ITO substrates. The epoxy is only applied at the edges, so a cavity is formed in the middle of the device. Sample is applied to the opening of the cavity and is heated above the isotropisation temperature. The liquid sample is drawn into the cavity by capillary effects,

effectively filling the space between the ITO electrodes. After cooling the device to the desired temperature, the TOF measurement can be performed as described in Section 3. A schematic representation of the device preparation is presented in Figure 5.22.

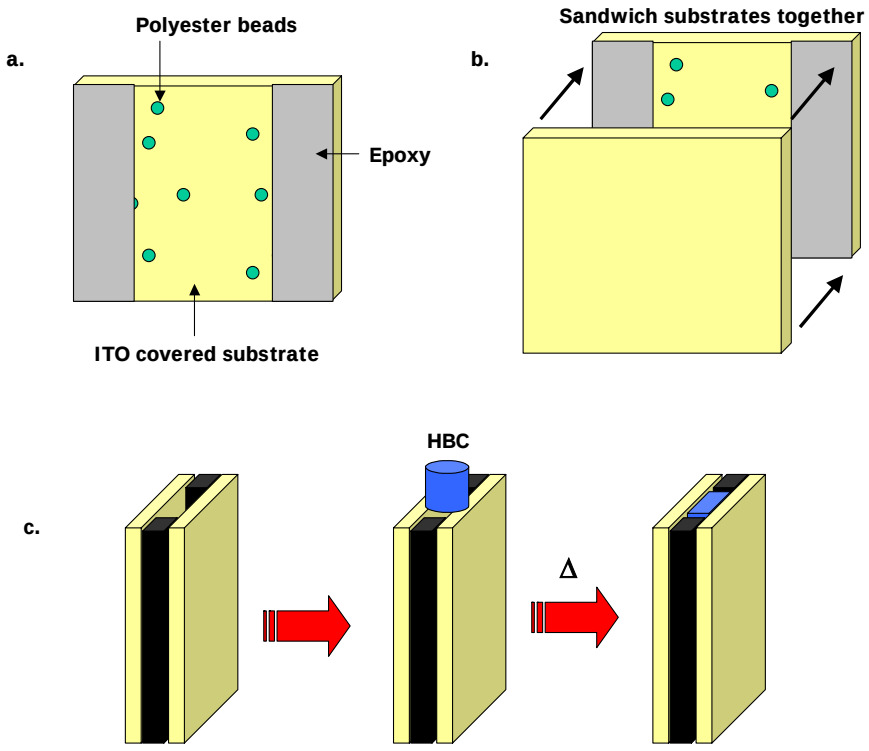

Figure 5.22. Schematic representation of device preparation. a. Polyester beads of a known diameter are deposited on an etched ITO substrate. b. Epoxy glue applied to the edges of the substrate then the beads sandwiched between another ITO substrate. c. HBC placed on the cavity opening, heated to isotropisation temperature, the fills the available volume by capillary forces.

The investigation of the charge carrier mobility of a mixture of **73** and HBC-$C_{10,6}$ by a TOF measurement is currently being undertaken.

5.3 Conclusion

The original target material of this project, a fully planarised 'super-indenofluorene', could not be obtained. Attempts to synthesise a diketone or tetraoctyl substituted 'super-indenofluorene' were both unsuccessful. This was due to difficulties in performing the cyclodehydrogenation reaction for the tetraoctyl super-indenofluorene, which led to incomplete ring closure and chlorination, whereas solubility was an issue for the diketone. As an alternative, a HBC bypass molecule has been synthesised. This bypass molecule consists of two HBC units linked by a conjugated indenofluorene spacer. This bypass molecule is such that the HBC units are free to rotate. The advantage to this material is that the HBC moieties are preformed and so the cyclodehydrogenation step of the bypass molecule is avoided. Although the purification of this material did not prove to be trivial, the target compound was obtained pure and characterised by MALDI-TOF MS and ^{1}H NMR.

The bypass molecule exhibited a UV-vis absorption spectrum that has more structural features, with an absorption maximum bathochromically shifted compared to single HBC discs. Likewise, the emission spectrum of the bypass material shows a large amount of structural features and is bathochromically shifted compared to HBC materials.

The packing behaviour of the bypass molecule was investigated by 2D-WAXS. The 2D-WAXS of an extruded fibre of the bypass molecule shows it orientates with the disc plane in the extrusion direction. Single HBC discs orient with the disc plane perpendicular to the extrusion direction. The bypass molecule has a longer dimension orthogonal to the HBC disc plane, and so this length turns in line with the extrusion direction when the fibre is formed. For single HBC discs the formation of columns with long range order means that the column is aligned with the extrusion direction. The distance between the HBC columns formed perpendicular to the extrusion direction of the bypass molecules is 2.82 nm. This is shorter than the calculated separation of the two HBC moieties in the bypass molecule, indication that the linking units of the bypass molecules don't align on top of each other. The HBC units of the

bypass material form columnar structures to give a 3D network of columns linked by indenofluorene moieties.

The film forming behaviour of the by-pass material was found to be dependent on the solvent that the films were drop-cast from. When prepared from *o*-xylene solutions the bypass material formed spherulites, while rhombic structures were formed when drop-cast from pyridine solutions. The DSC of the pure bypass material did not show any transitions up to the decomposition temperature. Similarly, the POM images of the bypass material heated to the decomposition temperature did not demonstrate any phase changes.

For the desired bypass mechanism to occur in a device, the molecule must be dispersed and integrated into the HBC columns. The bypass molecule was mixed with HBC-C8, 2, the HBC with the same alkyl chains. The DSC and POM results demonstrated that the low solubility of the bypass material means that homogenous mixing of these molecules is difficult. Instead, an HBC that has an isotropisation temperature below the decomposition point of the materials was chosen as the host. HBC-$C_{10,6}$ has a melting point at 90°C and was chosen as the matrix to dissolve the bypass molecule. The POM images of mixture of the bypass molecule and HBC-$C_{10,6}$ demonstrated that there is some incorporation of the bypass material into the host HBC, as on cooling from high temperatures the images showed liquid crystal behaviour at 125°C. It was demonstrated that films of the two materials prepared from CS_2 exhibited good mixing.

The synthesis of a bypass material may improve the performance characteristics of OFET's based on HBC's. The inclusion of conjugated pathways between the discotic columns in a device could allow charge carriers to migrate between columns. It is envisioned that this will increase the performance of the devices as the defect structures formed in the discotic material can be sidestepped, or bypassed, by the charge carriers. The charge carrier mobility of mixtures of the bypass molecule and HBC-$C_{10,6}$ are currently being measured using the TOF technique.

5.4 References

(1) Dimitrakopoulos, C. D.; Malenfant, P. R. L. *Advanced Materials* **2002**, *14*, 99-117.

(2) Newman, C. R.; Frisbie, C. D.; da Silva, D. A.; Bredas, J. L.; Ewbank, P. C.; Mann, K. R. *Chemistry Of Materials* **2004**, *16*, 4436-4451.

(3) Veres, J.; Ogier, S.; Lloyd, G.; de Leeuw, D. *Chemistry Of Materials* **2004**, *16*, 4543-4555.

(4) Pisula, W.; Menon, A.; Stepputat, M.; Lieberwirth, I.; Kolb, U.; Tracz, A.; Sirringhaus, H.; Pakula, T.; Mullen, K. *Advanced Materials* **2005**, *17*, 684-689.

(5) Wu, J. S.; Watson, M. D.; Tchebotareva, N.; Wang, Z. H.; Mullen, K. *Journal Of Organic Chemistry* **2004**, *69*, 8194-8204.

(6) Pisula, W.; Tomovic, Z.; Simpson, C.; Kastler, M.; Pakula, T.; Mullen, K. *Chemistry Of Materials* **2005**, *17*, 4296-4303.

(7) Stabel, A.; Herwig, P.; Mullen, K.; Rabe, J. P. *Angewandte Chemie-International Edition In English* **1995**, *34*, 1609-1611.

(8) Wu, J. S.; Watson, M. D.; Zhang, L.; Wang, Z. H.; Mullen, K. *Journal Of The American Chemical Society* **2004**, *126*, 177-186.

(9) Beier, J., PhD thesis, University Bayreuth, 2001.

(10) Kasha, M. *Discussions Of The Faraday Society* **1950**, 14-19.

(11) Adam, D.; Closs, F.; Frey, T.; Funhoff, D.; Haarer, D.; Ringsdorf, H.; Schuhmacher, P.; Siemensmeyer, K. *Physical Review Letters* **1993**, *70*, 457-460.

(12) Adam, D.; Schuhmacher, P.; Simmerer, J.; Haussling, L.; Siemensmeyer, K.; Etzbach, K. H.; Ringsdorf, H.; Haarer, D. *Nature* **1994**, *371*, 141-143.

(13) Pisula, W.; Kastler, M.; Wasserfallen, D.; Pakula, T.; Mullen, K. *Journal Of The American Chemical Society* **2004**, *126*, 8074-8075.

(14) Pisula, W. Dissertation, Johannes Gutenberg Universität, 2005.

6 Experimental

6.1 General procedures

All starting materials were obtained from commercial suppliers (Aldrich, Fluka, Fischer, Strem, Acros) and were used without further purification. All solvents were purified and freshly distilled prior to use according to literature procedures. Atmosphere-sensitive reactions were performed under argon using Schlenck techniques. Chromatography was carried out with silica gel 60 (230-400 mesh) from E. Merck. ^{1}H and ^{13}C NMR spectra were recorded on a Bruker AMX250 spectrometer (250 and 62.90 MHz respectively), a Bruker AC300 spectrometer (300 and 75.46 MHz respectively), a Bruker AMX500 spectrometer (500 and 125 MHz respectively), and a Bruker 700Ultrashield NMR spectrometer (700 and 175 MHz respectively) using the residual proton resonance of the solvent or the carbon signal of the deuterated solvent as the internal standard. Chemical shifts are reported in parts per million. FD mass spectra were performed with a VG-Instruments ZAB 2-SE-FDP. MALDI-TOF mass spectra were measured with a Bruker Reflex II and dithranol or TCNQ as matrix. UV-vis absorption spectra were recorded on a Perkin Elmer Lambda 9 specrophotometer, fluorescence spectra on a SPEX Fluorolog2 spectrometer. DSC was measured on a Mettler Toledo Star DSC with a heating and cooling rate of 10 K/min. POM was performed on a Zeiss POM with a Linkam THM 600 hot stage. The elemental analysis was carried out by the Microanalytical Laboratory of the University of Mainz, Mainz, Germany. Because of the high carbon content in some molecules, the combustion may have been incomplete (sooting) resulting in lower values than expected for the carbon content. Another reason for the wrong values can be the inclusion of solvent molecules in dendrimers or polymers, which are difficult to remove by vacuum.

6.2 Synthetic procedures

(4,4'-dibromo-biphenyl-2-yl)-bis-(4-trimethylsilanylethynyl-phenyl)-methanol (1)

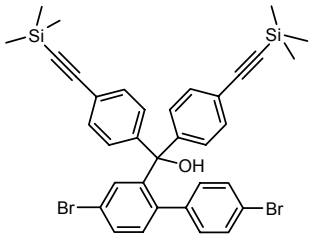

(4-Bromo-phenylethynyl)-trimethylsilane (1.15 g, 4.5 mmol) was dissolved in 11 mL of dry THF under argon, and cooled to -78°C in a dry ice/acetone bath. t-BuLi (3.1 mL, 4.7 mmol) was added and the reaction mixture stirred for 30 minutes. 4,4'-dibromo-biphenyl-2-carboxylic acid methyl ester (0.84 g, 2.2 mmol) dissolved in 22 mL dry THF was added, and the reaction mixture left to warm to room temperature, and stirred for 12 hours. The reaction was quenched with a ammonium chloride solution, the organic products extracted with methylene chloride, washed with water, dried over magnesium sulphate, and the solvents removed *in vacu*. The product was purified by column chromatography eluting with 0-2% ethyl acetate in hexane to give the title compound as a white powder. 0.9 g (57%). ^{1}H NMR (300 MHz): (CD_2Cl_2) δ 7.47 (dd, 1H, J=2.1Hz, J=8.1Hz), 7.38 (d, 4H, J=8.6Hz), 7.30 (d, 2H, J=8.5Hz), 7.05 (d, 1H, J=8.6Hz), 6.99 (d, 1H, J=8.1Hz), 6.90 (d, 1H, J=2.0Hz), 6.66 (d, 2H, J=8.5Hz), 2.77 (s, 1H), 0.25 (s, 18H) ppm. ppm. ^{13}C NMR (75 MHz): (CD2Cl2) δ 146.89, 146.69, 140.18, 139.48, 131.92, 131.47, 131.40, 128.17, 122.94, 122.13, 121.51, 104.81, 95.25, 82.99, 132.93, 130.80, 134.44, -0.06, ppm. MS (FS, 8kV): m/z (%) = 686.8 (100%, M^+) (calc. for $C_{35}H_{34}Br_2OSi_2$ = 686.64 g mol^{-1}). Elemental Analysis: Calculated C 61.22, H 4.99. Found C 59.90, H 5.02.

(4,4'-dibromo-biphenyl-2-yl)-bis-(4-ethynyl-phenyl)-methanol (2)

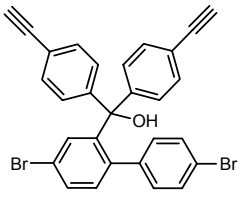

(4,4'-dibromo-biphenyl-2-yl)-bis-(4-trimethylsilanylethynyl-phenyl)-methanol (0.89 g, 1.3 mmol) and ammonium fluoride (190 mg, 5.2 mmol) was mixed in 18 mL dry THF under argon. Tetrabutylammonium fluoride (0.23 mL, 0.23 mmol) was added, and the reaction mixture stirred for 15 hours. The reaction was quenched with water, the organic products extracted with methylene chloride, washed with water, dried over magnesium sulphate, and the solvents removed in vacu. The product was purified by column chromatography eluting with 0-3% ethyl acetate in hexane to give the title compound as a white powder. 0.63 g (89%). ^{1}H NMR (250 MHz): (CD_2Cl_2)

δ 7.48 (dd, 1H, J = 2.1, 8.1Hz), 7.43 (d, 4H, J = 8.5Hz), 7.30 (d, 2H, J = 8.4Hz), 7.08 (d, 4H, J = 8.6Hz), 7.00 (d, 1H, J = 8.1Hz), 6.95 (d, 1H, J = 2.1Hz), 6.66 (d, 2H, J = 8.4Hz), 3.17 (s, 2H), 2.80 (s, 1H) ppm. ^{13}C NMR (63 MHz): (CD2Cl2) δ 147.15, 146.54, 140.11, 139.50, 134.46, 132.84, 132.17, 131.44, 131.37, 130.86, 128.21, 122.10, 121.84, 121.54, 83.39, 82.90, 78.02 ppm. MS (FS, 8kV): m/z (%) = 542.7 (100%, M^+) (calc. for $C_{29}H_{18}Br_2O$ = 542.27 g mol^{-1}). Elemental Analysis: Calculated C 64.23, H 3.35. Found C 63.12, H 3.69.

2,7-dibromo-9,9-bis-(4'-(2",3",4",5"-tetraphenyl benzene)-phenyl)-fluorene (3)

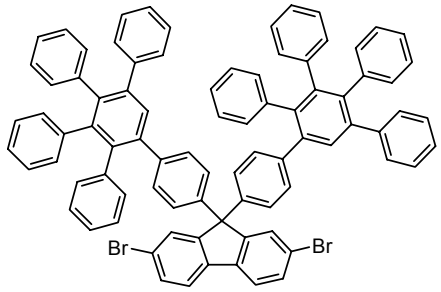

(4,4'-dibromo-biphenyl-2-yl)-bis-(4-ethynyl-phenyl)-methanol (212 mg, 0.4 mmol) and tetra phenyl cyclopentadienone (307 mg, 0.8 mmol)were mixed in 10 mL o-xylene, and degassed with bubbling argon for 30 min. The solution was heated to 140°C under argon for 14 hours. The reaction mixture was cooled, and the solvents removed *in vacu*. The intermediate was purified by column chromatography eluting with 0-5% ethyl acetate in hexane. The white powder was dissolved in 25 mL of acetic acid, and heated to 100 °C. Sulphuric acid (0.5 mL) was added and the white solution stirred for 12 hours at 100 °C. The reaction mixture was poured into water, the product filtered, washed with water and purified by column chromatography eluting with 0-5% ethyl acetate in hexane to give the title compound as a white powder. 420 mg (85%). ^{1}H NMR (250 MHz): (CD_2Cl_2) δ 7.62 (d, 2H, J=8.1Hz), 7.53-7.49 (m, 4H), 7.35 (d, 2H, J=1.5Hz), 7.14 (m, 10H), 7.01-6.79 (m, 36H) ppm. ^{13}C NMR (75 MHz): (CD_2Cl_2) δ 153.34, 142.57, 142.10, 142.01, 141.11, 141.08, 140.81, 140.64, 140.48, 140.28, 139.76, 138.44, 131.91, 131.85, 131.81, 130.33, 130.26, 127.89, 127.38, 127.17, 126.90, 126.60, 126.01, 125.94, 125.69, 122.04, 65.34 ppm. MS (FS, 8kV): m/z (%) = 1236.9 (100%, M^+) (calc. for $C_{85}H_{56}Br_2$ = 1237.20 g mol^{-1}). Elemental Analysis: Calculated C 82.52, H 4.56. Found C 83.00, H 4.59.

Poly-(9,9-bis-(4'-(2",3",4",5"-tetraphenyl benzene)-phenyl)-fluorene) (4)

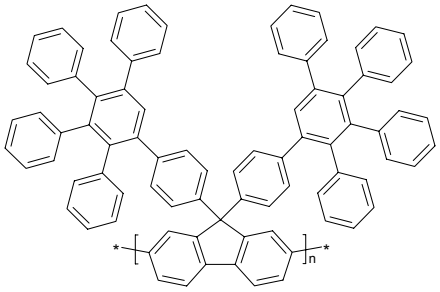

$Ni(COD)_2$ (73 mg, 2.7 x 10^{-4} mol), 2,2'-bipyridyl (41 mg, 2.7 x 10^{-4} mol) and COD (0.03 mL, 2.7 x 10^{-4} mol) was mixed with 1.5 mL dry DMF and 0.5 mL dry toluene in a glove box. The purple solution was heated to 80 °C for 30 minutes. 2,7-dibromo-9,9-bis-(4'-(2",3",4",5"-tetraphenyl benzene)-phenyl)-fluorene (137 mg, 1.1 x 10^{-4}) in 1.5 mL of dry toluene was added, and the solution stirred under argon, in absence of light, for 4 days. The reaction mixture was precipitated in a methanol/hydrochloric acid solution (4:1), filtered, subjected to Soxhlet extraction for 2 days in acetone, dissolved in THF, precipitated in methanol then filtered to give the title compound as a off white solid. 62 mg (52%). ^{1}H-NMR (300 MHz) δ 7.88 (d, 2H, J=7.4Hz), 7.55-7.40 (m, 6H), 7.10-6.46 (m, 48H) ppm. GPC analysis M_n = 9.8 x 10^3 g mol^{-1}, M_w = 1.8 x 10^4 g mol^{-1}, and D = 1.8 (against PS standard); M_n = 7.4 x 10^3 g mol^{-1}, M_w = 1.1 x 10^4 g mol^{-1}, and D = 1.6 (against PPP standard). Elemental Analysis: Calculated C 94.76, H 5.24. Found C 94.80, H 4.97.

(4,4'-dichloro-biphenyl-2-yl)-bis-(4-trimethylsilanylethynyl-phenyl)-methanol (5)

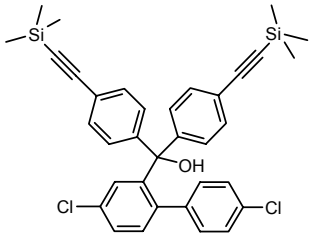

(4-Bromo-phenylethynyl)-trimethylsilane (1 g, 3.9 mmol) was dissolved in 15 mL of dry THF under argon, and cooled to -78°C in a dry ice/acetone bath. n-BuLi (2.6 mL, 4.2 mmol) was added and the reaction mixture stirred for 30 minutes. 4,4'-dichloro-biphenyl-2-carboxylic acid methyl ester (0.5 g, 1.8 mmol) dissolved in 5 mL dry THF was added, and the reaction mixture left to warm to room temperature, and stirred for 12 hours. The reaction was quenched with a ammonium chloride solution, the organic products extracted with methylene chloride, washed with water, dried over magnesium sulphate, and the solvents removed *in vacu*. The product was purified by column chromatography eluting with 0-2% ethyl acetate in hexane to give the title compound as a white powder. 0.95 g (88%). ^{1}H NMR (250 MHz): (CD_2Cl_2) δ 7.41 (d, 4H, J = 8.6Hz), 7.33 (dd, 1H, J=2.2, 8.1Hz), 7.17 (d, 2H, J=8.5Hz), 7.09-7.05 (m, 5H, J=2.9, 8.3Hz), 6.79 (d, 1H, J=2.2Hz), 6.75 (d, 2H, J=8.5Hz), 2.84 (s, 1H) 0.28 (s, 18H) ppm. ^{13}C NMR (63 MHz): (CD2Cl2) δ 146.95, 146.59, 139.71, 139.07, 134.31, 134.03, 133.38, 131.99, 131.34, 130.15, 128.50, 128.23, 127.83, 123.02, 104.92, 95.31, 83.09, 0.07 ppm. MS (FS, 8kV): m/z (%) = 595.7 (100%, M^+) (calc. for $C_{35}H_{34}Cl_2OSi_2$ = 597.74 g mol^{-1}). Elemental Analysis: Calculated C 70.33, H 5.73. Found C 70.03, H 5.42.

(4,4'-dichloro-biphenyl-2-yl)-bis-(4-ethynyl-phenyl)-methanol (6)

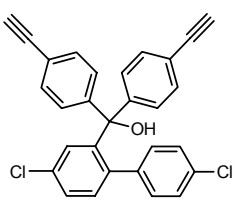

(4,4'-dichloro-biphenyl-2-yl)-bis-(4-trimethylsilanylethynyl-phenyl)-methanol (0.7 g, 1.2 mmol) and ammonium fluoride (270 mg, 7.4 mmol) was mixed in 30 mL dry THF under argon. Tetrabutylammonium fluoride (0.33 mL, 0.33 mmol) was added, and the reaction mixture stirred for 15 hours. The reaction was quenched with water, the organic products extracted with methylene chloride, washed with water, dried over magnesium sulphate, and the solvents removed *in vacu*. The product was purified by column chromatography eluting with 0-3% ethyl acetate in hexane to give the title compound as a white powder. 0.48 g (88%). ^{1}H NMR (250 MHz): (CD_2Cl_2) δ 7.43 (d, 4H, J=8.4Hz), 7.33 (dd, 1H, J=2.2, 8.1Hz), 7.15 (d, 2H, J=8.5Hz), 7.11-7.05 (m, 5H), 6.80 (d, 1H, J=2.1Hz), 6.73 (d, 1H, J=8.5Hz), 3.16 (s, 2H), 2.83 (s, 1H) ppm. ^{13}C NMR (63 MHz): (CD2Cl2) δ 147.21, 146.39, 139.64, 139.06, 134.30, 133.96, 133.35, 132.19, 131.27, 130.04, 128.44, 128.23, 127.84, 121.87, 83.42, 82.99, 78.01 ppm. MS (FS, 8kV): m/z (%) = 452.6 (100%, M^+) (calc. for $C_{29}H_{18}Cl_2O$ = 453.37 g mol^{-1}). Elemental Analysis: Calculated C 76.83, H 4.00. Found C 76.83, H 4.03.

2,7-dichloro-9,9-bis-(4'-(2",3",4",5"-tetraphenyl benzene)-phenyl)-fluorene (7)

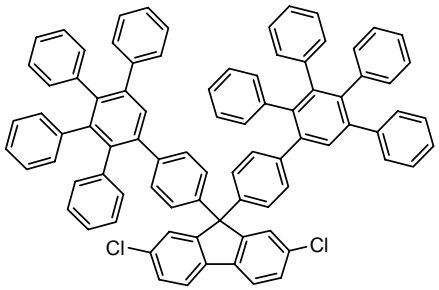

(4,4'-dichloro-biphenyl-2-yl)-bis-(4-ethynyl-phenyl)-methanol (280 mg, 6.17 x 10^{-4} mol) and tetra phenyl cyclopentadienone (533 mg, 1.36 x 10^{-3})were mixed in 15 mL o-xylene, and degassed with bubbling argon for 30 min. The solution was heated to 140°C under argon for 14 hours. The reaction mixture was cooled, and the solvents removed *in vacu*. The intermediate was purified by column chromatography eluting with 0-5% ethyl acetate in hexane. The white powder was dissolved in 10 mL of methylene chloride. $BF_3.OEt_2$ (0.2 mL) was added, and the intensely purple coloured solution was stirred for 12 hours. The reaction was quenched with methanol, and the product filtered, washed with methanol and dried *in vacu* to give the title compound as a white solid. 547 mg (83%). ^{1}H NMR (300 MHz): (CD_2Cl_2) δ 7.66 (d, 2H, J=8.1Hz), 7.49 (s, 2H), 7.35 (dd, 2H, J=1.9, 8.1Hz), 7.19 (d, 2H, J=1.8Hz), 7.14 (s, 10H), 7.00-6.79 (m, 38H) ppm. ^{13}C NMR (75 MHz): (CD2Cl2) δ 153.18, 142.66, 142.10, 142.01, 141.10, 141.06, 140.81, 140.65, 140.48, 140.29, 139.78, 137.99, 133.82, 131.90, 131.85, 131.81, 131.19, 130.31, 130.25, 128.43, 127.89, 127.37, 127.17, 126.90, 126.66, 126.60, 125.98, 125.69, 121.74, 65.30 ppm. MS (FS, 8kV): m/z (%) = 452.6 (100%, M^+) (calc. for $C_{85}H_{56}Cl_2$ = 1148.30 g mol^{-1}). Elemental Analysis: Calculated C 88.91, H 4.92. Found C 88.81, H 4.57.

Poly-(9,9-bis-(4'-(2",3",4",5"-tetraphenyl benzene)-phenyl)-fluorene) (8)

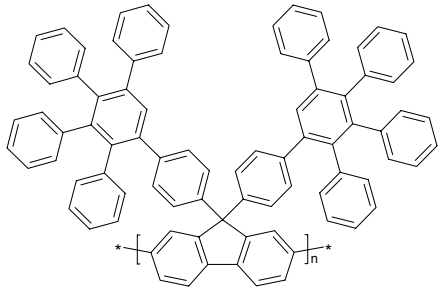

$Ni(COD)_2$ (257 mg, 9.4 x 10^{-4} mol), 2,2'-bipyridyl (146 mg, 9.4 x 10^{-4} mol) and COD (0.12 mL, 9.4 x 10^{-4} mol) was mixed with 4 mL dry DMF and 2 mL dry toluene in a glove box. The purple solution was heated to 80 °C for 30 minutes. 2,7-dichloro-9,9-bis-(4'-(2",3",4",5"-tetraphenyl benzene)-phenyl)-fluorene (450 mg, 3.9 x 10^{-4}) in 8 mL of dry toluene was added, and the solution stirred under argon, in absence of light, for 4 days. The reaction mixture was precipitated in a methanol/hydrochloric acid solution (4:1), filtered, subjected to Soxhlet extraction for 2 days in acetone, dissolved in THF, precipitated in methanol then filtered to give the title compound as a off white solid. 336 mg (80%). ^{1}H-NMR (300 MHz) δ 7.88 (d, 2H, J=7.4Hz), 7.55-7.40 (m, 6H), 7.10-6.46 (m, 48H) ppm. GPC analysis M_n = 3.2 x 10^4 g mol^{-1}, M_w = 8.7 x 10^4 g mol^{-1}, and D = 2.7 (against PS standard); M_n = 2.1 x 10^4 g mol^{-1}, M_w = 4.5 x 10^4 g mol^{-1}, and D = 2.1 (against PPP standard). Elemental Analysis: Calculated C 94.76, H 5.24. Found C 92.16, H 5.51.

2,7-dibromo-9,9-bis-(4'-(2",5"-diphenyl-",3",4"-bis-(triphenylamine)-benzene)-phenyl)-fluorene (11)

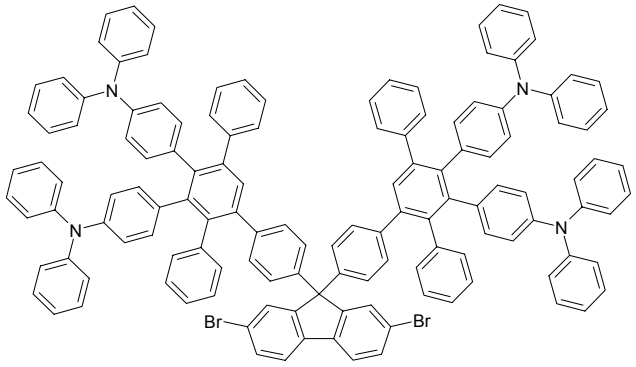

(4,4'-dibromo-biphenyl-2-yl)-bis-(4-ethynyl-phenyl)-methanol (100 mg, 0.2 mmol) and substituted tetra phenyl cyclopentadienone (300 mg, 0.42 mmol)were mixed in 7 mL o-xylene, and degassed with bubbling argon for 30 min. The solution was heated to 140°C under argon for 14 hours. The reaction mixture was cooled, and the solvents removed *in vacu*. The intermediate was purified by column chromatography eluting with 0-10% ethyl acetate in hexane. The yellow powder was dissolved in 15 mL of methylene chloride. $BF_3.OEt_2$ (0.2 mL) was added, and the intensely purple coloured solution was stirred for 12 hours. The reaction was quenched with methanol, and the product filtered, washed with methanol and dried *in vacu* to give the title compound as a yellow solid. 194 mg (51%). ^{1}H-NMR (300

MHz) δ 7.62 (d, 2H, J=8.3Hz), 7.51 (dd, 2H, J=1.8, 8.1Hz), 7.37 (d, 1H, J=1.8Hz), 7.24-7.13 (m, 26H), 7.03-6.84 (m, 42H), 6.79.6.64 (m, 16H) ppm. ^{13}C NMR (75 MHz): (CD2Cl2) δ 153.36, 148.14, 145.81, 145.50, 142.60, 142.05, 141.11, 141.06, 140.49, 140.35, 139.86, 139.65, 138.45, 136.03, 135.49, 132.91, 132.88, 132.08, 131.32, 131.08, 130.40, 129.57, 129.44, 129.38, 127.93, 127.43, 127.24, 126.69, 126.04, 124.00, 123.82, 123.61, 123.50, 122.70, 122.56, 122.13, 122.05, 121.86, 114.23, 65.37 ppm. MS (FS, 8kV): m/z (%) = 1901 (100%, M^+) (calc. for $C_{132}H_{92}Br_2N_2$ = 1906.05 g mol^{-1}). Elemental Analysis: Calculated C 83.81, H 4.87, N 2.94. Found C 83.78, H 4.89, N 3.02.

Poly-(9,9-bis-(4'-(2",5"-diphenyl-",3",4"-bis-(triphenylamine)-benzene)-phenyl)-fluorene) (13)

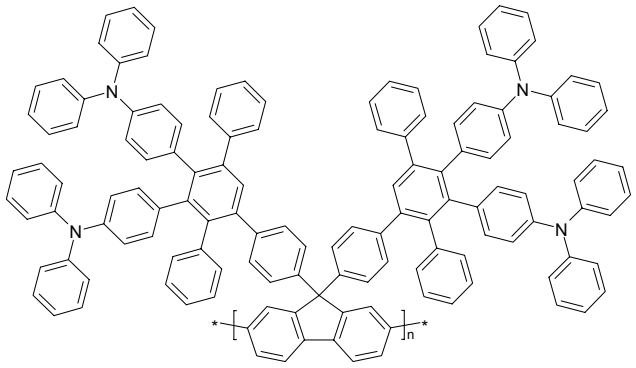

$Ni(COD)_2$ (67 mg, 2.4 x 10^{-4} mol), 2,2'-bipyridyl (38 mg, 2.4 x 10^{-4} mol) and COD (0.03 mL, 2.4 x 10^{-4} mol) was mixed with 2 mL dry DMF and 1 mL dry toluene in a glove box. The purple solution was heated to 80 °C for 30 minutes. 2,7-dibromo-9,9-bis-(4'-(2",5"-diphenyl-",3",4"-bis-(triphenylamine)-benzene)-phenyl)-fluorene (200 mg, 1.1 x 10^{-4}) in 5 mL of dry toluene was added, and the solution stirred under argon, in absence of light, for 4 days. The reaction mixture was precipitated in methanol, filtered, subjected to Soxhlet extraction for 2 days in acetone, dissolved in THF, precipitated in methanol then filtered to give the title compound as a yellow solid. 146 mg (80%). ^{1}H-NMR (250 MHz) δ 7.52-7.48 (m, 2H), 7.22-6.56 (m, 90H) ppm. GPC analysis M_n = 3.8 x 10^3 g mol^{-1}, M_w = 5.4 x 10^3 g mol^{-1}, and D = 1.4 (against PS standard); M_n = 3.1 x 10^3 g mol^{-1}, M_w = 4.0 x 10^3 g mol^{-1}, and D = 1.3 (against PPP standard). Elemental Analysis: Calculated C 91.48, H 5.32, N 3.21. Found C 83.31, H 3.87, N 3.04.

2,7-dichloro-9,9-bis-(4'-(2",5"-diphenyl-3",4"-bis-(triphenyl amine)-benzene)-phenyl)-fluorene (12)

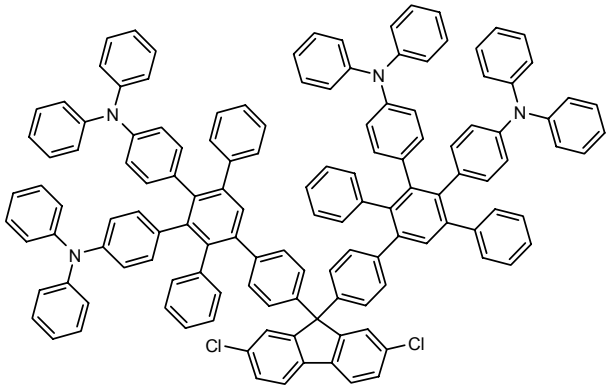

(4,4'-dichloro-biphenyl-2-yl)-bis-(4-ethynyl-phenyl)-methanol (115 mg, 0.25 mmol) and substituted tetra phenyl cyclopentadienone (444 mg, 0.62 mmol) were mixed in 15 mL o-xylene, and degassed with bubbling argon for 30 min. The solution was heated to 140°C under argon for 14 hours. The reaction mixture was cooled, and the solvents removed *in vacu*. The intermediate was purified by column chromatography eluting with 0-5% ethyl acetate in hexane. The yellow powder was dissolved in 5 mL of methylene chloride. $BF_3.OEt_2$ (0.2 mL) was added, and the intensely purple coloured solution was stirred for 12 hours. The reaction was quenched with methanol, and the product filtered, washed with methanol and dried *in vacu* to give the title compound as a white solid. 282 mg (62%). ^{1}H NMR (300 MHz): (CD_2Cl_2) δ 7.67 (d, 2H, J=8.2Hz), 7.52 (s, 2H) ppm 7.36 (dd, 2H, J=1.9, 8.2Hz), 7.23-7.14 (m, 28H), 7.06-6.85 (m, 42H), 6.79-6.65 (m, 16H) ppm. ^{13}C NMR (75 MHz): (CD_2Cl_2) δ 153.22, 148.16, 145.84, 145.52, 142.71, 142.08, 141.12, 141.08, 140.52, 140.39, 139.66, 138.02, 136.05, 135.51, 133.85, 132.93, 132.89, 132.09, 131.09, 130.42, 129.46, 129.40, 128.45, 127.95, 127.45, 127.24, 126.71, 126.02, 124.02, 123.85, 123.63, 122.72, 122.58, 121.76 ppm. MS (FS, 8kV): m/z (%) = 1817.0 (100%, M^+) (calc. for $C_{133}H_{92}Cl_2N_4$ = 1817.15 g mol^{-1}). Elemental Analysis: Calculated C 87.91, H 5.10, N 3.08. Found C 87.58, H 5.38, N 3.21.

Poly-(9,9-bis-(4'-(2",5"-diphenyl-3",4"-bis-(triphenyl amine)-benzene)-phenyl)-fluorene) (14)

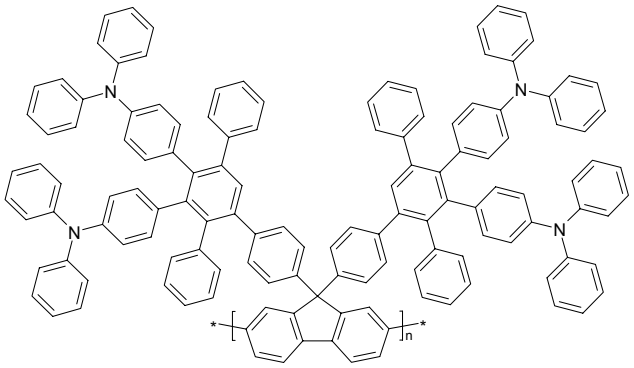

$Ni(COD)_2$ (85 mg, 0.31 mmol), 2,2'-bipyridyl (48 mg, 0.31 mmol) and COD (0.04 mL, 0.31 mmol) was mixed with 2 mL dry DMF and 1 mL dry toluene in a glove box. The purple solution was heated to 80 °C for 30 minutes. 2,7-dichloro-9,9-bis-(4'-(2",5"-diphenyl-3",4"-bis-(triphenyl amine)-benzene)-phenyl)-fluorene (235 mg, 0.13 mmol) in 5 mL of dry toluene was added, and the solution stirred under argon, in absence of light, for 4 days. The reaction mixture was precipitated in methanol, filtered, subjected to Soxhlet extraction for 2 days in acetone, dissolved in THF, precipitated in methanol then filtered to give the title compound as a off white solid. 45 mg (47%). ^{1}H-NMR (300 MHz): (CD_2Cl_2) δ 7.88 (d, 2H, J=7.4Hz), 7.55-7.40 (m, 6H), 7.10-6.46 (m, 48H) ppm. GPC analysis M_n = 1.7 x 10^4 g mol^{-1}, M_w = 3.1 x 10^4 g mol^{-1}, and D = 1.9 (against PS standard); M_n = 1.2 x 10^4 g mol^{-1}, M_w = 1.9 x 10^4 g mol^{-1}, and D = 1.6 (against PPP standard). Elemental Analysis: Calculated C 91.48, H 5.31, N 3.21. Found C 87.88, H 4.93, N 2.84.

2,7-dibromo-9,9-bis-(4'-(2",5"-diphenyl-3",4"-bis-(4'''-di-(4''''-isooctylphenyl)-amine-phenyl)-benzene)-phenyl)-fluorene (16)

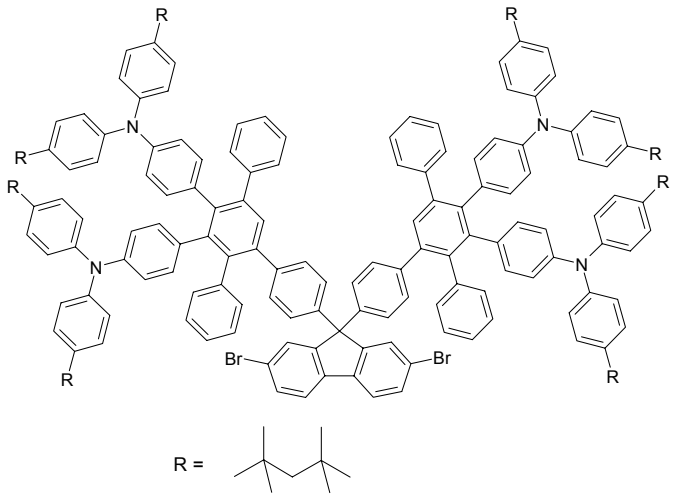

(4,4'-dibromo-biphenyl-2-yl)-bis-(4-ethynyl-phenyl)-methanol (45 mg, 8.6 x 10^{-5} mol) and substituted tetra phenyl cyclopentadienone (200 mg, 1.7 x 10^{-4} mol) were mixed in 3 mL o-xylene, and degassed with bubbling argon for 30 min. The solution was heated to 140°C under argon for 14 hours. The reaction mixture was cooled, and the solvents removed *in vacu*. The intermediate was purified by column chromatography eluting with 0-10% ethyl acetate in hexane. The yellow intemediate was dissolved in 15 mL of methylene chloride. $BF_3.OEt_2$ (0.2 mL) was added, and the intensely purple coloured solution was stirred for 12 hours. The reaction was quenched with methanol, and the product filtered, washed with methanol and dried *in vacu*. The product was purified by column chromatography eluting with 0-5% ethyl acetate in hexane to give the title compound as a yellow powder. 166 mg (66%). ^{1}H-NMR (300 MHz) δ 7.63 (d, 2H, J=8.1Hz), 7.52 (dd, 1H, J=1.7, 8.1Hz), 7.51 (s, 1H), 7.24-7.18 (m, 26H), 7.06-7.01 (m, 10H), 6.90-6.64 (m, 40H), 1.70 (s, 16H), 1.33 (s, 48H), 0.74 (s, 72H) ppm. ^{13}C-NMR (75 MHz) δ 219.54, 153.42, 146.13, 145.83, 145.39, 144.67, 144.53, 142.56, 142.39, 142.20, 141.24, 140.98, 140.47, 140.41, 140.03, 138.47, 134.34, 132.63, 132.12, 130.42, 127.94, 127.43, 127.23, 127.18, 123.68, 123.55, 122.07, 57.34, 38.43, 32.61, 31.87, 31.66, 23.07, 14.26, 1.14. MS

(FS, 8kV): m/z (%) = 2785.6 (100%, M^+) (calc. for $C_{196}H_{219}Br_2N_4$ = 2789.76 g mol^{-1}). Elemental Analysis: Calculated C 84.39, H 7.91, N 2.00. Found C 83.29, H 8.24, N 2.04.

Poly-(9,9-bis-(4'-(2",5"-diphenyl-3",4"-bis-(4'''-di-(4''''-isooctylphenyl)-amine-phenyl)-benzene)-phenyl)-fluorene) (17)

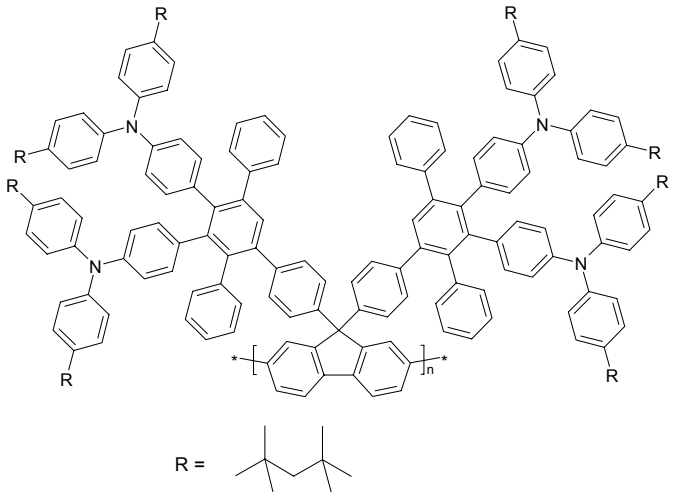

$Ni(COD)_2$ (23 mg, 8.6 x 10^{-5} mol), 2,2'-bipyridyl (13 mg, 8.6 x 10^{-5} mol) and COD (0.01 mL, 8.6 x 10^{-5} mol) was mixed with 0.5 mL dry DMF and 0.2 mL dry toluene in a glove box. The purple solution was heated to 80 °C for 30 minutes. 2,7-dibromo-9,9-bis-(4'-(2",5"-diphenyl-3",4"-bis-(4'''-di-(4''''-isooctylphenyl)-amine-phenyl)-benzene)-phenyl)-fluorene (100 mg, 3.6 x 10^{-5} mol) in 0.8 mL of dry toluene was added, and the solution stirred under argon, in absence of light, for 4 days. The reaction mixture was precipitated in a methanol/hydrochloric acid solution (4:1), filtered, subjected to Soxhlet extraction for 2 days in acetone, dissolved in THF, precipitated in methanol then filtered to give the title compound as a yellow solid. 35 mg (37%). ^1H NMR (300 MHz): (CD_2Cl_2) δ 7.50 (s, broad, 4H), 7.24-6.54 (m, 78H), 1.67 (s, 6H), 1.65 (s, 6H), 1.30 (s, 24H), 1.28 (s, 24H), 0.72 (s, 36H), 0.69 (s, 36H) ppm. M_n = 3.5 x 10^4 g mol^{-1}, M_w = 1.8 x 10^5 g mol^{-1}, and D = 5.2 (against PS standard); M_n = 2.4 x 10^4 g mol^{-1}, M_w = 8.5 x 10^4 g mol^{-1}, and D = 3.5 (against PPP standard). Elemental Analysis: Calculated C 89.51, H 8.36, N 2.13. Found C 86.91, H 7.16, N 2.48.

(4,4'-dibromo-biphenyl-2-yl)-bis-(4'-(2",5"-diphenyl-3",4"-bis-(4-acetylene benzene)-phenyl)-methanol (18)

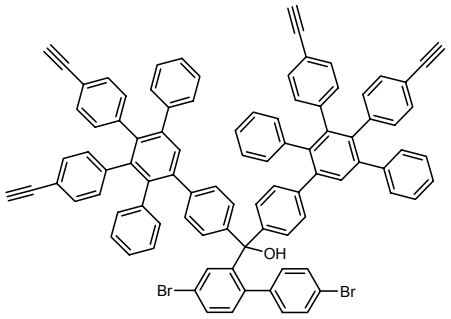

(4,4'-dibromo-biphenyl-2-yl)-bis-(4-ethynyl-phenyl)-methanol (163 mg, 0.3 mmol) and di-(TIPS acetylene)-tetra phenyl cyclopentadienone (500 mg, 0.67 mmol)were mixed in 13 mL o-xylene, and degassed with bubbling argon for 30 min. The solution was heated to 140°C under argon for 14 hours. The reaction mixture was cooled, and the solvents removed *in vacu*. The intermediate was purified by column chromatography eluting with 0-2% ethyl acetate in hexane. The white powder was mixed with ammonium fluoride (100 mg, 2.7 mmol) in 12 mL dry THF under argon. Tetrabutylammonium fluoride (0.14 mL, 0.14 mmol) was added, and the reaction mixture stirred for 15 hours. The reaction was quenched with water, the organic products extracted with methylene chloride, washed with water, dried over magnesium sulphate, and the solvents removed *in vacu*. The product was purified by column chromatography eluting with 0-15% ethyl acetate in hexane to give the title compound as a white powder. 373 mg (92%). ^{1}H-NMR (300 MHz) δ 7.55 (s, 2H), 7.43 (dd, 1H, J=2.0Hz, J=8.1Hz), 7.25 (d, 2H, J=8.4Hz), 7.20-6.76 (m, 46H), 6.54 (d, 2H, J=8.4Hz), 3.02 (s, 2H), 3.04 (s, 2H), 2.60 (s, 1H). ^{13}C-NMR (75 MHz) δ 147.45, 145.03, 141.57, 141.48, 141.27, 141.12, 140.41, 139.91, 139.69, 139.37, 138.78, 134.17, 132.98, 131.86, 131.79, 131.51, 131.27, 131.17, 130.90, 130.50, 130.22, 129.85, 128.11, 127.51, 127.46, 126.92, 126.44, 121.92, 121.29, 119.79, 119.50, 83.76, 82.89, 77.43, 77.31. MS (FS, 8kV): m/z (%) = 1353.7 (100%, M^{+}) (calc. for $C_{93}H_{58}Br_2O$ = 1351.31 g mol^{-1}). Elemental Analysis: Calculated C 82.66, H 4.33. Found C 82.62, H 4.43.

2,7-dibromo-9,9-bis-(4'-(2",5"-diphenyl-3",4"-bis(4'-(2",3",4",5"-tetraphenyl benzene)-phenyl)-benzene)-phenyl)-fluorene (20)

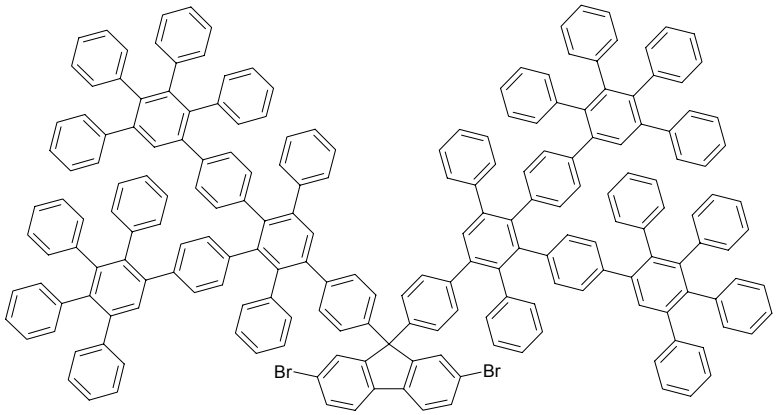

(4,4'-dibromo-biphenyl-2-yl)-bis-(4'-(2",5"-diphenyl-3",4"-bis-(4-acetylene benzene)-phenyl)-methanol (184 mg, 0.14 mmol) and tetra phenyl cyclopentadienone (313 mg, 0.82 mmol)were mixed in 5 mL o-xylene, and degassed with bubbling argon for 30 min. The solution was heated to 140°C under argon for 14 hours. The reaction mixture was cooled, and the solvents removed *in vacu*. The intermediate was purified by column chromatography eluting with 0-5% ethyl acetate in hexane. The white powder was mixed in 7 mL acetic acid, heated to 100 °C, 0.5 mL sulphuric acid was added and the mixture stirred for 12 hours. The reaction mixture was poured into water, the product filtered, washed with water, dried *in vacu* to give the title compound as a white powder. 313 mg (81%). ^{1}H-NMR (300 MHz) δ 7.61 (d, 2H, J=8.1Hz), 7.50 (dd, 2H, J=1.7Hz, J=8.1Hz), 7.45 (s, 2H), 7.41 (s, 2H), 7.37 (s, 2H), 7.33 (d, 2H, J=1.7Hz), 7.17-7.14 (m, 24H), 7.07-6.65 (m, 92H), 6.54 (d, 4H, J=8.3Hz) 6.49 (d, 4H, J=8.3Hz) ppm. ^{13}C-NMR (75 MHz) δ 142.26, 140.60, 140.42, 139.44,

132.04, 131.89, 131.41, 131.32, 130.28, 128.97, 127.97, 127.87, 127.22, 127.17, 127.13, 126.83, 126.56, 125.89, 125.61, 59.89, 144.13, 142.08, 141.08, 140.98, 140.82, 140.76, 139.56, 139.24, 138.88, 129.56, 128.70, 125.76, 122.04 ppm. MS (FS, 8kV): m/z (%) = 2757.9 (100%, M^+) (calc. for $C_{205}H_{136}Br_2$ = 2759.18 g mol^{-1}). Elemental Analysis: Calculated C 89.24, H 4.97. Found C 89.03, H 4.97.

(4,4'-dichloro-biphenyl-2-yl)-bis-(4'-(2",5"-diphenyl-3",4"-bis-(4-acetylene benzene)-phenyl)-methanol (19)

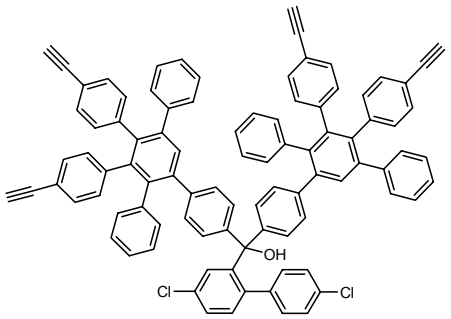

(4,4'-dichloro-biphenyl-2-yl)-bis-(4-ethynyl-phenyl)-methanol (242 mg, 0.53 mmol) and di-(TIPS acetylene)-tetra phenyl cyclopentadienone (875 mg, 1.2 mmol)were mixed in 20 mL o-xylene, and degassed with bubbling argon for 30 min. The solution was heated to 140°C under argon for 14 hours. The reaction mixture was cooled, and the solvents removed *in vacu*. The intermediate was purified by column chromatography eluting with 0-2% ethyl acetate in hexane. The white powder was mixed with ammonium fluoride (117 mg, 3.2 mmol) in 20 mL dry THF under argon. Tetrabutylammonium fluoride solution (1.1 mL, 1.1 mmol) was added, and the reaction mixture stirred for 15 hours. The reaction was quenched with water, the organic products extracted with methylene chloride, washed with water, dried over magnesium sulphate, and the solvents removed *in vacu*. The product was purified by column chromatography eluting with 0-20% ethyl acetate in hexane to give the title compound as a white powder. 354 mg (53%). ^{1}H NMR (300 MHz): (CD_2Cl_2) δ 7.57 (s, 2H), 7.28 (dd, 1H, J=2.2Hz, J=8.1Hz), 7.21-7.00 (m, 31H), 6.90-6.79 (m, 16H), 6.62 (d, 2H, J=8.3Hz), 6.60 (s, 1H), 3.04 (s, 2H), 3.02 (s, 2H), 2.63 (s, 1H) ppm. ^{13}C-NMR (75 MHz) δ 147.26, 145.04, 141.57, 141.48, 141.27, 141.12, 139.92, 139.87, 139.71, 138.88, 138.77, 133.96, 133.74, 133.01, 131.86, 131.80, 131.32, 131.17, 130.90, 130.22, 129.84, 128.34, 128.11, 127.45, 126.92, 126.43, 119.79, 119.51, 83.76, 82.93, 77.43, 77.31 ppm. MS (FS, 8kV): m/z (%) = 1260.9 (100%, M^+) (calc. for $C_{93}H_{58}Cl_2O$ = 1262.40 g mol^{-1}). Elemental Analysis: Calculated C 88.48, H 4.63. Found C 88.50, H 5.08.

2,7-dichloro-9,9-bis-(4'-(2",5"-diphenyl-3",4"-bis(4'-(2",3",4",5"-tetraphenyl benzene)-phenyl)-benzene)-phenyl)-fluorene (21)

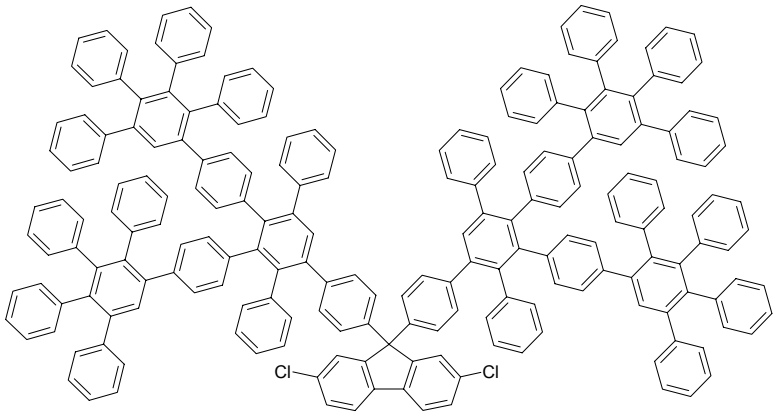

(4,4'-dichloro-biphenyl-2-yl)-bis-(4'-(2",5"-diphenyl-3",4"-bis-(4-acetylene benzene)-phenyl)-methanol (134 mg, 0.1 mmol) and tetra phenyl cyclopentadienone (167 mg, 0.44 mmol)were mixed in 10 mL o-xylene, and degassed with bubbling argon for 30 min. The solution was heated to 140°C under argon for 14 hours. The reaction mixture was cooled, and the solvents removed *in vacu*. The intermediate was purified by column chromatography eluting with 0-20% ethyl acetate in hexane. The white powder was dissolved in 5 mL of methylene chloride. $BF_3.OEt_2$ (0.2 mL) was added, and the intensely purple coloured solution was stirred for 24 hours. The reaction was quenched with methanol, and the product filtered, washed with methanol and dried *in vacu* to give the title compound as a white powder. 285 mg (91%). ^{1}H NMR (300 MHz): (CD_2Cl_2) δ 7.66 (d, 2H, J=8.1Hz), 7.45 (s, 2H), 7.41 (s, 2H), 7.37 (s, 2H), 7.35 (dd, 2H, J=1.9Hz, J=8.2Hz), 7.19-7.14 (m, 26H), 7.07-6.65 (m, 92H), 6.54 (d, 4H, J=8.3Hz), 6.49 (d, 4H, J=8.3Hz) ppm. ^{13}C NMR (75 MHz): (CD_2Cl_2) δ 153.19, 142.61, 142.23, 142.06, 141.53, 141.13, 141.06, 140.96, 140.80, 140.74, 140.71, 140.57, 140.40, 140.24, 139.78, 139.58, 139.54, 139.49, 139.42, 139.22, 138.86, 138.53, 138.21, 137.97, 133.81, 132.02, 131.87, 131.42, 131.37, 131.31, 130.30, 130.26, 128.97, 128.70, 128.42, 127.96, 127.86, 127.35, 127.16, 127.13, 126.83, 126.66, 126.56, 126.01, 125.88, 125.60, 121.74, 65.29 ppm. Elemental Analysis: Calculated C 92.21, H 5.13. Found C 92.15, H 5.15.

Poly-(9,9-bis-(4'-(2",5"-diphenyl-3",4"-bis(4'-(2",3",4",5"-tetraphenyl benzene)-phenyl)-benzene)-phenyl)-fluorene) (22)

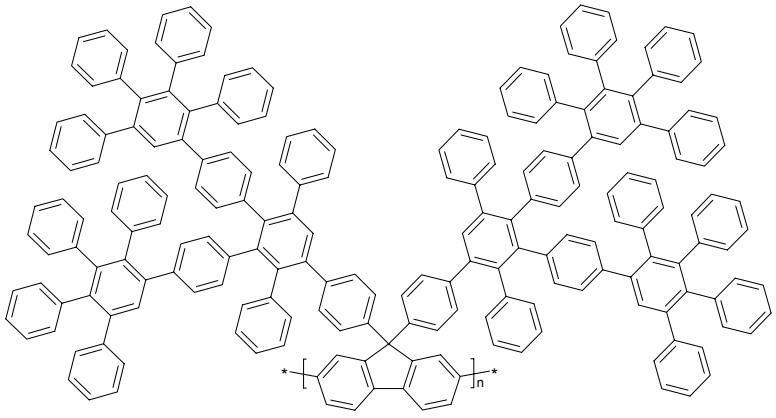

$Ni(COD)_2$ (50 mg, 0.18 mmol), 2,2'-bipyridyl (28 mg, 0.18 mmol) and COD (0.02 mL, 0.18 mmol) was mixed with 2 mL dry DMF and 0.5 mL dry toluene in a glove box. The purple solution was heated to 80 °C for 30 minutes. 2,7-dichloro-9,9-bis-(4'-(2",5"-diphenyl-3",4"-bis(4'-(2",3",4",5"-tetraphenyl benzene)-phenyl)-benzene)-phenyl)-fluorene (200 mg, 7.5 x 10^{-5} mol) in 4 mL of dry toluene was added, and the solution stirred under argon, in absence of light, for 4 days. The reaction mixture was precipitated in a methanol/hydrochloric acid solution (4:1), filtered, subjected to Soxhlet extraction for 2 days in acetone, dissolved in THF, precipitated in methanol then filtered to give the title compound as a yellow solid. 80 mg (41%). ^{1}H NMR (300 MHz): (CD_2Cl_2) δ 7.50-7.33 (m, 8H), 7.13-6.41 (m, 128H) ppm. M_n = 6.7 x 10^3 g mol^{-1}, M_w = 9.4 x 10^3 g mol^{-1}, and D = 1.4 (against PS standard); M_n = 5.2 x 10^3 g mol^{-1}, M_w = 6.7 x 10^3 g mol^{-1}, and D = 1.3 (against PPP standard). Elemental Analysis: Calculated C 94.73, H 5.27. Found C 92.00, H 4.92.

{4,4''-Dibromo-5'-[hydroxy-bis-(4-trimethylsilanylethynyl-phenyl)-methyl]-[1,1';4',1'']terphenyl-2'-yl}-bis-(4-trimethylsilanylethynyl-phenyl)-methanol (23)

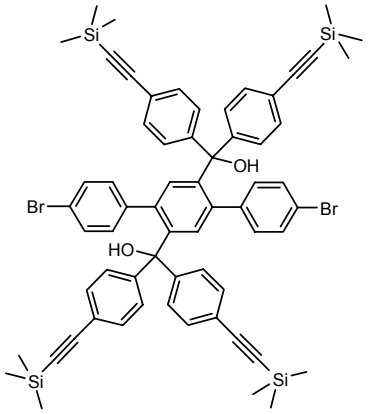

(4-Bromo-phenylethynyl)-trimethylsilane (0.575 g, 2.3 mmol) was dissolved in 10 mL of dry THF under argon, and cooled to -78°C in a dry ice/acetone bath. n-BuLi (1.6 mL, 2.5 mmol) was added and the reaction mixture stirred for 30 minutes. 4,4''-Dibromo-[1,1';4',1'']terphenyl-2',5'-dicarboxylic acid dimethyl ester (0.26 g, 0.5 mmol) dissolved in 10 mL dry THF was added, and the reaction mixture left to warm to room temperature, and stirred for 12 hours. The reaction was quenched with a ammonium chloride solution, the organic products extracted with methylene chloride, washed with water, dried over magnesium sulphate, and the solvents removed *in vacu*. The product was purified by column chromatography eluting with 0-5% ethyl acetate in hexane to give the title compound as a white powder. 0.45 g (76%). ^{1}H NMR (250 MHz): (CD_2Cl_2) δ 7.33 (d, 8H, J = 8.5 Hz), 7.25 (d, 4H, J = 8.5 Hz), 7.06 (d, 8H, J = 8.8 Hz), 6.61 (d, 4H, J = 8.2 Hz), 6.54 (s, 2H), 2.76 (s, 2H), 0.23 (s, 36H) ppm. ^{13}C NMR (63 MHz): (CD_2Cl_2) δ 147.27, 143.61, 140.63, 139.07, 134.35, 131.87, 131.47, 131.44, 128.15, 122.82, 122.09, 104.89, 95.20, 83.01, -0.04 ppm. MS (FS, 8kV): m/z (%) = 1136.7 (100%, M^+) (calc. for $C_{64}H_{64}Br_2O_2Si_4$ = 1137.37 g mol^{-1}). Elemental Analysis: Calculated C 67.59, H 5.67. Found C 67.57, H 5.47.

{5'-[Bis-(4-ethynyl-phenyl)-hydroxy-methyl]-4,4''-dibromo-[1,1';4',1'']terphenyl-2'-yl}-bis-(4-ethynyl-phenyl)-methanol (24)

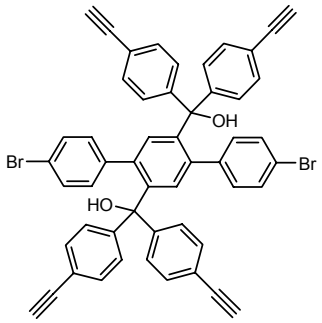

{4,4''-Dibromo-5'-[hydroxy-bis-(4-trimethylsilanylethynyl-phenyl)-methyl]-[1,1';4',1'']terphenyl-2'-yl}-bis-(4-trimethylsilanylethynyl-phenyl)-methanol (0.44 g, 0.39 mmol) and ammonium fluoride (190 mg, 5 mmol) was mixed in 30 mL dry THF under argon. Tetrabutylammonium fluoride (0.39 mL, 0.39 mmol) was added, and the reaction mixture stirred for 15 hours. The reaction was quenched with water, the organic products extracted with methylene chloride, washed with water, dried over magnesium sulphate, and the solvents removed *in vacu*. The product was purified by column chromatography eluting with 1:1 pentane/methylene chloride to give the title compound as a white powder. 0.19 g (59%). ^{1}H NMR (300 MHz): (CD_2Cl_2) δ 7.39 (d, 8H, J=8.5Hz), 7.24 (d, 4H, J=8.4Hz), 7.10 (d, 8H, J=8.5Hz), 6.62 (d, 4H, J=8.5Hz), 6.60 (s, 2H), 3.14 (s, 4H), 2.83 (s, 2H) ppm. ^{13}C NMR (75 MHz): (CD_2Cl_2) δ 147.48, 143.50, 140.49, 139.06, 134.30, 132.09, 131.41, 131.36, 128.14, 122.02, 121.65, 83.41, 82.86, 77.93 ppm. MS (FS, 8kV): m/z (%) = 848.8 (100%, M^+) (calc. for $C_{52}H_{32}Br_2O_2$ = 848.64 g mol^{-1}). Elemental Analysis: Calculated C 73.60, H 3.80. Found C 71.15, H 3.75.

2,8-Dibromo-6,6,12,12-tetra-(4'-(2",3",4",5"-tetraphenyl benzene)-phenyl)-indenofluorene (25)

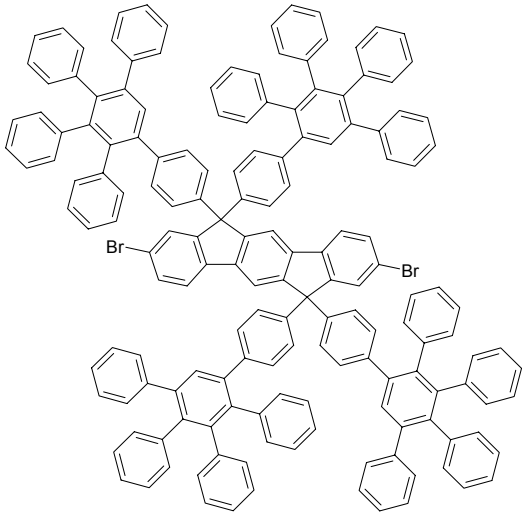

{5'-[Bis-(4-ethynyl-phenyl)-hydroxy-methyl]-4,4"-dibromo-[1,1';4',1"]-terphenyl-2'-yl}-bis-(4-ethynyl-phenyl)-methanol (150 mg, 0.18 mmol) and tetra phenyl cyclopentadienone (280 mg, 0.73 mmol)were mixed in 10 mL o-xylene, and degassed with bubbling argon for 30 min. The solution was heated to 140°C under argon for 14 hours. The reaction mixture was cooled, precipitated in methanol, filtered and dried *in vacu*. The white powder was dissolved in 5 mL of tetrachloromethane. $BF_3.OEt_2$ (0.2 mL) was added, heated to 70 °C and the purple coloured solution was stirred for 24 hours. The reaction was quenched with methanol, and the product filtered, washed with methanol and dried *in vacu* to give the title compound as a white powder. 251 mg (94%). ^{1}H NMR (300 MHz): (CD_2Cl_2) δ 6.85 (m, 10H), 6.45 (s, broad, 20H), 6.33-6.07 (m, 78H) ppm ^{13}C NMR (75 MHz): ($C_2D_2Cl_4$) δ 143.01, 141.95, 141.68, 140.78, 140.63, 140.51, 140.46, 140.19, 140.10, 139.56, 139.47, 139.41, 131.83, 131.09, 130.28, 127.82, 127.33, 127.28, 127.15, 127.06, 127.00, 126.85, 126.40, 125.72, 125.67, 125.42, 121.60, 74.45 ppm. MS (FS, 8kV): m/z (%) = 2239.3 (100%, M^+) (calc. for $C_{164}H_{108}Br_2$ = 2238.50 g mol^{-1}). Elemental Analysis: Calculated C 88.00, H 4.86. Found C 82.39, H 4.30.

Poly-(6,6,12,12-tetra-(4'-(2",3",4",5"-tetraphenyl benzene)-phenyl)-indenofluorene) (26)

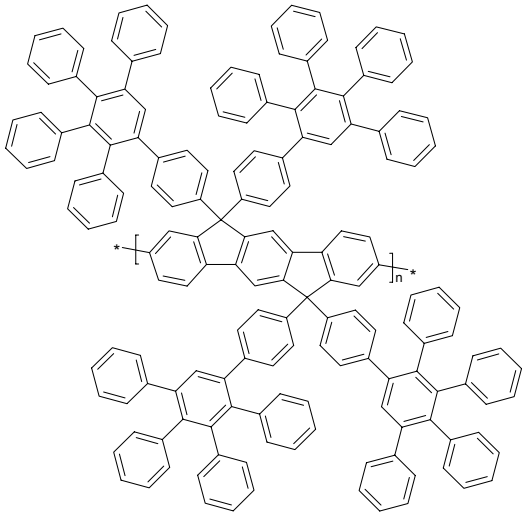

$Ni(COD)_2$ (60 mg, 0.22 mmol), 2,2'-bipyridyl (33 mg, 0.22 mmol) and COD (0.03 mL, 0.22 mmol) was mixed with 1.5 mL dry DMF and 0.75 mL dry toluene in a glove box. The purple solution was heated to 80 °C for 30 minutes. 2,8-Dibromo-6,6,12,12-tetra-(4'-(2",3",4",5"-tetraphenyl benzene)-phenyl)-indenofluorene (200 mg, 9 x 10^{-5} mol) in 4 mL of dry toluene was added, and the solution stirred under argon, in absence of light, for 4 days. The reaction mixture was precipitated in a methanol/hydrochloric acid solution (4:1), filtered, subjected to Soxhlet extraction for 2 days in acetone, dissolved in THF, precipitated in methanol then filtered to give the title compound as a yellow solid. 176 mg (94%). ^{1}H NMR (300 MHz): (CD_2Cl_2) δ 7.63-7.40 (m, 10H), 7.13-6.69 (m, 98H) ppm. M_n = 1.1 x 10^4 g mol^{-1}, M_w = 2.2 x 10^4 g mol^{-1}, and D = 1.9 (against PS standard); M_n = 8.3 x 10^3 g mol^{-1}, M_w = 1.3 x 10^4 g mol^{-1}, and D = 1.7 (against PPP standard). Elemental Analysis: Calculated C 94.76, H 5.24. Found C 93.56, H 5.34.

Aryl amine substituted dendronised fluorene co-polymer (27)

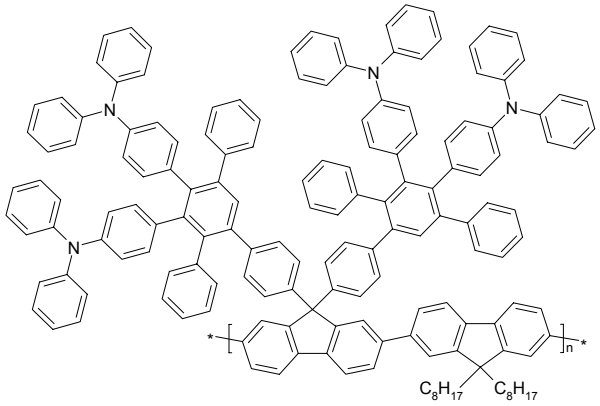

2,7-dibromo-9,9-bis-(4'-(2",5"-diphenyl-",3",4"-bis-(triphenylamine)-benzene)-phenyl)-fluorene (55 mg, 2.9 x 10^{-5} mol) and 2,7-bis-boronic ester 9,9-dioctylfluorene (19 mg, 2.9 x 10^{-5} mol) was dissolved in toluene (2 mL) and 2M K_2CO_3 solution (0.5 mL), and degassed with bubbling argon for 20 minutes. $Pd(PPh_3)_4$ (3 mg, 2.6 x 10^{-6} mol) was added and the solution heated at 80 °C for 12 hours. The reaction mixture was precipitated in a methanol, filtered, subjected to Soxhlet extraction for 2 days in acetone, dissolved in THF, precipitated in methanol then filtered to give the title compound as a yellow solid. 50 mg (80%). ^{1}H NMR (300 MHz): (CD_2Cl_2) δ 7.93-7.34 (m, 18H), 7.19-6.66 (m, 80H), 2.07 (s, broad, 4H), 1.19-1.06 (m, 20H), 0.75-0.69 (m, 10H) ppm. M_n = 3.2 x 10^3 g mol^{-1}, M_w = 6.9 x 10^3 g mol^{-1}, and D = 2.2 (against PS standard); M_n = 2.8 x 10^3 g mol^{-1}, M_w = 5.0x 10^3 g mol^{-1}, and D = 1.8 (against PPP standard). Elemental Analysis: Calculated C 91.14, H 6.23, N 2.62. Found C 71.84, H 4.81, N 2.27.

Second generation dendronised fluorene co-polymer (28)

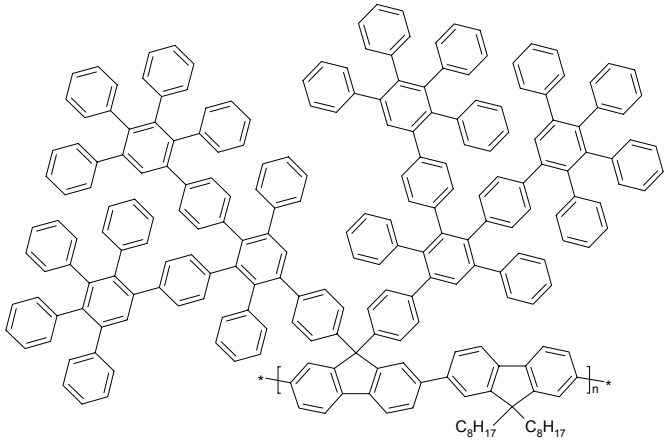

2,7-dibromo-9,9-bis-(4'-(2",5"-diphenyl-3",4"-bis(4'-(2",3",4",5"-tetraphenyl benzene)-phenyl)-benzene)-phenyl)-fluorene (244 mg, 8.8 x 10^{-5} mol) and 2,7-bis-boronic ester 9,9-dioctylfluorene (57 mg, 8.8 x 10^{-5} mol) was dissolved in toluene (2 mL) and 2M K_2CO_3 solution (0.4 mL), and degassed with bubbling argon for 20 minutes. $Pd(PPh_3)_4$ (10 mg, 8.8 x 10^{-6} mol) was added and the solution heated at 80

°C for 12 hours. The reaction mixture was precipitated in a methanol/hydrochloric acid solution (4:1), filtered, subjected to Soxhlet extraction for 2 days in acetone, dissolved in THF, precipitated in methanol then filtered to give the title compound as a yellow solid. 262 mg (90%). ^{1}H NMR (300 MHz): (CD_2Cl_2) δ 7.91-7.35 (m, 28H), 7.14-6.61 (m, 170H), 6.53-6.45 (m, 11H), 2.12-1.99 (m, 4H), 1.20-0.97 (m, 20H), 0.77-0.66 (m, 10H) ppm. M_n = 4.7 x 10^3 g mol^{-1}, M_w = 7.4 x 10^3 g mol^{-1}, and D = 1.6 (against PS standard); M_n = 3.8 x 10^3 g mol^{-1}, M_w = 5.4 x 10^3 g mol^{-1}, and D = 1.4 (against PPP standard). Elemental Analysis: Calculated C 94.06, H 5.94. Found C 90.18, H 5.67.

Dendronised indenofluorene copolymer (29)

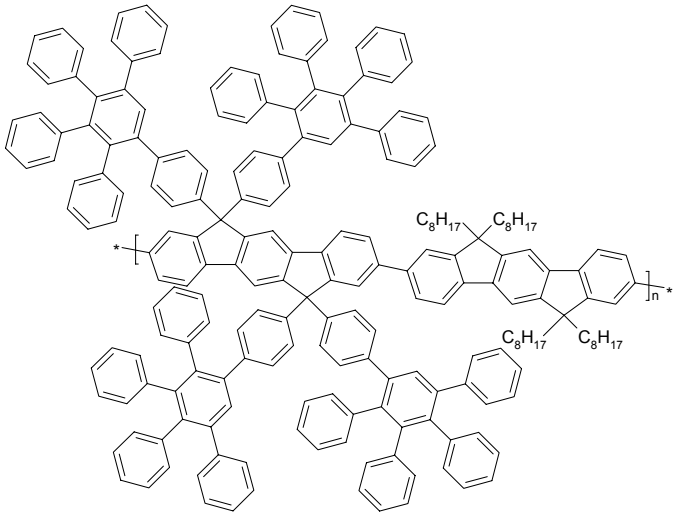

2,8-Dibromo-6,6,12,12-tetra-(4'-(2",3",4",5"-tetraphenyl benzene)-phenyl)-indenofluorene (200 mg, 8.9 x 10^{-5} mol) and 2,7-bis-boronic ester 9,9-dioctylfluorene (85 mg, 8.9 x 10^{-5} mol) was dissolved in toluene (2 mL) and 2M K_2CO_3 solution (1 mL), and degassed with bubbling argon for 20 minutes. $Pd(PPh_3)_4$ (8 mg, 6.9 x 10^{-6} mol) was added and the solution heated at 80 °C for 12 hours. The reaction mixture was precipitated in a methanol/hydrochloric acid solution (4:1), filtered, subjected to Soxhlet extraction for 2 days in acetone, dissolved in THF, precipitated in methanol then filtered to give the title compound as a yellow solid. 239 mg (96%). ^{1}H NMR (300 MHz): (CD_2Cl_2) δ 7.58-7.47 (m, 68H), 7.34 (d, 10H, J=1.5Hz) ppm 7.25 (m, 10H), 7.13-6.79 (m, 882H), 2.16-1.98 (m, 8H), 1.15-1.00 (m, 40H), 0.78-0.65 (m, 20H) ppm. M_n = 1.9 x 10^3 g mol^{-1}, M_w = 3.6 x 10^3 g mol^{-1}, and D = 1.9 (against PS standard); M_n = 1.7 x 10^3 g mol^{-1}, M_w = 2.8 x 10^3 g mol^{-1}, and D = 1.6 (against PPP standard). Elemental Analysis: Calculated C 93.33, H 6.67. Found C 86.72, H 4.90.

1,4-Dibromo-2,5-bis-(2“,3“,4“,5“-tetraphenyl benzene)-benzene (31)

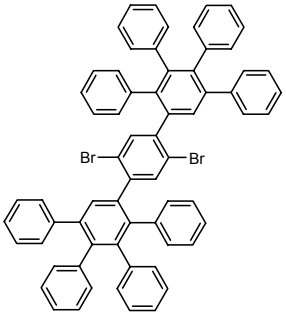

1,4-Dibromo-2,5-diethynyl-benzene (260 mg, 0.9 mmol) and tetra phenyl cyclopentadienone (770 mg, 2 mmol)were mixed in 10 mL o-xylene, and degassed with bubbling argon for 30 min. The solution was heated to 140°C under argon for 14 hours. The reaction mixture was cooled, and the solvents removed *in vacu*. The product was purified by column chromatography eluting with 0-5% ethyl acetate in hexane to give the title compound as a white powder. 684 mg (76%). ^{1}H NMR (300 MHz): (CD_2Cl_2) δ 6.85 (m, 10H), 6.45 (s, broad, 20H), 6.33-6.07 (m, 78H) ppm. ^{13}C NMR: not available due to low solubility. MS (FS, 8kV): m/z (%) = 997.1 (100%, M^+) (calc. for $C_{66}H_{44}Br_2$ = 996.89 g mol^{-1}). Elemental Analysis: Calculated C 79.52, H 4.45. Found C 80.22, H 3.97.

Poly(dendronised phenylene ethynylene) (32)

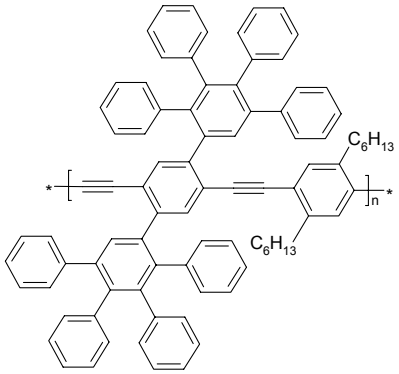

1,4-Dibromo-2,5-bis-(2“,3“,4“,5“-tetraphenyl benzene)-benzene (173 mg, 0.17 mmol), 1,4-Diethynyl-2,5-dihexyl-benzene (51 mg, 0.17 mmol), CuI (3 mg, 1.6 x 10^{-5} mol) and triphenylphosphine (4 mg, 1.6 x 10^{-5} mol) was mixed in 20 mL piperidine and degassed with bubbling argon for 30 minutes. $Pd(PPh_3)_4$ (50 mg, 3 x 10^{-5} mol) was added and the solution stirred at 80 °C for 48 hours. The reaction was quenched with water, the organic products extracted with methylene chloride, washed with 2M HCl solution then water, dried over magnesium sulphate, and the solvents removed *in vacu*. The material was dissolved in chloroform, precipitated in methanol then filtered to give the title compound as a yellow solid. 164 mg (85%). ^{1}H NMR (300 MHz): (CD_2Cl_2) δ 7.27 (s, 2H), 7.18 (m, 4H), 7.08-7.05 (m, 14H), 6.83-6.70 (m, 26H), 2.67 (m, 4H), 1.26-1.17 (m, 12H), 0.80 (m, 10H) ppm M_n = 6.6 x 10^2 g mol^{-1}, M_w = 9.8 x 10^2 g mol^{-1}, and D = 1.5 (against PS standard); M_n = 6.8 x 10^2 g mol^{-1}, M_w = 9.0 x 10^2

g mol^{-1}, and D = 1.3 (against PPP standard). Elemental Analysis: Calculated C 93.58, H 6.42. Found C 77.20, H 4.98.

Bis-{4-[5-(4-tert-butyl-phenyl)-[1,3,4]oxadiazol-2-yl]-phenyl}-(4,4'-dibromo-biphenyl-2-yl)-methanol (33)

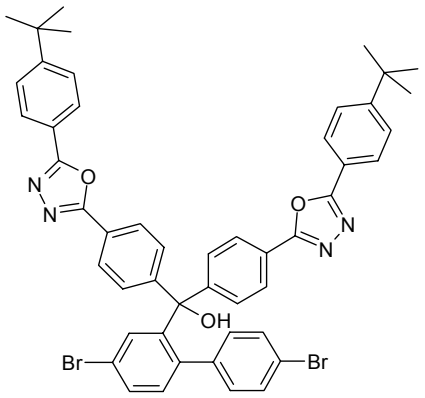

2-(4-Bromo-phenyl)-5-(4-tert-butyl-phenyl)-[1,3,4] oxadiazole (1.45 g, 4.1 mmol) was dissolved in 65 mL THF, and cooled to –78°C. nBuLi (2.3 mL, 3.7 mmol) was added slowly, and reaction mixture left stirring for 30 minutes. 4,4'-Dibromo-biphenyl-2-carboxylic acid methyl ester (0.6g, 1.62 mmol) in 20 mL THF added, and the solution was left to warm to room temperature. Stirred for 3 days. Ammonium chloride solution added and solution stirred for 30 minutes. The product were extracted into methylene chloride, washed with water, the organics were dried over magnesium sulfate, and the solvents were removed *in vacu.* The crude product was purified by column chromatography with 0-50% ethyl acetate in hexane eluent. Recrystallisation from toluene gave the title product. 0.57 g (38%). ^{1}H NMR (300MHz): (CD_2Cl_2) δ 8.14-8.09 (m, 8H), 7.58 (d, 4H, J=8.7Hz), 7.53 (dd, 1H, J=2.1Hz, J=8.1Hz), 7.38 (d, 4H, J=8.7Hz), 7.29 (d, 2H, J=8.5Hz), 7.11 (d, 1H, J=2.0Hz), 7.05 (d, 1H, J=8.1Hz), 6.75 (d, 2H, J=8.5Hz), 3.29 (s, 1H), 1.37 (s, 18H) ppm. ^{13}C NMR (75MHz): (CD2Cl2) δ 165.15, 164.35, 155.91, 149.82, 146.25, 140.06, 139.76, 134.64, 132.86, 131.56, 131.38, 131.14, 128.97, 127.00, 126.52, 123.90, 122.15, 121.73, 121.43, 126.97, 82.94, 35.36, 31.20 ppm. MS (FS, 8kV): m/z (%) = 894.7 (100%, M^+) (calc. for $C_{49}H_{42}Br_2N_4O_3$ = 894.71 g mol^{-1}). Elemental Analysis: Calculated C 65.78, H 4.73, N 6.26. Found C 65.88, H 4.66, N 6.32.

2,7-Dibromo-9,9-bis-(4-(5-(4-tert-butyl-phenyl)-2-oxadiazolyl)phenyl)-fluorene (34)

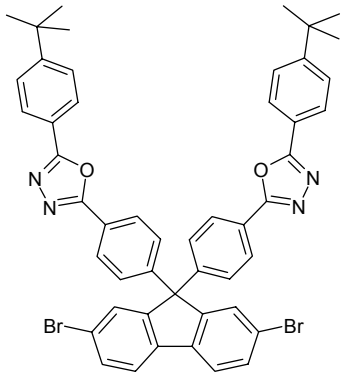

Bis-{4-[5-(4-tert-butyl-phenyl)-[1,3,4]oxadiazol-2-yl]-phenyl}-(4,4'-dibromo-biphenyl-2-yl)-methanol (0.23 g, 0.26 mmol) was dissolved in 4 mL methylene chloride. $BF_3.Oet_2$ (0.4 mL) was added, and the solution goes yellow. The reaction mixture was stirred for 10 hours, then 50 mL methanol added. The product was filtered and washed with methanol to give the title compound. 0.2 g (88%). ^{1}H NMR (300MHz): (CD_2Cl_2) δ 8.08-8.03 (m, 8H), 7.72 (d, 2H, J = 7.7 Hz), 7.61-7.56 (m, 8H), 7.37 (d, 4H, J = 8.7 Hz) 1.36 (s, 18H) ppm. ^{13}C NMR (75MHz): (CD2Cl2) δ 165.12, 164.27, 155.87, 151.96, 147.91, 138.67, 132.00, 129.58, 129.02, 127.59, 126.97, 126.50, 123.75, 122.52, 122.50, 121.45, 66.00, 35.35, 31.19 ppm. MS (FS, 8kV): m/z (%) = 877.8 (100%, M^+) (calc. For $C_{49}H_{40}Br_2N_4O_2$ = 876.70 g mol^{-1}). Elemental Analysis: Calculated C 67.13, H 4.60, N 6.39. Found C 65.32, H 4.13, N 6.21.

Poly(9,9-bis-(4-(5-(4-tert-butyl-phenyl)-2-oxadiazolyl)phenyl)-fluorene) (35)

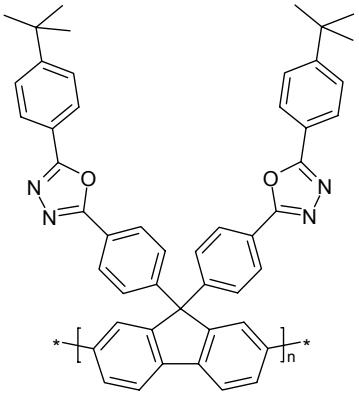

$Ni(COD)_2$ (113 mg, 0.4 mmol), 2,2'-bipyridyl (64 mg, 0.4 mmol) and COD (0.05 mL, 0.4 mmol) was mixed with 2 mL dry DMF and 0.5 mL dry toluene in a glove box. The purple solution was heated to 80 °C for 30 minutes. 2,7-Dibromo-9,9-bis-(4-(5-(4-*t*-butyl-phenyl)-2-oxadiazolyl)phenyl)-fluorene (150 mg, 1.7 x 10^{-4} mol) in 8 mL of dry toluene was added, and the solution stirred under argon, in absence of light, for 2 days. The reaction mixture was precipitated in a methanol/ammonia solution (1:1), filtered, subjected to Soxhlet extraction for 2 days in acetone, dissolved in hot toluene,

precipitated in methanol then filtered to give the title compound as a yellow solid. 67 mg (55%). ^{1}H-NMR (250MHz): ($C_2D_2Cl_4$) δ 7.98-7.31 (m, 24H), 1.26 (s, 18H) ppm. GPC analysis M_n = 6.5 x 10^3 g mol^{-1}, M_w = 1.8 x 10^4 g mol^{-1}, and D = 2.8 (against PS standard); M_n = 5.1 x 10^3 g mol^{-1}, M_w = 1.2 x 10^4 g mol^{-1}, and D = 2.3 (against PPP standard). Elemental Analysis: Calculated C 82.10, H 5.62, N 7.82. Found C 73.59, H 5.41, N 8.09.

2,7-Dibromo-9,9-bis(4-cyanophenyl)-fluorene (36)

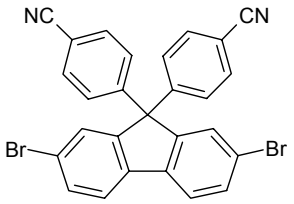

2,7-Dibromofluorene (5 g, 15.4 mmol), 4-fluorobenzonitrile (4.1 g, 34 mmol), 18-crown-ether-6 (2.1 g, 8 mmol) and K_2CO_3 (5.1 g, 37 mmol) was mixed in 13 mL DMF and 5 mL benzene under an argon atmosphere. The solution was heated to 160°C for 4 hours. Water formed during the reaction was removed by azeotropic distillation and collected in a Dean-Stark trap. After this period, the remaining benzene was removed by distillation. The reaction mixture was cooled to room temperature, and water was added. The precipitate was filtered, washed with water, and dried *in vacu*. The product was purified by recrystallisation from hexane, and washed with methylene chloride to give the title compound as a white solid. 1.05 g (13%). ^{1}H NMR (300MHz): (THF-d_8) δ 7.83 (d, 2H, J=8.1Hz), 7.66-7.60 (m, 8H) 7.36 (d, 4H, J=8.5Hz) ppm. ^{13}C NMR (75MHz): (THF-d_8) δ 152.01, 149.86, 139.37, 133.42, 132.79, 130.13, 129.71, 123.37, 123.09, 118.68, 112.80 ppm. MS (FS, 8kV): m/z (%) = 526.5 (100%, M^+) (calc. for $C_{27}H_{14}Br_2N_2$ = 526.23 g mol^{-1}). Elemental Analysis: Calculated C 61.63, H 2.68. Found C 61.51, H 2.93.

2,7-Dibromo-9,9-bis(4-tetraazolylephenyl)-fluorene (37)

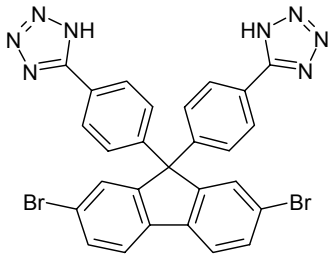

2,7-Dibromo-9,9-bis(4-cyanophenyl)-fluorene (0.8 g, 1.5 mmol), NaN_3 (0.3 g, 4.6 mmol) and NH_4Cl (0.26 g, 4.8 mmol) was dissolved in 3 mL DMF and stirred under argon for 20 minutes. The solution was heated at 150°C for 4 hours, then cooled to room temperature and poured into water. The water was acidified with 2M HCl, and the product filtered, washed with water and dried to give the title compound as a white solid. 0.87 g (95%). ^{1}H NMR (300MHz): (THF-d_8) δ 8.03 (d, 4H, J=8.5Hz), 7.85 (d, 2H, J=8.2Hz), 7.70 (d, 2H, J=1.6Hz), 7.60 (dd, 2H, J=1.8Hz, J=8.2Hz), 7.41 (d, 4H, J=8.5Hz) ppm. ^{13}C NMR (75MHz): (THF-d_8) δ 153.14,

147.84, 139.36, 132.37, 130.18, 129.58, 128.11, 125.97, 123.21, 122.86 ppm. MS (FS, 8kV): m/z (%) = 613.3 (100%, M^+) (calc. for $C_{27}H_{16}Br_2N_8$ = 612.29 g mol^{-1}). Elemental Analysis: Calculated C 52.97, H 2.63, N 18.30. Found C 51.57, H 2.78, N 17.57.

2,7-Dibromo-9,9-bis-(4-(5-(4-decyl-phenyl)-2-oxadiazolyl)phenyl)-fluorene (38)

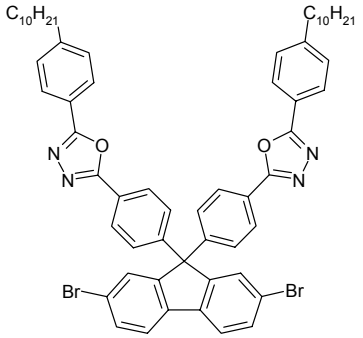

2,7-Dibromo-9,9-bis(4-tetraazolylephenyl)-fluorene (0.7 g, 1.14 mmol) was mixed in 5 mL pyridine. 4-Decyl-benzoyl chloride (0.96 g, 3.43 mmol) was added dropwise. The solution was heated to 125°C for 3 hours. The reaction mixture was poured into a 3:1 methanol/ water solution, and the crude product filtered. The product was purified by recrystallisation from methylene chloride to give the title compound as a white solid. 0.99 g (83%). ^{1}H NMR (300MHz): (THF-d_8) δ 7.98 (d, 4H, J = 8.5 Hz), 7.93 (d, 4H, J = 8.1 Hz), 7.69 (d, 2H, J = 7.9 Hz), 7.56 (s, 2H), 7.5 (d, 2H, J = 8.1 Hz), 7.31 (d, 4H, J = 8.1 Hz), 7.27 (d, 4H, J = 8.1 Hz), 2.6 (t, 4H, J = 7.4 Hz), 1.25-1.18 (m, 32H), 0.78 (t, 6H, J = 6.4 Hz) ppm. ^{13}C NMR (75MHz): (Toluene-d_8) δ 164.81, 163.95, 152.46, 147.42, 147.00, 138.52, 137.05, 131.87, 129.60, 127.20, 124.05, 122.68, 122.45, 122.21, 66.02, 36.29, 32.43, 31.57, 30.19, 30.03, 29.91, 29.77, 23.20, 14.38 ppm. MS (FS, 8kV): m/z (%) = 526.5 (100%, M^+) (calc. for $C_{27}H_{14}Br_2N_2$ = 526.23 g mol^{-1}). Elemental Analysis: Calculated C 70.11, H 6.17, N 5.36. Found C 68.76, H 5.75, N 5.23.

Poly(9,9-bis-(4-(5-(4-decyl-phenyl)-2-oxadiazolyl)phenyl)-fluorene) (39)

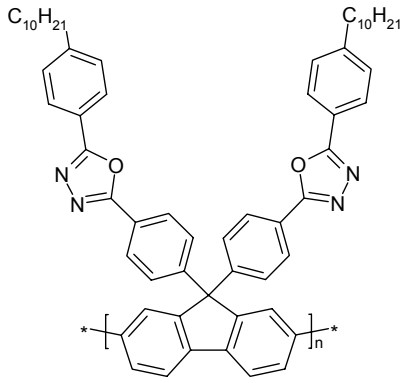

$Ni(COD)_2$ (303 mg, 1.1 mmol), 2,2'-bipyridyl (172 mg, 1.1 mmol) and COD (0.14 mL, 1.1 mmol) was mixed with 4 mL dry DMF and 2 mL dry toluene in a glove

box. The purple solution was heated to 80 °C for 30 minutes. 2,7-Dibromo-9,9-bis-(4-(5-(4-decyl-phenyl)-2-oxadiazolyl)phenyl)-fluorene (500 mg, 4.8 x 10^{-4} mol) in 10 mL of dry toluene was added, and the solution stirred under argon, in absence of light, for 2 days. The reaction mixture was precipitated in a methanol/ammonia solution (1:1), filtered, subjected to Soxhlet extraction for 2 days in acetone, dissolved in hot toluene, precipitated in methanol then filtered to give the title compound as a off white solid. 142 mg (33%). ^{1}H-NMR (700MHz): ($C_2D_2Cl_4$) δ 7.98-7.24 (m, broad, 16H), 6.59-6.28 (m, broad, 6H), 2.09 (s, broad, 4H), 1.09-0.61 (m, 36H), 0.36-0.31 (m, 10H) ppm. GPC analysis M_n = 1.6 x 10^4 g mol^{-1}, M_w = 3.9 x 10^4 g mol^{-1}, and D = 2.4 (against PS standard); M_n = 1.2 x 10^4 g mol^{-1}, M_w = 2.3 x 10^4 g mol^{-1}, and D = 2.0 (against PPP standard). Elemental Analysis: Calculated C 84.36, H 7.18, N 5.39. Found C 77.45, H 7.03, N 5.79.

2,7-Dibromo-4-amino-fluorene (41)

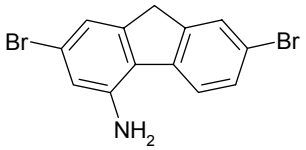

2,7-Dibromo-4-nitro-fluorene (6.3 g, 17.1 mmol) was mixed with 30 mL concentrated aqueous HCl and 80 mL ethanol. Tin powder (8.1 g, 68.3 mmol) was added slowly, and the mixture was heated to reflux for 30 minutes. The reaction was poured into ice, extracted with ethyl acetate, washed with sodium carbonate, dried over magnesium sulfate, and the solvents removed *in vacu* to yield the title compound as a white powder. 5.0 g (87 %). ^{1}H NMR (250MHz): (THF-d_8) δ 7.74 (d, 1H, J=8.3Hz), 7.64 (s, 1H), 7.47 (d, 1H, J=8.3Hz), 6.97 (s, 1H), 6.83 (s, 1H), 5.16 (s, 2H), 3.84 (s, 2H) ppm. ^{13}C NMR (75MHz): (CD_2Cl_2) δ 146.84, 145.28, 143.86, 140.03, 130.11, 128.38, 125.67, 122.72, 121.69, 119.68, 118.92, 117.92, 37.28 ppm. MS (FS, 8kV): m/z (%) = 337.4 (100%, M^+) (calc. for $C_{13}H_{10}Br_2N$ = 340.04 g mol^{-1}). Elemental Analysis: Calculated C 46.06, H 2.68, N 4.12. Found C 46.03, H 3.03, N 4.05.

2,7-Dibromo-4-iodo-fluorene (42)

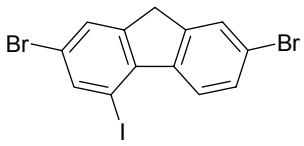

2,7-Dibromo-4-amino-fluorene (5.0 g, 14.7 mmol) was dissolved in a mixture of 75 mL water and 75 mL sulphuric acid and cooled to 0 °C. Afterwards a solution of soldium nitrite (1.06 g, 16 mmol) in 10 mL water was added slowly, while the temperature was kept below 5 °C. The mixture was stirred for additional 30 minutes, before potassium iodide (5.4 g, 33 mmol) dissolved in 10 mL water was added. The cloudy solution was brought to reflux and cooled down again. The precipitate was collected by filtration and purified by washing with 2M sodium hydroxide solution and water to afford the title product as an off-white crystalline material. 4.6 g (70 %). ^{1}H NMR (300MHz): (THF-d_8) δ 8.67 (d, 1H, J = 8.49), 8.05 (s, 1H), 7.74 (s, 2H), 7.60 (d, 1H, J = 8.49 Hz), 3.94 (s, 2H). ppm. ^{13}C NMR (75MHz): (CD_2Cl_2) δ 147.55,

146.30, 140.90, 140.48, 139.83, 128.84, 128.04, 127.88, 123.32, 121.64, 120.43, 87.51, 36.27 ppm. MS (FS, 8kV): m/z (%) = 450.4 (100%, M^+) (calc. for $C_{13}H_7Br_2I$ = 449.91 g mol^{-1}). Elemental Analysis: Calculated C 34.71, H 1.57. Found C 34.66, H 1.52.

2,7-Dibromo-4-iodo-9-fluorenone (43)

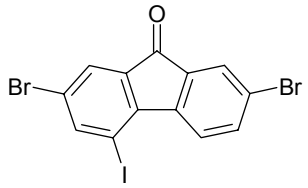

2,7-Dibromo-4-iodo-fluorene (4.2 g, 9.3 mmol) was dissolved in 100 mL pyridine. 10 mL of a 1M *tert*-Butyl ammonium hydroxide solution in methanol was added, and the solution stirred with bubbling air for 3 days. 1M HCl was added until an approximately neutral solution was achieved, and the mixture was poured into water and filtered. The product was purified by column chromatography eluting with 20% ethyl acetate in hexane to give the title compound as a yellow powder. 5.0 g (87 %). ^{1}H NMR (300MHz): (CD_2Cl_2) δ 8.49 (d, 1H, J = 8.23 Hz), 8.11 (d, 1H, J = 1.80 Hz), 7.80 (d, 1H, J = 1.98 Hz), 7.76 (d, 1H, J = 1.75 Hz), 7.74 (dd, 1H, J = 1.98 Hz, J = 8.24 Hz) ppm. ^{13}C NMR (75MHz): (CD_2Cl_2) δ 189.72, 148.05, 144.38, 142.98, 137.30, 135.80, 127.96, 127.58, 124.32, 123.58, 123.40, 88.86 ppm. MS (FS, 8kV): m/z (%) = 464.3 (100%, M^+) (calc. for $C_{13}H_5Br_2IO$ = 463.90 g mol^{-1}). Elemental Analysis: Calculated C 33.66, H 1.09. Found C 33.64, H 1.16.

2,7-Dibromo-4-trimethylsilylethynyl-9-fluorenone (44)

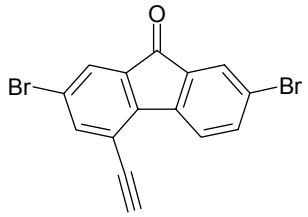

2,7-Dibromo-4-iodo-9-fluorenone (950 mg, 2.05 mmol), trimethylsilylacetylene (1.01 g, 10.3 mmol), triphenylphosphine (11 mg, 41 μmol), and copper (I) iodide (7.8 mg, 41 μmol) were dissolved in a mixture of 50 mL triethylamine and 10 mL THF and degassed. Bis(triphenylphosphin)palladium(II)chloride (29 mg, 41 μmol) was added and the reaction was stirred at room temperature for 12 hours. The solvent was removed *in vacuo* and the residue was purified by using preparative column chromatography with a hexane:ethyl acetate (4:1) eluent to yield a yellow crystalline material. This was dissolved in 10 mL THF and 1 mL water, and potassium carbonate (1.5 g) was added. The resulting green solution was stirred for 2 hours, neutralized with 2M HCl, and extracted with dichloromethane. The organics were washed with aqueous sodium carbonate solution, dried over magnesium sulfate, and the solvents removed *in vacu* to yield the title compound as a yellow powder. 0.28 g (84 %). ^{1}H NMR (300MHz): (CD_2Cl_2) δ 8.17 (d, 1H, J = 8.09 Hz), 7.79 (d, 1H, J = 1.94 Hz), 7.75 (d, 1H, J = 1.82 Hz), 7.74 (d, 1H, J = 1.85 Hz), 7.69 (dd, 1H, J = 1.92 Hz, J =

8.09 Hz), 3.65 (s, 1H) ppm. ^{13}C NMR (75MHz): (CD_2Cl_2) δ 190.18, 142.20, 141.48, 137.98, 135.77, 135.63, 132.24, 128.21, 127.81, 124.83, 124.18, 122.76, 84.94, 79.77 ppm. MS (FS, 8kV): m/z (%) = 362.4 (100%, M^+) (calc. for $C_{15}H_6Br_2O$ = 362.02 g mol^{-1}). Elemental Analysis: Calculated C 49.77, H 1.67. Found C 49.73, H 1.78.

2,7-Dibromo-4-(2,5-diphenyl-3,4-di(4-(2-decyl-tetradecyl)phenyl)phenyl)-9-fluorenone (45)

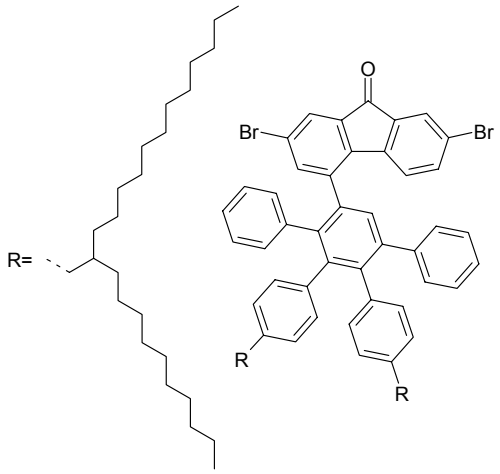

2,7-Dibromo-4-ethynyl-9-fluorenone (200 mg, 550 µmol) and 2,5-diphenyl-3,4-bis-(4-(2-decyl-tetradecyl)-phenyl)-cyclopenta-2,4-dienone (580 mg,550 µmol) were dissolved 1 mL *o*-xylene. The reaction mixture was heated to 160 °C in a closed tube for 12 hours. After the reaction, the solvent was removed *in vacuo* and the residue was purified by preparative column chromatography with a petroleum ether: methylene chloride eluent (7:3) to afford the title compound as a yellow oil. 520 mg (68%). ^{1}H NMR (300MHz): (CD_2Cl_2) δ 7.71 (d, 1H, J = 1.83 Hz), 7.58 (d, 1H, J = 1.86 Hz), 7.52 (dd, 1H, J = 1.94 Hz, J = 8.05 Hz), 7.50 (s. 1H), 7.41 (d, 1H, J = 1.85 Hz), 7.2-6.6 (m, 19H), 2.38 (d, 2H, J = 7.07 Hz), 2.32 (d, 2H, J = 7.04 Hz), 1.5-1.0 (m, 82H), 0.90 (dt, 12H, J = 1.75 Hz, J = 5.88 Hz) ppm. ^{13}C NMR (75MHz): (CD_2Cl_2) δ 211.48, 163.69, 162.23, 162.039, 162.01, 161.01, 160.73, 160.66, 160.31, 160.23, 160.02, 159.98, 159.84, 157.86, 157.82, 157.77, 157.74, 157.70, 157.66, 156.80, 156.53, 156.00, 152.51, 152.27, 151.58, 151.44, 151.09, 150.24, 148.85, 148.81, 148.52, 148.20, 147.98, 147.66, 147.33, 147.16, 147.13, 145.70, 144.76, 143.67, 142.84, 156.81, 60.71, 53.71, 53.62, 52.79, 51.59, 51.24, 50.90, 50.57, 50.23, 49.87, 47.23, 44.22, 43.53, 35.12, 34.33, 47.91, 54.25, 53.54, 52.99, 52.11, 52.05, 49.53, 46.57, 42.84 ppm. MS (FS, 8kV): m/z (%) = 1393.6 (100%, M^+) (calc. for $C_{91}H_{122}Br_2O$ = 1391.79 g mol^{-1}).

Poly-(4-(2,5-diphenyl-3,4-di(4-(2-decyl-tetradecyl)phenyl)phenyl)-9-fluorenone) (46)

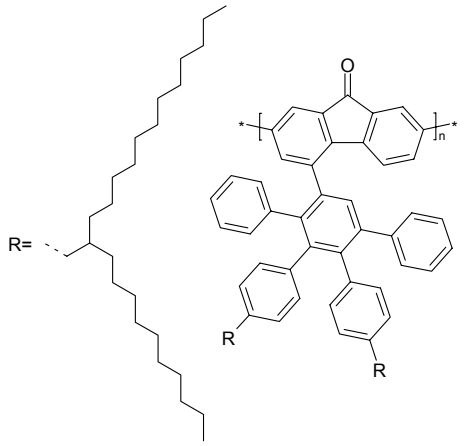

$Ni(COD)_2$ (112 mg, 0.4 mmol), 2,2'-bipyridyl (64 mg, 0.4 mmol) and COD (0.05 mL, 0.4 mmol) was mixed with 2 mL dry DMF and 0.5 mL dry toluene in a glove box. The purple solution was heated to 80 °C for 30 minutes. 2,7-Dibromo-4-(2,5-diphenyl-3,4-di(4-(2-decyl-tetradecyl)phenyl)phenyl)-9-fluorenone (240 mg, 0.17 mmol) in 3 mL of dry toluene was added, and the solution stirred under argon in absence of light for 2 days, before 0.5 mL of bromobenzene was added. The reaction mixture was precipitated in a methanol/HCl solution (4:1), filtered, subjected to Soxhlet extraction for 2 days in acetone, dissolved in THF, precipitated in methanol then filtered to give the title compound as a yellow solid. 170 mg (85%). ^{1}H-NMR (700MHz): ($C_2D_2Cl_4$) δ 7.87-7.32 (m, 6H), 7.16-6.61 (m, 17H), 2.32-2.25 (m, 4H), 1.42-0.83 (m, 106H) ppm. GPC analysis M_n = 4.1 x 10^4 g mol^{-1}, M_w = 1.5 x 10^5 g mol^{-1}, and D = 3.5 (against PS standard); M_n = 2.7 x 10^4 g mol^{-1}, M_w = 7.0 x 10^4 g mol^{-1}, and D = 2.6 (against PPP standard). Elemental Analysis: Calculated C 88.72, H 9.98. Found C 87.74, H 9.23.

[7-(2-Bromo-phenyl)-9,9-dioctyl-fluorene]-trimethyl-silane (48)

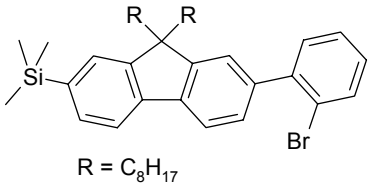

(7-Bromo-9,9-dioctyl-fluoren-2-yl)-trimethyl-silane (4.31 g, 7.96 mmol) and 2-Bromo-benzoboronic acid was dissolved in toluene (50 mL) and 2M K_2CO_3 solution (25 mL), and degassed with bubbling argon for 20 minutes. $Pd(PPh_3)_4$ (185 mg, 0.16 mmol) was added and the solution heated at 80 °C for 12 hours. The organic product was extracted with methylene chloride, washed with water, dried over magnesium sulphate, and the solvents removed *in vacu*. The product was purified by column chromatography using hexane as eluent to give the title compound as a colourless oil. 2.39 g (48%) ^{1}H NMR (250MHz): (CD_2Cl_2) δ 7.79 (d, 1 H, J = 9.2 Hz), 7.76 (d, 1 H, J = 9.5 Hz), 7.72 (d, 1 H, J = 8.9 Hz), 7.57 - 7.55 (m, 2 H,), 7.49 - 7.35 (m, 4 H), 7.24 (m, 1 H,), 2.04 (t, 4 H, J = 8.2 Hz), 1.25 - 1.10 (m, 20 H), 0.85 (t, 6 H, J = 6.8 Hz),

0.73 (m, 4 H), 0.36 (s, 9 H) ppm. ^{13}C NMR (63MHz): (CD_2Cl_2) δ 151.02, 150.72, 143.55, 141.78, 141.01, 140.37, 139.79, 133.60, 132.37, 131.81, 129.09, 128.32, 128.13, 127.89, 124.98, 123.21, 119.78, 119.53, 55.58, 40.58, 32.26, 30.41, 29.65, 29.64, 24.28, 23.09, 14.34, -0.70 ppm. MS (FS, 8kV): m/z (%) = 617.4 (100%, M^+) (calc. for $C_{38}H_{53}BrSi$ = 617.84 g mol^{-1})

9-[2-(9,9-Dioctyl-7-trimethylsilanyl-fluorene)-phenyl]-heptadecan-9-ol (49)

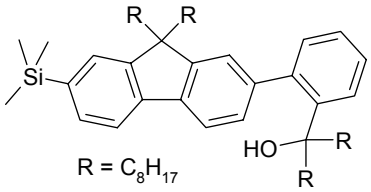

[7-(2-Bromo-phenyl)-9,9-dioctyl-fluoren-2-yl]-trimethyl-silane (2.39 g, 3.86 mmol) was dissolved in 50 mL of dry THF under an argon atmosphere, and cooled to –78 °C in a dry ice/acetone bath. n-BuLi (2.6 mL, 4 mmol) was added and the reaction mixture stirred for 30 minutes. Heptadecan-9-one (1.07 g, 4.2 mmol) dissolved in 25 mL dry THF was added, and the reaction mixture left to warm to room temperature, and stirred for 12 hours. The reaction was quenched with water, the organic products extracted with methylene chloride, washed with water, dried over magnesium sulphate, and the solvents removed *in vacu*. The product was purified by column chromatography eluting with 0-2% ethyl acetate in hexane to give the title compound as a colourless semi-solid. 1.6 g (75%). ^{1}H NMR (300MHz): (CD_2Cl_2) δ 7.72 (d, 1 H, J = 7.71 Hz), 7.69 (d, 1 H, J = 8.28 Hz), 7.62 (dd, 1 H, J = 1.1 Hz, 7.9 Hz), 7.53 - 7.50 (m, 2 H), 7.34 (dt, 1 H, J = 1.5 Hz, 7.6 Hz), 7.25-7.16 (m, 3 H), 7.07 (dd, 1 H, J = 1.5 Hz, 7.4 Hz), 2.36 (t, 4 H, J = 7.4 Hz), 1.96 (m, 4 H), 1.63 (s, 1 H), 1.52 (m, 8 H), 1.27-0.64 (m, 52 H), 0.32 (s, 9 H) ppm. ^{13}C NMR (75MHz): (CD_2Cl_2) δ 150.47, 150.23, 143.77, 143.35, 141.90, 140.87, 140.36, 139.55, 132.41, 132.27, 128.10, 128.01, 127.74, 127.33, 125.90, 124.01, 119.24, 119.23, 78.90, 55.49, 43.06, 32.32, 32.25, 29.81, 29.76, 29.57, 24.27, 24.21, 23.07, 14.29, 14.23, -0.82 ppm. MS (FS, 8kV): m/z (%) = 792.9 (100%, M^+) (calc. for $C_{55}H_{88}OSi$ = 793.40 g mol^{-1}). Elemental Analysis: Calculated C 83.26, H 11.18. Found C 83.28, H 11.03.

9-[2-(7-Bromo-9,9-dioctyl-fluorene)-phenyl]-heptadecan-9-ol (50)

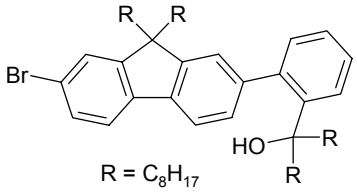

9-[2-(9,9-Dioctyl-7-trimethylsilanyl-fluoren-2-yl)-phenyl]-heptadecan-9-ol (3.9 g, 4.9 mmol) and sodium acetate (0.4 g, 4.9 mmol) was mixed in dry THF (90 mL) under an argon atmosphere, and cooled to 0 °C. Bromine liquid (0.5 mL, 9.8 mmol) was added dropwise, and the solution stirred for 35 minutes. Triethyl amine (1.5 mL) was added, and the reaction quenched with a sodium bisulphite solution. The organic products extracted with methylene chloride, washed with water, dried over magnesium sulphate, and the solvents removed *in vacu*. The product was purified by

column chromatography eluting hexane to give the title compound as a white powder. 2.04 g (52%). ^{1}H NMR (300MHz): (CD_2Cl_2) δ 7.67 (d, 1 H, J = 7.5 Hz), 7.62 (dd, 1 H, J = 1.1 Hz, 8.1 Hz), 7.61 (d, 1 H, J = 8.1 Hz), 7.51 - 7.46 (m, 2 H), 7.35 (dt, 1 H, J = 1.5 Hz, 7.6 Hz), 7.25 - 7.17 (m, 3 H), 7.05 (dd, 1 H, J = 1.5, 7.4 Hz), 1.96 (m, 8 H), 1.58 (s, 1 H), 1.28 - 0.62 (m, 56 H) ppm. ^{13}C NMR (75MHz): (CD_2Cl_2) δ 153.47, 149.89, 143.82, 143.72, 140.63, 140.46, 139.27, 132.31, 130.31, 128.35, 127.77, 127.43, 126.57, 125.92, 123.97, 121.39, 121.32, 119.27, 78.86, 55.92, 32.30, 32.23, 29.74, 29.54, 24.30, 24.17, 23.06, 23.02, 14.28, 14.23 ppm. MS (FS, 8kV): m/z (%) = 799.8 (100%, M^+) (calc. for $C_{52}H_{79}BrO$ = 800.11 g mol^{-1}).

2-Bromo-6,6,12,12-tetraoctyl-indenofluorene (51)

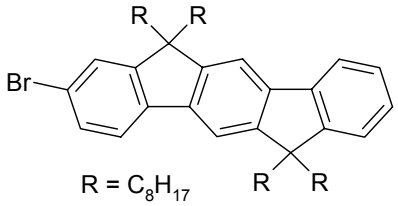

9-[2-(7-Bromo-9,9-dioctyl-fluoren-2-yl)-phenyl]-heptadecan-9-ol (2.04 g, 2.5 mmol) was dissolved in methylene chloride (10 mL). $BF_3.OEt_2$ (0.3 mL) was added dropwise, and the resulting dark blue solution was stirred at room temperature for 12 hours. Following the addition of methanol, a white solid was filtered and recrystalised from ethanol to yield the title compound as white crystals. 1.59 g (81%). ^{1}H NMR (300MHz): (CD_2Cl_2) δ 7.74 (dd, 1 H, J = 1.1 Hz, 6.4 Hz), 7.64 - 7.60 (m, 3 H), 7.49 - 7.45 (m, 2 H), 7.37 - 7.26 (m, 3 H), 2.00 (m, 8 H), 1.17 - 1.03 (m, 36 H), 0.78 (t, 12 H, J = 6.8 Hz), 0.61 (m, 8 H) ppm. ^{13}C NMR (75MHz): (CD_2Cl_2) δ 153.88, 151.54, 150.65, 150.09, 141.70, 141.52, 141.09, 139.83, 130.09, 127.22, 127.05, 126.54, 123.30, 121.07, 120.79, 119.77, 114.46, 114.33, 55.52, 55.16, 40.90, 40.85, 32.16, 30.33, 30.29, 29.62, 29.53, 24.15, 24.12, 22.96, 14.18 ppm. MS (FS, 8kV): m/z (%) = 783.9 (100%, M^+) (calc. for $C_{52}H_{77}Br$ = 782.10 g mol^{-1}) Elemental Analysis: Calculated C 79.86, H 9.92. Found C 80.08, H 9.98.

4,4,5,5-Tetramethyl-2-(6,6,12,12-tetraoctyl-indenofluorene)-[1,3,2]dioxaborolane (52)

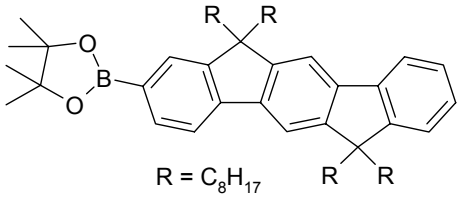

2-Bromo-6,6,12,12-tetraoctyl-indenofluorene (0.4 g, 0.51 mmol), Bis(pinacolato)diboron (0.143 g, 0.56 mmol), potassium acetate (0.15 g, 1.5 mmol) and $PdCl_2$(dppf) (11.5 mg, 1.53 x 10^{-5} mol) was mixed in dry dioxane (2 mL) under an argon atmosphere, and heated at 90 °C for 12 hours. The crude reaction mixture was filtered through silica to give the title compound as a white solid. 0.4 g (95%). ^{1}H NMR (250MHz): (CD_2Cl_2) δ 7.76 - 7.7.68 (m, 6 H), 7.37 - 7.29 (m, 3 H), 2.05 (m, 8 H), 1.38 (s, 12 H), 1.23 - 1.05 (m, 36 H), 0.78 (t, 12 H, J = 6 Hz), 0.62 (m, 8 H) ppm. ^{13}C NMR (63MHz): (CD_2Cl_2) δ 151.61, 151.05, 150.68, 150.43, 144.94, 141.84,

141.61, 140.78, 133.90, 129.09, 127.19, 127.05, 127.04, 123.29, 119.79, 119.01, 114.76, 114.37, 84.06, 55.16, 55.14, 41.00, 40.95, 32.21, 30.41, 30.38, 29.68, 29.59, 25.27, 25.19, 24.22, 24.17, 22.99, 14.25 ppm. MS (FS, 8kV): m/z (%) = 1817.0 (100%, M^+) (calc. for $C_{133}H_{92}Cl_2N_4$ = 1817.15 g mol^{-1}).

6,6,12,12-tetraoctyl-indenofluorene dimer (53)

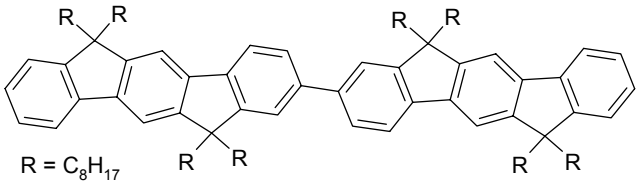

2-Bromo-6,6,12,12-tetraoctyl-indenofluorene (0.196 g, 0.25 mmol) and 4,4,5,5-Tetramethyl-2-(6,6,12,12-tetraoctyl-indenofluorene)-[1,3,2]dioxaborolane (0.25 g, 0.30 mmol) was mixed in toluene (6 mL) and 2M K_2CO_3 solution (3 mL), and degassed with bubbling argon for 20 minutes. $Pd(PPh_3)_4$ (15 mg, 1.26 x 10^{-5} mol) was added and the solution heated at 80 °C for 12 hours. The organic product was extracted with methylene chloride, washed with water, dried over magnesium sulphate, and the solvents removed *in vacu*. The product was purified by column chromatography using hexane as eluent to give the title compound as a yellow powder. 0.18 g (51%). ^{1}H NMR (300MHz): (CD_2Cl_2) δ 7.84 (d, 2H, J=7.8Hz), 7.77 (d, 2H, J=7.5Hz), 7.72-7.67 (m, 8H), 7.40-7.30 (m, 6H), 2.17-2.04 (m, 18H), 1.12-1.09 (m, 78H), 0-82-0.65 (m, 40H) ppm. ^{13}C NMR (75MHz): (CD_2Cl_2) δ 152.32, 151.56, 150.77, 150.54, 141.95, 141.16, 141.05, 140.72, 140.49, 127.04, 126.23, 123.29, 121.68, 119.95, 119.68, 114.39, 55.32, 55.16, 41.01, 32.19, 30.40, 29.68, 29.58, 24.28, 24.23, 22.97, 14.21 ppm. MS (FS, 8kV): m/z (%) = 1404.53 (100%, M^+) (calc. for $C_{104}H_{154}$ = 1404.39 g mol^{-1}). Elemental Analysis: Calculated C 88.95, H 11.05. Found C 88.86, H 11.07.

6,6,12,12-tetraoctyl-indenofluorene trimer (54)

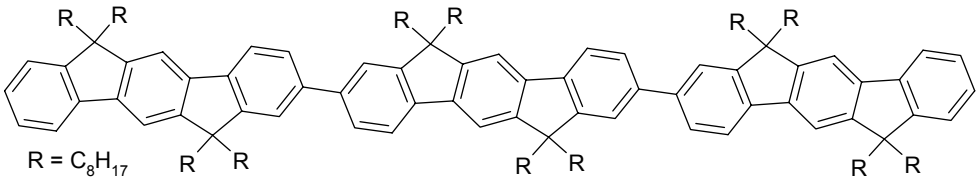

2,7-Dibromo-6,6,12,12-tetraoctyl-indenofluorene (0.189 g, 0.22 mmol) and 4,4,5,5-Tetramethyl-2-(6,6,12,12-tetraoctyl-indenofluorene)-[1,3,2]dioxaborolane (0.4 g, 0.48 mmol) was mixed in toluene (10 mL) and 2M K_2CO_3 solution (5 mL), and degassed with bubbling argon for 20 minutes. $Pd(PPh_3)_4$ (16.7 mg, 1.44 x 10^{-5} mol) was added and the solution heated at 80 °C for 12 hours. The organic product was extracted with methylene chloride, washed with water, dried over magnesium sulphate, and the solvents removed *in vacu*. The product was purified by column chromatography using hexane as eluent to give the title compound as a yellow powder. 0.192 g (41%) ^{1}H NMR (250MHz): (CD_2Cl_2) δ 7.89-7.62 (m, 18H), 7.51-7.28 (m, 8H), 2.16-2.07 (m, 24H), 1.28-1.11 (m, 120H), 0.81-0.69 (m, 60H) ppm. ^{13}C NMR (63MHz): (CD_2Cl_2) δ 152.35, 152.27, 151.57, 150.93, 150.78, 150.56, 141.96,

141.19, 141.08, 140.78, 140.74, 140.53, 140.50, 129.14, 127.43, 127.34, 127.06, 126.27, 126.16, 123.30, 121.87, 121.70, 119.98, 119.70, 114.49, 114.41, 114.38, 55.38, 55.35, 55.17, 41.03, 32.22, 30.43, 29.70, 29.60, 24.31, 24.24, 22.99, 14.23, ppm. MS (FS, 8kV): m/z (%) = 2104.3 (100%, M^+) (calc. for $C_{156}H_{230}$ = 2105.57 g mol^{-1}). Elemental Analysis: Calculated C 88.99, H 11.01. Found C 89.13, H 10.97.

Dibromo-(6,6,12,12-tetraoctyl-indenofluorene) dimer (55)

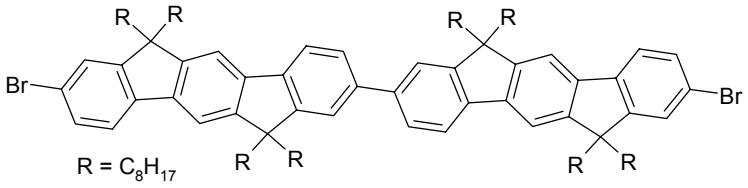

6,6,12,12-tetraoctyl-indenofluorene dimer (70 mg, 5 x 10^{-5} mol) and $CuBr_2$ on Alumina (250 mg) was mixed in 10 mL carbon tetrachloride and heated to reflux for 24 hours. The reaction mixture was cooled to room temperature, filtered through a wad of silica and washed with methylene chloride to give the title compound as a yellow powder. 73 mg (94%). ^{1}H NMR (300MHz): (CD_2Cl_2) δ 7.85 (d, 2H, J=7.8Hz), 7.73-7.69 (m, 8H), 7.65 (d, 2H, J=8.0Hz), 7.53-7.48 (m, 4H), 2.15-2.05 (m, 16H), 1.18-1.08 (m, 80H), 0.83-0.67 (m, 40H) ppm. ^{13}C NMR (75MHz): (CD_2Cl_2) δ 153.92, 152.37, 151.04, 150.27, 141.24, 141.11, 141.00, 140.67, 139.93, 130.16, 126.59, 126.32, 121.73, 121.13, 120.88, 120.10, 114.56, 114.45, 55.58, 55.39, 40.98, 40.91, 32.20, 30.35, 30.28, 29.65, 29.57, 24.27, 24.18, 24.12, 22.99, 14.23 ppm. MS (FS, 8kV): m/z (%) = 1562.6 (100%, M^+) (calc. for $C_{104}H_{152}Br_2$ = 1562.18 g mol^{-1}).

Perylene end-capped (6,6,12,12-tetraoctyl-indenofluorene) dimer (57)

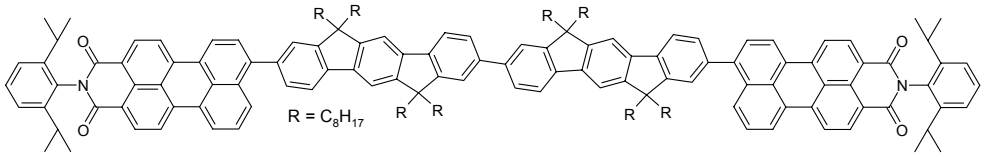

Dibromo-(6,6,12,12-tetraoctyl-indenofluorene) dimer (30 mg, 1.9 x 10^{-5} mol) and perylene boronic ester (25 mg, 4.2 x 10^{-5} mol) was dissolved in toluene (2 mL) and 2M K_2CO_3 solution (0.5 mL), and degassed with bubbling argon for 20 minutes. $Pd(PPh_3)_4$ (1.5 mg, 1.3 x 10^{-6} mol) was added and the solution heated at 80 °C for 12 hours. The organic product was extracted with methylene chloride, washed with water, dried over magnesium sulphate, and the solvents removed *in vacu*. The product was purified by column chromatography using petrol ether:methylene chloride (7:3) as eluent, and precipitated from methylene chloride in hexane to give the title compound as a red solid. 10 mg (22%). ^{1}H NMR (300MHz): (CD_2Cl_2) δ 8.70-8.57 (m, 12H), 8.15 (d, 2H, J=8.6Hz), 7.96 (d, 2H, J=8.2Hz), 7.89 (d, 2H, J=7.9Hz), 7.85-7.74 (m, 10H), 7.66 (t, 2H, J=7.8Hz), 7.60-7.58 (m, 4H), 7.51 (t, 2H, J=7.8Hz), 7.36 (d, 4H, J=7.7Hz), 2.78 (q, 4H, J=6.8Hz), 2.18-2.13 (m, 16H), 1.17-1.15 (m, 104H), 0.83-0.78 (m, 40H) ppm. MS (FS, 8kV): m/z (%) = 1181.5 (100%, M^{++}), 2362.3 (95%, M^+), 787.6 (61%, M^{+++}), (calc. for $C_{172}H_{204}N_2O_4$ = 2363.55 g mol^{-1}).

2-(9,9-Dioctylfluorene)-benzoic acid methyl ester (59)

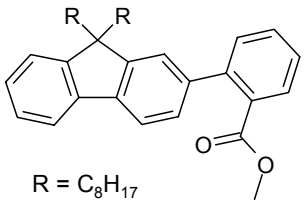

2-(9,9-Dioctyl-9H-fluoren-2-yl)-4,4,5,5-tetramethyl-[1,3,2]dioxaborolane (4.92 g, 9.5 mmol) and 2-bromobenzoic acid methyl ester (2.25 g, 10 mmol) was dissolved in toluene (50 mL) and 2M K_2CO_3 solution (25 mL), and degassed with bubbling argon for 20 minutes. $Pd(PPh_3)_4$ (346 mg, 3 x 10^{-4} mol) was added and the solution heated at 80 °C for 12 hours. The organic product was extracted with methylene chloride, washed with water, dried over magnesium sulphate, and the solvents removed *in vacu*. The product was purified by column chromatography using 0-2% ethyl acetate in hexane as eluent to give the title compound as a colourless oil. 4.55 g (91%). ^{1}H NMR (250MHz): (CD_2Cl_2) δ 7.80-7.73 (m, 3H), 7.57 (dt, 1H, J=1.5Hz, J=7.5Hz), 7.48-7.28 (m, 7H), 3.60 (s, 3H), 1.98 (t, 4H, J=7.8Hz), 1.21-1.06 (m, 20H), 0.81 (t, 6H, J=6.8Hz), 0.68-0.53 (m, 4H) ppm. ^{13}C NMR (63MHz): (CD_2Cl_2) δ 169.52, 151.31, 151.03, 143.04, 141.17, 140.66, 140.58, 131.78, 131.41, 131.10, 129.90, 127.44, 127.36, 127.30, 127.13, 123.47, 123.30, 120.03, 119.64, 55.49, 52.07, 40.74, 32.15, 30.40, 29.64, 29.59, 24.15, 22.95, 14.18 ppm. MS (FS, 8kV): m/z (%) = 524.8 (100%, M^+), (calc. for $C_{37}H_{48}O_2$ = 524.79 g mol^{-1}).

2-(9,9-Dioctylfluorene)-benzoic acid (60)

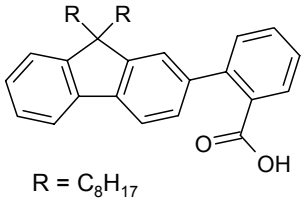

2-(9,9-Dioctyl-9H-fluoren-2-yl)-benzoic acid methyl ester (4.40 g, 8.4 mmol) and sodium hydroxide (3.2 g, 80 mmol) were mixed in 100 mL methanol and 40 mL water, and refluxed for 3 days. 2M hydrochloric acid was added, the product filtered and recrystallised from hexane to give the title compound as a white powder. 3.35 g (78%). ^{1}H NMR (250MHz): (CD_2Cl_2) δ 7.92 (d, 1H, J=7.8Hz), 7.76-7.71 (m, 2H), 7.59 (dt, 1H, J=1.3Hz, J=7.5Hz), 7.46-7.30 (m, 7H), 1.97 (t, 4H, J=8.3), 1.17-1.03 (m, 20H), 0.78 (t, 6H, J=6.8Hz), 0.72-0.53 (m, 4H) ppm. ^{13}C NMR (63MHz): (CD_2Cl_2) δ 173.06, 151.38, 150.90, 144.26, 141.17, 140.74, 140.39, 132.40, 131.70, 131.10, 129.66, 127.43, 127.14, 123.87, 123.31, 120.08, 119.63, 55.50, 40.68, 32.16, 30.47, 29.63, 24.20, 22.98, 14.19 ppm. Elemental Analysis: Calculated C 84.66, H 9.08. Found C 84.88, H 8.67.

12,12-Dioctyl-12H-indeno[1,2-b]fluoren-6-one (61)

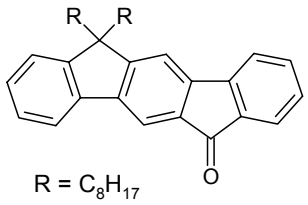

2-(9,9-Dioctyl-9H-fluoren-2-yl)-benzoic acid (3.30 g, 6.5 mmol) was mixed with 50 mL of freshly distilled thionyl chloride under argon, and refluxed for 24 hours. The thionyl chloride was removed by distillation under argon. The residue was dissolved in 70 mL of dry carbon tetrachloride and cooled in an ice bath. $AlCl_3$ (2.66 g, 20 mmol) was added and the blue solution stirred for 12 hours, then the reaction was quenched with ice. The organic product was extracted with methylene chloride, washed with water, dried over magnesium sulphate, and the solvents removed *in vacu*. The product was purified by column chromatography eluting with hexane, then recrystallised from methanol to give the title compound as a yellow solid. 0.74 g (23%). ^{1}H NMR (250MHz): (CD_2Cl_2) δ 7.97 (s, 1H), 7.77-7.74 (m, 1H), 7.63 (d, 1H, J=7.2Hz), 7.60 (d, 1H, J=7.3Hz), 7.55 (s, 1H), 7.52 (dt, 1H, J=1.3Hz, J=7.3Hz), 7.39-7.34 (m, 3H), 7.29 (dt, 1H, J=1.1Hz, J=7.4Hz), 2.05 (t, 4H, J=8.3Hz), 1.19-1.06 (m, 20H), 0.79 (t, 6H, J=6.8Hz), 0.70-0.57 (m, 4H) ppm. ^{13}C NMR (63MHz): (CD_2Cl_2) δ 193.74, 159.15, 150.98, 145.26, 144.26, 142.91, 140.42, 135.32, 134.97, 134.20, 129.10, 127.99, 127.42, 124.26, 123.27, 120.50, 120.27, 115.76, 115.52, 56.08, 40.60, 32.12, 30.30, 29.56, 24.15, 22.94, 14.16 ppm. MS (FS, 8kV): m/z (%) = 492.9 (100%, M^+), (calc. for $C_{36}H_{44}O$ = 492.75 g mol^{-1}). Elemental Analysis: Calculated C 87.75, H 9.00. Found C 87.63, H 8.69.

2,7-Di(2-benzoic acid methyl ester)-9,9-dioctylfluorene (62)

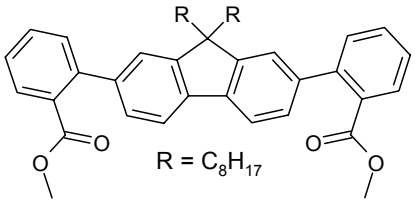

2,7-Bisboronic ester 9,9-dioctylfluorene (0.5 g, 0.78 mmol) and 2-bromobenzoic acid methyl ester (0.344 g, 1.6 mmol) was dissolved in 8 mL toluene and 4 mL 2M K_2CO_3 solution, and degassed with bubbling argon for 20 minutes. $Pd(PPh_3)_4$ (55 mg, 4.8 x 10^{-5} mol) was added and the solution heated at 80 °C for 12 hours. The organic product was extracted with methylene chloride, washed with water, dried over magnesium sulphate, and the solvents removed *in vacu*. The product was purified by column chromatography using 5% ethyl acetate in hexane as eluent to give the title compound as a colourless oil. 0.4 g (78%). ^{1}H NMR (250MHz): (CD_2Cl_2) δ 7.84-7.78 (m, 4H), 7.59 (dt, 2H, J=1.4Hz, J=7.3Hz), 7.51-7.41 (m, 4H), 7.34-7.32 (m, 4H), 3.63 (s, 6H), 2.05-1.98 (m, 4H), 1.22-1.10 (m, 20H), 0.82 (t, 6H, J=6.8Hz), 0.75-0.68 (m, 4H) ppm. ^{13}C NMR (63MHz): (CD_2Cl_2) δ 169.52, 151.28, 143.08, 140.72, 140.38, 131.79, 131.45, 131.13, 129.96, 127.53, 127.41, 123.51,

119.81, 55.63, 52.09, 40.89, 32.17, 30.47, 29.71, 29.64, 24.18, 22.97, 14.21 ppm. MS (FS, 8kV): m/z (%) = 658.8 (100%, M^+), (calc. for $C_{45}H_{54}O_4$ = 658.93 g mol^{-1}).

2,7-Di(2-benzoic acid)-9,9-dioctylfluorene (63)

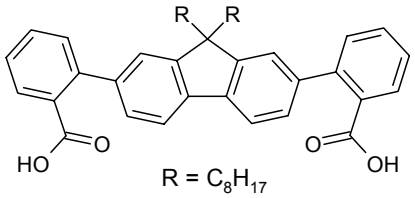

2,7-Di(2-benzoic acid methyl ester)-9,9-dioctylfluorene (0.4 g, 0.6 mmol) and sodium hydroxide (0.5 g, 13 mmol) were mixed in 10 mL methanol and 4 mL water, and refluxed for 3 days. 2M hydrochloric acid was added, the product filtered and recrystallised from hexane to give the title compound as a white powder. 0.36 g (95.2%). ^{1}H NMR (250MHz): (CD_2Cl_2) δ 8.03 (d, 2H, J=7.9Hz), 7.76 (d, 2H, J=7.8Hz), 7.60 (dt, 2H, J=1.5Hz, J=7.8Hz), 7.46-7.29 (m, 8H), 1.93-1.87 (m, 4H), 1.03-0.78 (m, 24H), 0.69 (t, 6H, J=7.0Hz) ppm. ^{13}C NMR (63MHz): (CD_2Cl_2) δ 151.11, 144.69, 140.25, 132.83, 132.10, 131.79, 128.90, 127.76, 127.44, 124.10, 119.84, 55.39, 40.44, 32.14, 30.86, 29.73, 29.67, 24.42, 22.97, 14.14 ppm. Elemental Analysis: Calculated C 81.87, H 7.99. Found C 81.82, H 7.88.

6,6-Dioctyl-indeno[1,2-b]-indeno[1,2-b']fluoren-12,15-dione (64)

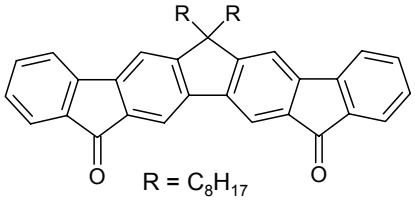

2,7-Di(2-benzoic acid)-9,9-dioctylfluorene (310 mg, 0.71 mmol) was mixed with 3 mL of freshly distilled thionyl chloride under argon, and refluxed for 24 hours. The thionyl chloride was removed by distillation under argon. The residue was dissolved in 7 mL of dry carbon tetrachloride and cooled in an ice bath. $AlCl_3$ (590 mg, 4.4 mmol) was added and the blue solution stirred for 12 hours, then the reaction was quenched with ice. The organic product was extracted with methylene chloride, washed with water, dried over magnesium sulphate, and the solvents removed *in vacu*. The product was purified by column chromatography using 50% ethyl acetate in hexane as eluent, then recrystallised from methanol to give the title compound as a yellow solid. 70 mg (17%). ^{1}H NMR (250MHz): (CD_2Cl_2) δ 7.97 (s, 2H), 7.66-7.51 (m, 8H), 7.32 (dt, 2H, J=1.0Hz, J=7.4Hz), 2.14-2.09 (m, 4H), 1.16-1.06 (m, 20H), 0.76 (t, 6H, J=6.8Hz), 0.72-0.63 (m, 4H) ppm. ^{13}C NMR (63MHz): (CD_2Cl_2) δ 193.39, 158.88, 145.02, 144.70, 141.77, 135.28, 135.04, 134.45, 129.34, 124.37, 120.63, 115.99, 115.44, 56.69, 32.10, 30.24, 29.52, 29.49, 24.17, 22.91, 14.13 ppm. MS (FS, 8kV): m/z (%) = 594.6 (100%, M^+), (calc. for $C_{43}H_{46}O_2$ = 594.84 g mol^{-1}). Elemental Analysis: Calculated C 86.83, H 7.79. Found C 85.44, H 6.80.

4,4''-Bis-(4-dodecyl-phenylethynyl)-[1,1';4',1'']terphenyl-2',5'-dicarboxylic acid dimethyl ester (65)

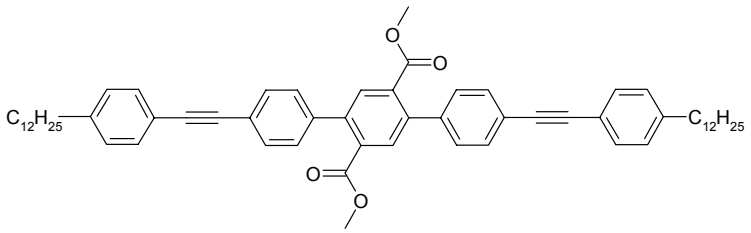

4,4''-Diiodo-[1,1';4',1'']terphenyl-2',5'-dicarboxylic acid dimethyl ester (650 mg, 1.08 mmol), 1-dodecyl-4-ethynyl-benzene (705 mg, 2.6 mmol), triphenylphosphine (7 mg, 26 µmol), and copper (I) iodide (5 mg, 26 µmol) were dissolved in 100 mL piperidine and degassed. $Pd(PPh_3)_4$ (30 mg, 26 µmol) was added and the reaction was stirred at 45°C for 24 hours. The solvent was removed *in vacuo* and the residue was purified by column chromatography eluting with 0-5% ethyl acetate in hexane to give the title compound as a white powder. 0.79 g (82%). ^{1}H NMR (250MHz): (d_8-THF) δ 7.84 (s, 2H), 7.57 (d, 4H, J=8.3Hz), 7.44 (d, 4H, J=8.1Hz), 7.39 (d, 4H, J=8.4Hz), 7.21 (d, 4H, J=8.2Hz), 3.64 (s, 6H), 2.67-2.61 (m, 4H), 1.70-1.58 (m, 4H), 1.35-1.30 (m, 36H), 0.89 (t, 6H, J=6.5Hz) ppm. ^{13}C NMR (63MHz): (d_8-THF) δ 168.32, 144.39, 141.32, 140.79, 134.48, 132.61, 132.28, 132.10, 129.38, 129.32, 123.93, 121.49, 52.28, 36.65, 32.87, 32.22, 30.60, 30.56, 30.45, 30.30, 30.21, 23.56, 14.42 ppm. MS (FS, 8kV): m/z (%) = 881.9 (100%, M^+) (calc. for $C_{62}H_{74}O_4$ = 883.28 g mol^{-1}). Elemental Analysis: Calculated C 84.31, H 8.44. Found C 84.36, H 8.45.

2,8-Bis-(4-dodecyl-phenylethynyl)-6,6,12,12-tetraoctyl-indenofluorene (69)

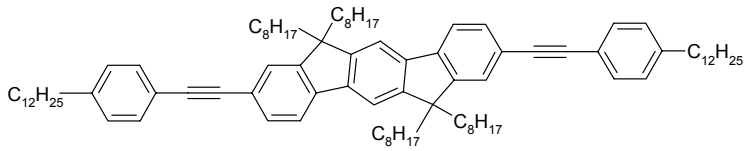

2,8-Dibromo-6,6,12,12-tetraoctyl-indenofluorene (280 mg, 0.33 mmol), 1-dodecyl-4-ethynyl-benzene (200 mg, 0.74 mmol), triphenylphosphine (2 mg, 7.4 µmol), and copper (I) iodide (1.7 mg, 7.4 µmol) were dissolved in 15 mL triethylamine and degassed. $Pd(PPh_3)_4$ (8.5 mg, 7.4 µmol) was added and the reaction was stirred at 75°C for 24 hours. The organic product was extracted with methylene chloride, washed with water, dried over magnesium sulphate, and the solvents removed *in vacu*. The product was purified by column chromatography eluting with hexane to give the title compound as a white powder. 0.35 g (85%). ^{1}H NMR (300MHz): (CD_2Cl_2) δ 7.74 (d, 2H, J=8.2Hz), 7.68 (s, 2H), 7.54-7.51 (m, 4H), 7.47 (d, 4H, J=8.1Hz), 7.21 (d, 4H, J=8.2Hz), 2.66-2.61 (m, 4H), 2.09-2-04 (m, 8H), 1.65-1.58 (m, 4H), 1.34-1.07 (m, 76H), 0.89 (t, 6H, J=6.7Hz), 0.78 (t, 12H, J=6.9Hz), 0.68-0.57 (m, 8H) ppm. ^{13}C NMR (75.46MHz): (CD_2Cl_2) δ 151.71, 151.00, 144.01, 142.00, 140.80, 131.68, 130.76, 128.95, 121.74, 120.84, 119.78, 114.65, 90.20, 89.91, 126.29, 55.25, 40.91, 36.23, 32.31, 32.16, 31.67, 30.33, 30.02, 29.96, 29.85, 29.73, 29.64, 29.54, 24.15, 23.07, 22.94, 14.26, 14.18 ppm. MS (FS, 8kV): m/z (%) = 1240.7 (100%, M^+), (calc. for $C_{92}H_{134}$ = 1240.09 g mol^{-1}). Elemental Analysis: Calculated C 89.11, H 10.89. Found C 89.24, H 10.77.

2,8-Bisethynyl-6,6,12,12-tetraoctyl-indenofluorene (72)

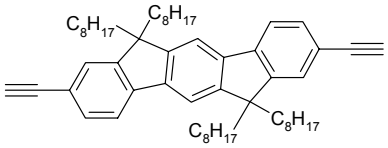

2,8-Dibromo-6,6,12,12-tetraoctyl-indenofluorene (500 mg, 0.58 mmol), triphenylphosphine (3 mg, 12 µmol), and copper (I) iodide (2 mg, 12 µmol) were dissolved in 10 mL triethylamine and degassed. $Pd(PPh_3)_4$ (13 mg, 16 µmol) and trimethylsilyl acetylene (0.18 mL, 1.28 mmol) was added and the reaction was stirred at 80°C for 12 hours. The organic product was extracted with methylene chloride, washed with 2M HCl solution, washed with water, dried over magnesium sulphate, and the solvents removed *in vacu*. The white solid was mixed with ammonium fluoride (119 mg, 3.2 mmol) in 20 mL dry THF, to which a solution of tetrabutyl ammonium fluoride was added (0.14 mL, 0.14 mmol). The solution was stirred for two hours under argon, before being quenched with water. The organic product was extracted with methylene chloride, washed with water, dried over magnesium sulphate, and the solvents removed *in vacu*. The product was purified by column chromatography eluting with hexane to give the title compound as a white powder. 0.30 g (68%). ^{1}H NMR (300MHz): (CD_2Cl_2) δ 7.71 (d, 2H, J=8.2Hz), 7.67 (s, 2H), 7.51-7.48 (m, 4H), 3.19 (s, 2H), 2.07-2.01 (m, 8H), 1.20-1.04 (m, 40H), 0.79 (t, 12H, J=6.9Hz), 0.61 (m, 8H) ppm. ^{13}C NMR (75.46MHz): (CD_2Cl_2) δ 151.69, 151.07, 142.59, 140.78, 131.39, 126.93, 120.39, 119.78, 114.81, 85.00, 77.26, 55.29, 40.84, 32.17, 30.30, 29.62, 29.54, 24.13, 22.96, 14.20 ppm. MS (FS, 8kV): m/z (%) = 751.7 (100%, M^+), (calc. for $C_{56}H_{78}$ = 751.25 g mol^{-1}). Elemental Analysis: Calculated C 89.53, H 10.47. Found C 89.58, H 10.44.

2,8-Bis(penta-(3,7-dimethyl octyl)-HBC-ethynyl)-6,6,12,12-tetraoctyl-indenofluorene (73)

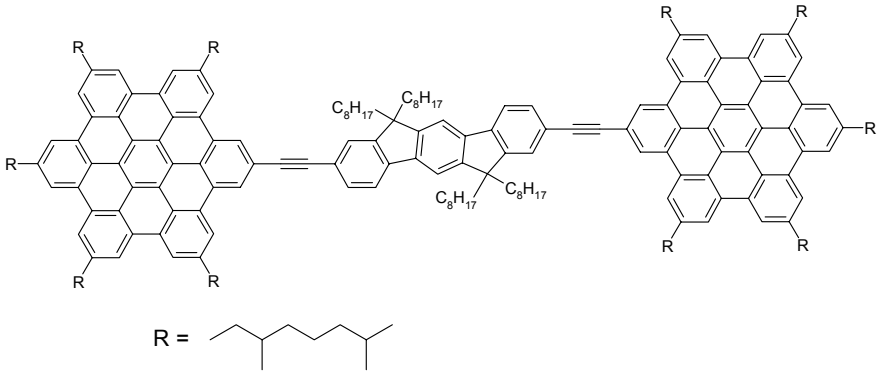

2,8-Bisethynyl-6,6,12,12-tetraoctyl-indenofluorene (80 mg, 0.11 mmol), monobromo penta(3,7-dimethyl octyl) HBC (284 mg, 0.22 mmol), and triphenylphosphine (4 mg, 17 µmol) were dissolved in 5 mL piperidine and degassed by freeze-pump-thaw (4x). $Pd(PPh_3)_4$ (19 mg, 17 µmol) and copper (I) iodide (3 mg, 17 µmol) was added and the reaction was stirred at 80°C for 12 hours under argon. The reaction mixture was cooled to 50°C, poured into methylene chloride, and the precipitate filtered. The precipitate was recrystallised from THF to yield the title

product as a yellow solid. 85 mg (24%). ^{1}H NMR (300MHz): (CS_2) δ 9.07 (s, 4H), 8.75 (s, 4H), 8.57 (s, 4H), 8.56 (s, 12H), 7.90-7.82 (m, 8H), 3.33-3.04 (m, 20H), 2.37-2.25 (m, 8H), 2.18-1.27 (m, 148H), 1.03-1.00 (m, 90H), 0.93 (t, 12H, J=6.6Hz) ppm. MS (MALDI-TOF, 8kV): m/z (%) = 3195 (100%, M^+), (calc. for $C_{240}H_{310}$ = 3195.15 g mol^{-1}). Elemental Analysis: Calculated C 90.22, H 9.78. Found C 86.83, H 9.61.